



The
University
Of
Sheffield.

Using Tribo-Chemistry Analysis to Understand Low Adhesion in the Wheel-Rail Contact

Benjamin White

Supervised by Professor Roger Lewis

A thesis submitted in fulfilment of the requirements for the degree of Doctor of
Philosophy

University of Sheffield
Faculty of Engineering
Department of Mechanical Engineering

19th April 2018

Summary

Low adhesion between wheel and rail is a recurrent problem for the rail industry. Low adhesion can lead to wheel slides and slips during acceleration and deceleration, which can cause large amounts of damage to the wheel and rail as well as causing safety issues and delays if a train cannot accelerate or decelerate when necessary.

Adhesion in the wheel-rail contact is affected by the third body layer which is present in the contact patch between wheel and rail. It is composed naturally from steel wear debris and iron oxides, but often contains other contaminants such as organic matter, ballast dust, soil and grease. Different environmental conditions such as temperature, precipitation and humidity change the properties of this third body layer and therefore change adhesion conditions on the railway.

Low adhesion has been well documented throughout the autumn season due to organic contamination, but also takes place throughout the year when no visible contamination is seen on the railhead, known as the “wet-rail” phenomenon. It is thought to occur when there are low levels of water on the railhead, formed by dew, mist or light rain, rather than heavy rain.

The conditions and mechanisms that cause the phenomenon are not fully understood. Low adhesion does not occur very often and under what is likely to be a narrow window of conditions, which means that it can be difficult to simulate and study.

The aim of this work was to use a combination of tribology and chemistry to better understand the cause of low adhesion throughout the year, known as the wet-rail phenomenon. It investigated low adhesion conditions that occur all year round, initially focusing on the role of iron oxide in low adhesion as it has previously been hypothesised that oxides could play a major role in the wet-rail phenomenon.

Testing was carried out over a range of conditions on three different tribological test rigs to attempt to simulate low adhesion due to the wet-rail phenomenon, which produced valuable information about the causes of low adhesion. It was found that, under certain conditions, a combination of iron oxides and water could cause low adhesion in a simulated wheel-rail contact. Test methods were designed to simulate the wet-rail phenomenon, which can be used as a platform to better understand the causes of low adhesion and to test future mitigation methods.

Nomenclature

1. **RSSB** - Rail Safety and Standards Board
2. **NR** - Network Rail
3. **LA** - Low Adhesion
4. **WSP** - Wheel Slide Protection
5. **SPAD** - Signal Passed At Danger
6. **RH** - Relative Humidity
7. **SRV** - Slip Resistance Factor
8. **SUROS** - Sheffield Univeristy Rolling Sliding Test Rig
9. **UMT** - Universal Mechanical Tester
10. **HPT** - High Pressure Torsion
11. **FSR** - Full Scale Rig
12. **Ra** - Roughness Average
13. **Sa** - Surface Roughness Average (area)
14. μ - Friction Coefficient
15. **XPS** - X-ray Photoelectron Spectroscopy
16. **wt %** - Weight Percentage of solid in a paste. Often referred to as “%” or solid oxide fraction (see below)
17. **Solid oxide fraction** - Fraction of solid in a paste

Contents

1	Introduction	1
1.1	Overview	2
1.2	Aims and Objectives	3
1.3	Novel Aspects and Impact	4
1.4	Thesis Layout	5
2	Literature Review	7
2.1	Introduction	8
2.2	The Wheel-Rail Contact	8
2.2.1	Friction and creepage	8
2.2.2	Rail surface conditions	11
2.2.3	Contact conditions	13
2.3	Effects of Iron Oxides on the Wheel-Rail Contact	14
2.3.1	Formation and transformations	14
2.3.2	Effects of oxides on the wheel-rail contact	17
2.3.3	Oxide analysis	26
2.4	Effects of Water on the Wheel-Rail Contact	32
2.4.1	Introduction	32
2.4.2	Amount of water	32
2.4.3	Contact conditions	33
2.5	Effects of Organic Contamination on the Wheel-Rail Contact	38
2.6	Summary and Hypotheses	43
3	Operational Data Analysis	47
3.1	Introduction	48
3.2	Data Collection	51
3.3	National Analysis	52
3.4	Local Analysis	57
3.5	Data Collation	61
3.6	WSP Analysis	67
3.7	Stockholm Case Study	70
3.8	Conclusions	71
4	Railhead Analysis	73
4.1	Introduction	74
4.2	Laboratory Full Scale Testing	74
4.2.1	Introduction	74

4.2.2	Methodology	75
4.2.3	Results	76
4.2.4	Discussion	81
4.3	Iron Oxide Rheometry	82
4.3.1	Introduction to tests	82
4.3.2	Methodology	83
4.3.3	Results	83
4.3.4	Discussion	86
4.4	Field Testing	88
4.4.1	Introduction to tests	88
4.4.2	Results	88
4.4.3	Discussion	91
4.5	Conclusions	91
5	Modelling	93
5.1	Introduction	94
5.2	Adhesion Model	94
5.3	Modifications	100
5.4	Conclusions	105
6	Test rigs and Preliminary Investigations	107
6.1	Introduction	107
6.1.1	Rig selection	108
6.1.2	Oxide and water application	110
6.2	Pendulum Testing	114
6.2.1	Introduction to test rig	114
6.2.2	Test apparatus	115
6.2.3	Methodology	117
6.2.4	Results	120
6.2.5	Discussion	126
6.2.6	Conclusions	128
6.3	Bruker UMT Tribometer Testing	129
6.3.1	Introduction to test rig	129
6.3.2	Test apparatus	129
6.3.3	Methodology	131
6.3.4	Results	135
6.3.5	Discussion	140
6.3.6	Conclusions	142
6.4	SUROS Twin Disc Testing	144
6.4.1	Introduction to test rig	144
6.4.2	Test apparatus	144
6.4.3	Methodology	146
6.4.4	Results	149
6.4.5	Discussion	155

6.4.6	Conclusions	160
6.5	Investigative Test Conclusions	162
7	Simulation of the Wet-Rail Phenomenon	165
7.1	Introduction	166
7.2	Methodology	166
7.2.1	SUROS traction testing	166
7.2.2	SUROS specimen roughness analysis	168
7.3	Results	169
7.3.1	SUROS traction testing	169
7.3.2	SUROS specimen roughness analysis	175
7.4	Discussion	178
7.4.1	SUROS traction testing	178
7.4.2	SUROS specimen roughness analysis	179
7.4.3	Links to the adhesion model	180
7.4.4	Hypotheses validation	181
7.5	Conclusions	182
8	Chemical Analysis of the Wet-Rail Phenomenon	183
8.1	Introduction	184
8.2	Methodology	184
8.3	Results	185
8.4	Discussion	190
8.5	Conclusions	191
9	Mitigation of the Wet-Rail Phenomenon	193
9.1	Introduction	194
9.2	Methodology	194
9.3	Results	195
9.4	Discussion	196
9.5	Conclusions	197
10	Discussion	199
10.1	Introduction	200
10.2	Incident Frequency and Weather Conditions	200
10.3	Oxide Paste Behaviour	201
10.4	Simulation of the Wet-Rail Phenomenon	202
10.5	Mechanisms and Hypotheses	203
10.6	Mitigation	205
11	Conclusions	207
11.1	Project conclusions	208
11.2	Publications Arising From This Work	210
	References	211

1 Introduction

1.1 Overview

Effective railway acceleration and braking is reliant on the small contact patch between wheel and rail. This is roughly 1 cm^2 and has to support high loads under numerous different conditions. Traction in the contact is generated as a result of torque being applied through the driving wheelsets and low levels of traction, often known as low adhesion, between wheel and rail can occur under certain conditions and cause difficulties when accelerating or braking.

The wheel-rail contact is an open system and therefore exposed to a number of conditions and contaminants that may influence adhesion. This can include natural contaminants such as leaves and organic debris [1], iron oxides [2] and wear particles [3], as well as artificial contaminants such as sand, oil and salt [4]. Some of the causes of low adhesion in the wheel-rail contact are well understood and can be predicted and mitigated, whilst others remain hard to prevent.

Low adhesion can cause a number of problems for the rail industry. Trains, unable to brake effectively, can collide with buffers and “signals passed at danger” involve a train passing a stop signal. Station overruns also have a large effect on the railway, where a train is unable to brake sufficiently for its intended station stop. Wheel slides due to low adhesion often result in wheel flat spots, which result in the wheels needing re-profiling or premature replacement.

Many UK railway lines are operating at full capacity which means it is more important than ever that acceleration and braking are efficient and reliable to prevent delays; better low adhesion prediction and mitigation methods will be key to achieving this.

A recent RSSB project [5] has highlighted that low adhesion incidents can occur without heavy precipitation or visible rail contamination, organic or otherwise. This has been named the “wet-rail” phenomenon, defined as the following:

“Poor adhesion conditions caused when low levels of moisture are present at the wheel-rail interface. These conditions are associated with dew on the rail head; very light rain, misty conditions and the transition between dry and wet rails at the onset of rain. These conditions are not associated with continuous rain”.

This phenomenon is currently not very well understood, difficult to replicate and therefore hard to predict. This work is being carried out to investigate the wet-rail phenomenon and better understand the conditions that cause it, to allow better prediction and mitigation of the problem.

Various types of traction enhancers such as sand or artificial traction gels are used to prevent low adhesion caused by leaf layers [6], these can be applied from the trains themselves or by using trackside applicators. These traction enhancers are often used in localised areas so are ineffective unless low adhesion conditions are known to be present there. It is currently unclear whether current traction enhancers will be effective against the wet-rail phenomenon.

Adhesion monitoring and forecasts are necessary to give drivers a warning system as to when low adhesion may occur. An example of this is the “Adhesion Index” [7], which estimates the amount of leaf fall and therefore likelihood of a low adhesion event caused by leaf contamination, but is only applicable for the autumn leaf fall season. If the wet-rail phenomenon was better understood, a similar year-round index could be created or modified to forecast particular periods and locations where a traction increasing product should be applied or a more cautious braking style should be used.

Driver braking style is an important factor and needs to be considered when assessing low adhesion events. Low adhesion conditions can be mitigated if drivers adjust their braking style which makes prediction of low adhesion conditions especially important. It also means that low adhesion conditions such as the wet-rail phenomenon, which occur on seemingly uncontaminated track, are particularly hard to adjust for. As a result it is especially important to better understand when and why this problem occurs.

The transitory nature of the wet-rail phenomenon becomes problematic when predicting the phenomenon. If it occurs under a specific set of conditions, these conditions may not occur for long stretches of rail. This leads us to the suggestion that the conditions may be able to “propagate” down the rail; where low adhesion causes a physical change in contact conditions, leading to further loss of adhesion.

1.2 Aims and Objectives

The aim of this work was to use a combination of tribology and chemistry to better understand the wet-rail phenomenon. It investigated low adhesion conditions that occur all year round, initially focusing on the role of iron oxide in low adhesion as it has previously been hypothesised that oxides could play a major role in the wet-rail phenomenon. The PhD was split into four work packages that are outlined below and a flow chart for the work is shown in Figure 1.1.

1. Use available data and field measurements to define the critical conditions that lead to adhesion loss, This involved analysing weather and low adhesion incident data to understand the conditions that may cause low adhesion on the railway network
2. Generate methods to simulate environmental and rail surface conditions on small scale test rigs
3. Perform small scale laboratory tests using different test rigs under different environmental and surface conditions to assess the impact they have on adhesion and attempt to produce representative low adhesion conditions
4. Perform full scale tests to overcome scaling effects and provide a platform to test mitigation methods

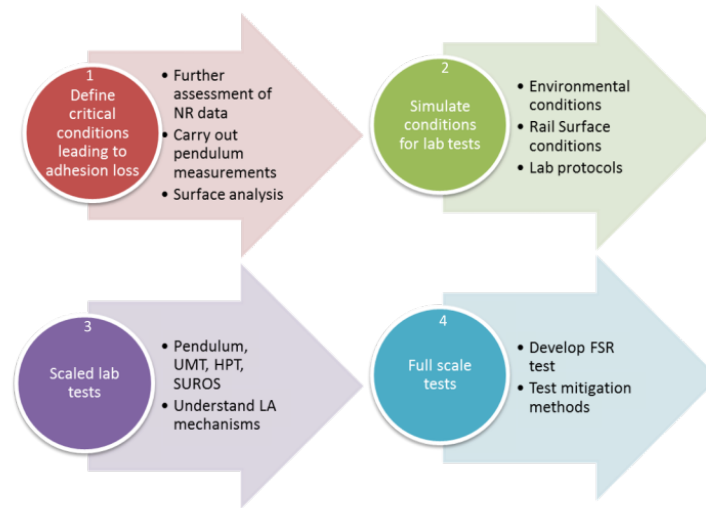


Figure 1.1: A flow chart of the work

1.3 Novel Aspects and Impact

The work comprehensively assessed the impact of iron oxides on adhesion levels. Sustained and repeatable low adhesion in a simulated wheel-rail contact due to iron oxides and water alone was produced in a laboratory for the first time and this was used to generate a better understanding of the wet-rail phenomenon, using a combination of techniques to generate and validate a hypothesis by which the wet-rail phenomenon may occur.

Mitigation techniques were tested in the laboratory on a wet-rail simulation and the information and methodology gained from this work can be used to inform and improve mitigation techniques to prevent the wet-rail phenomenon on the railways.

1.4 Thesis Layout

Chapter 2 reviews the role of iron oxides and water in the wet-rail phenomenon. It also reviews the role of organic contamination and water in low adhesion as a comparison. Hypotheses for the mechanism of the wet-rail phenomenon are created to examine in future work.

Chapter 3 presents an analysis of operational and weather data sets to look for any correlations between specific weather conditions and low adhesion events. Data was provided by Network Rail, Met Office, MetDesk, Virgin Trains and Greater Anglia trains.

Chapter 4 experimentally assesses how iron oxide and water will behave on the railhead in order to plan tests and support hypotheses made. This chapter makes use of a full scale wheel and rail rig so the impact of a full size contact patch on the rail head can be seen. Rheology measurements are carried out on oxide and water pastes to investigate their shear properties. Images from field testing on a working railway are also included to compare with laboratory results.

Chapter 5 looks at models available for use to predict friction in the wheel-rail contact. An existing model is then modified to investigate the dependence of oxide paste viscosity on friction in small scale test rigs. The work from this chapter allows a better understanding of how the wet-rail phenomenon may be replicated using small scale rigs and how it may occur in a real wheel-rail contact.

Chapter 6 uses a broad variety of conditions and test rigs to assess how iron oxides can affect the wheel-rail contact. This work builds up a better picture of the mechanisms in which iron oxides could reduce adhesion and how the wet-rail phenomenon could occur in a railway.

Chapter 7 uses the outcomes of chapter 6 to provide a more streamlined approach to testing the conditions that cause the wet-rail phenomenon, in order to investigate how and when it may occur.

Chapter 8 uses X-ray photoelectron spectroscopy to analyse both samples from a railhead and samples that have produced low adhesion in a laboratory to assess how iron oxides and organic contaminants change in the contact patch.

Chapter 9 tests mitigation methods in a controlled laboratory environment using methodologies described in chapter 7 that produce representative low adhesion conditions.

Chapter 10 discusses the outcomes of this thesis and outlines further work that could be carried out on the subject.

Chapter 11 provides conclusions to this thesis.

2 Literature Review

2.1 Introduction

This chapter will begin by introducing the wheel-rail contact, key principles such as friction will be introduced and the contact patch will be described.

The review that follows is split into three sections. The first primarily aims to look at the iron oxides that form in the wheel-rail contact and assess evidence for the contribution of iron oxide to low adhesion in the wheel-rail interface. The techniques used to measure both the chemical and tribological properties of oxide layers will be discussed and suggestions for future progress will be made.

A short review is then carried out on low adhesion due to water alone. This is added because the wet-rail phenomenon seems to occur with low water levels so it is important to compare the effects of water, often in high volumes, to that of water in combination with oxide at lower volumes. Another short review is carried out on low adhesion due to organic contamination. Organic contamination may also be present throughout the year and contribute to the wet-rail phenomenon, so a focus is put upon year round methods of contamination. The tribological behaviour of these is compared and contrasted to the behaviour of iron oxides and the combined effects on low adhesion are reviewed.

2.2 The Wheel-Rail Contact

The fundamental tribology of the wheel-rail contact has been described in detail in many other works, but a simplified version is included so that the reader understands the terminology of friction, adhesion and traction used in this thesis. This opening section reviews the contact conditions in the wheel-rail contact so the conditions needed to replicate this contact in future testing can be better understood.

2.2.1 Friction and creepage

Friction is the force operating that opposes the relative tangential motion at the boundary between sliding objects. It is often expressed as a friction coefficient, the ratio between the friction force and the normal force in the contact between two bodies. The static friction, opposing the movement of bodies from a static start is often higher than kinetic friction, which opposes the movement of bodies that are already in motion.

Friction is measured in a sliding contact but the wheel-rail contact is a rolling/sliding contact which means that traction needs to be considered, the force transmitted when a cylinder is driven along a flat plane. A schematic of the forces involved in the wheel rolling over the rail is shown in Figure 2.1. Torque is applied through the axis of rotation at the centre of the wheel which then moves with angular velocity

(ω) and linear velocity (v). This torque application causes a longitudinal tangential force called the traction force, F_x . The traction, or adhesion, coefficient (μ) is defined as this traction force, divided by the normal force in the contact.

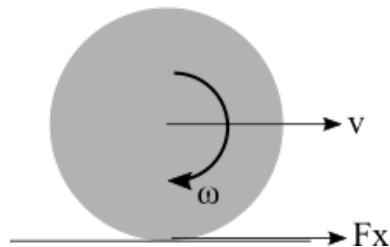


Figure 2.1: A schematic force diagram of the wheel rail contact [8]

A purely rolling contact is very rare and the contact will almost always involve sliding as well as rolling due to the wheel turning faster or slower than pure rolling. In a rolling/sliding contact the circumferential velocity is unequal to the linear velocity and causes slip, often known as creep, in the contact. Creep is often represented as a percentage of relative velocity compared to mean velocity of the wheel, with 0% being a purely rolling contact and 100 % being a purely sliding contact.

The relationship between traction force and slip, known as the creep curve, is shown in Figure 2.2. At 0 % creep the traction coefficient is 0, a purely rolling contact. At this point there is full “stick” in the contact patch, with no slipping between the wheel and rail [9].

An increase in traction force causes a rise in slip at the rear of the contact patch and a decrease in stick, which causes a rise in the traction coefficient along the creep curve, the slip and traction coefficient increase until at full slip the entire contact patch is slipping. At this point the traction coefficient is equal to the friction coefficient and cannot increase any further. The creep curve plateaus at the friction coefficient, known as saturated creep.

The traction coefficient is also known as the “adhesion coefficient”, whilst “adhesion” will refer to the general state of friction on the railhead, with “low adhesion” conditions referring to a railhead with low friction and therefore producing a low traction coefficient between wheel and rail [1].

Different conditions were tested on a laboratory-based twin disc test machine and the creep curves generated are shown in Figure 2.3. The contaminants producing low traction coefficients result in a saturated creep curve at much lower levels, with a less pronounced rise in traction coefficient with creep before saturation.

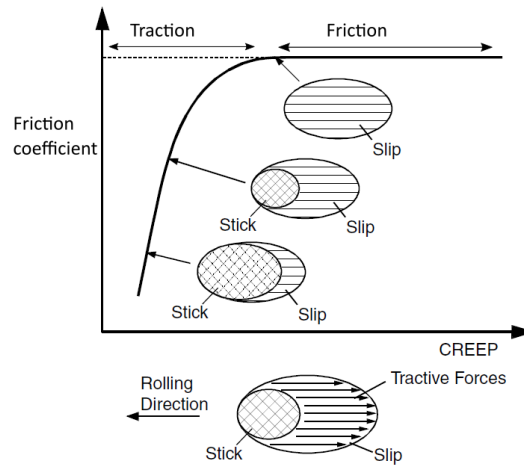


Figure 2.2: A theoretical creep curve, showing slip and stick regions in the contact patch [9]

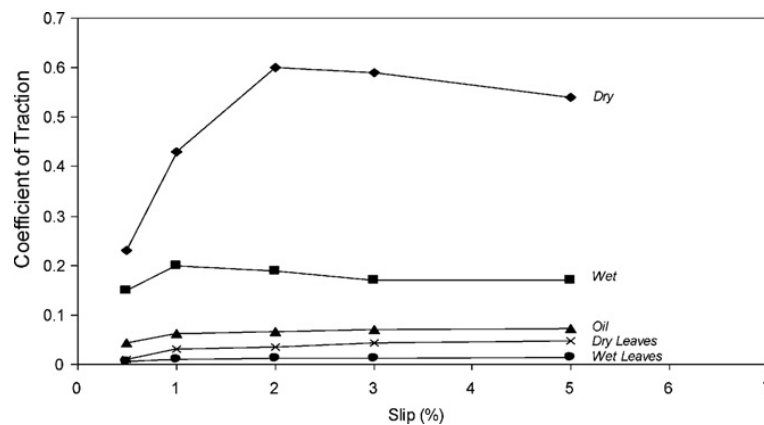


Figure 2.3: Creep curves generated using a twin disc test rig under different conditions [10]

The lowest wheel-rail friction coefficient limits that are deemed acceptable by different railways are shown in Table 2.1 [11].

	Friction coefficient for deceleration	Friction coefficient for acceleration
UK	0.09	0.2
Stockholm public transport	0.15	0.18
Netherlands	0.07	0.17

Table 2.1: Wheel-rail friction limits deemed acceptable by different railways [11]

2.2.2 Rail surface conditions

On the surface of both the wheel and rail lies the third body layer which is present at all times, even when the rail appears dry and uncontaminated. The third body layer lies above the modified surface steel microstructure and the bulk steel microstructure, as shown in Figure 2.4 [3]. The layer can be complicated to study as it is comprised of a number of materials and subjected to a variety of conditions, all of which can affect the tribological properties of the layer. An emphasis will be put on the effect on iron oxides in the layer, however it needs to be remembered that iron oxides are just one of many constituents and any tribological effect of the layer may be due to a combination of materials and conditions rather than iron oxides alone. As such, the main constituents and environmental factors that affect the third body layer will be discussed, before moving on to a more detailed explanation of the role that iron oxides may play in the layer.

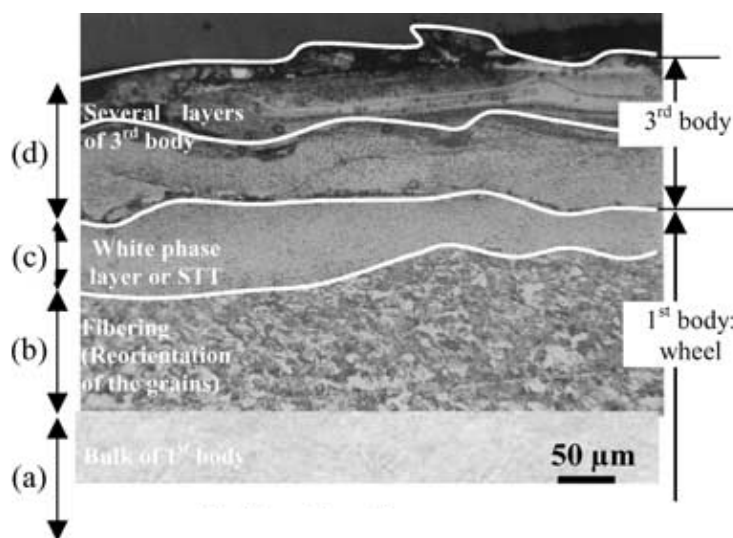


Figure 2.4: A cross section of used wheel, showing the third body layers on the surface [3]

Studies have been carried with the aim of better understanding the third body layer between wheel and rail, under both field and laboratory environments. Some key findings are described here. Perhaps most important of all is that the third body layer has been found to be between 15 and 100 μm thick [2]. The average roughness of wheel and rail vary throughout the working lifespan, but studies have shown it to be 10 μm when freshly ground and dropping to 1 μm within the first 2.5 days of traffic on one site, as shown in Figures 2.5 and 2.6 [12]. The third body layer is therefore often thicker than the combined roughness of wheel and rail and will play a direct role in the tribological effects in the contact patch.

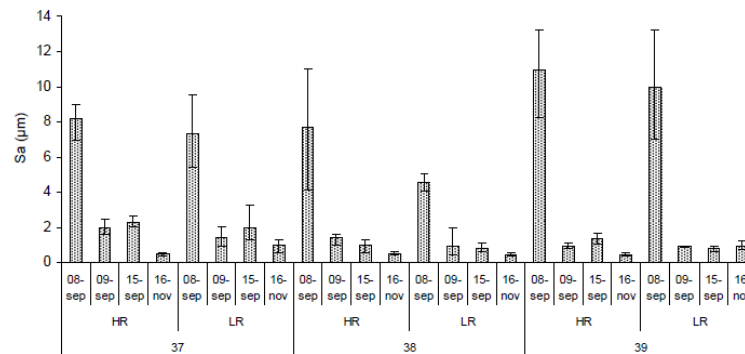


Figure 2.5: The change in rail roughness over time [12]

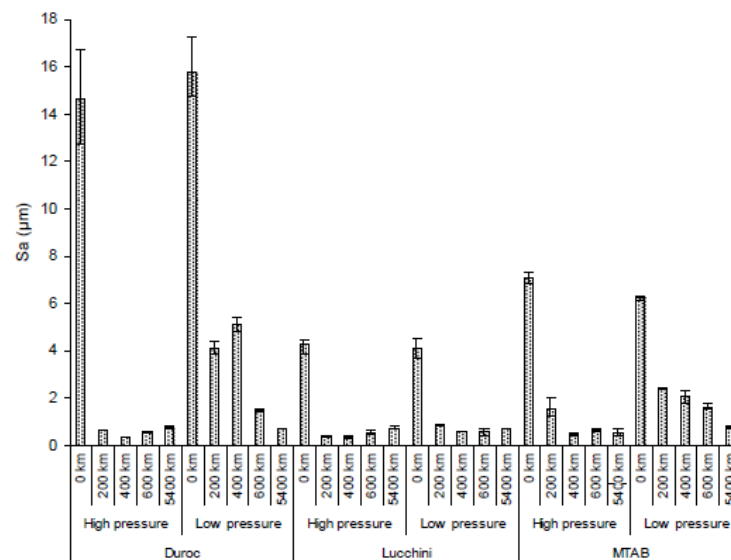


Figure 2.6: The change in wheel roughness over time [12]

2.2.3 Contact conditions

The physical characteristics of the contact patch such as load, speed and temperature will have a role in the behaviour of the third body layer, iron oxides and water. These are especially important when comparing small scale laboratory based testing to real world examples so that any similarities and differences can be examined.

The load on an axle varies between vehicles, with small metro vehicles having an axle load as low as 90 kN [13] and a freight axle having loads up to 300 kN [14]. There are three regions of contact between wheel and rail as shown in Figure 2.7. Each will produce different forces, contact patch sizes and contact pressures. *Region A*, the rail head and wheel tread is where contact most often occurs on straight track or large radius curves and produces the minimum contact stresses. *Region B*, between wheel flange and rail gauge, occurs during tight radius curves and produces high contact stresses. *Region C*, the field side, does not occur often but also produces high stresses. *Region A*, the wheel and rail tread, is most likely to occur during low traction on straight rail so this will be focussed on in this work.

Typical contact pressures between wheel tread and the railhead is 900-1500 MPa, but this can vary due to the dynamic forces at high speeds. A passenger locomotive is likely to be at the lower end of this range whilst a heavy freight vehicle will be at the upper end. The contact pressure will vary depending on which area of the wheel and rail are contacting, as seen in Figure 2.8 [14].

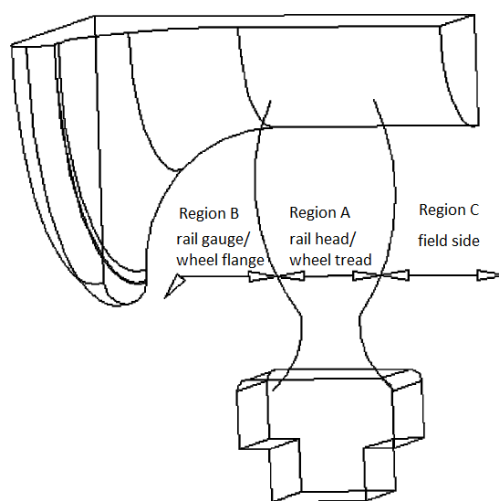


Figure 2.7: Wheel-rail contact regions [14]

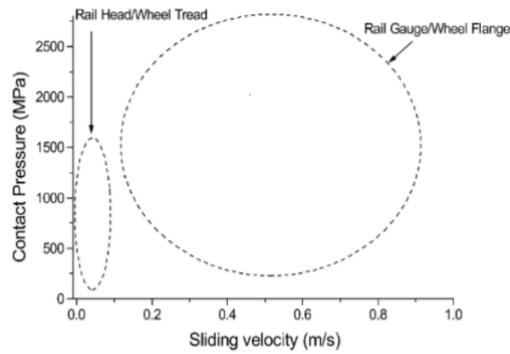


Figure 2.8: Contact pressure dependence on velocity, for various wheel-rail contact situations [15]

2.3 Effects of Iron Oxides on the Wheel-Rail Contact

2.3.1 Formation and transformations

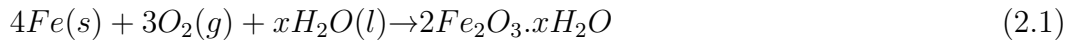
There are fifteen types of iron oxide which differ in composition, the valence of Fe and crystal structure. After analysis using in situ X-ray diffraction spectroscopy (XRD), only five have been found to form under the environmental conditions found on rail track [16]. These can either form on top and attached to the bulk surface of the railhead, or from wear particles which have detached from the main bulk.

These can be split into two groups, the oxides magnetite (Fe_3O_4) and hematite (Fe_2O_3), along with the oxyhydroxides goethite ($\alpha\text{-FeOOH}$), lepidocrocite ($\gamma\text{-FeOOH}$) and akaganeite ($\beta\text{-FeOOH-Cl}$). The hydrated oxides are known as rust and can only form in the presence of water and oxygen. Wustite (FeO) was not found in the previously mentioned study, but has been included because it can be formed at temperatures above $600\text{ }^\circ\text{C}$, which may be possible under wheel slip conditions [17]. Oxides can be formed under atmospheric conditions on the rail, but will also form in the wheel-rail contact patch. Oxides in the interface could either enter as a contaminant, be already present on the substrate, or be formed in the contact under heat and pressure. The properties of individual oxides are noted in Table 2.2.

Iron oxides on rails can be formed by electrochemical corrosion which involves the oxidation of iron metal by an oxidising agent [19], usually oxygen, under an aqueous layer which acts as an electrolyte. In wet conditions or at a high relative humidity, water will cover the rail-atmosphere interface which acts as an electrolyte, with the amount of available water acting as the rate controlling factor. The electrochemical corrosion of iron is shown in (2.1) Electrochemical corrosion occurs via a redox mechanism (2.2) with iron metal first oxidised to Fe^{2+} ions. Oxygen is reduced in the second half reaction (2.3)

Name	Formula	Colour	Magnetic
Hematite	Fe ₂ O ₃	Red	No
Magnetite	Fe ₃ O ₄	Black	Yes
Goethite	α-FeOOH	Yellow-brown	No
Lepidocrocite	γ -FeOOH	Orange	No
Akaganeite	β-FeOOH-Cl	Yellow-brown	Ni
Wustite	FeO	Black	No

Table 2.2: Properties of iron oxides found in the wheel-rail contact [18]



Fe²⁺ precipitates as Fe(OH)₂, a thin and insoluble layer that can passivate the metal against further attack. The loose and powdery layers of hydrated iron oxide or “rust” typical of atmospheric corrosion are formed when Fe²⁺ is oxidised further in the presence of OH⁻ to Fe³⁺, precipitating into a number of hydrated iron oxides, Fe₂O₃·xH₂O. The products of electrochemical corrosion under different conditions are shown in Table 2.3.

Type of corrosion	Conditions	Composition of oxide
Electrochemical	Oxygenated water	Gt, Lp
Electrochemical	Sea water	Mt, Lp, Gt, Ak
Electrochemical	High SO ₂	Mostly Gt
Electrochemical	High Cl ⁻	Mostly Ak
Thermal	Air (room temperature)	Mt
Thermal	Air, 250-550 °C	Mt, Hm
Thermal	Air, 600 °C	Wu, Mt, Hm

Table 2.3: The likely composition of oxide layers under different conditions. Gt: goethite ; Lp: lepidocrocite ; Ak: akaganeite ; Hm: hematite ; Mt: magnetite ; Wu: wustite [20]

An oxide layer can be formed without water via thermal corrosion, with the reaction occurring in the oxide rather than the electrolyte and oxygen concentration acting

as the limiting factor. This oxide is rapidly formed on clean metal as a coherent film, which acts as a barrier to oxygen and the reaction rate subsequently falls. At room temperatures the oxide produced is only approximately 0.1 nm thick, but a thicker layer is formed as temperatures are elevated. Magnetite is found as an invisible thin film at normal temperatures, with film thickness increasing as temperatures rise [20].

The alternating wet and dry cycles that are common under atmospheric conditions result in cyclic composition changes of the rust, breaking up the morphology and preventing adhesion to the metal underneath. Magnetite is often found at the steel/oxide interface and lepidocrocite or goethite on top. Magnetite and lepidocrocite often occur when there are large amounts of Fe(II) ions present. Goethite is particularly thermodynamically stable so is often produced from transformation of another oxide. Lepidocrocite often transforms into goethite, but also into magnetite if there is a large amount of Fe(II) available [20].

Transformations between oxides can occur via two mechanisms. The atoms in the solid crystal structure can rearrange under heat or pressure which is known as topotactic transformation and may occur under wheel slippage. One of the most likely transformations that could occur via this mechanism would be the dehydroxylation of FeOOH polymorphs to form their anhydrous counterparts [21], occurring at 140-500 °C. The other rearrangement mechanism is reconstructive, occurring when an oxide is dissolved in a solvent and then precipitates out of solution as a new structure. Little literature is available regarding transformations on the railhead which may affect oxide analysis, but possible transformations are shown below in Table 2.4 [20].

Precursor	Product	Type of transformation
Goethite	Hematite	Topotactic, Thermal dehydroxylation
Goethite	Magnetite	Reconstructive, Hydrothermal dehydroxylation
Lepidocrocite	Hematite	Thermal dehydroxylation
Lepidocrocite	Magnetite, Goethite	Reconstructive, in alkaline solution
Akaganeite	Hematite	Thermal dehydroxylation
Akaganeite	Goethite	Reconstructive, in alkaline solution
Akaganeite	Hematite	Reconstructive, in acid solution
Magnetite	Hematite	Oxidation in air
Wustite	Magnetite	Disproportionation in air

Table 2.4: The possible transformations of iron oxides found in the wheel-rail contact [20]

Oxide formation can be analysed by creating artificial environments for them to grow in; controlling factors such as humidity, salinity and wear to produce different oxides and compositions. Small differences in preparative conditions can greatly affect the properties of the oxide, such as surface area and crystal morphology.

Uniform corrosion occurs on smooth metal surfaces with minimal defects which means the entire steel surface will corrode at a uniform rate. Pitting corrosion occurs when the passive oxide layer is weakened by a defect or where individual water droplets are located, resulting in localised corrosion. This local corrosion creates small pits where the oxygen concentration is lower at the base of the pit, destabilising the passive oxide film and increasing corrosion. The rate of pitting corrosion can be increased when chloride ions are present.

The study of the influence of atmospheric gases such as sulphur dioxide on oxide formation has been limited so far but a study was recently carried out [22]. In an atmosphere containing high levels of sulphur dioxide, the gas can react with iron to form FeSO_4 , which is oxidised to form iron oxide. SO_4^{2-} is released during the oxidation which acidifies, corroding the iron and repeating the process. SO_2 has been found to increase the formation of iron oxide and over time transform other oxides into goethite [22].

2.3.2 Effects of oxides on the wheel-rail contact

The wheel-rail contact is open to the elements and therefore undergoes repeated wetting and drying cycles under working conditions. This leads to electrochemical corrosion of the iron contained in both the rail and the wheel. Oxide layers will form on the steel surface, some may remain intact during contact, but others will be removed as wear particles. Under dry conditions there has been shown to be little difference between the adhesion coefficients of oxidised and non-oxidised railhead [4], probably due to the speed at which the oxidised layer is removed as a train passes. When both water and oxide are present, levels of adhesion drop and stay low, possibly because the water prevents the high rates of wear on oxides that occurs on dry rails. When oxide wear particles are removed they form a third body layer, a solid interfacial layer in the wheel-rail contact. It is always present to some extent and contains a significant proportion of oxides along with wear debris and outside contaminants; a cross-section of this layer is shown in Figure 2.9 [2].

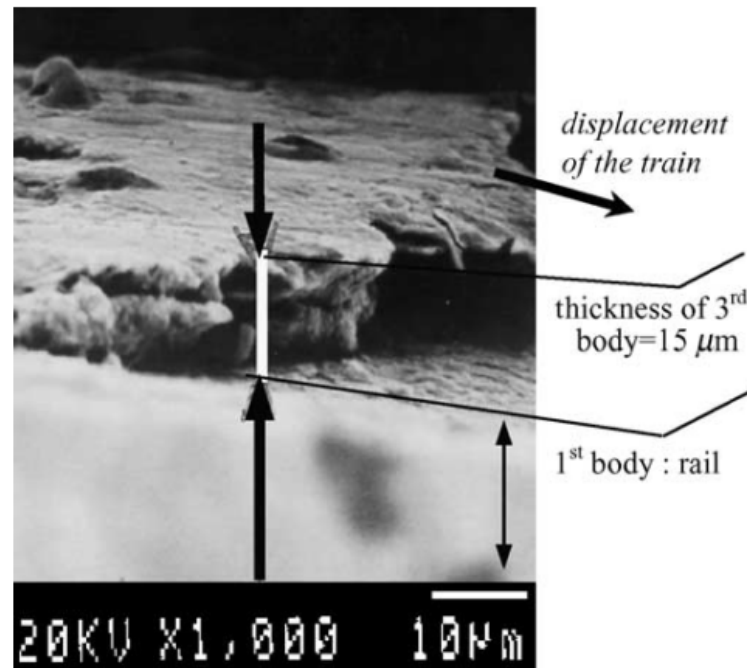


Figure 2.9: Metallographic cross section of a rail and third body layer [2]

Sliding in the wheel-rail contact, which would occur if a wheel slips, produces oxidised steel debris as a powder, some of which is compacted onto the clean metal surface by the sliding force. Here it mixes with other metallic debris which helps to break up the particles over time, creating a larger surface area and eventually forming particles which are completely oxidised. These can be agglomerated and compacted by the sliding force to form a glaze, or remain particulate in the contact and cause three body abrasive wear. The rheological properties of the third body layer were tested by Berthier et al. [3][23], who deposited heaps of aluminium powder on the railhead before repeated train passes in order to analyse whether a third body layer could affect the wheel-rail interface or simply be swept of the track.

After multiple train passes it was found that the aluminium layer was first compacted and then spread along the track by the passing of each wheel, with the properties of the powder changed by the heat and pressure of the wheel-rail contact and the absorption of other third body contaminants such as oil as the powder was transported along the railhead. In the study, a fragment of ballast with a volume of 1 cm^3 was transported 150 m after the passage of 20 wheels, with the particles crushed and becoming smaller with each successive wheelset and hardened into a compressed layer on the railhead due to heat and pressure.

The moving wheel-rail contact creates a dynamic third body layer which can be simplified into two particle flows. An external flow involves the passage of the third body into and out of the contact but there is also an internal flow of the third body within the contact itself. A schematic diagram of this is shown in Figure 2.10.

Oxides could either enter as an external flow (EF) or be formed in the contact during the internal flow (IF).



Figure 2.10: The third body flow, external flow (EF) and internal flow (IF)

Although the particles did not contain iron oxides, low adhesion problems occur on roads when the first rains fall after long dry spells. Particles such as soil and tyre debris build up on the road surface under dry conditions but are washed away after rainfall. Work has shown that adhesion levels are reduced when a longer dry period is followed by rainfall, rather than a shorter dry period [24]. A similar mechanism may occur on the rail where third body debris is built up after a dry period so it is important to analyse oxidised wear particles and other detached contaminants, as well as the iron oxide layers that are bonded to the railhead or wheel.

Beagley [25] reported that the lowest friction coefficient was found when a paste was formed from iron oxide and wear debris, mixed with low quantities of water. The results for various contaminant types are shown in Table 2.5. The results are taken from a high pressure torsion test rig under a realistic $5 \times 10^4 \text{ N}$ contact pressure but the test rig is purely sliding and slow speed, therefore very different from the wheel-rail contact.

Material	Coefficient of friction under 10^5 N load
Precipitated Fe_2O_3	0.2
Fe_2O_3 + 7.5 % oil	0.08
Leaf Debris	0.05
Fe_2O_3 / H_2O	4.4×10^{-4}

Table 2.5: Properties of rail contaminants, tested by Beagley [25]

Pin-on-disc results using a number of temperature and humidity values are shown in Figure 2.11. Test specimens are shown in Figure 2.12. G0 is a clean sample whilst G2 is lightly oxidised to form a speckled coating [26]. Higher humidity appears to lower the friction coefficient up to a relative humidity of around 67%, the friction coefficient then stays level after this point. Other methods of measuring the friction coefficient are shown in Table 2.6.

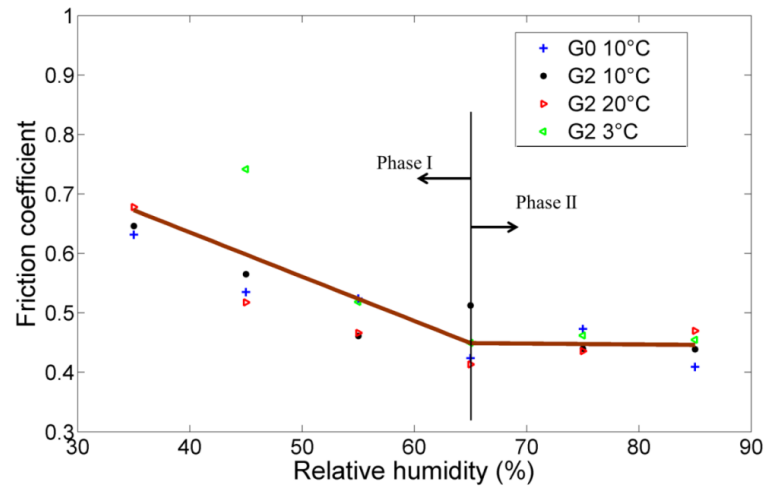


Figure 2.11: The variation of friction coefficient with humidity using oxidised samples [26]



Figure 2.12: Oxidised rail discs; G0 (left), G1 (middle), G2 (right) [26]

Reference	[26]	[27]	[4]	[25]	[28]
Test Method	pin-on-disc	Pendulum	Twin disc	Sliding ball, rolling disc tribometer	Twin disc
Test Variables	Pre oxidised, temperature, humidity	Water, oil, leaf residue, friction modifiers	Salt, moisture, pre oxidised	Oil type, humidity	Dry, Wet, slip ratio, thick and thin oxide
Friction coefficient	0.2-0.8	0.01-0.8	0.04-0.25	0.03-0.6	0.14-0.67
Other analysis	SEM, Raman, XRD				XRD, EDX

Table 2.6: Test methods used to obtain railhead friction coefficients

An RSSB project, T1077 [29], was conducted in order to investigate the effects of water on adhesion levels in the wheel-rail contact, aiming to develop a model that would be able to predict adhesion levels under different moisture conditions. Different amounts of water were applied dropwise to a full scale wheel-rail rig in order to produce a creep curve for each condition. The results in Figure 2.13 show that under very low levels of moisture the adhesion coefficient reaches a very low value for a long period of time. During this very low adhesion a band of wear particles, which likely contains high levels of iron oxides, is seen in the contact. The iron oxide here seems to be formed in the contact itself rather than entering from external sources as no intentional pre-oxidation was carried out, as seen in Figure 2.14.

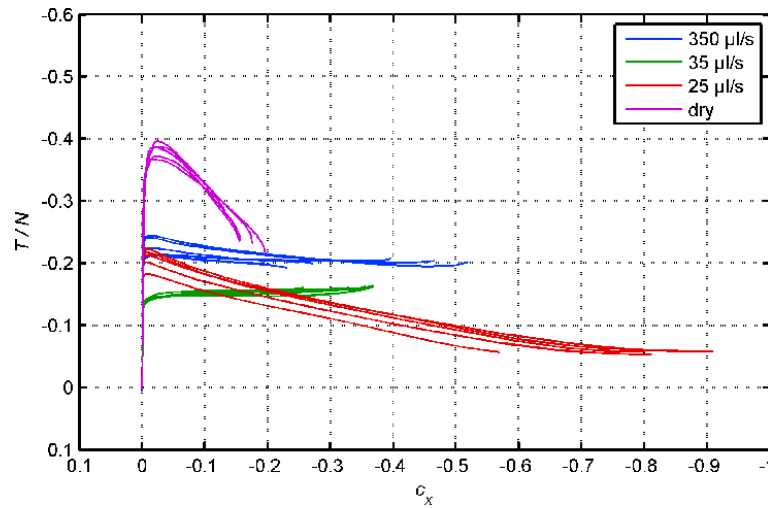


Figure 2.13: Creep curves from water droplet tests showing variation of water rate at fixed load and speed [29]

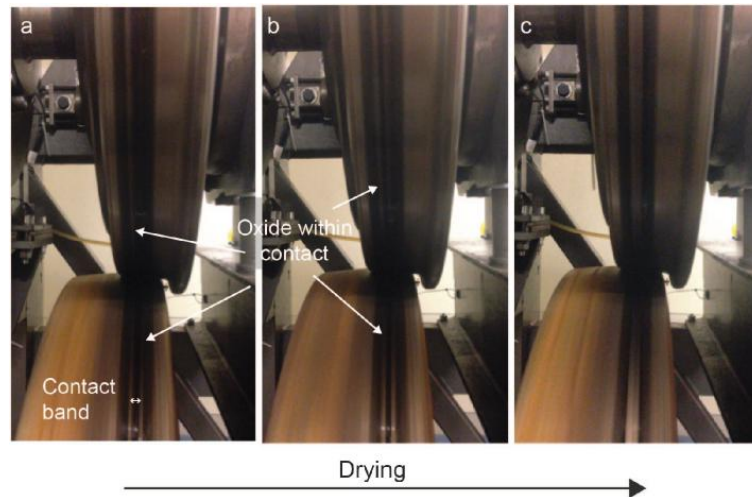


Figure 2.14: Images showing the visible oxide layer in the contact band during full scale testing [29]

Pre-oxidation is often necessary in order to study the oxide layers. This can be achieved in an environment chamber where the temperature and humidity can be adjusted. An example of an oxidation procedure [16] is to keep the temperature constant and alternate between a high humidity of 95% and a low humidity of 28% over 40 hours, shown in Table 2.7.

	Thick oxides (Five Cycles)	Thin Oxides (Five Cycles)
Step 1	Exposure in air for 0.5 h at 40 °C and relative humidity (RH) >90%	Exposure in air for 2 h at 40 °C and RH > 90%
Step 2	Exposure in air for 0.5 h with 1% NaCl solution spray at 40 °C and RH >90%	Exposure in air for 6 h at 40 °C and RH < 30%
Step 3	Exposure in air for 1 h at 40 °C and RH > 90%	-
Step 4	Exposure in air for 6 h at 40 °C and RH < 30%	-

Table 2.7: A method of oxidising the sample [26]

Spraying water on the railhead and leaving for a period of time is effective and a NaCl solution can also be used to promote more rapid oxidation where thick layers are necessary. An ultrasonic humidifier has been used to produce oxides for analysis on railhead samples, shown in Figure 2.15. The thickness of the produced oxide layer may vary as well as the coverage, sometimes forming as a uniform layer over the rail surface but sometimes forming in much more localised patches. It is unknown whether these different methods form different oxide layer compositions.

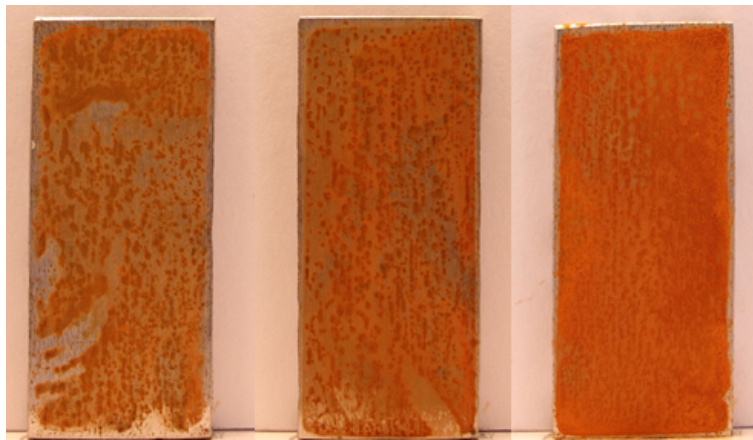


Figure 2.15: Unpublished work by L Buckley Johnstone showing oxide formed over 4 hours using an ultrasonic humidifier: Left (1 hour) ; Centre (2 hours) ; Right (4 hours). The steel specimens had a width of 19 mm and a height of 50 mm

The influence of chloride ions on adhesion and corrosion has been investigated [4]. Chloride ions can be present due to marine environments or carried onto the track from road crossings when salt is used on roads during icy conditions. They can cause

pitting in the steel surface which causes the destructive pitting corrosion to occur. More ions result in water on the iron surface acting as a better electrolyte which speeds up oxidation. The results, shown in Table 2.8, showed that the adhesion coefficient was significantly reduced under wet conditions when an oxide layer was present during twin disc testing. The low adhesion also lasted longer than when a dry oxide was used, with the water acting as a lubricant to prevent the oxide being removed. Scanning electron microscopy, SEM, showed that the oxidised surface was smoother than the clean surface.

Condition	Dry (no oxide)	Dry (oxidised)	Wet (no oxide)	Wet (oxidised)	Oil
Traction Coefficient	0.22	0.23	0.18	0.03	0.02

Table 2.8: The effect of oxidisation on the traction coefficient [4]

Magnetite is very hard and forms a protective layer on the bare steel surface under oxygen rich conditions. This effectively reduces abrasive wear although oxidative wear still occurs [26]. Aside from this early work there has been very little research into the tribological properties of specific oxides, which may play a part in low adhesion events. The low adhesion due to akaganeite was found to be an issue in Japan's Kita-Kyushu tunnel [30], where a thin layer of oxide formed in the chlorine rich conditions. The ascending slopes meant a large driving force was applied through the wheels, amplifying the problem. The paper established that a method of avoiding this could be the introduction of a new type of steel to be used around problem areas. Pearlitic steel is commonly used, but its high carbon content of around 0.6% means it is more susceptible to corrosion. The corrosion resistance of bainitic steel, an alternative rail steel microstructure, in comparison to the pearlitic microstructure has been researched [31]. Similar corrosion rates were seen between the two types of steel but the frictional properties of the different microstructures of oxidised steel could be further explored.

Wear between two or more surfaces will occur in the wheel-rail contact, causing surface damage and material loss. The contact is subjected to a number of wear mechanisms but only oxidative wear is relevant to this review, a mild mechanism that creates a smoother surface after wear takes place. Oxidative wear occurs when the oxidised surface layer reaches a critical point, between 1-3 μm . The oxide layer is removed as platelets and the metal underneath will then oxidise, before being worn away again [32]. These oxide wear particles may remain in the contact and cause adhesion loss, a possible mechanism for oxide entering the contact as wear particles. Oxides on the gauge corner are more quickly removed than on the top of the rail. This leads to varying oxide compositions on different sites of the railhead, with goethite being found on top and magnetite at the gauge corner [16].

Zhu and Olofsson [26] used a pin-on-disc tribometer in order to assess the differ-

ences in wear rates in the wheel-rail contact between oxidised and non-oxidised disk samples. A normal force was applied to a pin which can be pushed into contact with a rotating disc. It was found that oxidised samples at high humidity generally had a lower wear rate than clean samples under the same conditions. The highest wear rates on both samples were found at the lowest tested temperature and humidity, 3 °C and 40%. At higher temperatures and humidity oxides were formed on the clean disks during testing, the oxide layer was hypothesised as protecting the sample from severe wear. This protection did not occur at 3 °C, even at high humidity. The majority of the wear on pre oxidised disks was severe due to removed oxide acting as a third body layer, but became milder with increased humidity.

Figure 2.16 shows the worn surfaces of pins after a tribometer test at 900 MPa and 0.01 ms⁻¹, wear is more severe at a lower temperature. Figure 2.17 shows an optical microscopy image of the oxide wear debris after each test, with lower temperatures resulting in small oxide fragments.

With large amounts of water such as heavy rain, the third body layer forms a slurry and is removed from the track when the wheels pass. However, when smaller amounts of water mixes with the oxides and other wear debris it can form a viscous low shear strength paste [33] which remains on the wear band and lubricates the contact.

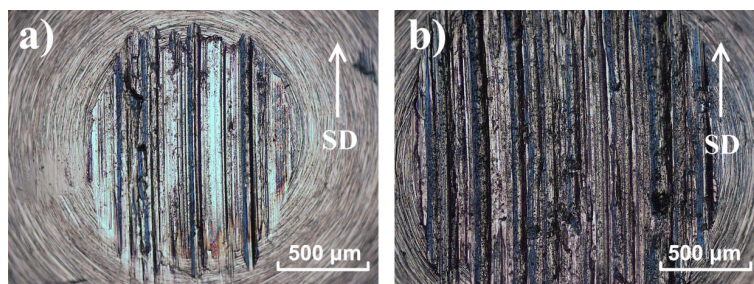


Figure 2.16: Worn surfaces of the pins after tested at a) 3 °C and b) -15 °C [26]

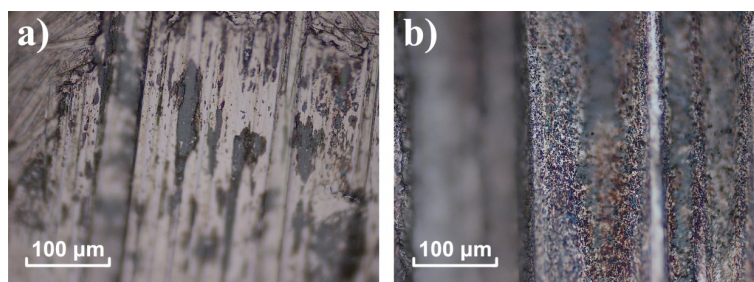


Figure 2.17: Morphologies of the oxides generated on the pin surfaces tested at a) 3 °C and b) -15 °C [26]

2.3.3 Oxide analysis

A number of methods can be used to analyse iron oxide layers, Table 2.9 lists the previously used methods.

Name	Capabilities	Previous use
Colour chart	Can distinguish pure oxides. Issues if mixed oxide layer formed or varying colour with thickness. Very easy to use.	-
X-Ray diffraction (XRD)	Powerful technique to distinguish oxide type and unknown compounds. Quantity, unit cell parameters and crystallinity can be obtained. Penetration depth varies between material and spectrometer but approximately 100 μm .	[16][28][26]
Energy dispersive x-ray (EDX)	Gives elemental information when paired with an SEM, can determine if oxide is present. Penetration depth approximately 1 μm .	[16][4][34]
Scanning electron microscopy (SEM)	Secondary electron shows morphology. Backscatter can show atomic density, able to show an oxide layer exists but cannot characterise.	[26]
Infrared (FTIR)	Distinguish type, crystal morphology, degree of crystallinity, extent of Al substitution. Would be very hard to distinguish oxide types in a mixture. Penetration depth from 0.5-5 μm .	[31][35]
UV-vis	Simple to use but variations in results limits the suitability for identification in absorbance mode.	[36]
X-Ray photoelectron (XPS)	Measure elemental composition. Penetration depth approximately 2 μm .	[37]
Raman	Complementary to IR. Water peak not seen. Penetration depth varies with instrument but approximately 1 μm .	[26][35]
Auger electron	Able to measure the depth of an oxide layer using sputter. Penetration depth approximately 2 μm .	[35]
Glow discharge (GDOES)	Bulk and depth analysis. Can also be paired with mass spec. Penetration depth approximately 100 μm .	[37, 38, 39, 40]

Table 2.9: Iron oxide analysis methods

Each oxide has its own distinct colour and can be identified, if present alone, using a colour chart. This technique is not so useful when mixtures of oxides are present

due to the change in colour. Optical microscopy is useful for assessing wear scars and basic oxide formations, but does not have the resolution for analysing small oxide particles. SEM can be used to view the crystal structures of each oxide, with each having distinct morphological features. Figure 2.18 shows an SEM image of an oxide layer on steel. Multiple types of oxide can often be found together. Layer type structures form when there is a chemical gradient, with the Fe (II) oxides often found on the inner layer. The varying composition means that more advanced analysis is often needed to distinguish oxide types. Figures 2.19 to 2.22 show unpublished work by Olofsson using SEM and optical microscopy on oxide flakes generated using pin-on-disc testing.

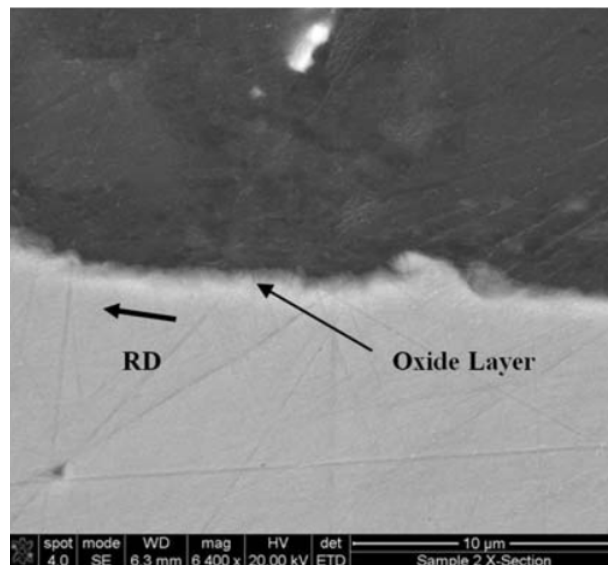


Figure 2.18: SEM image of an oxide layer on steel [4]

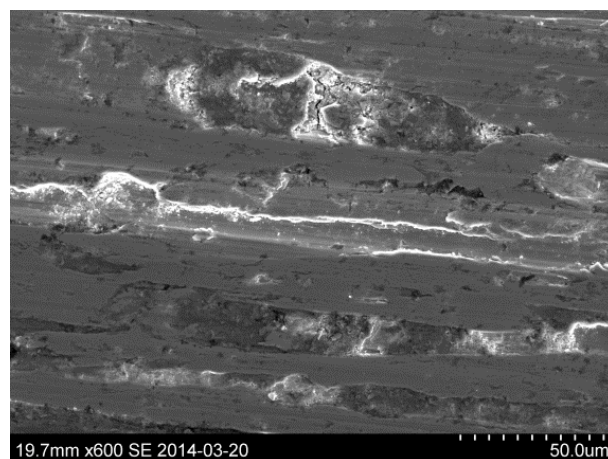


Figure 2.19: Secondary electron SEM images of an oxide flake, showing the morphology of the flake. The brighter regions are in the foreground



Figure 2.20: Backscattered electron SEM images of an oxide flake which shows atomic density. The oxide flake contains a higher percentage of oxygen which has a lower atomic number than iron, therefore showing up as a darker region on the image

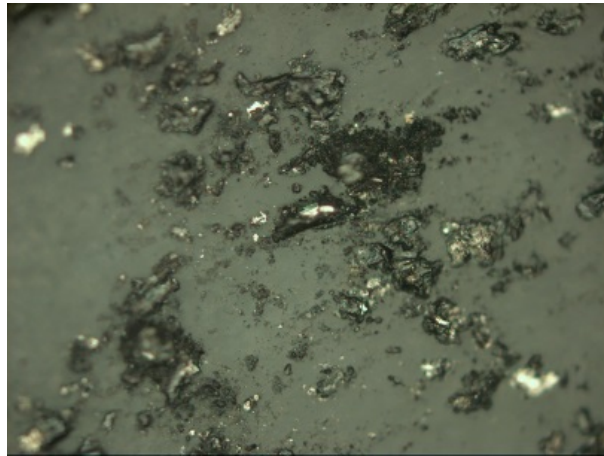


Figure 2.21: Optical microscopy of wear debris that appears to be the black oxide, magnetite



Figure 2.22: Optical microscopy of wear debris that appears to be the red oxide, hematite

Fourier transform infrared spectroscopy (FTIR) is a quick and useful technique, able to detect very low concentrations of chemicals. It is useful when there are trace amounts of different oxides in the bulk (for example traces of goethite in hematite), or when impurities have arisen. Infrared spectrums of common oxide varieties vary in the region between 400 cm^{-1} and 1000 cm^{-1} and can be used to distinguish between oxide types, shown in Figure 2.23. The technique has been used previously to study oxide formation on novel steel types [31]. Raman spectroscopy uses a similar principle, but has the advantage of being unable to resolve any water present in the sample.

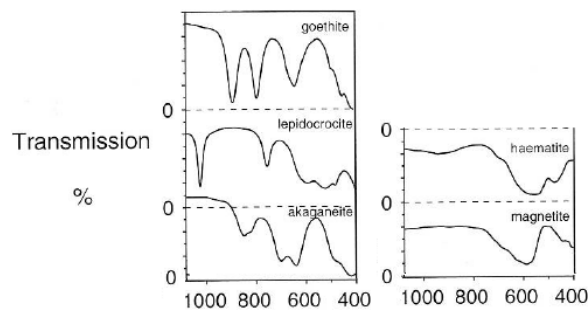


Figure 2.23: $400\text{-}1000\text{ cm}^{-1}$ IR spectrum of common oxide layers [20]

The lack of portable spectroscopic equipment often means that oxides found on the rail need to be transported to a laboratory for analysis. This creates some limitations, most notably the fact that the layer of oxide may change composition throughout the day, affected by factors such as heat and moisture.

In-situ spectroscopy can overcome these problems, but is currently limited by the small number of portable instruments. Suzumura and Sone [16] have started to

tackle this problem by adapting a portable X-ray diffraction fluorescence (XRDF) spectrometer so that it can be used on the railhead. The results were positive, with spectroscopic measurements showing how the oxide layers changed conformation with time under differing conditions and different numbers of train passings. As expected, akaganeite was found when oxide formed under saline conditions. Unfortunately this method of spectroscopy still takes a considerable amount of time to analyse a sample, by which time the oxide composition may have changed. The study noted the difference in oxide composition between a mountainous and marine rail site, which highlights the importance of surrounding conditions when assessing low adhesion. It was also concluded that akaganeite provided the low friction characteristics associated with oxides whilst other FeOOH conformations actually increased adhesion. Track was oxidised using harsh conditions over relatively long time periods which may be more relevant to the mountain tunnel mentioned in the literature, rather than the milder conditions and short time intervals between trains that are often found in the UK. The XRDF spectrometer used could not analyse the thin layer of oxide found on the mildly oxidised samples.

One of the most reliable analytic techniques is X-ray Diffraction, XRD. This technique can analyse the distinctive crystalline structure of each iron oxide, alongside structural properties and the degree of isomorphous substitution. Oxides are often removed and ground into a fine powder before XRD spectroscopy [22, 26]. Olofsson and Zhu [26] used XRD to establish the oxide composition on both lightly and heavily oxidised samples. No oxides were found on the less oxidised sample which highlights one of the limitations of this technique. A sample area of approximately 1 mm^2 is needed to direct the beam onto and XRD cannot be used on very thin films so may only be useful on more heavily oxidised samples.

Energy dispersive X-ray, EDX, is a technique that has been used previously. It involves directing a beam of charged particles at a sample to eject an electron. A higher energy electron will fill this hole and emits energy in the form of an X-ray which provides information about the elemental composition. When combined with SEM it can be used to find the thickness of an oxide layer.

Glow discharge optical emission spectroscopy, GD-OES, analyses chemical composition as a function of depth and can be used to establish the thickness of oxide layer as shown in Figure 2.24. The thickness of this layer could be obtained from the depth of the crossing point (D_0) of the iron and oxygen concentration curves. The depth of friction reducing layer over a number of months has been plotted by Zhu et al. [37] and shown in Figure 2.25, with rail samples being cut and replaced. Three samples were taken in October: a visibly uncontaminated sample; a sample with a visible leaf residue and a tarnished sample. The oxide layer was $0.28 \text{ }\mu\text{m}$ thick on the October tarnished sample and dropped considerably over all other months. It can be noted that even the seemingly uncontaminated sample contained an oxide layer. The thick oxide tarnished layer appeared to be produced after leaf contamination had reacted with the bulk material.

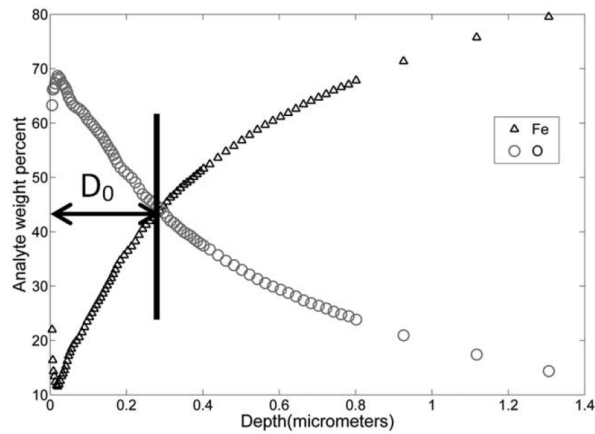


Figure 2.24: Iron and oxygen depth profile from ‘Ooctarnished’ sample. The crossing point (D_0) between the iron and oxygen contents is indicated [37]

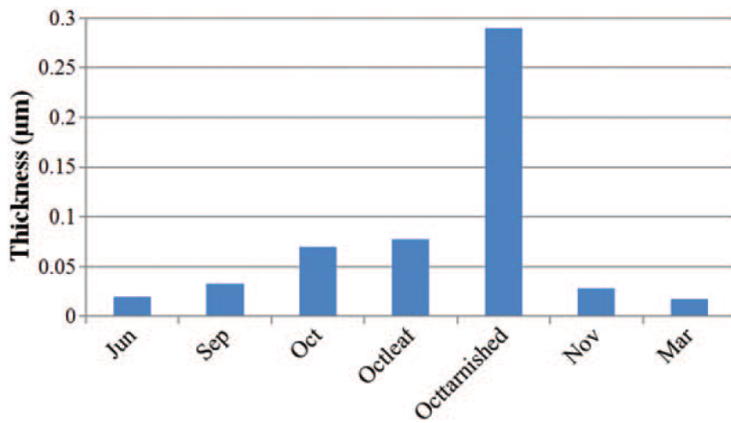


Figure 2.25: Thickness of superficial oxide sub layer over a number of months [37]

X-ray photoelectron spectroscopy (XPS) has previously been used for elemental analysis when looking at organic compounds in low adhesion related papers, shown in [41], but it may also be useful as a method to distinguish types of iron oxide in future. A study on distinguishing different types of iron oxides using XPS was carried out, but the study was not railway focussed [42].

2.4 Effects of Water on the Wheel-Rail Contact

2.4.1 Introduction

This section of the review covers the effect of water in the wheel rail contact, so that comparisons can be made between a water lubricated contact and a contact lubricated by a combination of water and oxide. It is important to remember that the railhead will always have some sort of third body layer so a contact with “pure” water will be unobtainable in the real wheel rail contact. The RSSB T1077 project [29] provides a number of review papers on the subject so this review will focus on those that are most relevant to this topic. The T1077 report concluded the following:

1. Water in combination with other contaminants (wear debris, iron oxides, leaves, etc.) creates liquids with significantly increased viscosity and as a result there may be significant hydro-dynamic effects.
2. Pure boundary lubrication between wheel and rail caused by pure water or water in combination with other contaminants (wear debris, iron oxides, leaves, etc.) resulting in significantly reduced adhesion.

The following section of this review will summarise the findings of the previous report and add some further relevant information. Without the presence of third body contamination, the factors effecting the wheel rail contact patch will be the physical characteristics of the wheel and rail, as well as the chemical characteristics of the water. Material types will not be analysed here so the main factors affecting wheel and rail are amount of water, roughness, temperature and speed.

Water will be present on the railhead due to either precipitation, condensation or artificially via human influence. As the wet-rail phenomenon will occur throughout the year, hail and snow will not be considered. Rain will fall onto the railhead and then be rolled over by a passing wheel, but the amount of water falling onto the railhead will vary with rain intensity and duration. Fog or mist will also wet the railhead surface with smaller volumes of water. It has been discussed previously that low volumes of water will contribute to the wet-rail phenomenon, wetting the third body layer to form a viscous paste whilst larger volumes of water may completely or partially wash the third body layer off the railhead or dilute the solids sufficiently that low adhesion does not occur.

2.4.2 Amount of water

It is hard to predict and quantify how much water will be found on the railhead, but the T1077 report [29] produced a table of the amount of water that is assumed to be on the railhead for a contact area of 100 mm², shown in Table 2.10. Water vapour will condense on the railhead when the rail temperature is cooler than the surrounding air temperature to leave a small amount of water on the railhead. The

volume of water that will condense onto the railhead will depend on temperature and humidity of the air as well as railhead temperature.

Rainfall (mm/hour)	Volume of rainfall in contact (mm ³ /hour)	Volume of rainfall in contact (mm ³ /minute)
0.1	10	0.17
0.2	20	0.33
0.3	30	0.50
0.4	40	0.67
0.5	50	0.83
1	100	1.7
2	200	3.3
4	400	6.7

Table 2.10: Amount of water assumed to be present on the railhead per wheel-rail contact area [29]

2.4.3 Contact conditions

Although the exact role of water has yet to be confirmed, viscosity changes may be key to understanding the wet-rail phenomenon and the viscosity of water will be affected by temperature and pressure. There has been work to show the flash point of steel during a sliding wheel rail contact and this heat will be conducted to some extent into the surrounding water if it is present in the contact during a wheel slide. Contact conditions may vary in temperature and pressure so it is important to understand how the viscosity of water varies with temperature and pressure. Figure 2.26 shows this dependence, which may play a role in the different change in traction coefficients seen during tests run at different temperatures.

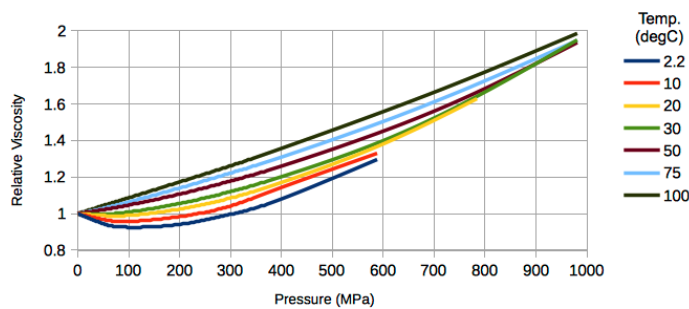


Figure 2.26: The change in water viscosity with temperature and pressure [43]

Experimental results were obtained using a mini traction machine to show the effects of roughness, temperature and speed on a water lubricated ball-on-flat contact [44]. Results, shown in Figures 2.27 and 2.28 show a decrease in traction coefficient in the smoother specimens. Lower temperatures also produced a lower traction coefficient on the rougher samples, with a less noticeable effect on smooth samples. An Ra of $0.15\ \mu\text{m}$ was used for the rough sample and an Ra of $0.01\ \mu\text{m}$ was used for the smooth sample, which is likely to be smoother than would be encountered in a real rail/wheel contact.

A similar trend was seen using a twin disc rig [45]. Discs were ground to three different roughness values and the discs contacted at 750 MPa. A large volume, 400 ml/min, of water was pumped into the contact at three different temperatures under high pressure to simulate very wet conditions. Experimental results are shown in Figures 2.29 and 2.30. The traction coefficients are all higher in this set of testing, although once again the lower temperature and smoother samples produced a lower traction coefficient. Speed effects were also explored, with a higher speed producing a lower traction coefficient.

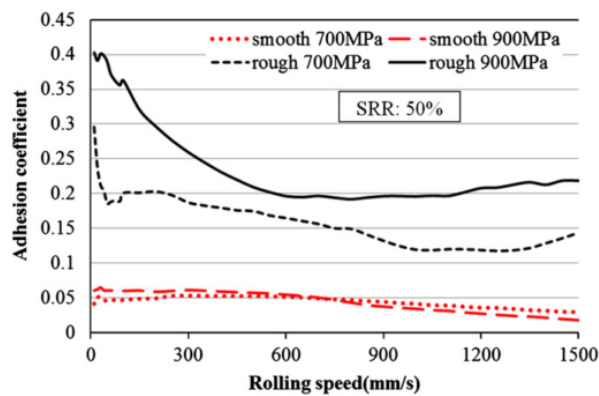


Figure 2.27: Adhesion coefficient plotted against rolling speed for smooth and rough surfaces, under wet conditions at different pressures [44]

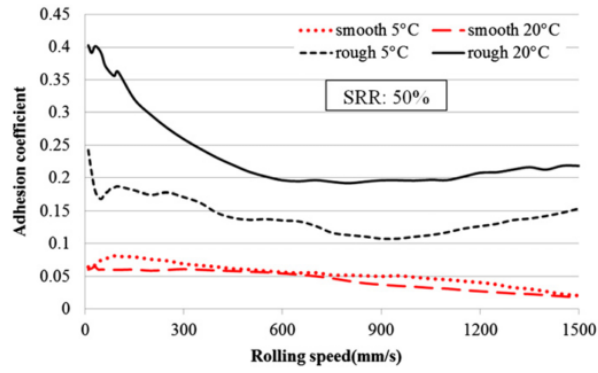


Figure 2.28: Adhesion coefficient plotted against rolling speed for smooth and rough surfaces, under wet conditions at different temperature [44]

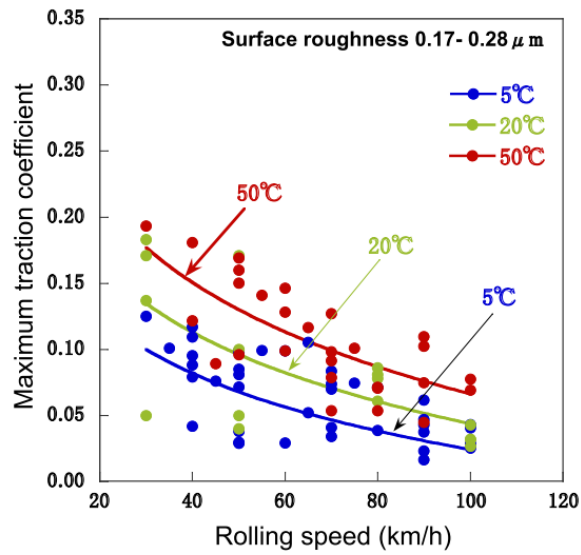


Figure 2.29: Traction coefficient change with rolling speed, at different temperatures [45]

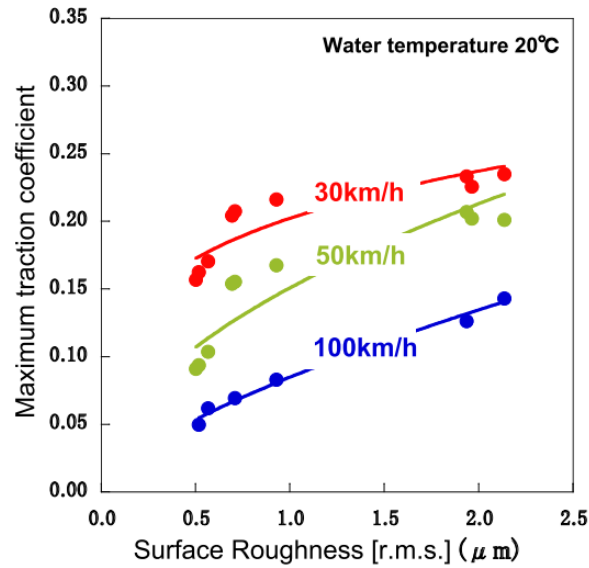


Figure 2.30: Traction coefficient change with surface roughness, at 30 km/h, 50 km/h and 100 km/h [45]

Chen et al. [46] have used a simplified line contact model that was created in (numerical analysis for the influence of water film) to create a model that describes the change in adhesion coefficient, using contact load, surface roughness and water temperature as input values. The models allow very high speeds to be looked at which could not be tested in small scale test rigs. The following graphs have been added to show the dependence of traction coefficient on the input parameters when pure water is used, with results shown in Figures 2.31, 2.32 and 2.33.

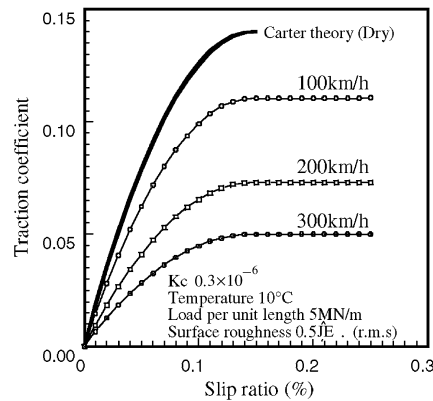


Figure 2.31: A graph showing the change in modelled traction coefficient at different speeds with increasing slip [46]

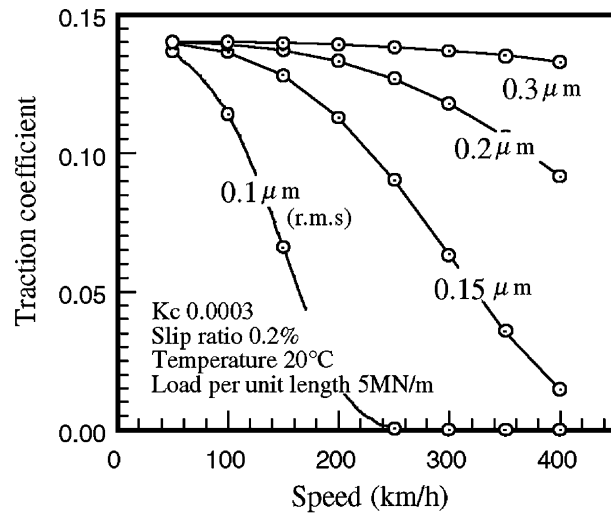


Figure 2.32: Modelled change in traction coefficient with speed for different roughnesses [46]

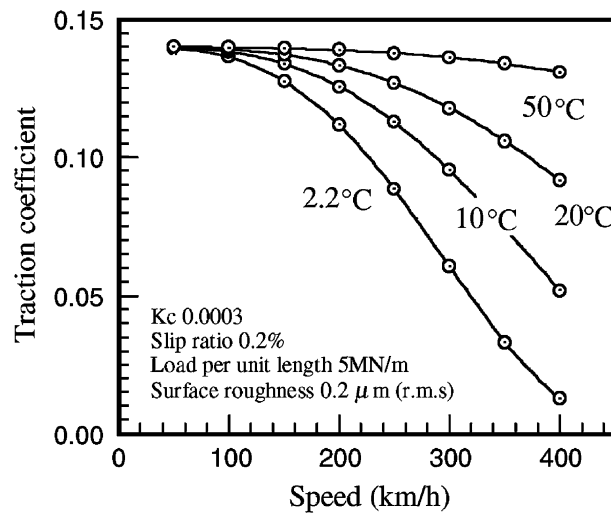


Figure 2.33: Modelled change in traction coefficient with speed at different temperatures [46]

2.5 Effects of Organic Contamination on the Wheel-Rail Contact

Although this review focuses primarily on the role of oxides in the wet-rail phenomenon, which occurs with no visible contamination, organic and specifically leaf contamination has been found as a layer that includes iron oxides. The hard, black organic layer is most commonly seen as the adhesion reducing leaf layer, made up from compacted leaf layers and well bonded to the steel substrate [1]. Previous analysis of Network Rail autumn data has shown that this leaf contamination has been associated with 50% of station overruns in the autumn period [5]. More station overruns, attributed to the wet-rail phenomenon, may be caused by either invisible contamination or contamination that has caused low adhesion, but has been removed by the slipping wheel before inspection. The main leaf fall season is from September to November with different trees shedding their leaves at different times [47], shown in Figure 2.34.

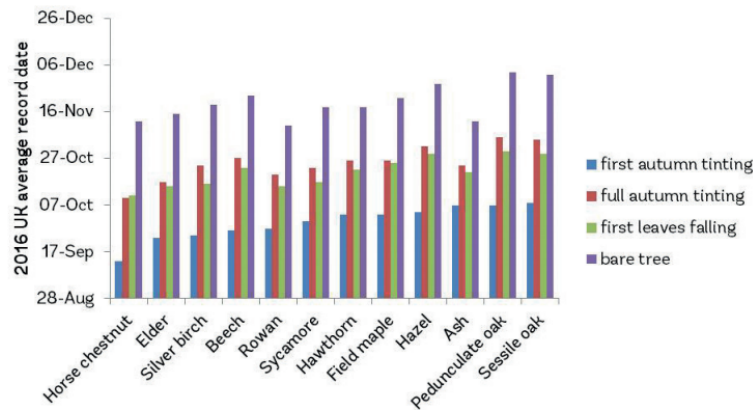


Figure 2.34: Leaf shedding times for UK trees [47]

Solid leaves have been used previously to produce low adhesion on small scale test rigs and have been well researched. The loss of adhesion when leaves are added to small scale test rigs are shown in Figure 2.35. Images of the leaf contaminated test specimens are shown in Figure 2.36.

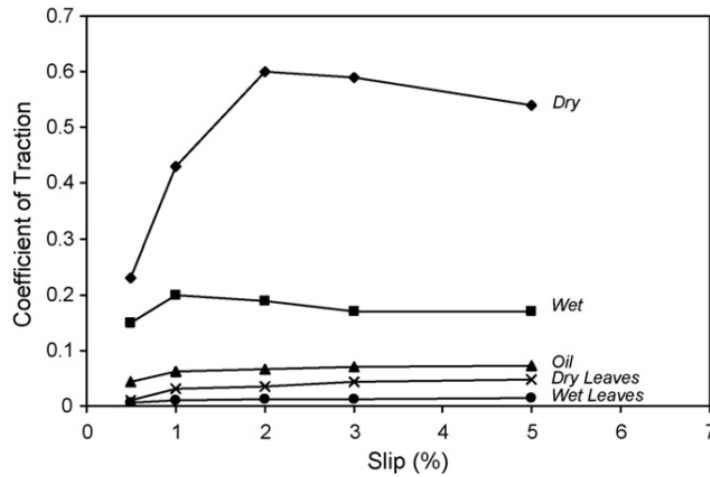


Figure 2.35: Leaf contamination in a twin disc test rig [10]

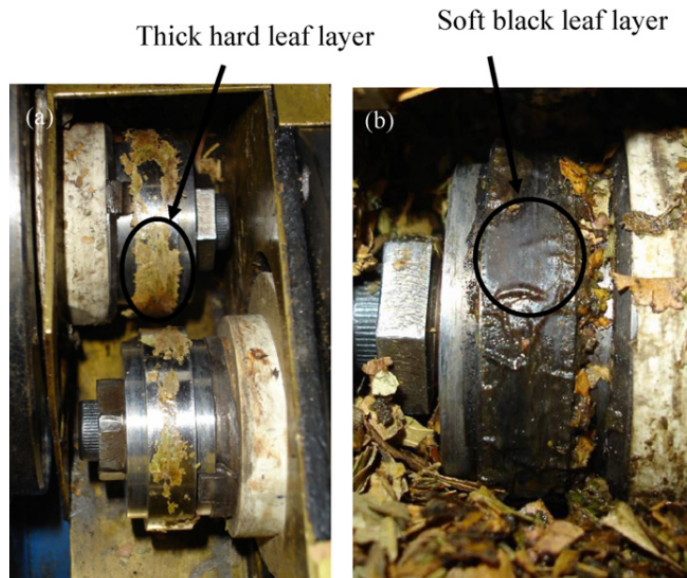


Figure 2.36: Images of the leaf contaminated discs after (a), a dry test and (b), a wet test [10]

The leaf contamination tested has often been thick and obvious layers that look similar to the black surface layers seen on rail so is unlikely to be linked to the wet-rail phenomenon. Water soluble leaf extract has been used which could be less obvious when on a railhead so may contribute to the wet-rail phenomenon[48].

The British Rail Tribotrain was a locomotive that collected adhesion data by applying its brake force linearly and measuring how much brake force was needed to achieve a wheelslide [49]. Data shown in Figure 2.37 shows adhesion loss, plotted

on modern software, when the train entered Kegworth cutting, a notorious area for low adhesion. Natural adhesion, with “dry” rails shows an adhesion drop to 0.1, but when the rails are sprayed with water the adhesion drops further to approximately 0.05. It is important to remember that although the conditions were thought to be dry, low levels of moisture may still be found on the railhead.

In comparison, outside the cutting the difference between the natural and artificially wetted rails is far less pronounced. The reasons for this could be that organic contamination had fallen onto the track due to the foliage in the cutting or that the more humid conditions that will form inside a cutting will cause a larger amount of iron oxide to be formed which produces the lower adhesion coefficient.

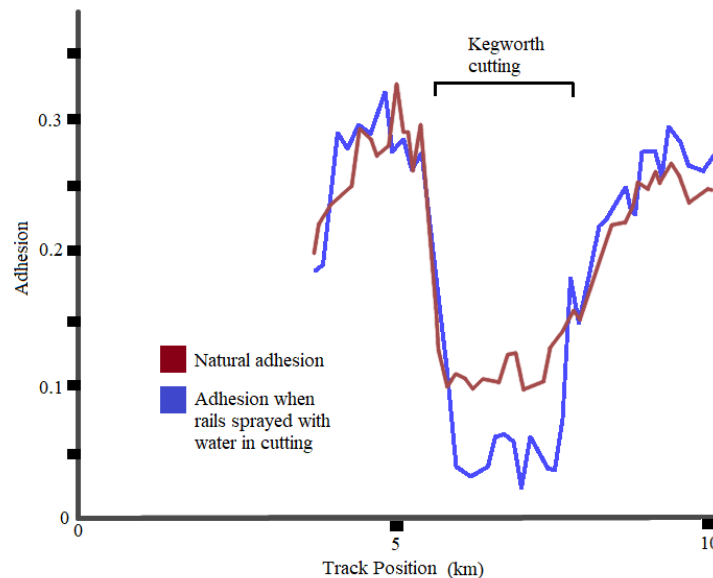


Figure 2.37: Adhesion loss when a train passes through a cutting, both in a natural state and when sprayed with water [49]

Adhesion data, collected from the same cutting after 18 hours of continuous rain, are shown in Figure 2.38. This led to an adhesion drop to 0.15. This is a higher traction coefficient than is seen in the “natural” state and much higher than when artificially wetted. This may be because the large amount of water falling onto the railhead over 18 hours washed away any contamination on the railhead. Alternatively a layer may remain but be covered by a film of water so low adhesion effects are not seen,

possibly due to a lower viscosity. After 24 hours of drying the adhesion is much lower again. Contamination has either returned, oxide has regrown or the water layer has decreased to allow the layer that caused low adhesion to be exposed once again.

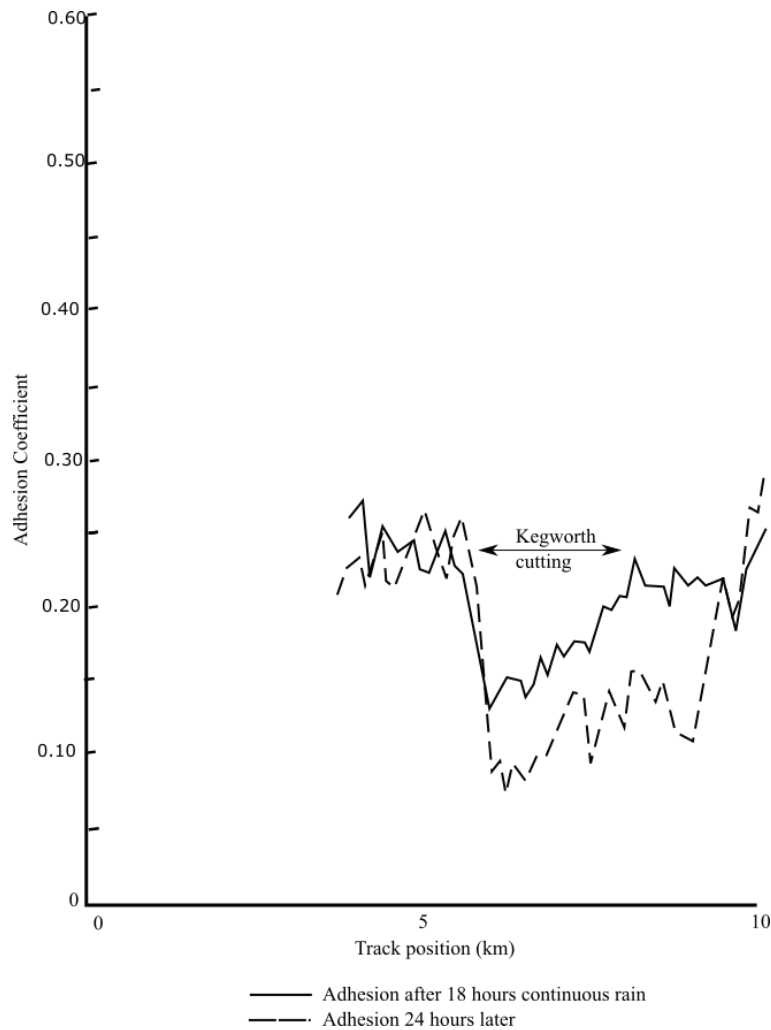


Figure 2.38: Adhesion loss in the Kegworth cutting straight after rainfall and then retested 24 hours after rainfall [49]

Tribotrain data was obtained for a longer stretch of track [49] and it was noted where tree locations were found, shown using double headed arrows in Figure 2.39. During early morning tests the adhesion drops to very low values near these trees, whilst the later test shows higher adhesion. The low adhesion data here is likely to be due to organic contamination under the trees, especially as leaves may be falling in November.

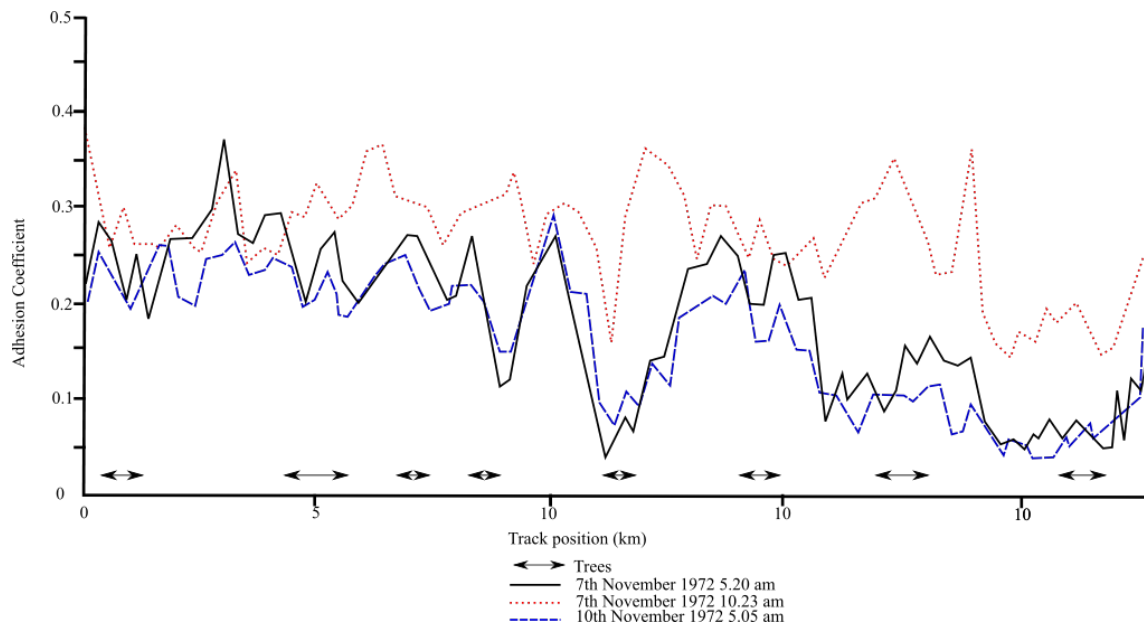


Figure 2.39: Adhesion levels plotted against tree locations [49]

Although primarily thought of as an autumn problem, leaf fall can occur all year round. A sudden change in environmental conditions, such as hotter or cooler temperatures can cause leaves to drop. High winds can also cause leaves to be blown off the tree at any time of year. Droughts, extended wet periods or even insect pressure can be enough for a tree to shed large numbers of leaves earlier than expected. Seed pods can also fall throughout the year and dead flowers known as catkins drop in large numbers at different times of year dependent on the tree species. For instance, Oak will grow and drop catkins around April and May and Hazel will drop its catkins in February.

“Paper tape” is used in a well documented method to simulate low adhesion in both small and large scale laboratory testing. This provides a smooth surface (tape) with a hydrocolloid known as acacia gum on the surface. When mixed with water, a viscous and slippery layer is formed which reduces adhesion. Organic compounds on the railhead may act in a similar manner to this, forming a viscous layer that causes low adhesion.

These hydrocolloids may be the friction reducing components that cause the wet-rail phenomenon, pectin is a hydrocolloid that has been found to make up a large proportion of water soluble organic matter when leaves have been left in water for a period of time [48]. Hydrocolloids are hydrophilic polymers, the long polymer chains bind with water, forming bonds that are as strong or stronger than the water-water bonds, which leads to a change in the properties of the solution. Pure hydrocolloids are often translucent so are hard to see when deposited in a thin film so could be hard to detect on the railhead.

The large radius of gyration of the hydrocolloids results in a large quantity of water being affected by a small amount of polymer, affecting properties such as viscosity [50]. This means that very small quantities of contamination on the railhead could cause a significant change in the properties of any water lying on the railhead.

The properties of a hydrocolloid solution are concentration dependent. A thin and invisible layer of these organic compounds could be deposited on the railhead and could reduce the friction coefficient when dissolved in dew or drizzle, but be washed away or become too dilute at higher levels of precipitation. Hydrocolloids also act as stabilisers, any dispersed particles in the solution will remain separate rather than agglomerating together. Iron oxide particles may remain particulate in the contact, or the hydrocolloid could move into the porous top layer of oxide. Water that has been bound by hydrocolloids often exhibits non-Newtonian behaviour, shear thinning and shear thickening.

Chemical reactions could occur between organic material and iron oxides. Long chain fatty acids, which can be found in plant material, can react with iron oxide in the presence of water to form a lubricating soap. Tingle provided evidence that a steel surface can be lubricated by a single monolayer of long chain fatty acids [51]. This could explain why low levels of water under certain conditions can reduce friction. Low levels of moisture will allow the reaction between long chain fatty acid and iron oxide to form a soap, too much water will dilute or wash away this soap monolayer. Another hypothesis is that the bonding between iron oxides and organic contamination may also simply mean that organic contamination is harder to remove when it binds with an oxide layer, reducing adhesion for longer periods of time. Natural organic matter is present in rainwater and has been found to bond with iron oxide particles, which could play a role in the bonding between rail and any organic matter [52].

2.6 Summary and Hypotheses

The main objective of this literature review was to provide a better understanding of the “wet-rail” phenomenon which will help develop test methods to replicate low adhesion and develop mitigation methods. It is clear from the reviewed literature that a naturally formed oxide layer will affect adhesion. The oxide could enter the contact from the external source flow, likely mixed with water and possibly the other contaminants that have been mentioned in this review. It will also be created in the internal flow of the contact, where wear particles oxidise under the applied heat and pressure.

This review has highlighted some knowledge gaps that need to be addressed in future work. In the UK especially, time intervals are relatively short between train passings. If a train removes oxide upon passing, any oxides that could lower adhesion would have to form a thin layer in a short time span, limiting the spectroscopic techniques

that can be used. It would be beneficial for research to focus on oxide layers that have been produced over a much shorter time span or actually within the wheel-rail contact itself to better simulate working conditions.

A second issue that will need further analysis is the time that the oxide will remain on the rail as the train passes. A thin layer will be easily removed and much of the discussed literature has relatively long testing times. It would be beneficial to conduct some tests over shorter time periods to establish whether it is purely the initial oxide contact that provides the low adhesion characteristic of the “wet-rail” phenomenon, as current tests may remove the oxide coating quickly and therefore any change in friction coefficient may be missed. More sensitive in-situ spectroscopy may be necessary to obtain a detailed analysis of the oxides forming on rail over short time periods; however, a more effective option may be to design a method of removing recently formed oxides that prevents chemical or mechanical changes during transportation to a laboratory. Experiments could be designed in order to distinguish between oxides already present on the rail, formed in the contact or entering as contaminants. The oxide composition and morphology is likely to differ between these scenarios but this has not been confirmed. It is currently unclear what oxides are being formed in each situation and how these affect adhesion. A further understanding of how oxide type depends on generation method would help solve this issue.

Mechanisms for friction reduction due to iron oxides have been proposed, based on the knowledge gained through this review. These hypotheses can be tested in future work to assess the role of iron oxides in the wet-rail phenomenon.

The first is that a low shear strength oxide containing paste is formed which can aid lubrication between wheel and rail. Work from Beagley et al. [25] suggests that dilatant, or shear thickening, behaviour is seen when a Fe_2O_3 and H_2O mixture has a high solid content, which causes this paste to remain on the railhead rather than being pushed aside, a schematic diagram is seen in Figure 2.40.



Figure 2.40: A possible hypothesis for low adhesion

Other hypothetical mechanisms rely on modifying the shear strength of the layers between wheel and rail using a thin oxide layer without any other contamination. Zhao et al. [40] hypothesised that the iron oxide coating on steel was divided into sub-layers due to an oxygen concentration gradient, with the $1\ \mu\text{m}$ superficial sub layer of Fe_3O_4 being the most friction reducing. The middle layer is around $10\ \text{nm}$ thick with a lower oxygen content, the layer bonded to the steel surface contains a

very low oxygen content. A schematic of this is shown in Figure 2.41. The lower layers provide support to the low shear strength superficial layer. As a result, friction is low when only the superficial layer is in contact; friction levels will increase if this layer is broken. The top layer is stable up to approximately 1 μm as it relies on the support of the lower layers.

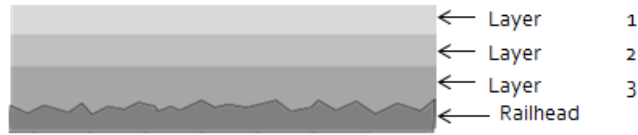


Figure 2.41: The three layer model of iron oxide layers

A schematic for a coherent magnetite film with a thin layer of water, possibly from dew, on the surface is shown in Figure 2.42. Once on the surface, the water may mix with the third body layer or organic contamination. A hard and strongly bonded layer of magnetite could provide a supporting surface for a viscous combination of third body layer and water on top. Another possibility is that the viscous paste contains organic compounds such as lignin or pectin which may provide the lubricating properties whilst a magnetite film provides the supporting surface.

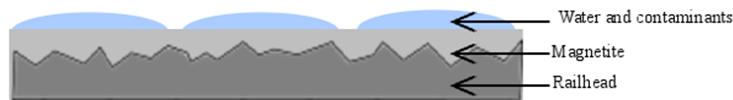


Figure 2.42: A magnetite film with a layer of surface water

If the surface is left moist, electrochemical corrosion will occur and a thicker oxide such as hematite will grow on the surface, the layer has been labeled “thicker oxide” due to the different oxide compositions that could be formed. Repeated wet and dry cycles will allow this layer to grow further, shown in Figure 2.43. Water may settle on top and or be absorbed by the thicker layer which could change the surface shear properties.

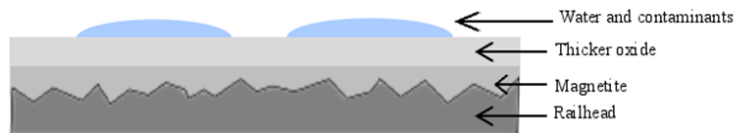


Figure 2.43: Two oxide layers with a layer of surface water

All these situations could potentially cause low adhesion, experimental methods are necessary to test each hypothesis out. Some mechanisms rely on oxide debris whilst

others rely on an oxide being present as a bonded layer on the railhead. It is not yet clear whether either set of mechanisms, or a combination of the two, may be causing low adhesion. The tribological circuit has been discussed and concluded that iron oxide can enter as an external flow as the wheel rolls over the rail or be created or modified in the contact itself, as an internal flow.

A number of methods used to determine the friction coefficient have been covered. It is clear that adhesion levels are dependent on a huge number of variables, which is complicated further by different test methods producing different results. If the adhesion coefficient associated with different oxide types were compared directly it would be necessary to choose a single method and control as many variables as possible, comparing relative adhesion levels rather than focusing on absolute values. The sliding UMT tribometers provide an excellent means of doing this but a rolling twin disc test provides a more realistic contact. If a viscous paste is producing low adhesion then a high speed rig may be necessary to produce low adhesion in a laboratory, which would not be possible on a slow moving test rig where the paste may be pushed out of the way.

Organic contamination may play a role in the wet-rail phenomenon. There are a number of ways that organic contamination can reach the railhead throughout the year and these may be unseen during an inspection of the track. These organic contaminants may be the sole cause of low adhesion or mix with iron oxides to produce what we know as the wet-rail phenomenon.

Although it is unlikely that water alone causes very low adhesion, it is likely to play a key part in the wet-rail phenomenon, likely when water is found in low volumes with either oxides or organic contamination. A series of tests involving iron oxides will be necessary to assess their role in lowering the adhesion between wheel and rail. Low adhesion due to organic contamination has been more documented but will be used as a comparison.

Two distinct mechanisms for friction reduction due to iron oxides have been proposed. The first is that an oxide containing paste is formed which, if of a sufficient viscosity, can result in lubrication between wheel and rail. Work from Beagley et al. [25] suggests that dilatant behaviour is seen when a Fe_3O_4 and H_2O mixture has a high solid content, which causes this paste to remain on the railhead. Zhao et al. [40] hypothesised that the iron oxide coating on steel was divided into sub layers, with the superficial sub layer of around $1\ \mu\text{m}$ being the most friction reducing. The first mechanism relies on oxide debris whilst the second relies on an oxide being present as a bonded layer on the railhead. It is not yet clear whether either mechanism, or a combination of the two, may be causing low adhesion.

3 Operational Data Analysis

3.1 Introduction

The purpose of this chapter is to analyse data to see if there are any trends of low adhesion periods throughout the year and explore any links between low adhesion and weather conditions. This will help to understand which low adhesion events throughout the year may be attributed to the wet-rail phenomenon and then look at the specific conditions that may cause it. If low adhesion causing conditions are found, the information can be used to steer laboratory testing, carried out later in this work, towards the specific conditions which cause low adhesion. This will result in the production of more realistic test methods that can recreate low adhesion in laboratory tests, leading to a better understanding of the problem and more realistic testing of mitigation methods.

Adhesion forecasts are particularly important to warn drivers that a more conservative braking style may be necessary on certain days. For instance, the autumn low adhesion index is a forecast that predicts adhesion conditions during the autumn season so that so that days with very low adhesion due to leaf fall can be predicted and mitigation methods can be used. The index is based on a model that uses daily leaf fall, wind and progress through the leaf fall season as its main inputs. It can be used as a UK average or for individual regions. An example of this is shown in Figure 3.1.

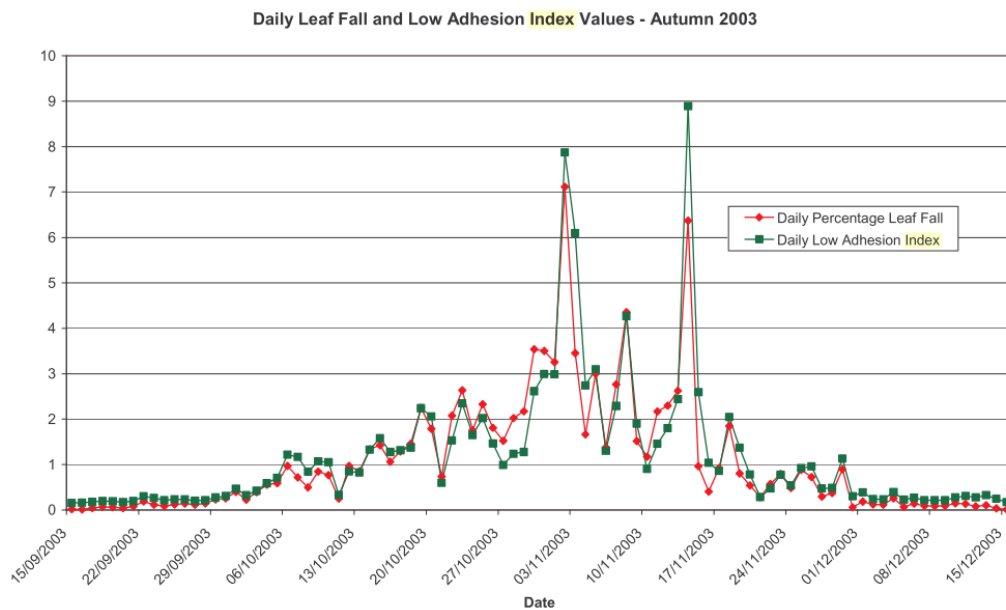


Figure 3.1: Daily national average percentage leaf fall and low adhesion index for autumn 2003 [7]

Adhesion forecasts currently focus on leaf fall, but low adhesion attributed to the

wet-rail phenomenon happens throughout the year and often unexpectedly. Any trends found between specific weather conditions and the wet-rail phenomenon could be used to design a year round adhesion forecast that does not just focus on leaf fall.

A previous RSSB report, T1042 [5], provided a starting point for this work, analysing operational performance data from 2010-2012 and UK wide weather data. It highlighted an increase in morning and evening low adhesion incidents where no organic contamination was found on the railhead after the incident. This could be linked to dew on the rail and the wet-rail phenomenon. A graph of incidents per hour, normalised by number of station stops to prevent bias towards busy periods, is shown in Figure 3.2.

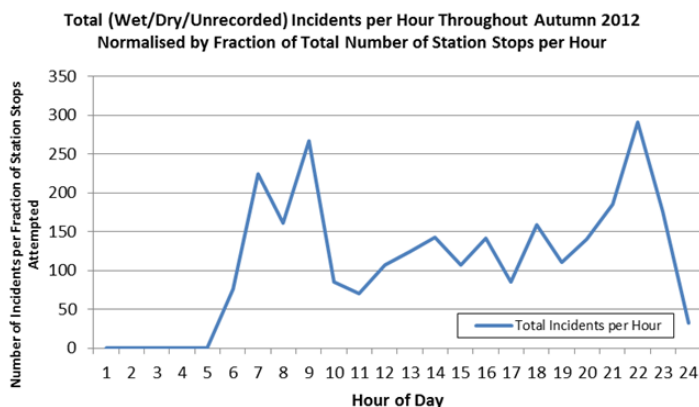


Figure 3.2: Plotting total number of station overruns per hour normalised by hourly traffic [5]

As well as updating the data, a key aim for this next stage was to focus on local rather than national conditions. Weather varies dramatically across the UK so focusing on weather data that has been taken from near to the site of an incident will help to assess if it is specific weather conditions that will cause low adhesion due to the wet-rail phenomenon. To achieve this the following work looked at areas which have known problems with adhesion levels, before compiling the data to develop a wider view on any weather related trends that are occurring.

A MET office report for the Adhesion Working Group (AWG) in 2003 [7] has also provided a useful basis for this work. It began by analysing SPAD, signals passed at danger, events from 2003 and summarised the impact of certain environmental factors that support this work:

- Some low adhesion events seem to be associated with damp rails, even without leaf contamination. Approximately half of low adhesion events that were studied involved leaf contamination, the other half involved damp or wet rail conditions without leaf contamination.

- Conditions where rails are only slightly damp seem to cause more problems than when the rails are very wet. 60% of low adhesion incidents analysed occurred in damp weather conditions characterised by high relative humidity values (>80%) when either mist, fog, drizzle or light rain were reported. Heavy rain accounted for a further 9% of cases, freezing conditions another 6% with just 25% of events occurring in dry weather conditions.
- Days with low (0-5mm) and moderate (5-10mm) rainfall had 30% and 60% more delays respectively, compared to dry days. Interestingly, very wet days (rainfall > 10mm) had 10% less delays than the dry day baseline, implying that heavy rain does not cause low adhesion.

The report then provided case studies where individual events were analysed. It looked at only 22 events, rather than the larger number seen in the T1042 report, however, each case study has a detailed review which lead to some interesting conclusions that can be expanded during the course of this work. Both leaf fall and meteorological data is extracted for each SPAD event and analysed. Meteorological data is collected within 30 km from the incident so it gives a clear idea of where this work can progress with looking at more localised data.

Precipitation is likely to have fallen within an hour directly prior to 4 out of 22 events, with precipitation falling 6 hours prior to 2 further events. 10 of the events had no precipitation for 24 hours prior to incident. However, dew would likely have been on the railhead for 7 of these events. A total of 16 out of 22 incidents would have likely had dew on the rail if there was no precipitation remaining and in 4 of these incidents the dew may have frozen to form a railhead frost. In total, after looking at which incidents may have had a moist railhead due to precipitation, dew or frost, only 4 or 5 incidents were likely to have occurred on a “dry” railhead. A full table of conditions for each incident is seen in Figure 3.3 [7].

3.2 Data Collection

Event No.	1	2	3	4	5	6	7	8	9	10	11	12	13	14	15	16	17	18	19	20	21	22
Date	07/10	22/10	02/11	04/11	04/11	05/11	06/11	06/11	06/11	07/11	08/11	08/11	09/11	11/11	12/11	13/11	15/11	21/11	22/11	22/11	27/11	29/11
Time	09:13	10:25	18:16	05:10	09:20	20:46	15:20	17:58	18:18	16:21	09:29	10:55	07:09	18:10	09:39	06:40	08:12	10:16	11:45	14:45	00:02	06:57
Signal Number:	GB871	YS198	HJ53	AD623	CBP26	D1002	H2	MR5	HN15	K622	ES34	WK708	TB16	CE189	E81	WR4	CO614	W1	W193	T239	L490	K1211
SPADS at signal since 1/1/85	8	2	1	1	1	2	1	1	1	1	1	1	1	1	2	6	1	1	1	1	1	1
Report of railhead	slippery	poor	wet	none	none	dry	none	rain	slippery?	dry	none											
Report of visible contamination	No visible	Good rail	slight	yes	yes	slight	yes	yes	yes	none	yes	none	yes	none	none	yes	yes	none	none	none	none	heavy
Leaf Fall (LF) area	LF6	LF4	LF6	LF15	LF15	LF1	LF5	LF7	LF6	LF12	LF6	LF15	LF13	LF6	LF14	LF14	LF13	LF7	LF15	LF15	LF13	LF7
Adhesion Code (% & colour)	g	a	f	g	g	a	a	g	g	a	f	f	g	a	a	a	f	g	g	g	g	g
Low Adhesion Index	0.68	1.65	9.85	1.94	1.94	5.83	1.32	1.21	1.66	2.59	6.13	6.01	1.90	1.67	3.20	5.06	3.33	0.17	0.97	0.97	0.30	1.03
% leaf fall on day	0.5	2.3	8.0	0.8	0.8	(4.3)*	2.5	1.0	1.1	3.1	5.7	6.3	1.5	2.2	3.4	4.5	0.5	0.1	1.1	1.1	0.2	0.9
Cumulative % leaf fall previous 3 days	1.0	4.2	14.0	13.0	13.0	(15.4)*	10.1	5.7	7.8	7.0	6.9	7.6	9.1	7.7	6.5	8.1	13.3	2.6	2.8	2.8	1.9	1.4
No precipitation last 24 hrs					▼	▼	▼	▼	▼	▼	▼	▼				▼						▼
>10mm precipitation in last 24 hrs			▲																		▲	
>10mm precipitation in last 48 hrs	▲			▲	▲															▲	▲	▲
Slight precipitation last hr		△	△																	△	△	
Slight precipitation in last 6 hrs	△	△	△												△					△	△	
Slight precipitation in last 24 hrs	△	△	△	△									△	△				△	△			△
Relative humidity (%)	79	82	88	97	98	85	74	na	92	57	97	70	95	87	92	95	91	95	93	97	75	89
Dew likely on railhead			?	<	<	?		?	<	<	<	<	<	<	<	<	<	<	<	<	<	<
Dew point temperature	5.6	1.3	6.9	3.5	5.6	8.7	8.9	na	12.0	2.8	5.7	3.3	2.8	7.2	10.0	9.4	6.0	4.2	8.0	7.9	2.6	5.9
Min air temp overnight if morning event	7	3	/	4	0.5	/	/	/	/	/	6	8	3	/	11	3	7	4	8	/	7	6
Air temp at time of event if evening			9			11	13.4	10.9	13.3	10.8				9.3						8.4		
Frost possible on railhead				*	*								*			*						

Figure 3.3: Autumn 2003 MET Office SPAD analysis [7]

A similar approach was used for the current work, but focusing only on incidents that could be linked to the wet-rail phenomenon, where no visible contamination was seen upon inspection after incident.

3.2 Data Collection

The data used in the course of this study came from a variety of sources. The bulk analysis was based on data provided by Network Rail, a list of incidents that have been attributed to low adhesion events during the autumn periods of 2010-2014, from the 1st September to 10th December. The data consisted of station overruns, signals passed at danger (SPADs) and wrong side track circuit failures.

The data included the time, date and coordinates of incident. Extra notes were sometimes included that were taken during rail inspection after incidents, such as the presence of any visible contaminant or whether the railhead was in wet or dry condition. Data is not collected by Network Rail throughout the rest of the year so only autumn could be investigated.

Wheel slide protection data sets have also been analysed as a comparison, which provides a large low adhesion data set over the full line throughout the year rather than just the autumn season, but does not provide any information of whether there was obvious contamination that caused the low adhesion.

The national and local weather analysis focused on building upon the T1042 report and linking station overruns to weather data obtained from SMT weather, a website

which provided specialist meteorological data for Network Rail [53]. Weather data was available from a large number of weather stations across the UK and contained hourly measurements for the amount of precipitation, air temperature and wind speed. Humidity data was sampled from the MET office. This analysis only used station overruns that have been attributed by Network Rail to weather conditions and not visible contamination or driver error. Only station overruns have been examined because these occur more often than the other previously mentioned types of incident, the larger number of incidents enabled better data analysis. A flow chart describing the sequence of work used to analyse this data is shown in Figure 3.4.



Figure 3.4: A flow chart explaining the structure of the work

3.3 National Analysis

As explained above, national analysis of Network Rail incident data during the autumn period was performed in the RSSB T1042 report [5] and some interesting trends were found. For example, in the 2010-2012 data sets it was reported whether leaf contamination was present or not after inspection following an incident. The reported numbers of incidents from both categories are shown in Table 3.1. It can be noted that the numbers of contaminated and non-contaminated incidents are roughly similar for all years. Data from the years 2013 and 2014 has not been included due to changes in incident recording.

Data set	Leaf contamination reported	No leaf contamination reported
2010	85	82
2011	20	27
2012	80	67
Total	185	176

Table 3.1: Rail contamination reported after an incident, taken from the Network Rail autumn incident data

The following reasons were proposed as to why a large number of incidents have been reported as non-contaminated [5]:

1. There was no leaf contamination in the contact and the overrun was caused by another factor (not necessarily low adhesion).

2. Leaf contamination was not present on the railhead, but was present on the wheels of the train.
3. The railhead condition was assessed at a position where leaf contamination was not present, but was present elsewhere in the stopping zone.
4. Leaf contamination was present at the point of assessment, but was not detectable by the assessor's methods (most commonly visual inspection).
5. Water or moisture was present on the railhead and perhaps in combination with other third body contaminants, caused low adhesion.

It is unlikely that the overruns are caused by human factors or mechanical issues because Network Rail analyses driver records for each incident in order to assess if anyone is at fault and have determined the incidents used here as “weather related”. It is unlikely that leaf contamination would purely be found on the wheels, few leaves would settle on them and contamination would quickly be removed due to the rotation and, if it was, the low adhesion is likely to be much more short lived because the high forces acting upon the same area of the wheel during slide would remove contamination. Proposals 3 and 4 are perhaps more likely due to the visual inspection method, although the hard black layer typically associated with leaf contamination is usually visibly obvious and notoriously difficult to remove.

The final proposal will be considered and other mechanisms of low adhesion that do not involve leaf contamination will be investigated. During visibly poor conditions, drivers anticipate low adhesion and make adjustments to their brake timing. If these seemingly uncontaminated low adhesion events are caused by low levels of water, the drivers may be unaware of these poor conditions and will not adjust their driving style.

It has been previously proposed that adhesion in the wheel-rail contact is lowest when the track is drying out [54]. Drying rain or dew may reach a critical moisture level, lowering the friction coefficient sufficiently for the train to experience low adhesion. If this was to occur, any moisture present on the railhead may have dried by the time the track is inspected and dry conditions reported.

The current work began by updating the previous work with 2013 and 2014 data, ensuring that there were no significant differences in more recent incidents compared to previous years. The only type of low adhesion event used in the following figures are station overruns that have been attributed to weather conditions by Network Rail, ensuring as far as possible that the weather conditions are causing these issues rather than leaf fall.

Another major finding of the previous report was the bias towards weather related station overruns taking place in the morning and evening. Figure 3.5 plots a summation of station overruns throughout the day for years 2010-2014. It can be seen from Figure 3.5 that there is a substantial increase in station overruns during the hours of 0600-0900 and a smaller increase at 2000-2200. It is during these times that dew may be present on the railhead. Data has been normalised by taking into account the average total number of station stops for each hour, the numbers for

which have been provided by Network Rail in the previous RSSB T1042 report [5]. Number of station stops per hour was only obtained from 2012 data, but for the purposes of this report it was decided that using this normalisation on all yearly data sets was sufficient. Interestingly a peak is not present at the busy time around 1700 hours in Figure 3.5, which supports the proposal that it is environmental conditions causing an increase in station overruns and not simply increased traffic volume. It can be noted that the 2014 data contains fewer incidents than previous years over the course of the entire day. Station overrun occurrence during these hours, as a percentage of the total overruns during the day, is similar to previous years as shown in Table 3.2. The incidents that have occurred between 0000 and 0500 have been included but the amount of traffic between these hours is very low and results in a single incident plotting very high up the Y axis.

When rails were inspected after a low adhesion incident, it was often noted whether the track was wet or dry. Figure 3.6 plots the normalised number of station overruns for each hour of the day, this time splitting up the data into 3 categories of dry, wet and those in which no track condition was recorded. It can be seen that the total number of dry incidents throughout the day is very low compared to the other categories, but with a substantial peak between 0500 and 0900 hours. This supports the previous hypothesis that dew may result in a low adhesion incident and dry before the track can be inspected or that oxides are formed overnight. The smaller peak after 2000 hours could also be caused by dew formation, possibly smaller because of previous traffic preventing oxide and third body layer build-up. The data used to generate Figures 3.5 and 3.6 has been analysed elsewhere to support geospatial analysis of low adhesion events [55].

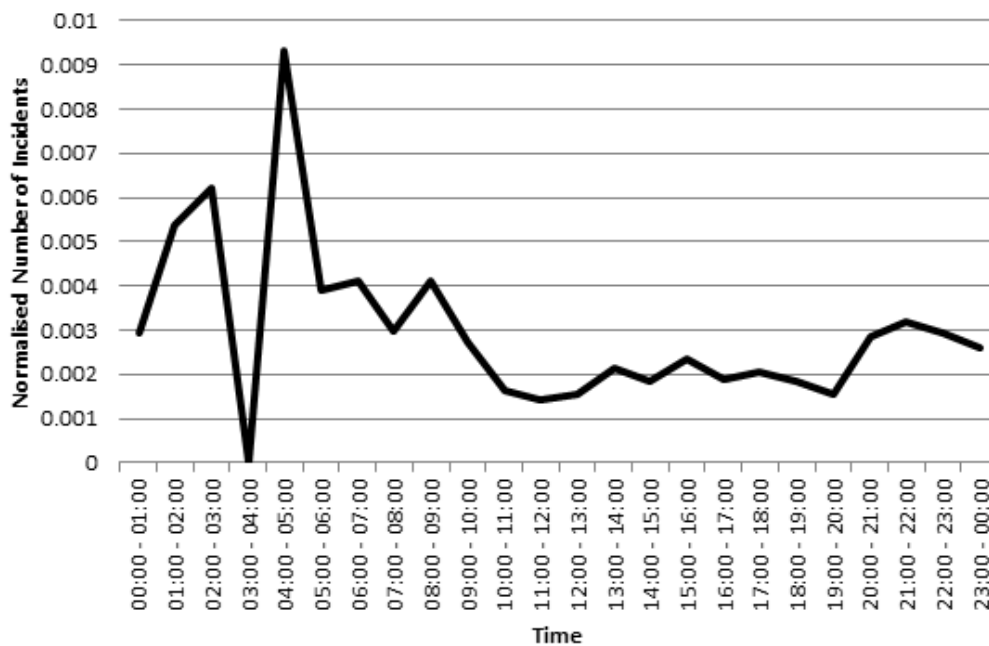


Figure 3.5: Number of station overruns plotted against hour of the day for 2010-2014, normalised by average number of station stops

	Incidents 0600-1000	Total Incidents	Percentage
2010	65	167	39
2011	17	47	36
2012	42	147	29
2013	65	217	30
2014	27	90	30

Table 3.2: Incidents between 0600-1000 hours, as a percentage of total incidents

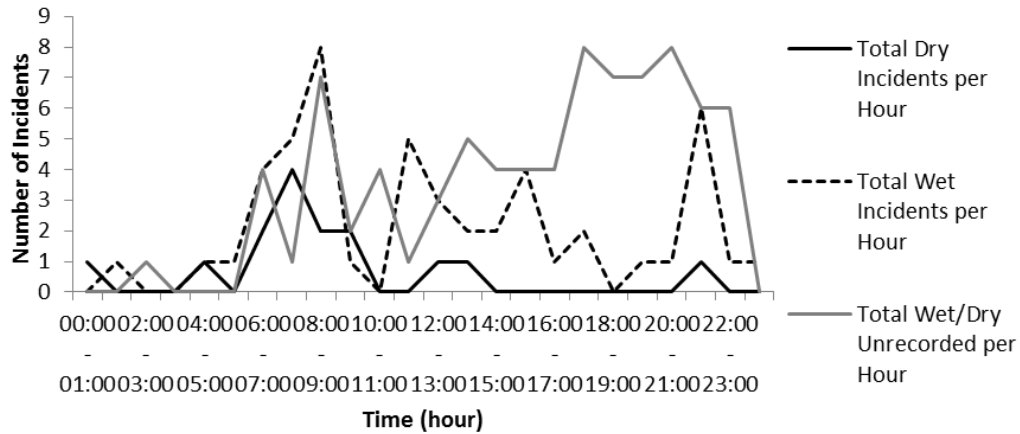


Figure 3.6: Total wet/dry/unrecorded incidents per hour, during the 2012 autumn season

Incidents per day were plotted over the entire autumn period and are shown in Figure 3.7. As seen in the prior report, incident numbers rose dramatically on certain days rather than being consistent throughout the season. The most obvious difference in data sets is that the number of station overruns is much lower in 2014 than 2013, with 217 station overruns in 2013 and 90 in 2014. This was out of a total of 397 low adhesion events in 2013 and 215 in 2014, so the percentage of events attributed to weather conditions is similar.

Figure 3.8 plots the number of incidents per day throughout the autumn season. Also shown are the daily UK average conditions for precipitation, air temperature and wind speed. UK average conditions were obtained by averaging a spread of 31 inland weather stations from across the United Kingdom. This needed further examination using more accurate weather data as conditions across the UK can vary significantly. To achieve this, local weather data was used to narrow down the specific conditions that occur during periods of low adhesion.

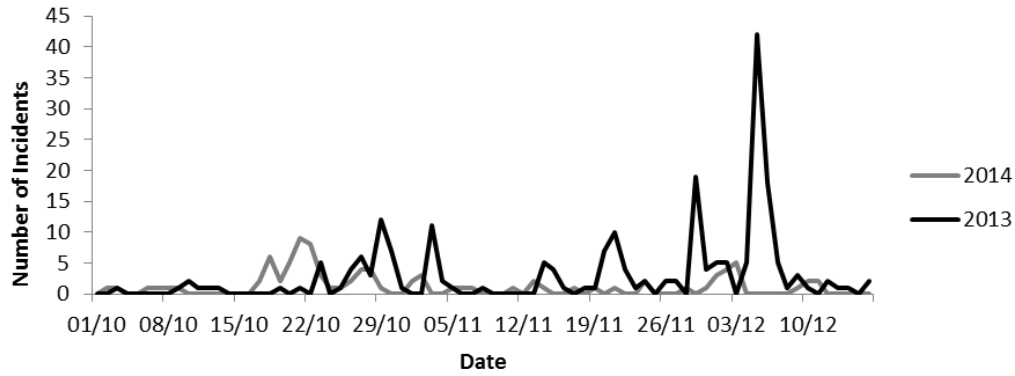


Figure 3.7: Number of station overruns plotted against date, throughout the autumn season

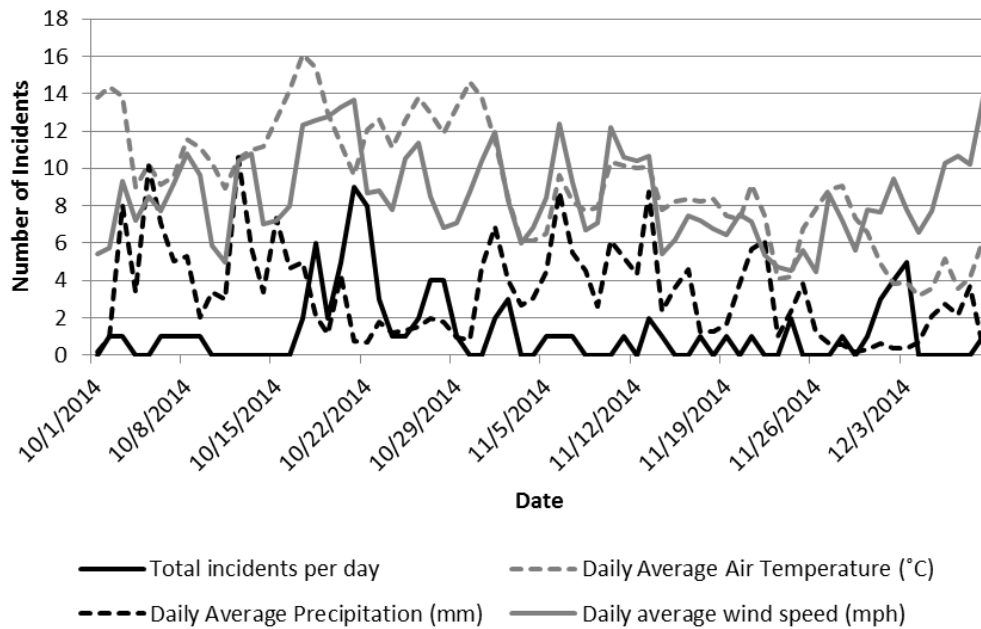


Figure 3.8: Category of incidents throughout autumn 2014, comparison of the daily average weather data to the total number of incidents

3.4 Local Analysis

The next stage of this work was to expand upon the national level analysis by analysing the weather conditions at the time of incidents on a local scale. This was achieved by linking low adhesion events to their nearest weather station available via SMT weather.

Network Rail incidents contained latitude and longitude coordinates which were logged into a map using ArcMap geographical information system (GIS) mapping software, allowing a visual representation of incident positions. The software enabled the viewing of incident locations during a particular time period, which was used for daily, weekly and monthly analysis. ArcMap was used to find specific problem periods and areas, with hourly data from local weather stations sites plotted alongside time of incident.

A number of incidents were plotted alongside their corresponding weather data. One particular period stood out as having a large number of low adhesion incidents, a total of 62 station overruns took place between 05/12/2013-07/12/2013, mostly in the Wessex and Kent areas.

Nearby weather stations available were plotted onto a map in order to find the nearest weather station to each incident. Weather data was plotted against incident time, the weather data was extended before and after the main incident period so that any changes that might cause or prevent these incidents could be observed. Incidents used were linked to a weather station within a 20 km radius to ensure that the weather data would be as reliable as possible.

A number of incidents in some locations were seen to be grouped together. Graphs of individual stations were plotted on a number of scales, looking at the weather trends over a long period before focusing on individual problem days. Figure 3.9 plots the weather data from Wisely and the incident times within a 20 km radius of the weather station have been added. Precipitation data has been multiplied by 10, improving visibility on the graph. Weather data from many other sites was plotted; a graph for Hurn is shown in Figure 3.10.

Incidents in Figure 3.9 and 3.10 seem to be grouped around precipitation. The spread of data points could possibly be due to the onset time of precipitation varying between locations, even if distances are short. These present weather data over a 5 day period, useful to show the weather conditions at the time of incident occurred and clearly showing that precipitation is linked to some of the low adhesion conditions. The graphs suggest that incidents tend to occur during precipitation or shortly after, but this is unclear due to the hourly resolution. It was also noted that incidents seemed to occur when precipitation was coupled with a large temperature fluctuation; however this may be due to incidents happening in the morning, or due to the weather fronts that bring in precipitation. Whilst it was seen that precipitation has a role in low adhesion conditions in a number of cases, some incidents occur when no precipitation has been recorded. A similar pattern is seen for Figure 3.11, plotted using 2014 data from Wisely. Incidents are mostly seen grouped around precipitation, but also occurring when a large temperature drop occurs on the evening of 21/10/2014.

3.4 Local Analysis

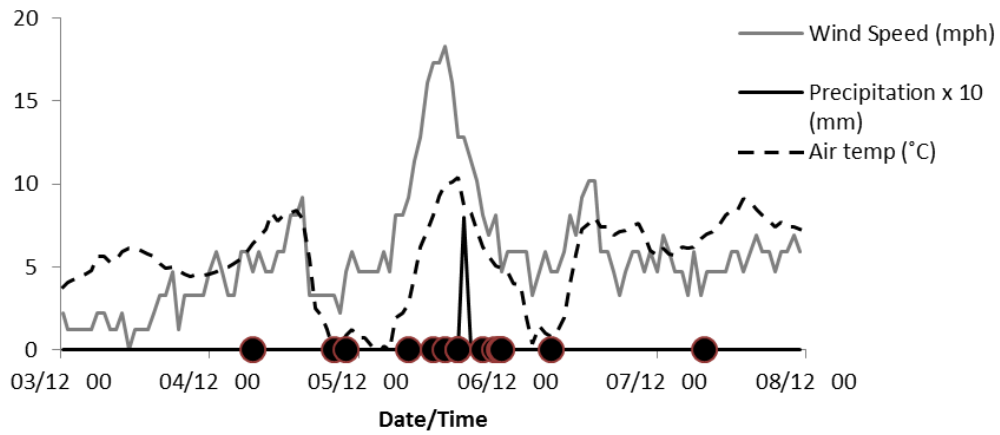


Figure 3.9: Incidents occurring within 20 km of Wisely, plotted against 2013 Wisely weather data

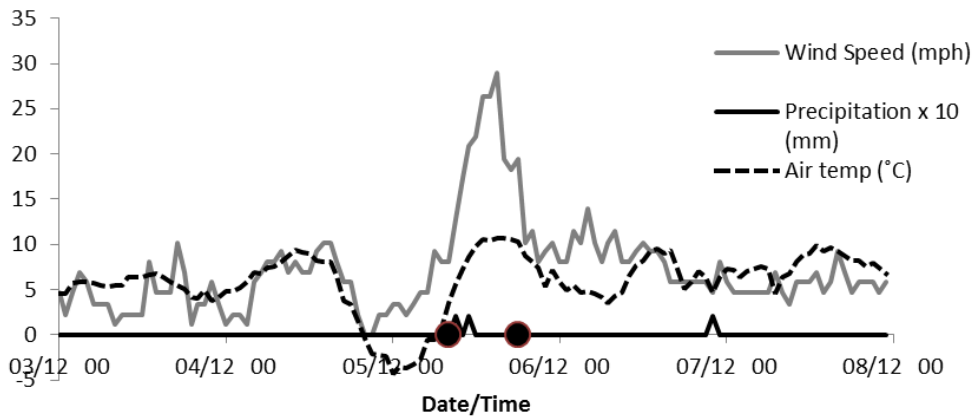


Figure 3.10: Incidents occurring within 20 km of Hurn, plotted against 2013 Hurn weather data

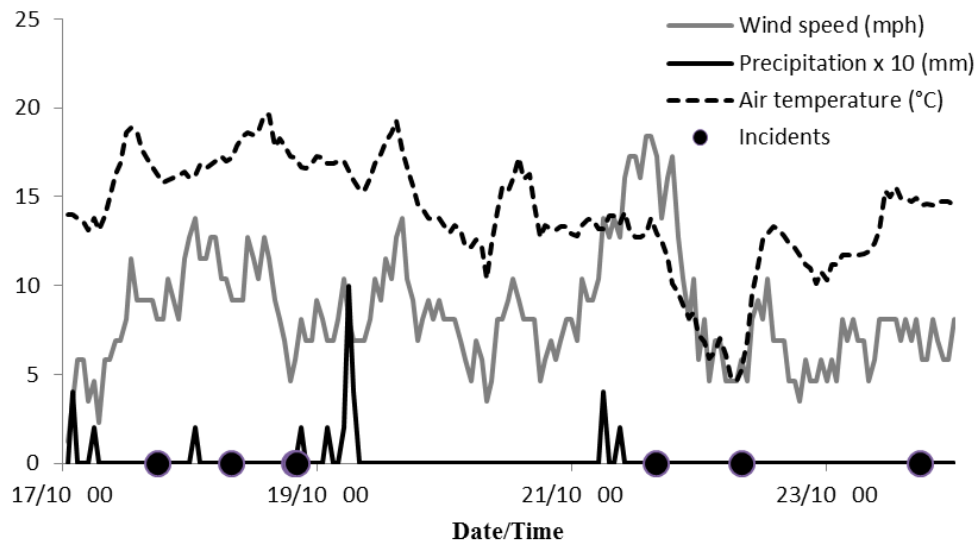


Figure 3.11: Incidents occurring within 20 km of Wisely, plotted against 2014 Wisely weather data

It was hypothesised that by expanding the time period, the conditions before and after the low adhesion event could be analysed and give an insight into why some conditions resulted in incidents whilst others did not. Figure 3.12 illustrates this, with incidents near Crosby plotted against weather data over a much longer period of time. The Crosby data also suggests that low adhesion events occur during large temperature fluctuations over the day, with incident groups at the beginning and end of the period having large fluctuations whilst the centre portion has smaller fluctuations and no incidents. These large fluctuations may be caused by clear skies, the large difference between day and night temperatures will cause more dew to be formed. No pattern was found between any change in wind direction and number of incidents. The wind speed is seen to increase during low adhesion periods, although this could be tied in with precipitation falling as a weather front passes, which may also explain the change in temperature.

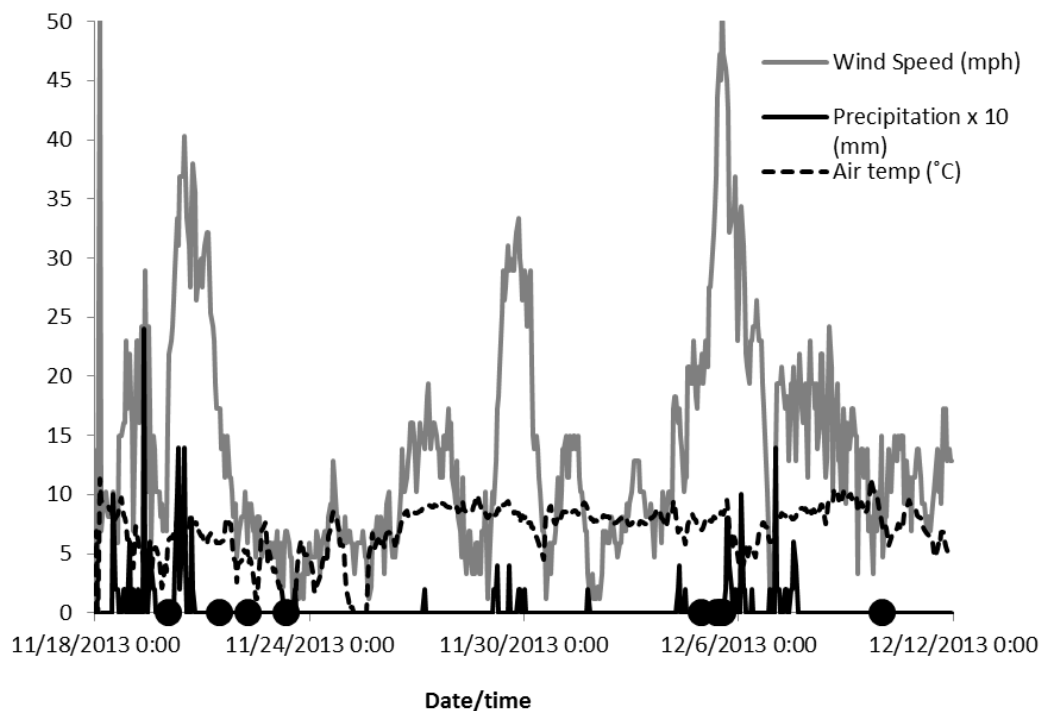


Figure 3.12: Incidents occurring within 20 km of Crosby, plotted against the corresponding 2013 Crosby weather data

3.5 Data Collation

A method of compiling data was needed to fully interpret the results, rather than analysing large numbers of individual graphs. In order to explore the correlation between precipitation and incidents, Figure 3.13 was produced. Figure 3.13 places incidents into 2 groups: incidents that occurred within 12 hours after precipitation and those where no precipitation occurred for over 12 hours before the incident. The 160 data points from the 2013 and 2014 Network Rail data were chosen because they were within 20 km of available weather stations, which allowed accurate categorisation. It is seen using Figure 3.13 that the majority of incidents are early morning and late at night, however, it needs to be noted that this graph has not been normalised due to the spread of data across the country, so this could possibly be due to the larger number of station stops during busy time periods.

Figure 3.13 does, however, provide a further insight into the cause of these low adhesion events as the ratio of categories will not change with normalisation. Although there are a few spikes, the incidents that involve precipitation are largely spread out evenly throughout the day, perhaps becoming more prevalent around noon. On the other hand, the incidents that did not involve precipitation within 12 hours occur more regularly during the high risk hours between 0600-1800 and 2000-2300. Of all

160 incidents logged in Figure 3.13, 64 are within 4 hours of precipitation, a further 22 are within 12 hours of precipitation and 74 have no precipitation 12 hours prior to the incident. With only 54% of incidents occurring within 12 hours of precipitation, other factors may play a role in many low adhesion events.

In some situations the rail may dry well before 12 hours so the same analysis was carried out but deeming any incident that did not occur 4 hours after precipitation was logged as “not involving precipitation” to assess if the data spread would change, a graph is shown in Figure 3.14. The significant difference between the two graphs is that at 2200 and 2300 hours, there are a large number of incidents occurring with precipitation falling between 4 and 12 hours prior to incident. With the current available data it is unclear if the railhead would have dried in this period time or not but the cooler temperatures at this time may mean that the railhead has not dried within 12 hours after precipitation and the rail remaining damp for this long period of time may result in the wet-rail phenomenon.

Relative humidity is a measurement of how much water vapour the air can hold, which depends on temperature. At 100% the air is fully saturated so water will condense if the temperature drops, water can also condense on any feature that is cooler than the air temperature. It can be seen that the 12 and 4 hour data set follows the average relative humidity throughout the day in Heathrow, shown in Figure 3.15 [56], with more incidents occurring at high relative humidities.

Human factors could be involved. The higher number of station stops and decreased time intervals for trains will put extra pressure on drivers which may result in station overruns caused by late braking. However, this is unlikely due to the nature of the Network Rail data. All station overruns in the data set have been attributed to weather conditions, after it has been established that neither the driver nor rolling stock are at fault. High pressure water jetting is often used to remove organic leaf matter throughout the autumn season. Tracks are often water jetted at night which could explain the station overruns located at 12:00 AM and 01:00 AM, but any incident that is obviously related to water jetting is unlikely to be designated by Network Rail as weather related.

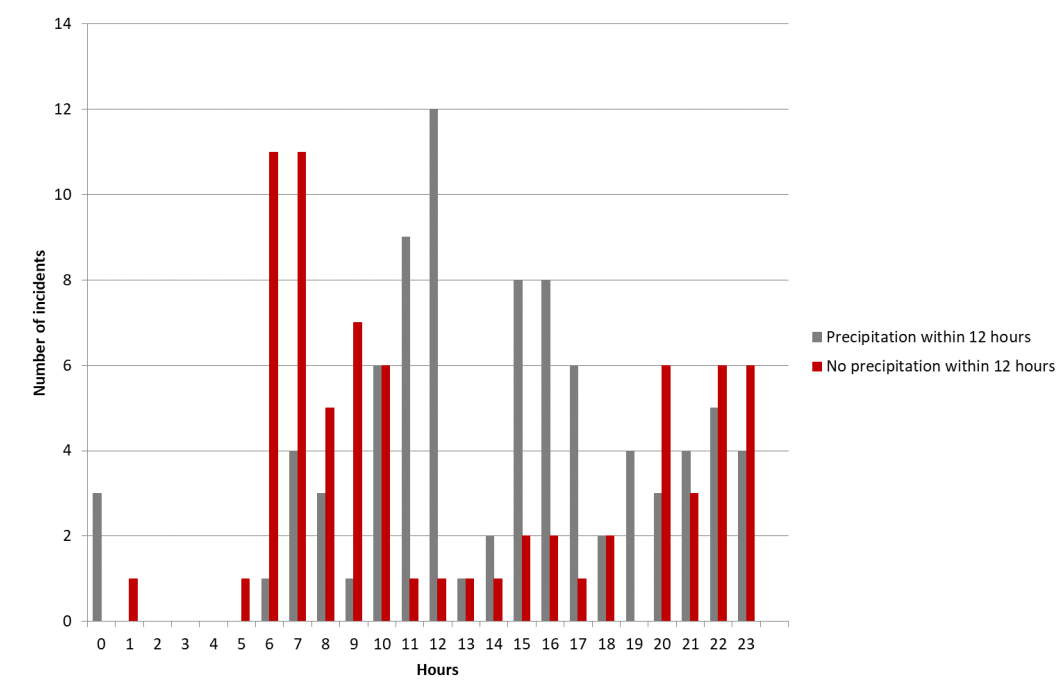


Figure 3.13: A graph showing the effect of recent precipitation on low adherence incidents, using 2013 and 2014 data

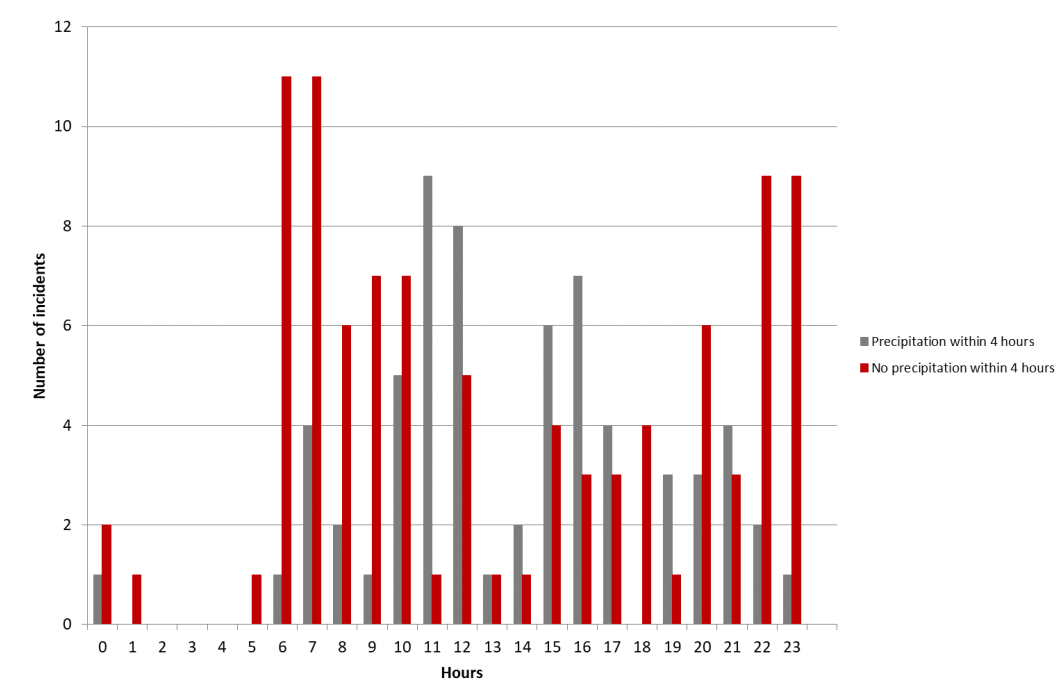


Figure 3.14: A graph showing the effect of recent precipitation on low adherence incidents, using 2013 and 2014 data

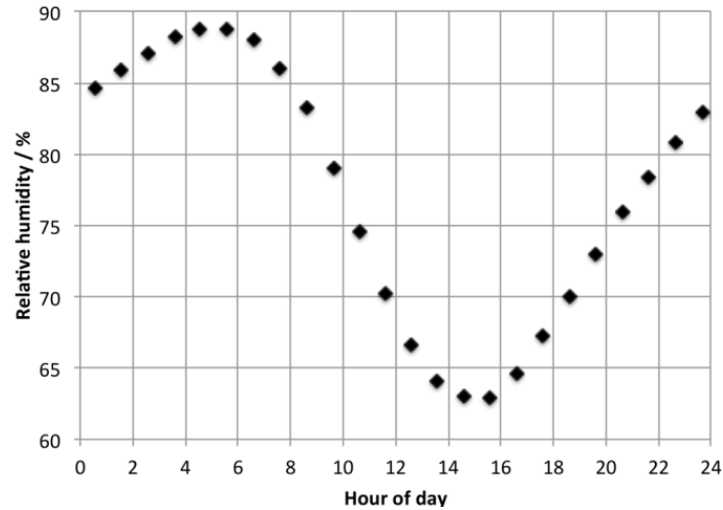


Figure 3.15: The diurnal humidity at Heathrow, average for a thirty year period 1981-2010 [56]

Correlations between temperature and incidents were looked at using Figure 3.16. Using SMT weather, the temperature for every hour during the autumn period could be obtained. This was averaged over 10 different sites to obtain average hourly temperature data for the south of England and this was used to find the percentage of time throughout the autumn season spent at each temperature. The percentage of incidents that took place at certain temperatures was calculated, which was plotted against the percentage of time spent at those temperatures. For instance 6 % of the autumn season was spent at 4 °C, but 18 % of incidents occurred at 4 °C. It can be seen that the number of incidents occurring at temperatures between 4-7 °C are disproportionate to the percentage of time where temperatures were in this range. This is in agreement of the laboratory tests results presented in Zhu et al. [44][57], that a lowering of the temperature decreases the friction level both for humidity and water lubricated contacts.

It has been noted from driver reports that lowest adhesion often occurs on cool mornings on shaded rail, which may explain the increase in incidents at lower temperatures. This may be because the lower temperature allows dew to remain on the rail for a longer period of time before it evaporates.

The railhead temperature is likely to be the factor that contributes to low adhesion, rather than air temperature, but can be difficult to obtain. The rail temperature change throughout the day has been studied previously [58]. If the rail temperature is lower than the air temperature then the rail will act as a condenser and dew will be formed in humid air. It can be seen from Figure 3.17, data collected in the course of this work, that the rail reaches its lowest temperature in spring at approximately 0300 hours and the temperature changes dramatically after 0600 hours when in direct sunlight. The temperature change from a day in winter, shown in Figure 3.18, show

a different pattern [58], with the rail cooling down quicker, staying colder for longer and reaching a peak temperature in the afternoon rather than the morning. In sunny conditions especially, the railhead temperature needs to be assessed because it can vary greatly from the air temperature and any moisture will dry far quicker if the railhead temperature is significantly above the air temperature.

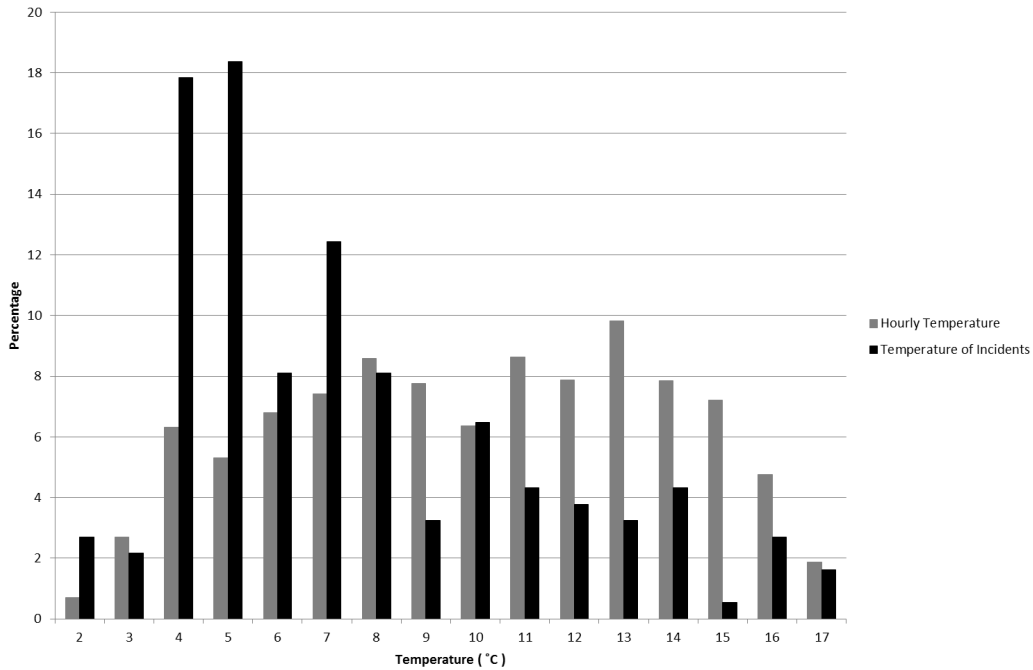


Figure 3.16: A graph plotting the percentage of incidents that occur at certain temperatures, against average temperatures

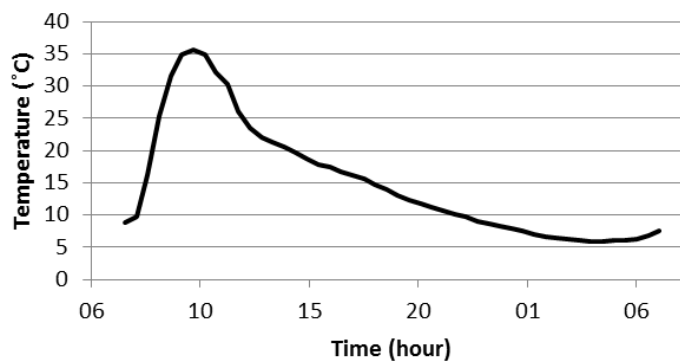


Figure 3.17: The variation of rail temperature during a sunny spring day

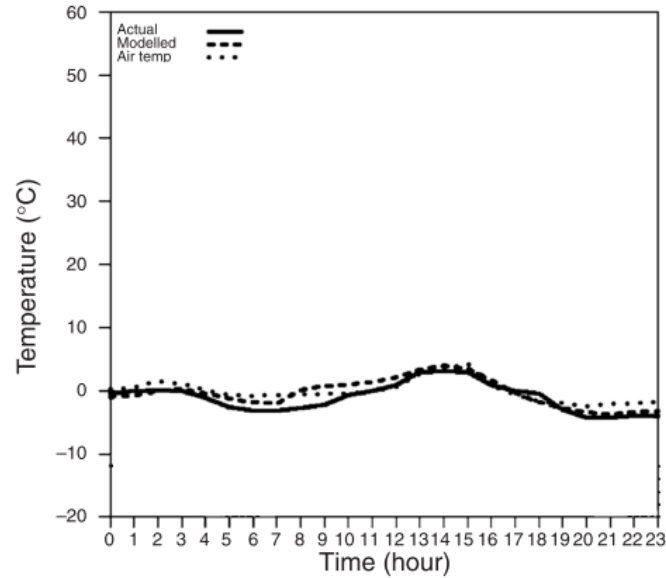


Figure 3.18: The variation of rail temperature during a day in winter [58]

Temperature data was compiled to look at whether temperature fluctuations resulted in more low adhesion incidents. The derivative of average UK temperature readings throughout the autumn season was plotted alongside station overruns and shown in Figure 3.19. The results suggest that the station overruns are not dependent on temperature fluctuations, but it needs to be remembered that this is based on average air temperature readings rather than location specific railhead temperature readings. This could be due to the temperature fluctuations having little effect unless they lead to a significant change in railhead conditions, for example freezing or reaching the dew point.

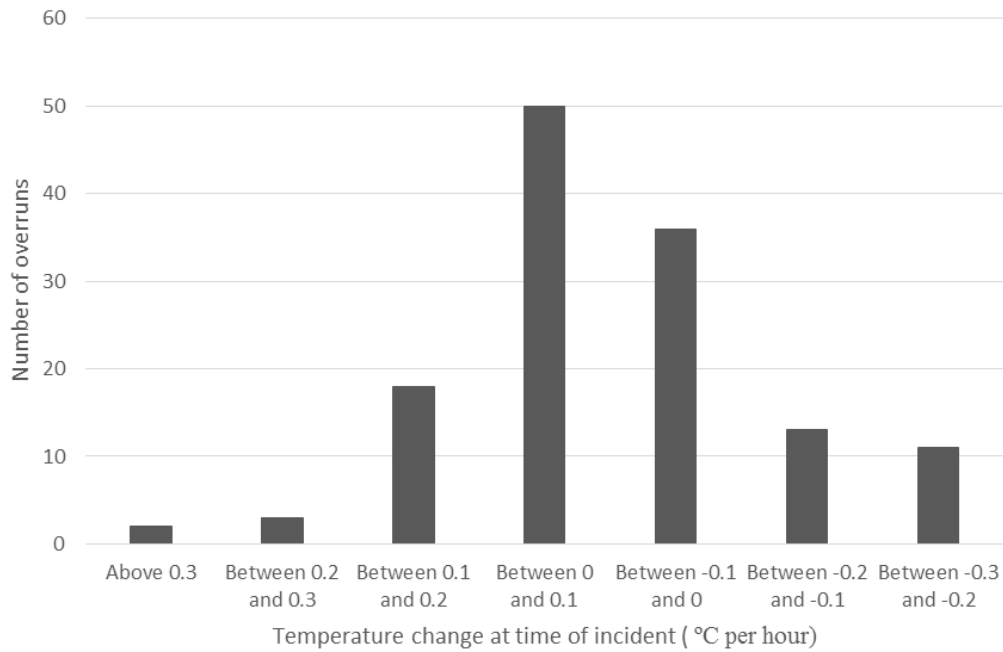


Figure 3.19: Number of station overruns plotted against UK average air temperature derivation, change in °C per hour, averaged over 3 hours at time of incident

3.6 WSP Analysis

Wheel slide protection data was provided by Virgin trains for class 390 vehicles on the west coast mainline. Wheel slide protection is an electronic braking system which is designed to detect wheel slide and adjusts the braking torque to prevent wheel slide from happening. A WSP system is designed to make the best use of available adhesion for all intended operating conditions by a controlled reduction and restoration of the brake force to prevent wheel sets from locking and uncontrolled sliding due to low adhesion. Thus the stopping distance is optimized and extension of stopping distance minimised.

Analysis was initially carried out on the speed of WSP activation. WSP provided a huge amount of data so only the incidents where WSP was activated for more than 5 seconds has been used to focus on longer periods of low adhesion that would be seen in the wet-rail phenomenon. Time duration of WSP activation rather than distance of WSP activation was used to prevent a bias towards high speed activation rather than low speed activation near station stops. The number of WSP activations plotted against speed at the time of activation is shown in Figure 3.20. Data is shown for WSP activations longer than 5 seconds, longer than 10 seconds, longer than 20 seconds and longer than 30 seconds. The data analysis shows that there are significantly more incidents of WSP activation for above 5 seconds at higher speeds

between 80 and 120 km/h. A similar trend is seen for all WSP activation lengths, these results are to be expected due to the increased time needed to slow down when travelling at higher speeds.

WSP data near specific sites was analysed using the same method used in Figure 3.14. The sites chosen were Crosby and Coventry due to the availability of weather data. All data used is taken from within 1 km from the station, this reduces the error due to precipitation falling at different times over a region and means that all wheel slide incidents will likely be at a slower speed when approaching or pulling away from a station. Data for Crosby is shown in Figure 3.21 and data for Coventry is shown in Figure 3.22. The pattern seen in Figure 3.14 is not as distinct in this case.

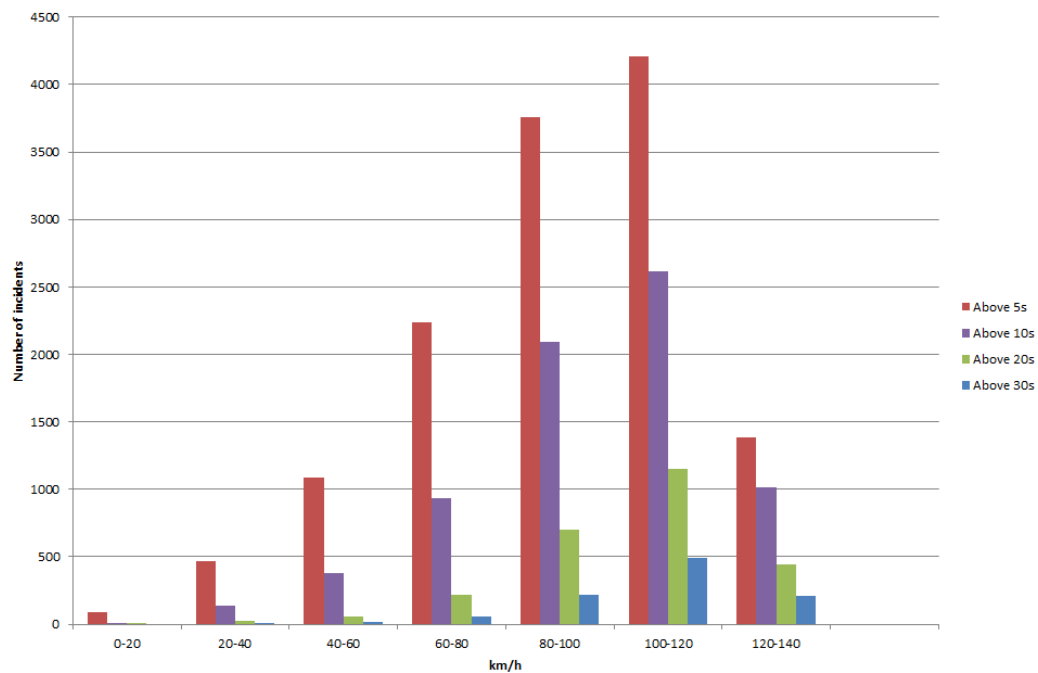


Figure 3.20: Speed of WSP events for different WSP activation periods

3.6 WSP Analysis

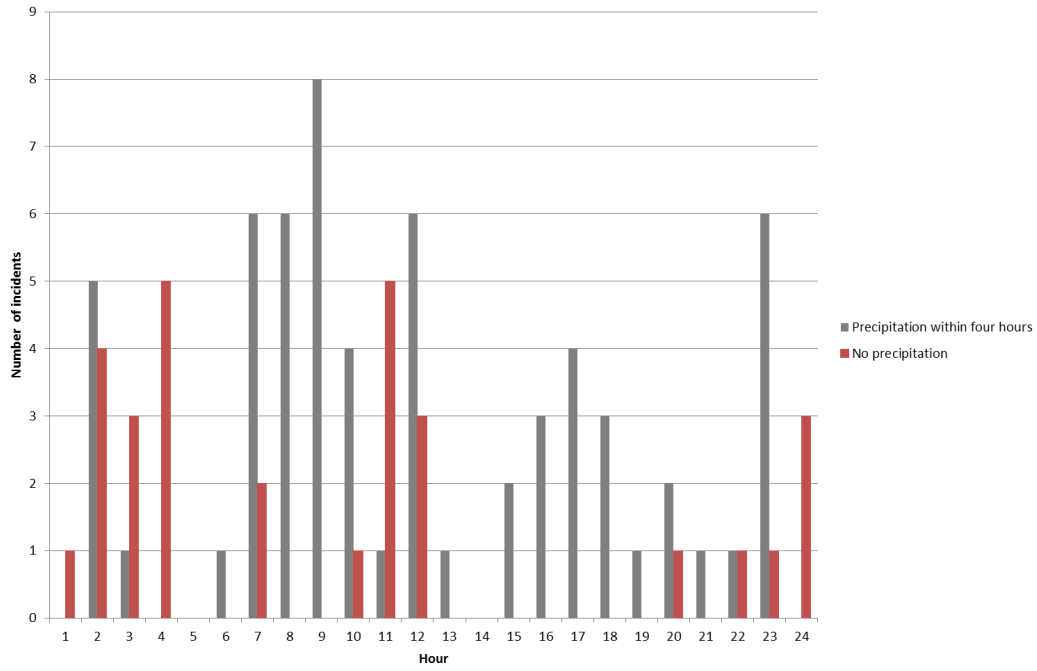


Figure 3.21: WSP events for Crosby station, plotted against precipitation data

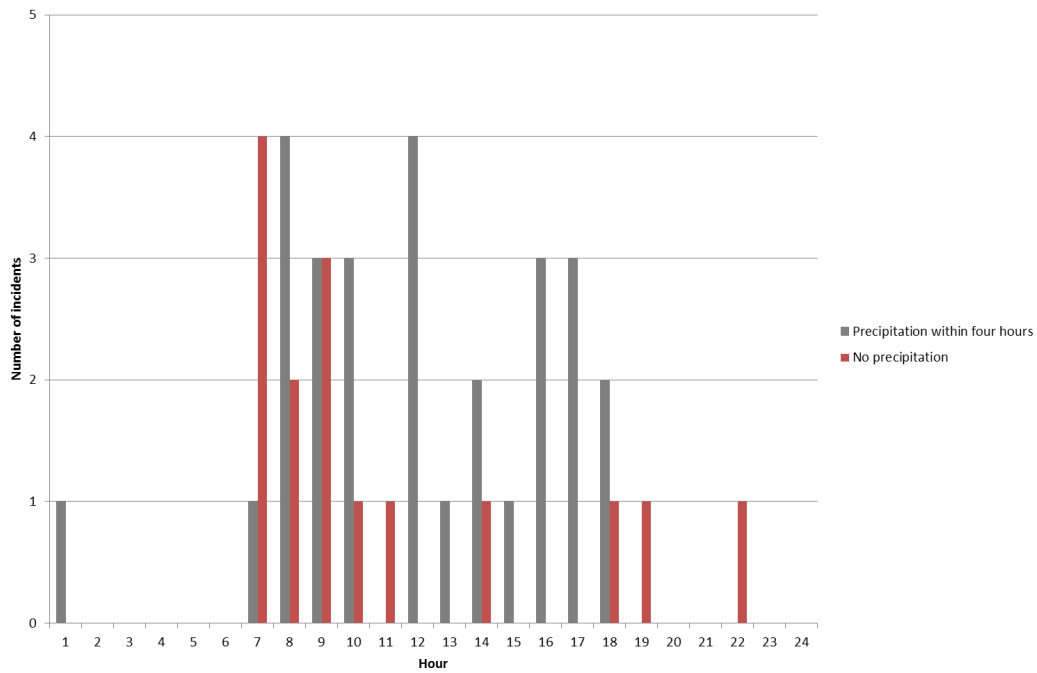


Figure 3.22: WSP events for Coventry station, plotted against precipitation data

3.7 Stockholm Case Study

Stockholm weather conditions in October 2006 were analysed and linked to a period of low adhesion between the 26th and 29th October in the Stockholm underground. Stockholm underground is divided into three lines, one is completely run in a tunnel environment and the other two are partially run in open air and thus subjected to a larger variation in environmental conditions. A substantial increase in the number of vehicles out of service due to wheel flats, often attributed to low adhesion, could be noted for the vehicles operating on the two lines run in open air, see Figure 3.23. The tunnel line however, showed no significant increase in wheel flats.

Data from a track based weather station is presented in Figure 3.24. This time period included a period of higher than average rains in the days prior to incidents and then no precipitation but mist, strong winds, decreasing temperature, and finally ice and frost on the days of increased wheel flats, as summarized in Figure 3.25. There was reduced cloud cover which likely led to decrease temperatures and an increased chance of dew or frost on the railhead. Strong winds may have also blown any remaining leaves onto the railhead.

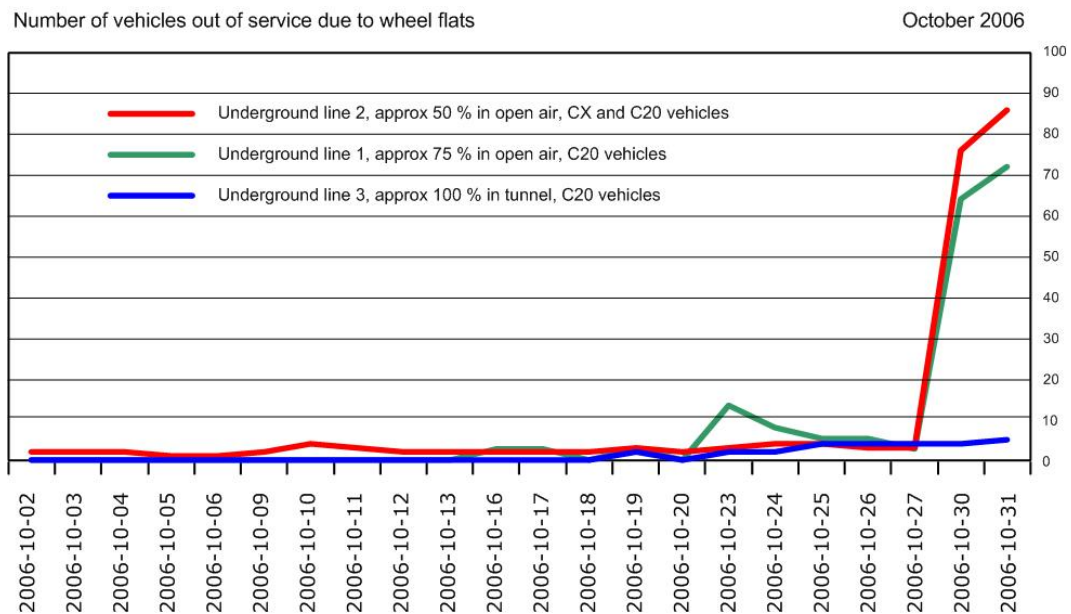


Figure 3.23: Number of wheel flats during October 2006

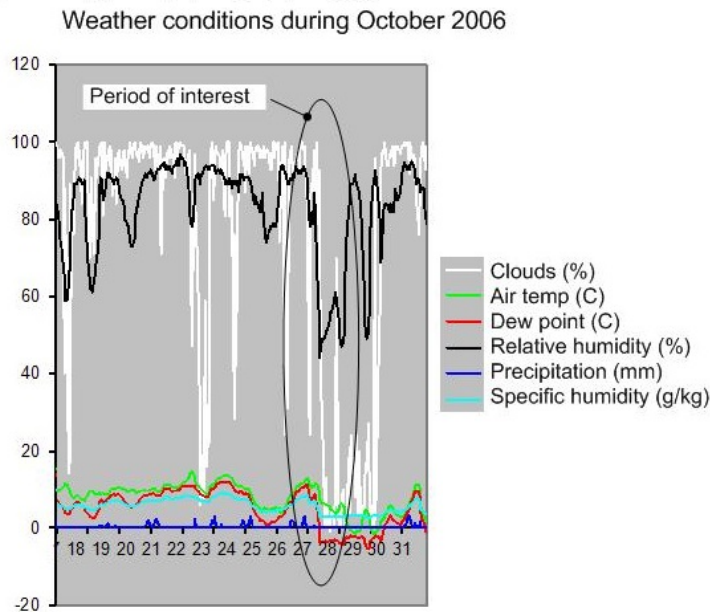


Figure 3.24: Weather conditions during October 2006

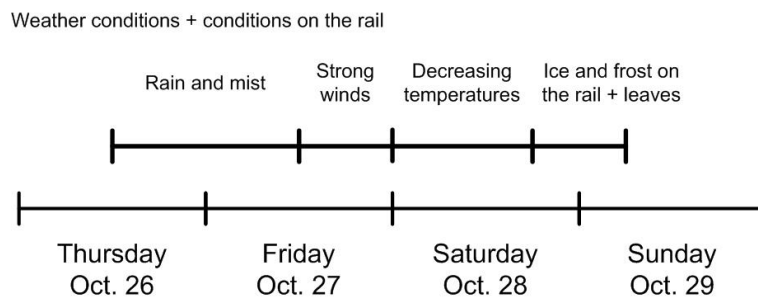


Figure 3.25: Summary of the weather conditions during the period of increasing number of wheel flats

3.8 Conclusions

The addition of 2013 and 2014 data to the previous RSSB T1042 project [5] emphasised the key trends found, notably the high number of incidents during the hours of 0600-0900 and the large number of incidents that occur in seemingly uncontaminated conditions. After mapping the Network Rail data, incident grouping could be seen around certain regions on certain dates. Individual analysis of problem periods, shown in Figures 3.9-3.11, were able to provide an insight into the conditions that may lead to low adhesion incidents occurring, notably the tendency for incidents to occur after precipitation and large temperature fluctuations.

The precipitation data from various sites was shown visually. It shows a strong link between precipitation and low adhesion incidents between 1100 and 1700 hours. Many more incidents occur in the morning and evening that do not seem to correlate to any precipitation. These incidents also closely match the average diurnal humidity graph which supports the hypothesis that dew may be involved

These results are also in agreement with a Stockholm Underground case study of wheel flats which found that decreasing temperatures along with dew or frost on the line caused a number of wheel flats resulting from low adhesion.

WSP analysis shows an increase in low adhesion during morning and evening hours but the trend is not as clear as that seen in the Network Rail analysis. This may be because during the Network Rail analysis, the station overruns caused by organic contamination or driver error could be removed from the dataset. The WSP data cannot give any information on whether leaf contamination was present on the rail or whether there was driver error, which may explain why there are still a large number of WSP activations during the middle of the day with no precipitation. More WSP activations of a duration of 5 seconds or longer were seen at higher speeds, above 80 km/h which may be due to an inverse relationship between speed and traction coefficient, which was seen in the previous literature review. However, station overruns still occur when a train fails to stop in time for the station at lower speeds.

The previous literature review was able to provide a number of ways that iron oxides and water alone could provide the low adhesion seen in the wet-rail phenomenon. This chapter highlighted the large numbers of incidents that could be attributed to the wet-rail phenomenon, either involving no leaf contamination or an invisible layer. It was able to support the evidence of the wet-rail phenomenon occurring in morning and evening hours, especially where there was likely to have been dew on the rail or precipitation, and therefore highlights the importance of using small amounts of water and high humidities during future tests to replicate the wet-rail phenomenon.

4 Railhead Analysis

4.1 Introduction

The literature review in chapter 2 proposed mechanisms that could result in low adhesion due to the wet-rail phenomenon and the previous operational data chapter highlighted the number of low adhesion incidents that could be linked to the wet-rail phenomenon. Future laboratory tests will try to replicate the wet-rail phenomenon and modelling work will look into how changing iron oxide, water, and environmental conditions may affect low adhesion. A key input in all of the hypotheses, laboratory tests and modelling work is knowing what is on the railhead at any time and how any railhead materials such as iron oxides and water will behave in the wheel-rail contact. This chapter will focus on understanding the behaviour of iron oxides on the railhead and in the wheel-rail contact rather than their tribological properties, which will be analysed in future chapters.

This chapter is split into three sections that investigate iron oxide behaviour on the railhead and in the wheel-rail contact. The first uses the University of Sheffield full scale wheel/rail test rig to help understand how an iron oxide layer behaves in the contact patch. Oxide paste rheology continued the work carried out by Beagley et al. [25], looking at the shearing behaviour of iron oxide pastes. The final section focusses on images and notes taken from field track testing, helping generate more information to better understand how the wet-rail phenomenon may occur and how to generate representative conditions in the laboratory.

4.2 Laboratory Full Scale Testing

4.2.1 Introduction

The following section will focus on the fundamentals of oxide growth and movement on the railhead and in the wheel-rail contact to attempt to provide a better understanding of the quantity and behaviour of iron oxides or wear particles in the contact patch before, during, and after wheel passes

Investigations were carried out on 260 grade, previously used rail and the tests made use of the full scale wheel-rail (FSR) rig which provides a realistic contact patch size and shape, the materials are identical to those seen in a real wheel rail contact and that the correct contact pressure was applied.

The hydraulic actuators on the FSR move a rail under the full size wheel to cause it to rotate on an axle. A normal force is applied to the wheel axle using a hydraulic actuator, 75 kN has been chosen because it is approximately the single wheel load in a UK passenger locomotive. A chain is attached between the wheel and a hydraulic actuator, the chain can be pulled as the rail is moving to induce creep in the contact by rotating the wheel at a higher speed. A load cell is mounted that can measure the tangential force and by dividing by normal force the friction coefficient can be found,

which can be read throughout the wheel cycle. A schematic of FSR movement is shown in Figure 4.1.

The sequence of FSR movement is as follows:

1. Rail moved so that the wheel is at the zero point of the railhead
2. Wheel lowered and 75 kN normal force applied
3. Wheel rolled relative to rail, chain used to induce creep in wheel
4. Wheel raised and rail moved back to zero position and cycle repeated if necessary

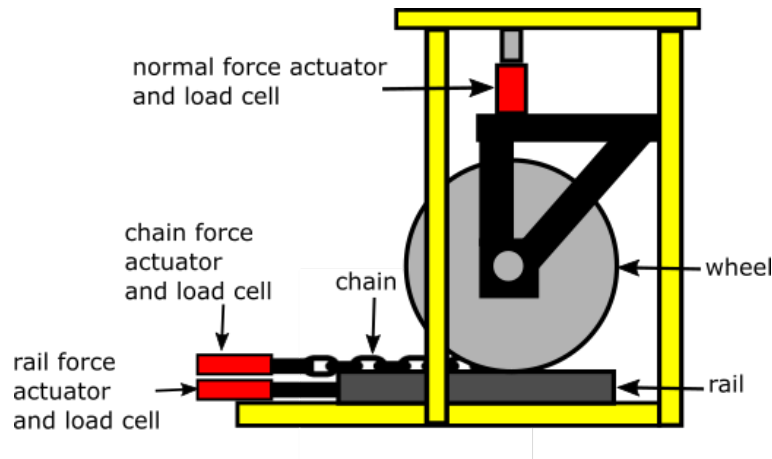


Figure 4.1: A schematic diagram of the full scale rig

4.2.2 Methodology

4.2.2.1 Oxide development

As discussed in the literature review, railhead oxide will become present very quickly after wetting and increases in depth over time. The rate of oxide growth over time depends on conditions such as rail condition, temperature, humidity and railhead moisture. Images were taken of an oxidising rail to assess how quickly an oxide layer would grow on the railhead in the laboratory. A small section of cut rail was used so that it would be easy to study. The rail material was cleaned with abrasive paper and water, then wiped to remove excess debris. This provided a shiny finish that looked similar to a rail that has had a recent wheel pass. The rail was not cleaned with solvents because the conditions were designed to be as realistic as possible.

Water volumes of 0.5 ml and 2 ml were added to the railhead using a syringe. The oxide growth was imaged over time to see how the oxide coating changed. This was repeated on the FSR test rail to assess the durability of these oxide layers upon wheel passage, but at 3 % slip these oxide layers were removed in a single cycle.

4.2.2.2 Oxide paste transfer

The railhead was again cleaned with abrasive paper and water, then wiped to remove excess debris. Iron oxide pastes were made to a particular weight percentage using water and hematite powder. Hematite was used because as highlighted in the literature review, it is likely to be the main oxide type found in surface rust, it could easily be purchased in bulk quantities and its bright red colour was very visible on the railhead.

Hematite powder was mixed with water to produce pastes with different weight percentages (wt %) of hematite to water. A known mass of paste was added to the railhead, 50 mm along on the rolling line of contact to ensure the wheel rolled through the paste rather than sitting on top of it at the beginning of the test. The paste was added to the contact running band where possible but at low viscosities or high volumes it typically spread out across the railhead away from the running band.

The FSR was run at 75 kN load, 3% slip and a velocity of 100 mm/s over a 350 mm contact patch, different weight percentages of hematite pastes were used between 40 % and 80 %, covering the region of high viscosity that was thought to produce low adhesion. The distance that the oxide paste was pushed along the railhead was measured with a ruler, images were taken and any observations were noted.

4.2.3 Results

4.2.3.1 Oxide development

Images were taken at regular intervals of a wetted railhead until the railhead was dry to document how rapidly the oxidation took place. Pictures for the 0.5 ml water application are shown on a timeline in 4.2 and pictures for the 2 ml water application shown in 4.3.

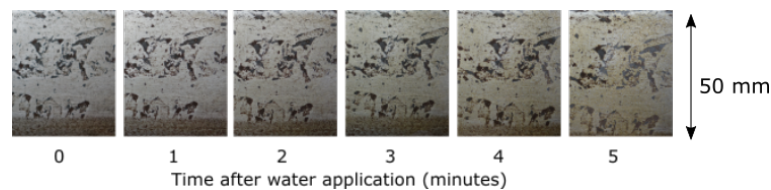


Figure 4.2: 0.5 ml water applied to the railhead

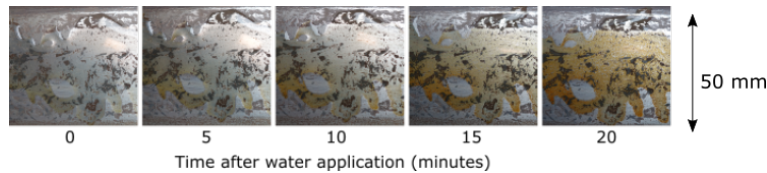


Figure 4.3: 2 ml water applied to the railhead

In both situations, a faintly visible orange layer was seen within 1 minute after water application. The larger volume of water will eventually form a thicker oxide layer, but the smaller volume of water spread thinly will form a thin oxide layer at a faster rate. This is likely due to the faster evaporation of a thinner layer of water to leave behind an oxide layer on the steel.

4.2.3.2 Investigations into oxide paste transfer

10 ml of 60 % weight hematite paste was initially added to the clean railhead, 50 mm away from the start position of the FSR contact so that the wheel could roll through the paste. After a single wheel pass the contact patch seemed to be completely dry, with the vast majority of oxide paste having been pushed out of the way. The oxide left was deposited as a compressed powder which was hard to remove from the railhead, with water being forced out. After 5 cycles the results are very similar, but the compressed layer in the contact patch seemed to be thicker, possibly due to new paste “pulled” into the contact. The iron oxide that was still present in the contact becomes a darker shade of red in places, this could either be due to change of morphology due to contact heat/pressure, or alternatively the oxide could have been mixed with other wear particles and oil. Images of the paste after 1 and 5 cycles are shown in Figure 4.4.

It can be seen that the water is important as a “carrier” in this situation, the oxide particles in the contact will only travel as far as the bulk water will go and oxide powder is deposited along the rail running band, the oxide paste sticks to the wheel and is spread further along the railhead. The oxide travelled 150 mm down the railhead over 5 cycles. Figure 4.5 shows the end of the oxide paste layer, where it could not be pushed any further along the railhead. There is a concentrated, dry pile of oxide at the end of the paste layer where it has not been pushed any further, possibly because at this point the water had been squeezed out the line of contact and the oxide became too dry to push any further along the railhead.

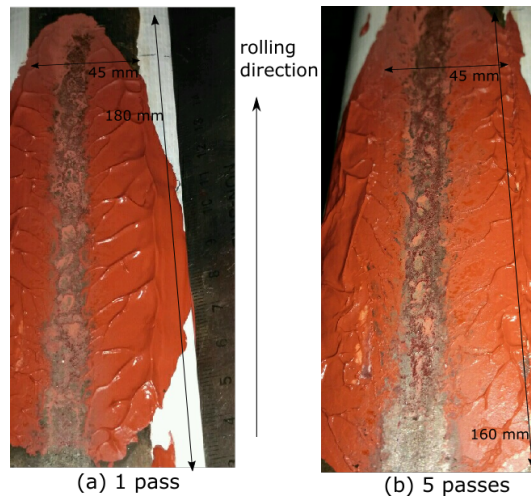


Figure 4.4: 10 ml of 60 % hematite paste (a) 1 pass; (b) 5 passes

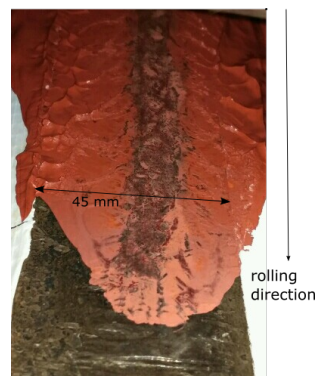


Figure 4.5: The end of the paste “trail”

A much smaller amount, 2 ml of oxide paste, was then used using the same method to see if this changes the spread of oxide along the rail. It was seen in Figure 4.6 that the 2 ml oxide travelled just as far as the 10 ml of oxide, with less excess oxide having been pushed out of the contact patch. This implies that the contact patch could be saturated with just 2 ml of oxide and anything extra is pushed out of the contact band quickly before it can be rolled along the railhead. There is still a lot of excess oxide paste present, so lower quantities of oxide may still be able to travel down the railhead.

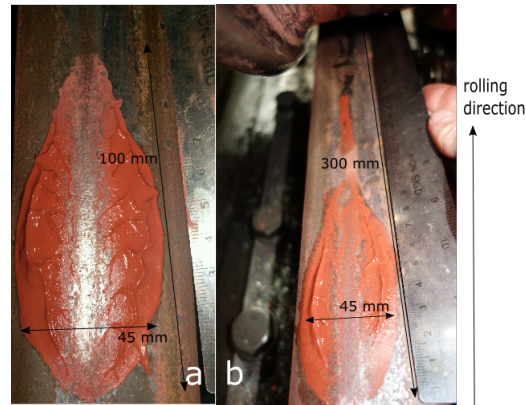


Figure 4.6: 2 ml of 60 % hematite paste after 5 cycles

A series of tests were carried out to assess the behaviour of different wt % of oxide paste. 2 ml of different weight percentages of hematite paste, ranging from 40% to 80% were placed as far under the wheel as possible and the FSR run for 10 cycles for each test. The maximum distance that the oxide paste was pushed along the railhead contact patch after 1, 5 and 10 cycles was measured. Results are shown in Table 4.1.

40 % hematite paste behaved in a similar manner to the 50 % paste, the wheel easily pushed the paste out of the way, running over the sides and covering the entire 300 mm contact band with a very thin oxide layer. A difference between these two percentages may have been seen if a smaller volume of oxide was used or the contact length was larger. Images for 50% oxide paste are pictured in Figure 4.7.

A large difference in results was seen between 50 and 60 wt % paste. The 60 wt % paste was only pushed 120 mm along the contact band but a much thicker layer was deposited in the line of contact as shown in 4.6.

In a real wheel-rail situation water may lay on top of a more viscous oxide layer so this was simulated. 2 ml of 60% oxide paste was rolled 5 times and then left on the railhead for 5 minutes, then sprayed on the upper surface with approximately 0.2 ml water mist. 5 wheel passes were once again made and the difference was notable as seen in Figure 4.8. The water being sprayed directly on top of the oxide meant that new paste seemed to be pulled into the contact and oxide paste was spread down the entire 30 cm contact length in a similar manner to the lower viscosity tests. In these 60 % oxide plus mist addition tests there seemed to be a lower amount of oxide at the end of the contact patch, so it may not have spread as far down the railhead as the 50 % if the wheel could continue over a longer length. However, there was a visibly thicker layer oxide along the contact band than on the 50 % oxide tests, the oxide was stickier and more compacted with less oxide runoff over the sides of the railhead.

A control test was carried out by replicating the same conditions as the previous test but without the water spray. 5 wheel passes were carried out on the oxide paste, before waiting 5 minutes and then the wheel was passed another 5 times. In this case no new oxide spread was seen on the second set of wheel passes, the dry oxide is unable to be pushed further along the rail without the addition of surface water.

70 % hematite spread over a shorter distance, 80 mm, but resulted in a thicker layer of hematite deposit than the 60 %. 80 % behaved in a similar way.

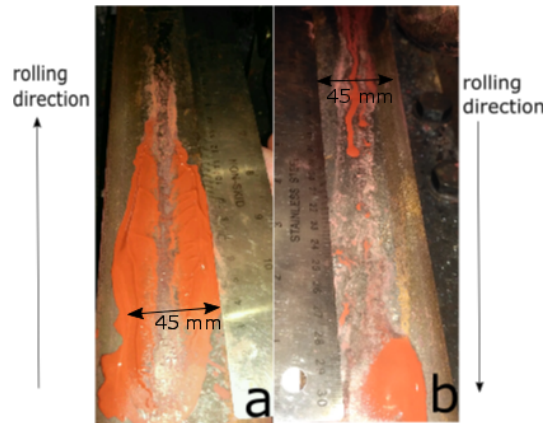


Figure 4.7: 2 ml of 50 wt % hematite paste. (a) beginning of contact (b) end of contact

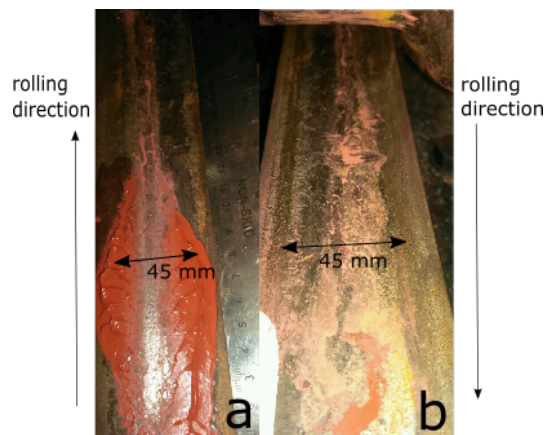


Figure 4.8: 2 ml of 60 wt % hematite paste after misting. (a) beginning of contact (b) end of contact

Wt % hematite	Distance (mm) 1 Pass	5 Passes	10 Passes	Notes
40	300	300	300	Very watery, lots of runoff
50	160	200	300	Watery layer, lots of runoff
60	100	120	120	Thick oxide layer
60 (+ water mist)	300	300	300	Thick oxide layer
70	80	80	80	Very thick oxide layer
80	80	80	80	Very thick oxide layer

Table 4.1: Railhead travel distances for different wt % hematite pastes

4.2.4 Discussion

The 50 and 60 % oxide pastes had very different properties. The 60 % iron oxide paste kept its shape and remained as a thick layer on the railhead, but did not travel as far, whilst 40 and 50 wt % covered the railhead, but did not produce a thick layer and were easily pushed out of the contact patch. This may show why low amounts of water can cause the wet-rail phenomenon by making a paste, yet high amounts of water will dilute the third body layer too much so it does not build up a layer in the contact patch.

The paste sticks to the wheel as it rolls over the rail and is subsequently transported and compressed along the railhead in a similar way to the aluminium powder that was discussed in the literature review [23]. Hematite pastes of 60 wt % and higher have a dry patch of oxide at the end of the contact patch where not enough water is available to carry the oxide any further whilst less viscous oxide pastes have a “puddle” of less viscous oxide and water at the end of the contact patch, where the water has been pushed further than the oxide powder. This shows a distinct difference in behaviour between 50 and 60 wt % hematite pastes.

If a locomotive with multiple carriages and wheelsets were to roll over a patch of oxide with the correct viscosity and volume of water, the oxide paste could be pushed along the railhead. This means that if caused by a paste, low adhesion conditions would not have to be consistent down a railhead and after a wheel pass, patches of paste could become one continuous band of paste covered railhead. Patches of less viscous paste could be pushed a long way down the railhead and then dry out over time to produce the viscous paste in one continuous band that could produce low adhesion over long distances.

In Figure 4.8, a small amount of 60 % paste was initially dried and compacted after 5 cycles. Upon mist addition, more paste was pulled into the contact. This could provide a mechanism to how low adhesion can occur for long periods of time over a number of wheel passes, the paste may be “used up”, pushed out or compacted in the contact, however under the right conditions when water settles on the railhead, the contaminants surrounding the contact band may be pulled into the contact patch.

The 60 wt % oxide may bear similarities to that seen in dew, mist or light rain in a real railway situation. A dry oxide layer may be re-wetted with a surface layer of dew or light rain to provide an easily sheared surface layer on top of a more viscous and supportive bottom layer. The 40 and 50 wt % may reflect what could happen under heavier rain, with the oxide mixing with large amounts of water and washing off the railhead.

The work carried out here provides information about how a paste could move down the railhead, as well as providing information about the quantities of oxides needed for testing. In particular it highlights how little paste would be needed to coat a railhead, the 2 ml paste tests still have a lot of excessive paste which is pushed out of the contact patch, so only a small quantity of paste would be needed to coat the railhead contact.

4.3 Iron Oxide Rheometry

4.3.1 Introduction to tests

As highlighted in the literature review, previous data from Beagley et al. [25] has suggested that an oxide paste is able to reduce the traction coefficient and could cause the wet rail phenomenon. Beagley found the yield shear stress of these pastes using a parallel plate plastometer, a device that can be used to measure the rheometry of viscous materials such as oxide pastes.

The parallel plate plastometer works by loading a sample between two parallel plates and applying a normal force, the increase in diameter as the sample is loaded and the height of the sample layer under load can be related to the yield shear stress of the paste.

Beagley et al. [25] then used the yield shear stress and limiting height of the sample under load as input values into a model which could predict the friction coefficient when a wheel passed over an oxide coated rail. This provides a way to better understand the conditions that cause wet-rail phenomenon and also to efficiently compare the effect of different contaminants on the friction coefficient. If the model can be validated with experimental data, it could provide an method to simulate the effect of a drying railhead, where reducing moisture levels can play a large role in the changing friction coefficient.

Test equipment has become more sophisticated since Beagley's work so a modern rheometer was used to repeat the tests, with a schematic of the rheometer shown in Figure 4.9. The modern rheometer is able to gather changes in shear stress with increased shear rate and may be used to increase the understanding of how iron oxides behave in the wheel-rail contact. It consists of two parallel plates, these compress a sample mounted onto the lower plate to a specified "gap height", the distance between the two plates. Torque is then applied to the upper plate and the speed of rotation as torque increases is logged.

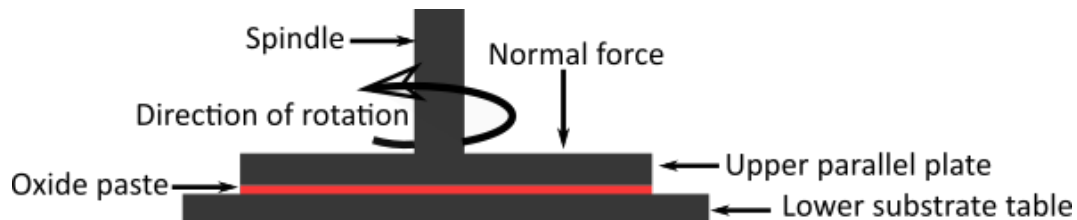


Figure 4.9: A schematic of the parallel plate plastometer

4.3.2 Methodology

Hematite pastes and water were made to different weight percentages and shaken before testing to ensure they were mixed. A TA Instruments AR 2000 rheometer was set up with a 40 mm parallel plate geometry. Hematite paste was added to the substrate table and the parallel plate lowered to 1 mm above the table surface. The parallel plate was then spun with increasing torque until spinning at 100 rpm. The torque, converted to shear stress, needed to spin the parallel plate at increasing rate is logged, with the yield shear stress being the point at which the sample begins to shear.

4.3.3 Results

The shear stress of 50-70 wt % of hematite pastes is plotted against the increasing shear rate between 0.01 and 100 cycles per second, data for two repeats is shown in Figures 4.10 and 4.11. Hematite pastes above 70 wt % could not be tested due to shear force limitations of the rheometer.

Alternative plots of shear rate against viscosity for each repeat are shown in Figures 4.12 and 4.13.

The point at which the torque applied is high enough to shear the material and start rotating the geometry is known as the yield shear stress. Values were averaged over two repeats and plotted in Figure 4.14, alongside the data from Beagley's previous paper [25].

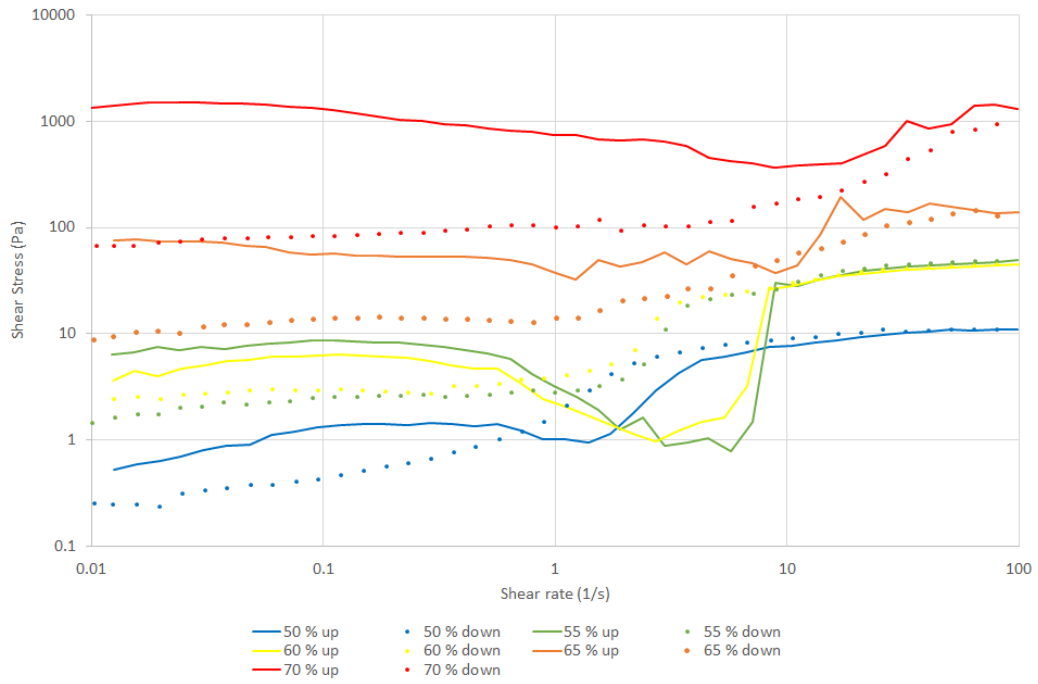


Figure 4.10: Shear rate plotted against shear stress for different hematite wt % (repeat 1)

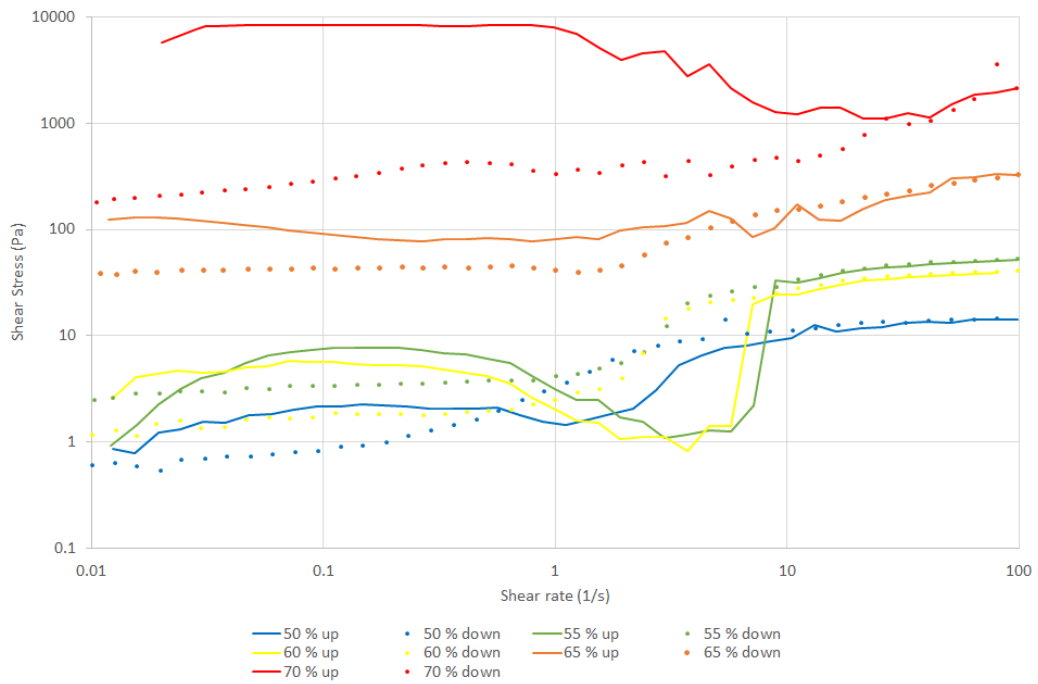


Figure 4.11: Shear rate plotted against shear stress for different hematite wt % (repeat 2)

4.3 Iron Oxide Rheometry

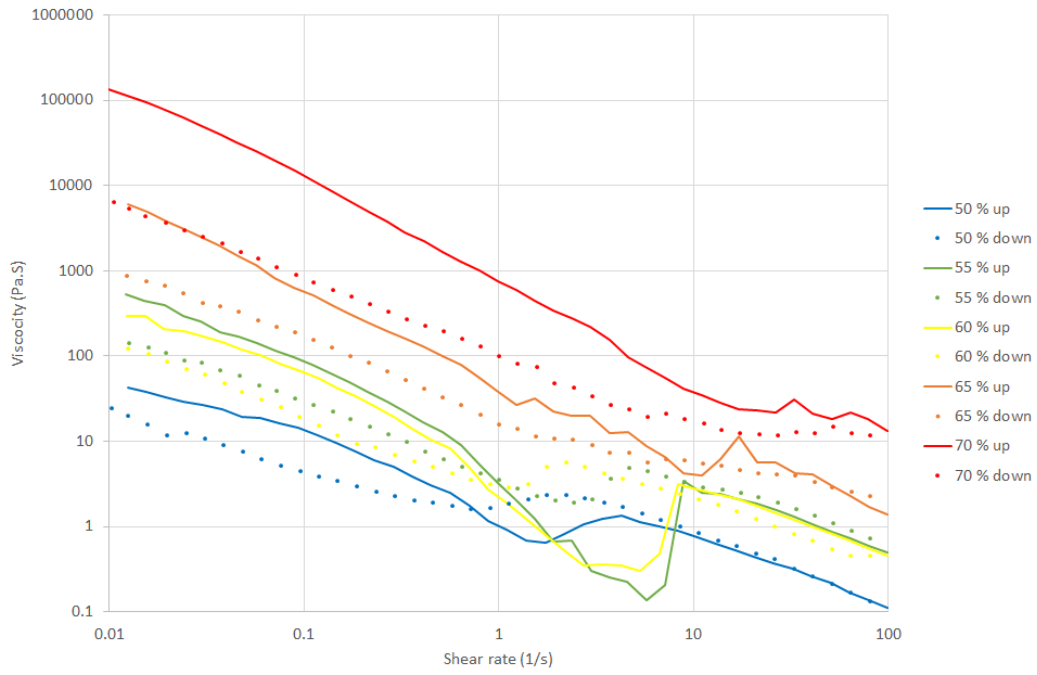


Figure 4.12: Shear rate plotted against viscosity for different hematite wt % (repeat 1)

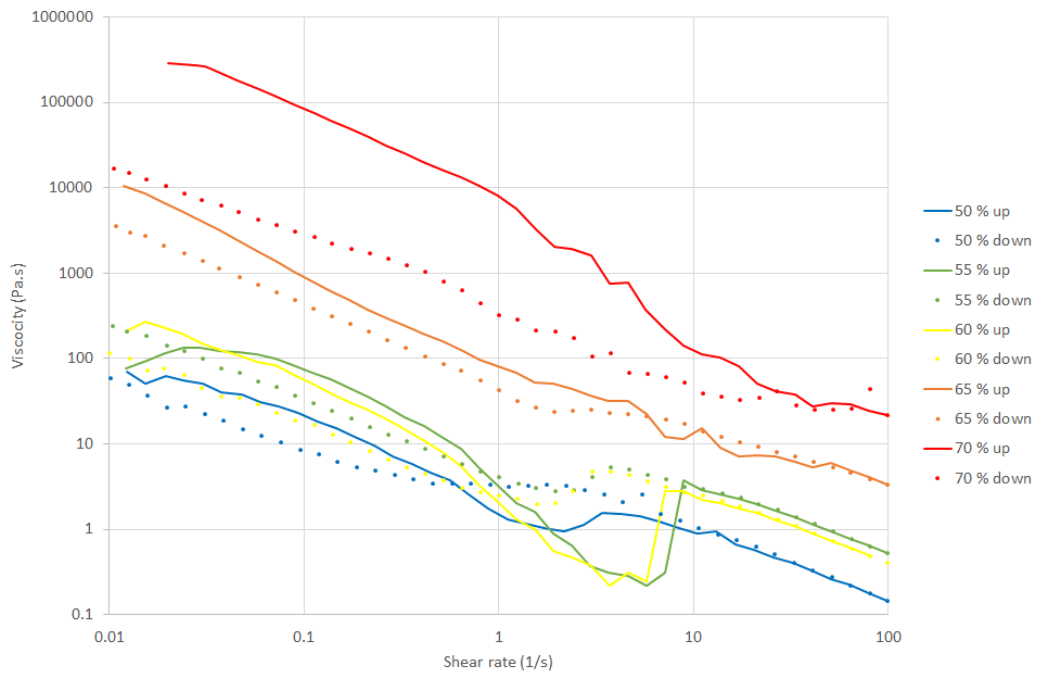


Figure 4.13: Shear rate plotted against viscosity for different hematite wt % (repeat 2)

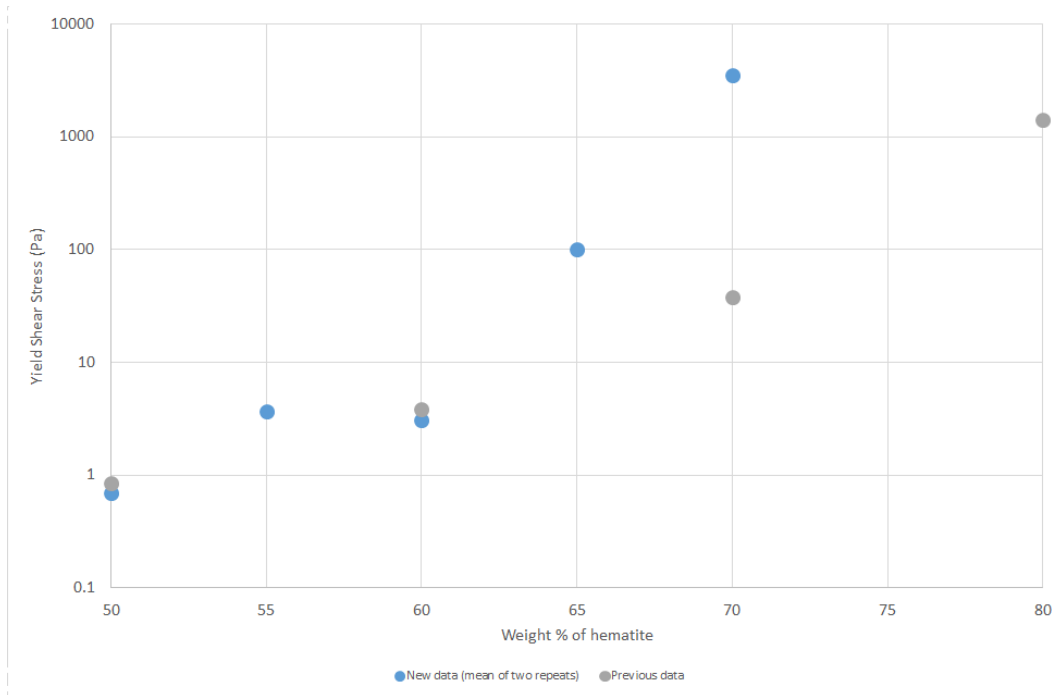


Figure 4.14: Yield shear stress of the new data, plotted against Beagley’s previous data [25]

4.3.4 Discussion

The yield shear stresses of different weight percentages of hematite paste have been previously gathered but their behaviour over different shear rates is something that has not been previously investigated. The iron oxides exhibited complex non-newtonian behaviour which may explain how the wet-rail phenomenon can be difficult to replicate, as the pastes behave differently at different shear rates.

The hematite pastes mostly show a decrease in viscosity over the test duration, although there is a rapid thickening mid way through the tests for 55 and 60 weight %. Previous reports have stated that rate dependent shear thinning is unlikely to occur for granular suspensions such as these pastes [59], so the effect seen here is likely to be time dependent. The paste is initially difficult to shear, but when the paste starts flowing it becomes easier. This effect could be due to the breakdown of the electrostatic network between particles as shear occurs. These tests occur over 10 minutes which is long in comparison to the time that an oxide paste will be sheared in the wheel/rail contact so it is important to focus on the initial yield stresses. This may explain why the wet-rail phenomenon can be difficult to replicate on continuously running test rigs, for instance a twin disc test may involve continuous movement of any oxide paste rather than having time to stabilise between train wheel passes.

The rheometer used here has a very low normal load of 1 N whilst Beagley's data replicated the real wheel-rail contact load. The shear stress is likely to be even higher under a larger load due the fact that liquid is likely to be squeezed out because it is more mobile than the solid phase whilst the affinity between liquid and solid phase will remain constant. As a result, the solid particle concentration will increase and particles will "jam" more readily, which produces rapid increases in shear stress [60]. More water may be squeezed out of the paste as creep increases up to sliding point between wheel and rail which would increase the shear stress. When full sliding occurs the paste may be pushed in front of the wheel, which will continue the low adhesion situation by pushing the paste further along the railhead.

An example of this "jamming" behaviour is seen for 55 and 60 wt % hematite at a shear rate between 1 and 10 s⁻¹. The overall trend is one of shear thinning, but at a shear rate of approximately 7 s⁻¹ there is a stage of rapid shear thickening. A shear thickening effect has been noted previously in iron oxides [25] and it was surprising that it was not seen in these results. Shear thickening may only occur at higher pressures than seen in this work, but also may only occur at a specific shear rate which would explain the sudden shear thickening seen in this work. Due to the pressure limitations on the available rheometer, it would be beneficial for these tests to be repeated on a rheometer that could obtain realistic wheel-rail contact pressures of approximately 1 GPa to assess if these results remain valid.

The hematite paste was seen to separate at the end of some tests in a similar way to that seen in the previous full scale testing. The phenomenon of "shear banding" was seen during some preliminary tests. This occurs when a shear plane is formed due to phase separation in the paste, in this situation water is likely to separate from the solid particles due to being more mobile and create a band across the sample [61]. This occurred during these tests when water was placed outside the sample to prevent the exposed edge from drying, a common rheological practice. The yield shear stress remained similar to the sample without added water but the behaviour upon yielding was dramatically different. Without the water addition there is a gradual increase in shear rate after the yield point, however, with water addition there was a rapid increase in shear rate after yielding so the test had to be stopped early. This is likely because water was pulled in from outside the sample and rather than mixing with the paste, forming a shear band on top of the viscous paste. This is useful information when looking at how water can be "pulled" into the contact from outside and how small amounts of water can sit on top of the third body layer rather than mixing, which may provide a mechanism for very low adhesion.

The hematite will become saturated in the paste at a certain point, at which point any extra hematite added will simply be found as a dry powder. This would be difficult to determine for hematite powder due to the range of particle sizes, but needs to be considered when looking at very high wt % of pastes.

The yield shear stress data shown in Figure 4.14 shows a a rapid increase in yield shear stress at lower wt % of hematite than Beagley's data [25]. This could be due

to more modern experimental equipment or differences in particle size of hematite powder used. Beagley [25] used a much higher load when collecting yield shear stress data, but this is likely to cause the opposite effect and increase the yield shear further, as discussed previously.

The work done in this section is able to show the large differences between different wt % of iron oxide paste. The behaviour under shear is able to provide hypotheses for how the wet-rail phenomenon may occur and propagate down the railhead. The yield shear stresses can be used for future modelling work, updating the data that Beagley [25] gathered.

4.4 Field Testing

4.4.1 Introduction to tests

Field testing was carried out using a locomotive on a 3 mile loop of track in Long Marston. The train was braked on a 3 m section of wetted rail and the stopping distance was noted. Weather data was collected using a trackside weather station and images were taken. This field testing was carried out for another project so although the braking results will not be published here, the images taken during the course of the work provide useful information on the mechanisms that could cause the wet-rail phenomenon.

4.4.2 Results

Weather data for the track over 3 days of testing is shown in Figure 4.15. 3 weather stations were located around the track, station 2 being close to where the train was braked. On October 12th, during the third day of testing, the rail temperature in the morning was above that of the dew point so dew was formed on the railhead.

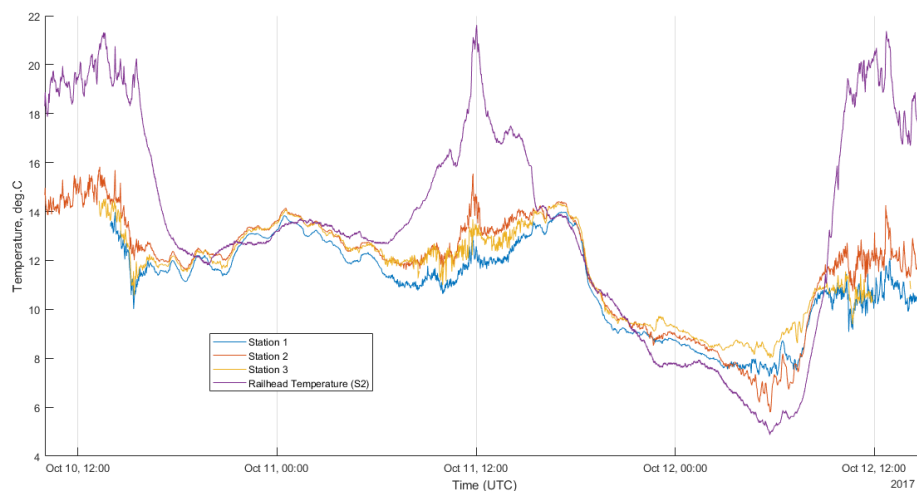


Figure 4.15: Data from 3 weather stations throughout the track testing

The first images, shown in Figure 4.16, were from a railhead with dew present in the morning before testing. The running band was initially a metallic silver, but upon rubbing it was clear that there was a brown paste on the surface, shown in image “A”. When this dried, the paste settles back onto the surface to create a visible but loosely bonded layer that could be wiped off, which would become the third body layer during a wheel pass, shown in image “B”.

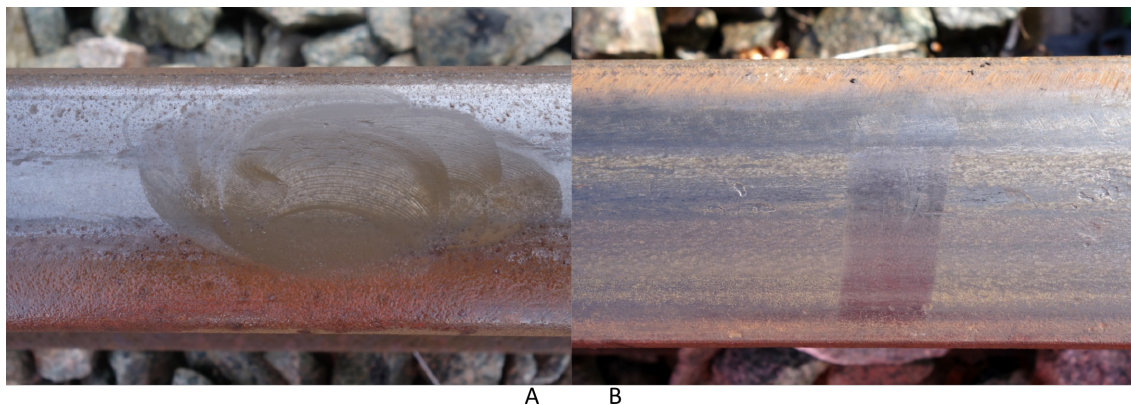


Figure 4.16: Iron oxide and dew present on the railhead when wet (A) and when dry (B)

Large wheel slides occurred in testing and the running band after a wheel slide during wet conditions is shown in Figure 4.17. Image “A” shows the railhead directly after wheel slide, while image “B” shows the railhead 10 minutes after wheel slide. The images are not taken from the same area but they are from the same railhead, approximately 1 m apart and subjected to the same conditions. It is clear that

any oxide layer formed would be removed, steel fragments have been worn from the railhead and the light blue colour of these fragments suggests that the railhead was heated to approximately 330 °C. After wheel sliding in wet conditions, a thick, orange iron oxide layer formed very quickly after less than 10 minutes after the wheel pass. This was likely because the passivating oxide film, along with any contaminants, were removed by the wheel so the steel is exposed and rapidly oxidised to form a much more strongly bonded oxide than that seen on the early morning dew railhead. The oxide formed in this stage was removed during the next wheel slide, but showed how a paste could be formed on the railhead when this oxide and wear debris mixes with water such as the dew shown in Figure 4.16.

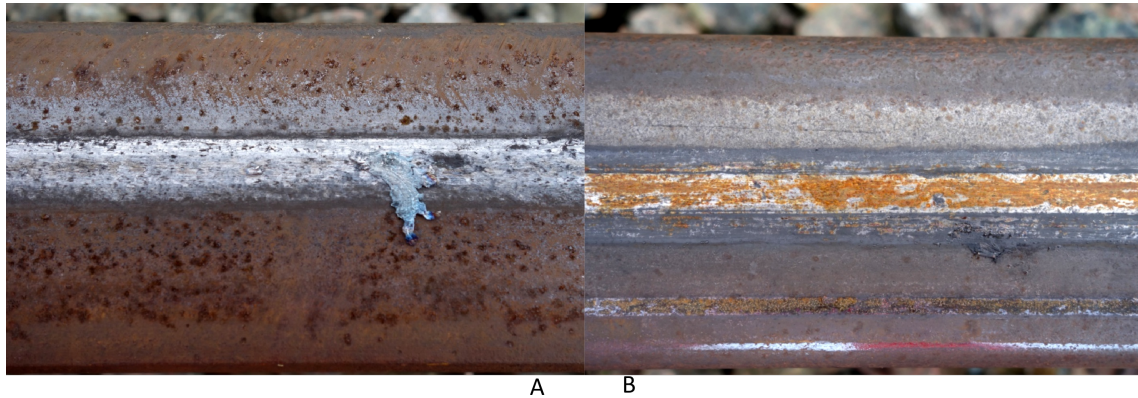


Figure 4.17: A wetted railhead (A) approximately 1 minute after a wheel slide, (B) approximately 10 minutes after a wheel slide

When this oxide layer was artificially wetted before the next test and once again wiped, it shows a paste that is similar to that seen in the early morning dew railhead, this time with a visible oxide layer underneath that seemed to be strongly bonded to the steel and was difficult to remove when the surface was scratched, meaning that the oxide was bonded to the main steel substrate rather than separated wear particles. An image of this paste on top of an intact oxide layer is shown in Figure 4.18.



Figure 4.18: A paste formed on top of the railhead after artificial wetting

4.4.3 Discussion

In terms of the hypotheses proposed in chapter 2, it seems unrealistic to suggest that an iron oxide layer could remain intact if the sliding forces and heat are high enough to remove pieces of steel as large as those seen in Figure 4.17. However, this is an example of an extreme wheelslide on a closed track, in reality the driver or WSP system would attempt to reduce the braking force to prevent such a long wheelslide. The oxide layer may remain intact until the wheels slide, at which point it is removed, but combines with the paste formed in the internal source flow to create a more viscous paste and lower adhesion levels further. It also seems likely that any water settling on top would mix with the loosely bonded third body layer and mix further in the contact itself so a paste would be formed rapidly.

A strongly bonded oxide layer formed quickly after a wheel slide, likely because of the exposed steel. It was also noted that during periods of high humidity, condensation formed on the railhead between tests so a layer of water would be once again present on the railhead shortly after a wheel slide. The literature review highlighted how there is almost always some sort of iron oxide layer between the steel and the third body layer formed from loose iron oxides, wear debris and water, but this can vary in thickness, which may change its behaviour.

It is currently unclear whether this thick underlying oxide layer is essential for low adhesion conditions or whether the paste alone could cause low adhesion, so subsequent tests will use both intact and naturally formed iron oxide layers, as well as oxide pastes, to investigate how the wet-rail phenomenon may occur.

4.5 Conclusions

The testing using the FSR highlighted the different behaviour of oxide pastes when rolled over in a replica wheel-rail contact. The low viscosity pastes below 60 %

spread a long way down the railhead but did not build up a layer of oxide on the railhead, whilst the viscous pastes of 60 % and above did not spread as far over the railhead but built up a thick layer of compressed oxide powder between wheel and rail. This work helped to understand how pastes behave in the contact itself with water pushed out and the paste essentially becoming more viscous in the contact, something that would be difficult to observe outside a laboratory. The FSR runs at slower speeds than most railway situations but the separation of water and oxide may be even more prevalent at higher speeds due to the dynamic forces acting upon the pastes.

A more detailed study into hematite paste behaviour in the rheometry work helped understand how the pastes respond to increasing shear rates over time. The yield shear stresses from this study provide valuable input data towards the modelling that will be carried out in chapter 5. Unfortunately the rheometry work did not distinguish between time or rate dependent shear thinning, but the former is more likely after assessing previous studies.

The images from Long Marston track testing showed that the dew mixed with a third body layer on top of the railhead to form a paste as hypothesised in the literature review. The track condition after testing showed that it was unlikely that an oxide layer could remain intact after a low adhesion induced wheel slide or multiple wheel passes so it was likely that the pastes formed would cause the wet-rail phenomenon rather than an intact oxide layer. The track that was still wetted after testing oxidised quickly, this oxide layer may be removed in the contact and help form the paste.

These three studies of iron oxides highlighted a number of behaviours that can help understand the mechanism of the wet-rail phenomenon, design test methodologies to replicate the wet-rail phenomenon and more effectively create and test mitigation methods.

5 Modelling

5.1 Introduction

The literature review showed that low adhesion due to iron oxides and water alone had been achieved using some test methods, but was not seen in others. The operational data analysis highlighted that low adhesion conditions could occur unexpectedly and only under specific conditions. As discussed previously, a huge number of factors could be affecting adhesion and low adhesion due to the wet-rail phenomenon is likely to only occur under very specific conditions, therefore it is important to make sure any tests carried out will focus on the most likely low adhesion conditions.

The objective for this chapter is to use modelling in order to develop a better understanding of low adhesion conditions and discover which conditions are most likely to cause low adhesion, so the test methods used to recreate them can be more effective.

The modelling will provide a better understanding why the wet-rail phenomenon is difficult to replicate, as well as allowing simulation of adhesion conditions may change with contact conditions. The modelling will also help in understanding how the methods and conditions used to replicate low adhesion need to change between test rigs used over the course of this work, and why low adhesion may be unobtainable using certain methods yet still occur in the real wheel-rail contact. As such, a successful model will be able to determine how friction will change in the wheel-rail contact as conditions vary, but also be transferable to other test rigs in order to assess how factors such as contact patch size, contact patch geometry and speed will affect adhesion levels.

A number of models have been created to model adhesion in the wheel rail contact, including those for a dry contact and with water. The effects of substances in the contact that are not pure water are harder to predict and less understood so there are fewer models available. The RSSB T1077 project [29] produced a comprehensive list of models which analyse the effects of water on the railhead and looked at models that could be modified to show how iron oxide or other third body contaminants could affect the wheel rail contact. Modelling was a useful addition, but not the main focus of this thesis so a model was needed that was freely available for use, could assess changes in third body layer, could be used relevantly with the test rigs in this work and was able to operate simply with low computational power. A model for low adhesion which suits these criteria has been created in collaboration between RSSB and Virtual Vehicle, known as the “adhesion model” [62].

5.2 Adhesion Model

The adhesion model was designed to estimate the friction coefficient (known in this model as the adhesion coefficient) of a high pressure torsion (HPT) contact where a paste of a known yield shear strength is present. It is not designed to provide

absolute values but to be used as a tool which can predict the change in adhesion coefficient when certain contact conditions are changed. A detailed description of the adhesion model is contained in Buckley-Johnstone et al. [62] and should be referred to if necessary, but this chapter will provide a summary to outline the key equations. This chapter at first replicates the model and then modifies it to suit the current work using the SUROS twin disc test rig. It also analyses in more detail the sensitivity of the model to different input parameters.

Key parts of this model were taken from previous work using parallel plastometers [63] so it is essential to provide a basic understanding on how these operate. A parallel plastometer is shown below. A known volume of paste, in this case iron oxide and water, is placed between two parallel plates, of radius a , that are pushed together with a normal force, N . The plates are enclosed in a cylinder so that the paste is limited to a circle of a known radius when compressed. The separation of the two plates due to the iron oxide paste, h , can be linked to the yield shear strength of the paste.

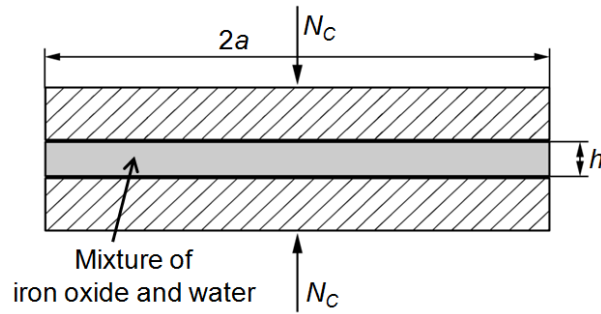


Figure 5.1: A schematic parallel plate plastometer [62]

The adhesion coefficient, f , can be taken as the tangential force in a contact, divided by the normal force applied. Therefore the coefficient in this model can be taken as the sum of the tangential forces from the asperities (T_B) and the iron oxide (T_C), divided by the sum of the normal force upon the asperities (N_B) and iron oxide (N_C). A schematic of this is shown in Figure 5.2 and it can be written as (5.1).

$$f = \frac{T_B + T_C}{N_B + N_C} \quad (5.1)$$

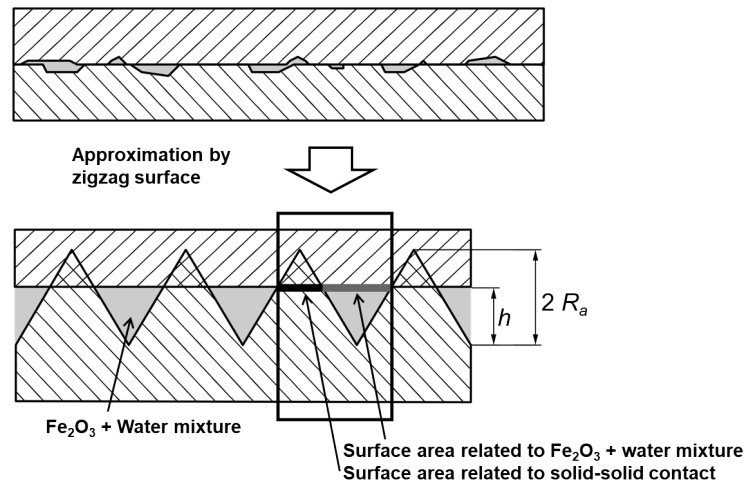


Figure 5.2: A schematic of the parallel plate contact, showing surface area related to the oxide paste and the solid-solid contact [62]

The adhesion model uses the following variables that could be changed to represent changing wheel rail contact conditions

- yield shear strength of the iron oxide and water paste
- the amount of paste that enters the contact
- surface roughness
- boundary friction value between metal and metal contact (where no paste is present)

Yield shear strength values for the iron oxide and water paste were initially taken from Beagleys results [64, 25] and the shear strength for varying weight ratios of iron oxide and water (replicated and plotted in modern software) are plotted in Figure 5.3.

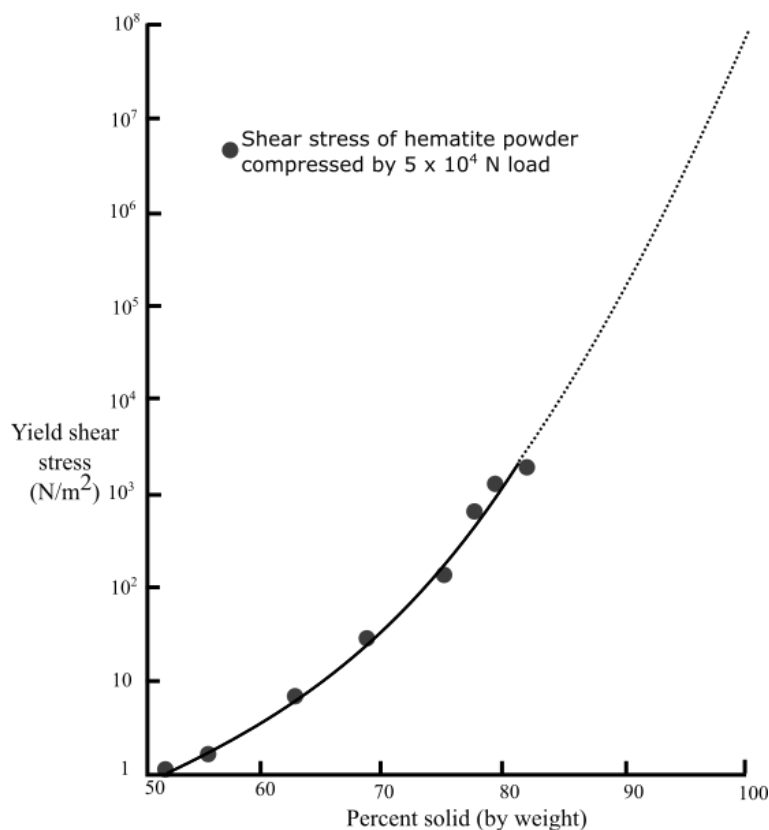


Figure 5.3: Percentage solid plotted against yield shear stress [25]

The relationship between the yield shear stress and percentage solid was used as a key initial input into the adhesion model. The separation of the surfaces is dependent on the yield strength and squeeze flow theory [63] is applied to determine the surface separation. For a circular contact and static separation when using the parallel plate plastometer, equation 5.2 can be used to find the static separation of the two plates:

$$N_C = \frac{2\pi a^3 \tau}{3h} \quad (5.2)$$

Where h is separation, a is plate radius and τ is shear yield stress. N_B can then be determined by subtracting N_C from N .

Friction is metal-metal asperity dominated at low yield strength of iron oxide paste, which results in the friction coefficient being equal to the boundary friction coefficient. As the yield strength increases, the iron oxide paste is able to support more of the normal force and therefore influences the adhesion coefficient

The adhesion coefficient of a wet contact, without oxide addition, is used as an upper boundary friction. The low viscosity of water will not support the parallel

plate load so the boundary friction is used to provide an upper friction limit which is entirely metal on metal. Increasing the wt % of iron oxide will reduce the amount of metal-metal contact between the plates because the increased oxide viscosity. Up to a certain point, an increasing thickness of paste in the contact will reduce the metal-metal contact and therefore reduce the friction coefficient. The tangential force transmitted by the hematite paste is calculated as equation 5.3. A_C is the area associated with the hematite paste in the contact, obtained by subtracting the area associated with asperities from the total area, worked out using a gaussian height distribution.

$$T_C = A_C \tau \quad (5.3)$$

The surface roughness will also play a role in the amount of metal-metal contact due to the importance of the oxide paste/surface roughness ratio, a rough contact will increase the amount of steel-steel contact between asperities. A lower surface roughness and therefore lower asperity height compared to paste thickness will result in lower volumes of iron oxide paste needed to reduce the metal-metal contact to a point in which low adhesion can occur.

The outputs of the model as used in the previous paper [62] are shown in Figure 5.4. The resulting change in the coefficient of adhesion at 3 different roughness (Ra) values, 0.1 μm , 1 μm and 10 μm are shown in Figure 5.5. The roughness values used are based on the information gained from the literature review [12], 10 μm represent a freshly ground rail, 1 μm a worn rail and 0.1 μm a very worn rail. A lower roughness value produces low adhesion at a lower solid oxide fraction. 0.1 μm and 1 μm will still result in very low adhesion, but the range of solid oxide fractions that cause low adhesion is larger for the lower roughness. At 10 μm , low adhesion is not produced at any solid oxide fraction value.

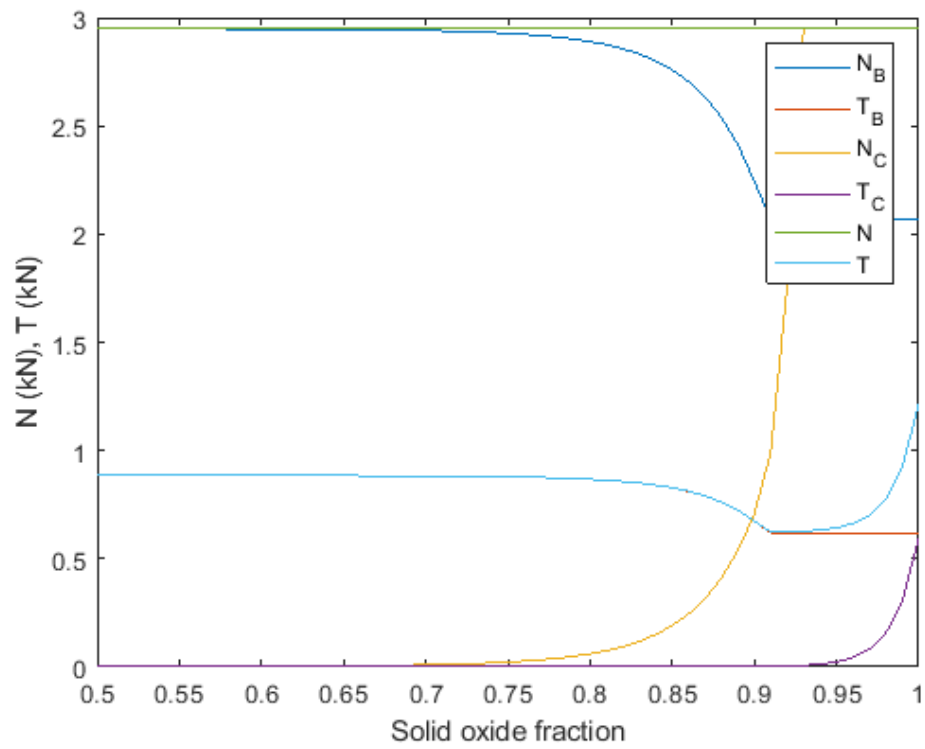


Figure 5.4: Model outputs for increasing solid oxide fraction with input values $N = 2.9$ kN, $Ra=1$ μm , $\mu=0.3$

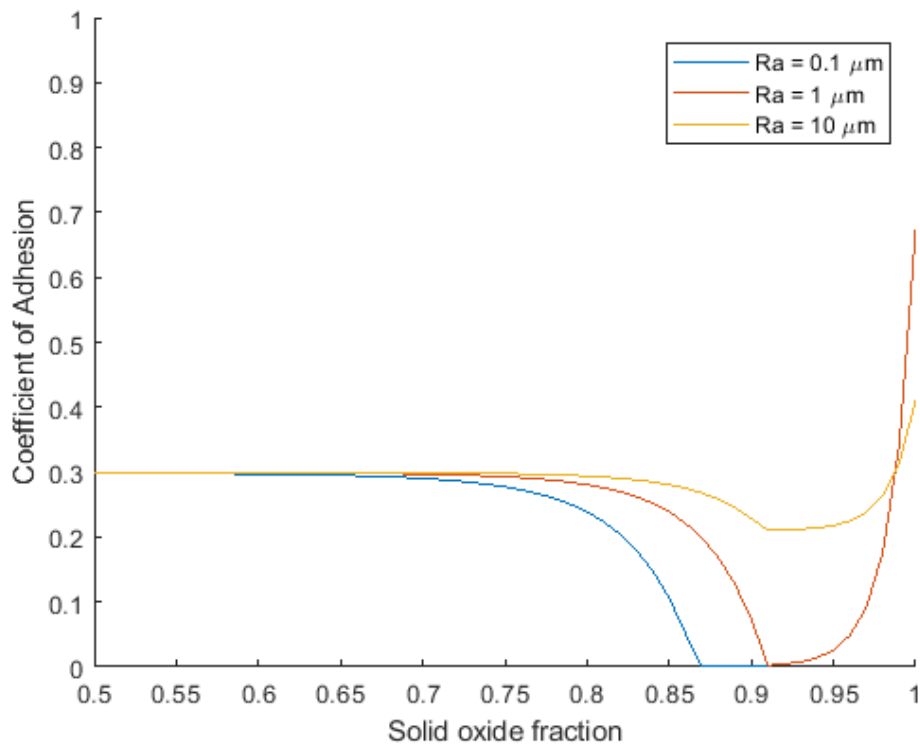


Figure 5.5: The change in coefficient of adhesion at different roughness values

5.3 Modifications

Work was carried out to modify this model for the Sheffield University rolling sliding twin disc test rig, SUROS, described in detail in chapter 6, so it could be used later in this work. The original low adhesion model was developed for parallel plate plastometry and cannot be completely modified to fit the twin disc contact, a rectangular contact between two cylinders, due to the different mechanism of contact. The parallel plate is approximated as a quasi-static contact in the adhesion model, whilst there are more dynamic effects occurring in the twin disc contact, the model is also based around a large circular contact which cannot be used for the twin disc. Attempts have been made to add these modifications to the model, but applied in combination they remove the model too far from its original use and produce erroneous results due to the very small area of contact, so instead the impact of each change on the model will be discussed separately.

Even if it is unable to be completely modified, analysing how the model can be changed to fit the twin disc test rig and looking at the output data may help understand any changes in adhesion. The overall concept of the model remains similar so the results may be comparable and show how certain conditions may effect ad-

hesion, rather than focusing on absolute values. Even with a change in contact patch and dynamic effects, the higher wt % hematite paste is still able to support a higher fraction of the normal and tangential forces and therefore produce a lower adhesion coefficient than a lower wt % paste where a larger fraction of the load will be supported by steel-steel contact so the results are still useful to interpret.

A simple modification is that the base adhesion coefficient will change. The wet value, with no oxide addition, of the twin disc tests is approximately 0.18 so the model can be changed to match this. The lower baseline adhesion, shown in Figure 5.6, shows similar results to the previous data in Figure 5.5. The solid oxide fraction at which adhesion is reduced remains the same, with the only change seen in the boundary adhesion at lower solid oxide fractions.

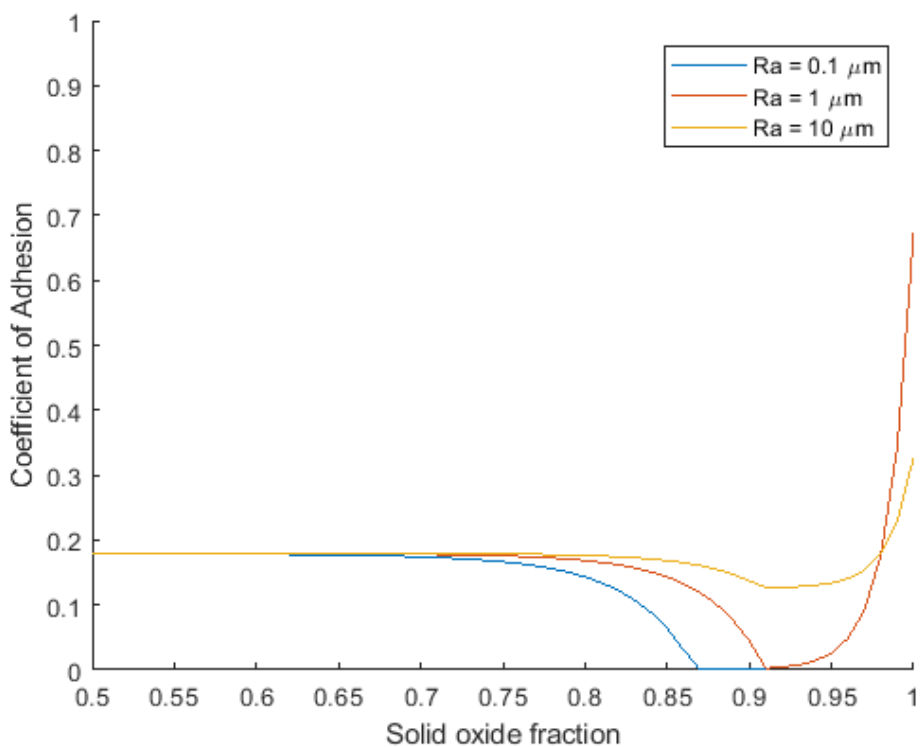


Figure 5.6: The change in coefficient of adhesion at different roughness values

The rheometry results in the previous chapter provided new data for the shear behaviour of iron oxides. The yield shear strength of the higher percentage oxides is higher than that of the previous results [25]. The new results, plotted with a line of best fit against those previously determined, are shown in Figure 5.7. The key difference in test methods between the previous and new results is that the previous results used a representative load of 10^4 N, but this could not be represented on the modern rheometer.

After the saturation point, the ratio of paste to dry oxide will decrease. With some water likely to be squeezed out, this makes it more likely that the twin disc and real wheel/rail contacts will give dry adhesion values after this point so the adhesion coefficient will rise rapidly. As such, τ may rise even more steeply after a solid oxide fraction of 0.7 as predicted here, but experimental evidence for this would be difficult to gather due to the high viscosity. The model is used to predict where the minimum value in traction may be and so values after this point have not yet been considered, in reality the traction coefficient would likely rise up to a maximum dry value and plateau, experimental data for this will be collected later in this work but it has not been added to the model.

The model was updated with the new τ values and a graph was plotted for the previously used values, shown in Figure 5.8. In comparison to Figure 5.6, the adhesion drops to low values at lower solid oxide fractions, due to the model predicting a larger oxide layer thickness for each oxide fraction due to the increased τ .

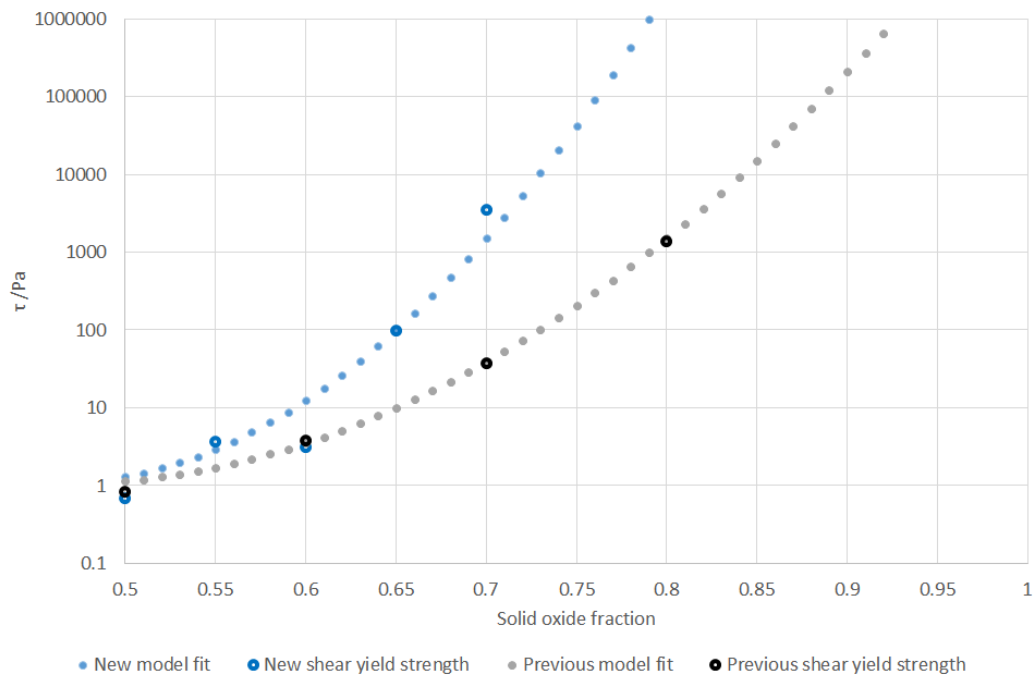


Figure 5.7: The yield shear strength, τ , of different oxide fractions. Data collected in this work is plotted against the previous data [25]

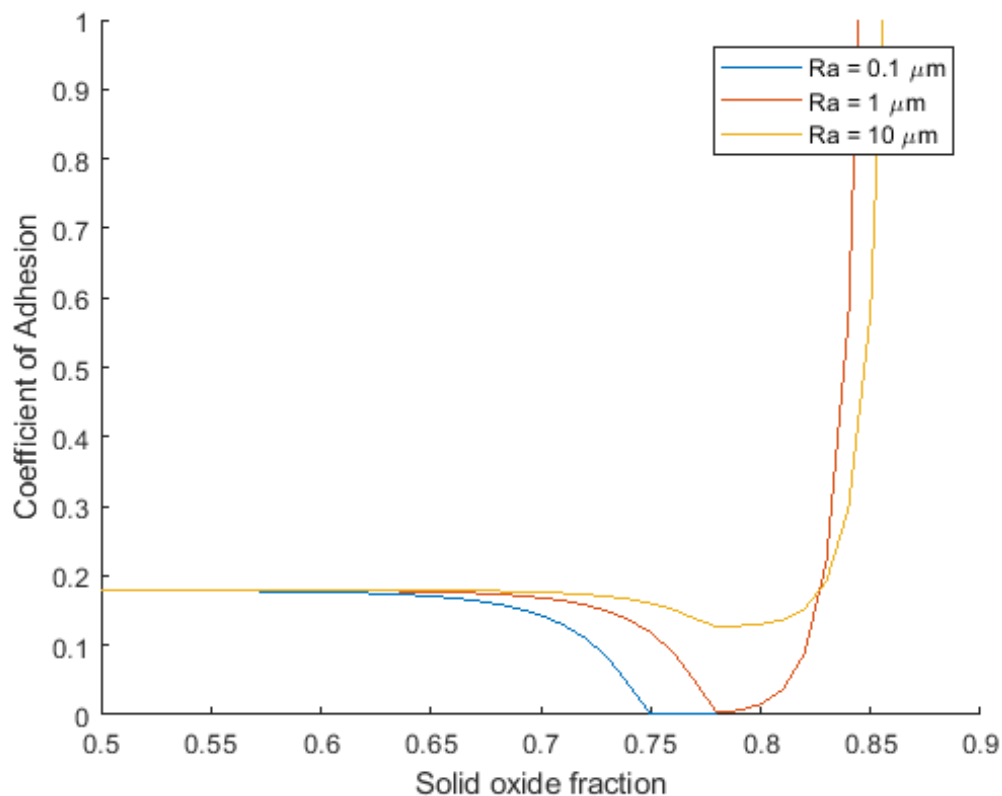


Figure 5.8: Coefficient of adhesion plotted against solid oxide fraction for different Ra values, using the updated τ values

The twin disc rig has a much smaller contact patch than the HPT, which the previous model was based on and the parallel plate plastometer, which the equations for this model were derived from. The twin disc contact patch size was estimated using Hertzian contact approximations and used as an input value into this model, alongside the updated τ value. The twin disc contact is rectangular rather than circular but is still a useful input into the model to assess how a smaller contact may change adhesion levels. The output is shown in Figure 5.9. With the smaller contact patch, the adhesion coefficient drops to a minimum at a higher solid oxide fraction.

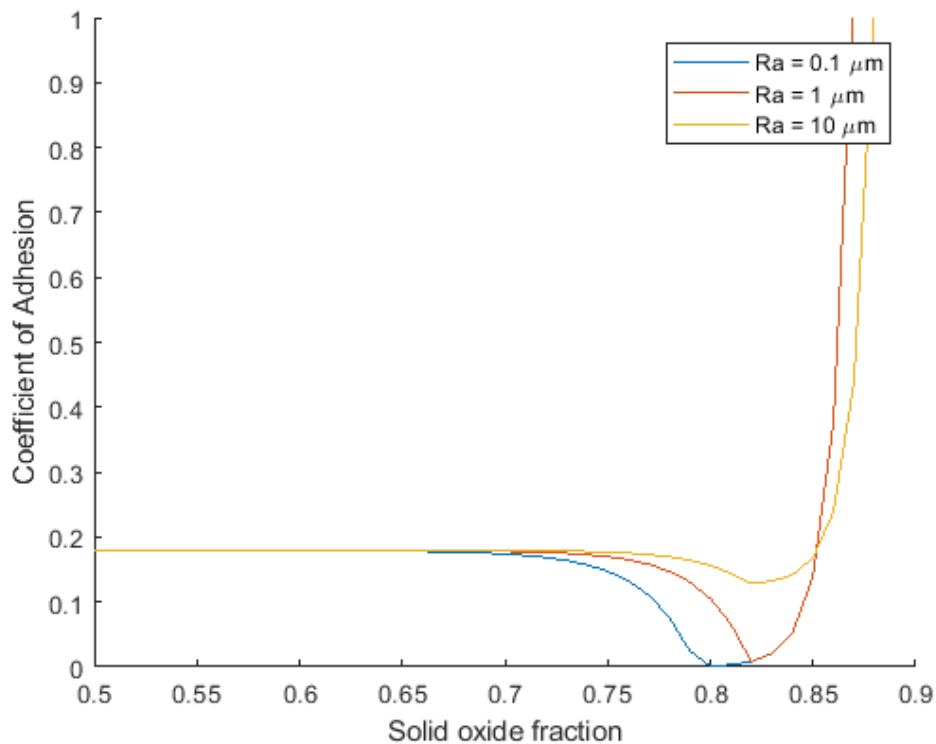


Figure 5.9: Coefficient of adhesion plotted against solid oxide fraction for different Ra values, using a contact patch size based on the twin disc test rig

As seen in the railhead investigations, iron oxide paste in the contact is likely to separate into water and oxide powder to some extent. The full scale testing in chapter 4 showed water being squeezed out of the contact, leaving a layer of viscous oxide paste or dry oxide powder in the contact.

Because of this, the viscosity of the paste in the contact is likely to be higher than the paste that was added to the contact, potentially “shifting” the equivalent friction coefficient on the model so that lower friction coefficients occur at lower wt % of hematite. This would be difficult to integrate into the model due to not being able to work out how much water is squeezed from the contact, but the predicted change is that low adhesion would occur at a lower solid oxide fraction than is currently predicted in the model and “shift” the curves to the left.

The model described here does not take into account dynamic conditions. Iron oxide added between two bodies in a dynamic contact will initially have a lower separation due to leakage. A lower separation, h , will be found for each oxide fraction but this may be offset by the increased likelihood of water being squeezed out preferentially to oxide particles as discussed in the rheology work. The separation of a dynamic contact should be based upon shear stress rather than yield shear strength values due to the applied shear on the paste, if shear thickening behaviour occurs as seen

in Beagley's work [25] then this will cause an increase in τ values for each solid oxide fraction and "shift" the curves further left with low adhesion occurring at a lower solid oxide fraction than predicted.

In a rolling sliding contact there will be a continuous flow of solids and liquids through the contact and some of the debris in the contact is likely to be squeezed out by the increased pressure. The metal-to-metal contact forces (Nb) are likely to increase due to the oxide being squeezed out of the contact. However, the moving contact patch will ensure a continuous supply of oxide and water paste as long as conditions remain consistent. The thickness of oxide layer is likely to be lower for the dynamic movement than the quasi-static conditions described in the original model.

5.4 Conclusions

The new data suggests that the τ value for each solid oxide fraction may be higher than previously suggested and may be higher still with increased loads. As a result, the model here predicts that the lowering of adhesion will occur at a lower solid oxide fraction for contacts with a low combined roughness. This may be even lower when the effects of increased shear rate and oxide paste thickening due to water separation in the contact itself are considered. This fits in well with the saturation point of the iron oxide paste which may occur at approximately 0.7 solid oxide fraction as discussed in the previous chapter.

The model was not able to be completely modified for the twin disc contact and a completely new model may have to be created in order to represent the small contact and dynamic effects. However, the model here serves its purpose in predicting how different conditions may affect adhesion. The model does not currently include an "upper limit" for dry friction coefficient, which is typically around 0.6 for the twin disc rig. The low roughness value of Ra 0.1 μm produced low adhesion that does not rise to a dry value, a change in the model to predict the rise in adhesion to a dry value at saturation point could be added but these were not essential here, with the model serving its purpose to predict the changes in producing low adhesion, but could be investigated if necessary in future work.

The narrow window of conditions that cause low adhesion seen in this model provide support to the observations seen from the operational analysis that low adhesion is very rarely seen for long periods of time. The key predictions from the model that can be taken forward into future testing are that low roughness values and high solid oxide fractions, as long as they are below the suspension saturation point, are most likely to produce low adhesion.

6 Test rigs and Preliminary Investigations

6.1 Introduction

The literature review in chapter 2 highlighted the difficulties with recreating low adhesion conditions due to the wet-rail phenomenon in the laboratory using existing methods and showed that no studies had successfully replicated low adhesion for significant periods of time using iron oxide and water alone. Very little research had been carried out to assess whether low adhesion could be produced using iron oxide and water alone, or whether the wet-rail phenomenon needs organic contamination to occur. The following chapter was designed to increase knowledge of the wet-rail phenomenon by recreating the conditions that may cause low friction using small scale rigs and observe whether certain conditions will lower friction. The results from this work will be used to investigate the hypotheses proposed in the literature review.

Small scale testing allows the large range of conditions that could produce the wet-rail phenomenon to be tested far quicker and with more control than would be achievable using full scale tests. Specimens can be analysed to better understand any changes in friction or morphology that took place during the test.

Based on the information gained from the literature review, an ideal small scale test that could be used to repeatably replicate and better understand the wet-rail phenomenon would achieve the following:

1. To be able to generate representative and repeatable low friction values
2. To be able to vary contact conditions such as pressure, velocity and creep
3. To be able to vary the type and quantity of oxide used
4. To be able to vary the quantity of water used, using different application methods
5. To be able to vary environmental conditions, such as temperature and humidity
6. To be able to remove samples after testing to perform tribological and chemical analysis

A single rig and method was not able to achieve all of these points, so different rigs and methods were used, with each having its own benefits and problems. When a reliable method of producing low adhesion was found, a more comprehensive set of

tests were carried out which are detailed in chapter 7, to see how low adhesion is affected by different conditions, based on the knowledge gained from this chapter.

A number of different rigs and conditions needed to be tested over a large range of different conditions. If a method was clearly not going to produce low adhesion then a full set of results was not carried out before moving onto the next to maximise the chances of finding a method that produced low adhesion in the time available. The same contact conditions and methodology were used where possible to ensure a systematic approach to the problem, but this was often difficult to implement due to the variation between rigs.

The modelling work highlighted the importance of focussing small scale testing on low roughness values and high oxide viscosities so tests were focussed on this.

The initial structure of this chapter was as follows:

- Identify the most useful test rigs to use and explain the workings and capabilities of each test rig, before showing the methodologies that were used during this work
- Decide which oxide and water application methods should be used during this work
- Carry out preliminary tests using different equipment over a wide range of conditions to assess if any are able to reproduce low adhesion
- Use knowledge gained to understand why the wet-rail phenomenon may occur and to design a more comprehensive series of tests in the next chapter

6.1.1 Rig selection

A number of tribological test rigs were available for use in this project and three rigs were focussed on to carry out this testing. An overview of each method is shown in Table 6.2.

Test Rig and contact type	Advantages	Disadvantages	Previous use
Pendulum Rig (uni-directional sliding contact)	<ul style="list-style-type: none"> • μ can be obtained • Portable and quick • Rail can be left to oxidise • Third bodies can be pre-applied 	<ul style="list-style-type: none"> • Produces a slip resistance value rather than friction coefficient • Not capable of realistic contact pressures 	[27] [65]
Bruker UMT (linear reciprocating or rotational sliding contact)	<ul style="list-style-type: none"> • Humidity can be controlled • Realistic contact pressure (1500 MPa) • Versatile, modular construction • Higher speeds than other test rigs (2 m/s) 	<ul style="list-style-type: none"> • Third bodies can be pre-applied or applied during test • Specimens can be oxidised • Purely sliding rather than rolling/sliding contact 	[26] [66] [39]
SUROS twin disc (rolling-sliding contact)	<ul style="list-style-type: none"> • Rolling/sliding contact (0-100 % slip) • Can use realistic materials for both discs • Discs can be pre-oxidised and third bodies can be pre-applied or applied during test • Realistic contact pressure (1500 MPa) 	<ul style="list-style-type: none"> • Maximum disc speed of 1 m/s 	[28] [4]

Table 6.2: Test method matrix

The pendulum rig was chosen initially due to the ease of testing under a variety of conditions. The main benefit was that it is portable so data could be collected on rail outside the laboratory.

The Bruker UMT rig was also chosen. Contact conditions such as velocity and normal force could be easily controlled which would allow the conditions that may cause the wet-rail phenomenon to be investigated. Samples could be made from steel, third body oxide powders could be applied or the specimens themselves could be oxidised. It was also the only rig available that had a purpose built humidity chamber and the literature review showed that high humidities may have a key role in the wet-rail phenomenon.

The SUROS rig produced a rolling/sliding contact which is most similar to that seen in a real wheel-rail contact. It allowed for water to be dripped into the contact and contaminants manually added so it was decided that this would provide the final small scale test method in this study.

Each rig will be introduced later in this chapter. The methodologies used for each rig to investigate the wet-rail phenomenon will be described and the results presented before a discussion of the results. All tests were carried out at room temperature (between 20 and 24 °C) and unless otherwise mentioned, at a relative humidity between 40 and 60 %.

6.1.2 Oxide and water application

6.1.2.1 Oxide application

Both naturally “generated” and artificially “applied” iron oxides were used over the course of this testing. Methods were created that could be used on as many of the test rigs as possible to allow continuity between methods. The difference in specimens meant that the same method could not be used between test rigs, but the methods were kept as similar as possible.

Naturally “generated” oxides could be formed on steel test specimens. This was often done by simply cleaning and then wetting the steel surface, allowing oxide to form as it dried. A humidity chamber was used if a thicker oxide layer was required. When using the SUROS rig, the heat and pressure of the contact could produce an oxide layer without needing any water addition.

These generated layers produced a natural oxide layer which better replicates what would occur on the railhead, but the oxide formed varied in thickness and colour so tests were often hard to repeat and small differences in conditions could have a large impact on the final oxide layer.

To create a more repeatable oxide layer, iron oxide and water pastes were used. Iron oxide pastes were formed from iron oxide particles and water and applied to the contact, allowing conditions to be kept more constant than those in the generated

oxides due to not having a condition dependent pre-oxidation step. The pastes were made by mixing a known mass of iron oxide powder, bought from a chemical supplier, with a known mass of water in a beaker to form a suspension of particles in a liquid. Hematite and magnetite powders were used because the literature review found them to be two common oxides found on the railhead and were readily available as powders.

The pastes are made as a weight percentage (wt %), for example with 10 g of 60 % hematite paste being made by mixing 6 g of hematite powder and 4 g water. Hematite (Fe_2O_3) and magnetite (Fe_3O_4) powders were used, each with a large size distribution of particles which were thought to better resemble what would be seen in a real wheel-rail contact, rather than very small particle size distributions. SEM images of the hematite and magnetite powders that were used are shown in Figures 6.1 and 6.2.

The pastes could be applied in a specific volume using a syringe. The oxides, especially the higher viscosities, would spread out very little when dropped onto a surface so it was difficult to add the same thickness of oxide paste for the UMT and pendulum rigs in particular. However, the amount of excess oxide pushed out during each test implies that the contact was saturated with oxide paste and the excess pushed out, which may mean that over a certain threshold, the thickness does not effect the results.

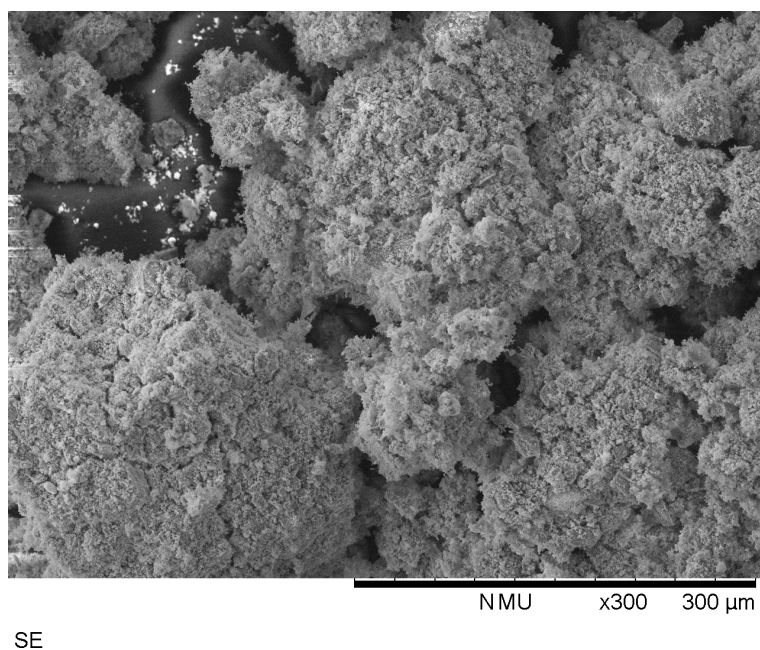


Figure 6.1: SEM image of hematite powder

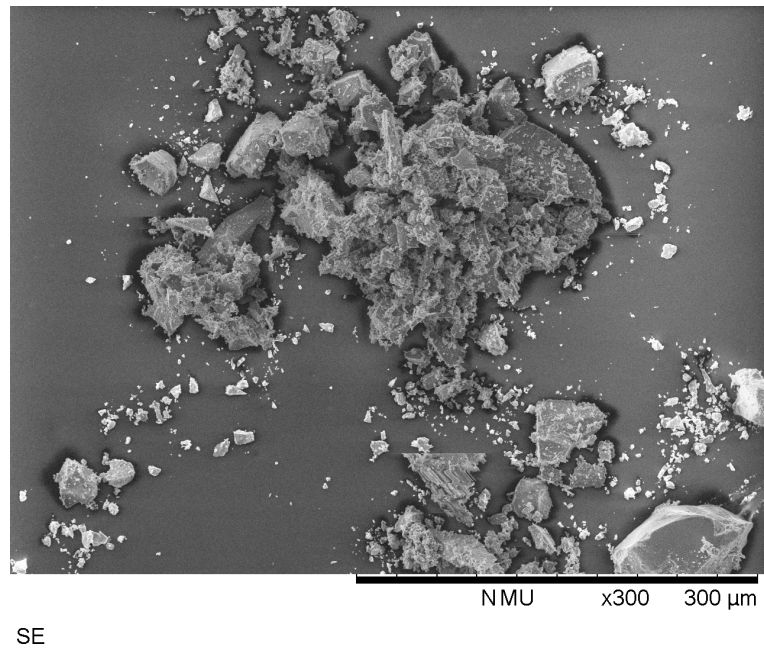


Figure 6.2: SEM image of magnetite powder

The two types of iron oxide particles look very different, the red hematite having a much more rounded structure than the black and more angular magnetite, Magnetite seems to be present as separate particles whilst the hematite is present as an agglomerate, it was expected that the pastes would have different properties in the contact. Particle size distributions were not available for these powders but these powders were chosen because of the large particle size distribution as would likely be found in the real contact, compared to those that could be bought with a known distribution, which generally had a limited range. Hematite paste was more stable and “stickier”, meaning it remained as a suspension and stuck to any substrate it was left on. Magnetite in comparison, separated into a layer of powder below a layer of water very quickly and ran off any substrate unless it was level, rather than sticking to it. The difference between the two suspensions is seen in Figure 6.3. Each rig has been tested with both naturally “generated” and artificially “applied” oxide pastes to allow a range of conditions to be assessed.



Figure 6.3: 50 wt % hematite (left) and magnetite (right), 2 minutes after mixing

6.1.2.2 Water application

Water is known to play a large role in low adhesion and both the volume and application method will likely affect test results, as discussed in the literature review. Due to the variation in test rigs and methods, the water application method could not be kept identical between test methods but the application was kept as consistent as possible.

Water was applied using 4 main methods. A syringe was used for the majority of this work, able to simply apply an accurate volume of water. When a continuous water application was needed the syringe could be used with a syringe plunger, which pushed the syringe at a user defined rate so the correct water flow rate could be achieved.

A micro-pipette was used to accurately dispense water when smaller water volumes were needed. An issue with both of these methods was that water could only be applied to a small area and surface tension often meant that large droplets were formed, rather than a thin layer over a larger area.

To overcome this a “spray” bottle was used. This sprayed water over a large area when the trigger was pulled and ensured better coverage than a syringe. The amount sprayed for each trigger pull was not completely consistent but was measured to be approximately 7 ml.

An aerosol water spray was used in later tests, this was a bottle containing water and nitrogen that could finely mist the surface that it was sprayed on, producing very small droplets of water. Once again the spray was not accurate at dispensing specific amounts of water, but the water dispensed per second of spraying was measured to be approximately 0.7 ml/sec.

6.2 Pendulum Testing

6.2.1 Introduction to test rig

Work has been previously carried out to modify a pendulum slip resistance meter, often used as a road friction assessment tool, for railhead use to provide an efficient means of determining railhead friction levels [27][65]. It provides a portable method to obtain values of railhead friction that can be used in both the laboratory and elsewhere. It is quick and simple to set up which means it is especially good for testing transient conditions, such as a drying railhead. The following work used the pendulum rig with and without iron oxide using different amounts of water to assess if oxides are having a noticeable effect on the friction coefficient.

Testing was carried both in the laboratory and on a piece of rail left outside at different times of day under different weather conditions to assess if any trends could be found between varying conditions and low adhesion. Particular emphasis was put on data collection when dew had settled in the morning to assess the role of this on low adhesion.

Previous work tested a range of railhead conditions and used different contaminants with the pendulum results clearly showing which conditions produced low levels of friction on the railhead and which did not, with values ranging from a dry high friction of approximately 0.65, to a low oil contaminated friction of approximately 0.15 [65]. Results for different railhead conditions are shown in Figure 6.4.

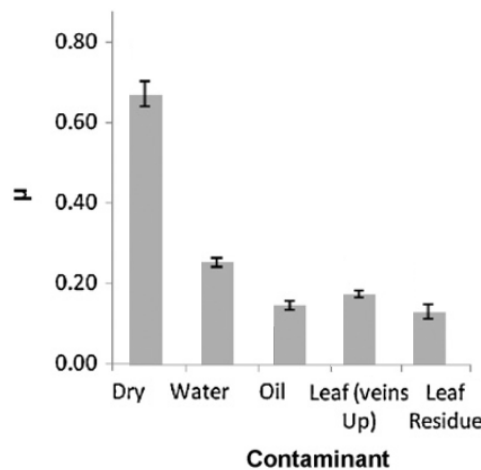


Figure 6.4: Levels of friction logged using the pendulum under different conditions [65]

6.2.2 Test apparatus

A schematic diagram of the pendulum is shown in Figure 6.5. The pendulum is an aluminium structure that operates similarly to the Charpy impact test, an arm is pulled back to the release mechanism and released when required using a lever. Energy is lost as the pad scuffs the rail surface after the pendulum arm is released, higher friction levels result in a higher slip resistance value (SRV) which is read from the scale.

The pendulum has an arm, (*c*) on Figure 6.5, that pivots around point (*b*). A rubber pad (*d*), also known as the slider, is mounted to the end of the arm and shown in Figure 6.7. The slider can use various different pads but the hardest rubber has been chosen for this work as these have been used previously to obtain similar friction coefficients to those seen in hand pushed tribometer testing. The slider has 45 degree, 5 mm chamfer at the contact end and is spring loaded to the pendulum arm which ensures that contact between pad and surface is maintained throughout the swing. The pendulum arm is swung from a set position which pushes the pointer up the scale, the arm and therefore the pointer travels further if there is less friction.

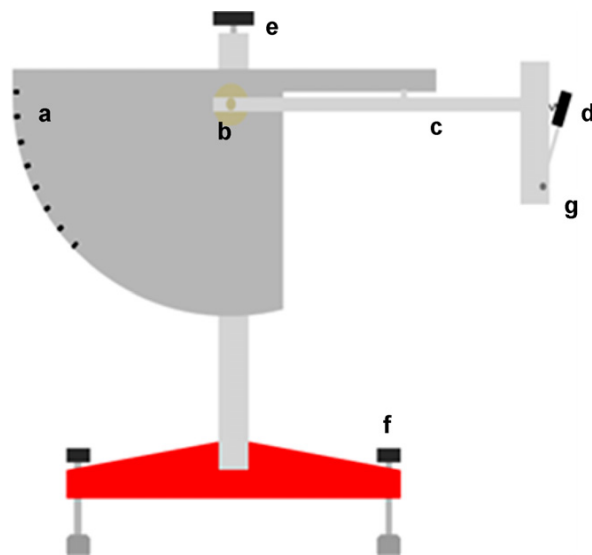


Figure 6.5: Schematic representation of the pendulum rig showing: (*a*) energy loss scale; (*b*) height-adjustable pivot; (*c*) pendulum swing arm; (*d*) spring mounted slider (rubber pad attached here); (*f*) height adjustable feet [27]

A wooden base has been manufactured to sit over a standard piece of rail so that the slider can contact, shown as used in the field in Figure 6.6. The wooden base is adjustable so that it can be used on uneven ground, the pendulum also has a bolt on each of its three feet that are used to keep the rig level, which can be checked using a built in spirit level.

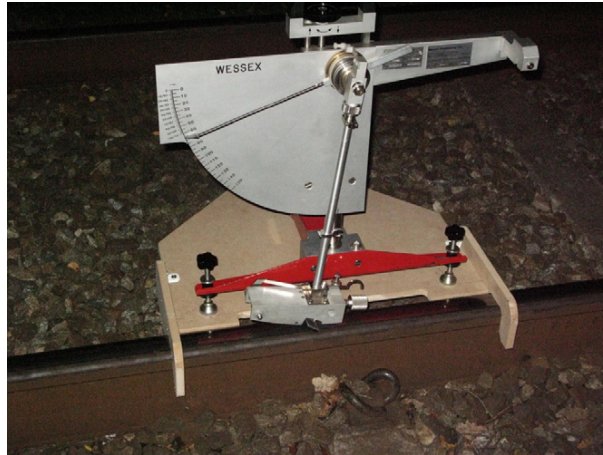


Figure 6.6: Field testing on rail with the pendulum mount [27]

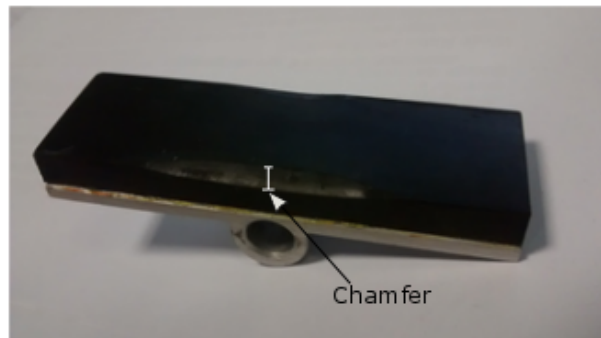


Figure 6.7: A pad slider with 5 mm chamfer

A 1000 mm section of 260 grade rail was used as the test surface. Surface rust was removed using an angle grinder and the rail head finished with p280 abrasive paper to produce a clean railhead contact patch that looked similar to those seen on track testing. The rail had been used previously so there was some surface pitting seen on the surface. A Four-S rubber pad with an IRHD hardness of 96 and was used for the majority of testing, as this was shown in previous tests to produce a consistent loss of force and the change in resistance was similar to those obtained from a hand pushed tribometer [65].

Another slider was manufactured with the same dimensions as the rubber chamfered pad, but using EN24 steel so that a comparison could be made between the rubber/steel and a steel/steel contact. This had an identical chamfer to the rubber slider on one side and a rounded fillet on the other to use as a comparison.

6.2.3 Methodology

The pad was conditioned between each set of tests and then cleaned between every test. The aim of conditioning was to make sure the rubber slider was clean and also had the same roughness and profile between each test. The pad was conditioned and returned to a standard finish by scuffing over P400 abrasive paper 3 times, followed by wetted 3M emery paper 10 times. The rail was cleaned between tests by scuffing over wetted 3M emery paper 3 times which removed any solid residue.

The pendulum was zeroed by adjusting the vertical adjustment knob and raising the pendulum arm to ensure there is no slider impact. The pendulum arm was released and caught on its return swing. The friction ring was adjusted in small increments using the clamp adjustment knob and the pendulum swung repeatedly until the pointer is pushed to zero for three consecutive swings.

The height of the pendulum arm was adjusted so that the spring loaded slider contacts the substrate for a distance of 127 mm during a swing. The pendulum was then swung using the following sequence:

1. The pendulum swing arm was raised and clipped in to its starting position.
2. The pendulum was released from its swing arm using a lever
3. Approaching 90 degrees into the swing, the rubber pad scuffed the test specimen
4. The pointer was pushed along by the pendulum arm until it reached a maximum value on the pendulum upstroke
5. The pendulum arm was caught by hand on the back swing to prevent any changes to the pointer
6. The energy lost due to friction was measured using the pointer position on a scale during the pendulum arm upstroke

The slip resistive value (SRV) can be converted to a comparable friction coefficient by using the equation shown in (6.1). It is important to remember that this is simply an approximation and not derived from the tangential and normal force as with the other rigs used in this work, but is useful when comparing approximate values. The high dry friction and low wet friction (approximately 0.6 and 0.15) do however provide compatible values to the dry and wet friction coefficients found on the other rigs [27]. For the purposes of comparison between other test method used in this work, pendulum results will be recorded as an approximate “friction coefficient”, converted from the SRV value using this equation [27].

$$\mu = \left(\frac{110}{SRV} - \frac{1}{3} \right)^{-1} \quad (6.1)$$

The pad was conditioned and cleaned, then water was applied in different quantities to generate a basic understanding of how water will affect friction when using the pendulum rig to act as a baseline. Water was applied using a syringe, “drizzling” the

water over the largest area of railhead possible to maximise coverage. An average of 3 repeats were taken for each water volume, shown in Figure 6.3.

Another set of tests were carried out, applying water using a “spray bottle” rather than a syringe. This was a less accurate method of dispensing water but ensured better railhead coverage than a syringe. The spray bottle was found to dispense approximately 7 ml of water with each spray and the results for the average friction coefficient over 3 repeats for different numbers of sprays are shown in Table 6.4. The spray bottle lowered the friction coefficient more effectively with a smaller volume of water than when the same volume of water was applied using a syringe, which may be because a better surface coverage can be achieved with a spray bottle.

Water volume (ml)	Average friction coefficient	Standard deviation
0	0.72	0
2	0.35	0.0058
5	0.26	0.0058
10	0.21	0.012
20	0.18	0.012
30	0.18	0.012
40	0.18	0

Table 6.3: Friction coefficient dependence on volume of water, applied using a syringe, on a clean railhead

Number of sprays	Estimated volume of water (ml)	Average friction coefficient	Standard deviation
0	0	0.74	0
1	7	0.19	0.0058
2	14	0.18	0.012
3	21	0.18	0.0058
4	28	0.18	0

Table 6.4: Friction coefficient dependence on volume of water, applied using a spray bottle, on a clean railhead

6.2.3.1 Generated oxides

A method was created to test the changing friction of a drying, oxidised rail. Applying a thin layer of water to the clean railhead and letting it evaporate was seen to produce a thin, orange layer of iron oxide. The oxide became visible approximately 100 seconds after water application and grew more visible as water evaporated, until

the railhead had completely dried. A test method was established in order to compare the friction coefficient of this freshly oxidised railhead to a “cleaned” railhead. Two sets of tests were carried out, one using a pre-oxidised railhead and another using a railhead with no visible oxidation.

In the pre-oxidised set of tests the railhead was first cleaned using P400 abrasive paper to remove any oxide layer and then rubbed with a clean cloth soaked in acetone to remove any oil residue. The area of pendulum contact on the railhead was taped off with masking tape, so only the 127 mm long contact area was exposed. 1 spray of approximately 7 ml of water was applied to this contact area using a squirt bottle, creating a thin film of water. This water was left to dry which took approximately 8 minutes and this formed a thin orange film of iron oxide on the railhead. After 10 minutes the dry railhead was re-wetted with 1 spray of water using the spray bottle again and the pendulum swung every 20 seconds until the railhead was visibly dry and a dry slip resistance value was reached.

Another set of tests were carried out without the pre-oxidation step as a comparison, the railhead was cleaned using P400 abrasive paper and acetone, then the contact patch was once again taped off. The railhead was then wetted with 1 spray from the bottle but this time testing was started straight away so that the oxide layer was not formed. Once again the pendulum was swung every 20 seconds until a dry slip resistance value was reached. A summary of the two test methods is shown in Table 6.5.

Step	Clean testing	Pre-oxidised testing
1	Rail cleaned	Rail cleaned
2	Rail wetted (7ml)	Rail wetted (7ml)
3	Test until dry	Wait 10 minutes
4	-	Rail re-wetted
5	-	Test until dry

Table 6.5: Test method to compare a clean and pre-oxidised railhead

6.2.3.2 Applied oxide

Magnetite and hematite oxide powder were also tested in paste form, as described in the introduction to this chapter, to assess any effects on friction levels. The pastes were made to a 50 wt % suspension using 3.5 g of oxide powder and 3.5 g of water. The 7 g of oxide paste was then spread over the surface of a freshly cleaned and non oxidised railhead, all the paste was added inside the area that the pendulum slider would contact and created a thin film of oxide paste that covered the contact patch. Tests were carried out using the same method used previously, the pastes were added and then a reading was taken every 20 seconds until the rail dried out and the friction coefficient returned to high values. As before, the results have been plotted against both time and number of pendulum swings.

A short series of tests under the same conditions were carried out with a pendulum slider that had been manufactured out of a piece of steel to assess if the steel on steel rather than rubber on steel contact would change any results.

6.2.3.3 Field testing

The effect of dew and weather conditions on the friction coefficient was assessed by testing on a piece of rail left outside so that the railhead could be exposed to natural conditions. The piece of rail was cleaned with abrasive paper and acetone in the evening and left overnight before readings were taken in the morning, beginning before dawn to assess if the dew point had a notable effect on friction characteristics. The rail was kept in an enclosed area outside the building, placed in between the outside building wall and a wooden fence which was surrounded by foliage. This means humidity levels were high and the rail was in a similar situation to that seen in a railway “cutting”.

The pendulum was zeroed and set up as outlined previously. The pendulum was left in the same position and not moved throughout the day, this meant that there was some wear of the rail surface oxide with each strike but it allowed comparable readings without having to set up the correct strike distance with every test which could cause further errors. This also better simulated the removal and regrowth of iron oxide by a wheel pass over a shorter time period rather than letting the railhead oxidise all day.

Three days were tested with readings at least every hour, but more regularly in the mornings as this was expected to be when dew was present and therefore important in the wet rail phenomenon.

The first two days contained a mixture of wet and dry conditions, on the first day the railhead surface oxide was abraded before the first pendulum reading to simulate a wheel pass and assess how quickly the friction coefficient would drop post abrasion. On the second day no morning abrasion was carried out so the railhead was oxidised heavily after being left outside the previous night.

The third morning of testing was used as a control, it was a dry day with a winds speed of 30 mph, which meant there was neither dew or precipitation and the railhead remained dry.

6.2.4 Results

6.2.4.1 Generated oxide results

The “generated oxide” method was repeated 3 times each for both clean and pre-oxidised rail. Testing was performed at alternate times (clean, then pre-oxidised, then clean), over 2 days to help eliminate any issues with environmental changes

such as temperature and humidity, along with physical changes such as pad wear or rail roughness. Average results are shown in Figure 6.8. The clean average friction coefficient starts at approximately 0.21 and drops slightly to 0.2 after 40 seconds, 2 swings. It then plateaus at 0.2 until 120 seconds and begins to climb until it reaches a dry value of 0.63 at 420 seconds. The friction coefficient then seems to drop slightly to 0.6 between 450 and 500 seconds.

The friction coefficient of the first swing of the pendulum using the pre-oxidised method averages slightly lower at 0.19. The friction coefficient then drops to approximately 0.14 at 150 seconds, before rising slightly to 0.15 at 200 seconds. At this point the friction coefficient then climbs back up to a dry value similar to that seen in the clean testing at 430 seconds. An image of the railhead after oxidised testing is shown in Figure 6.9.

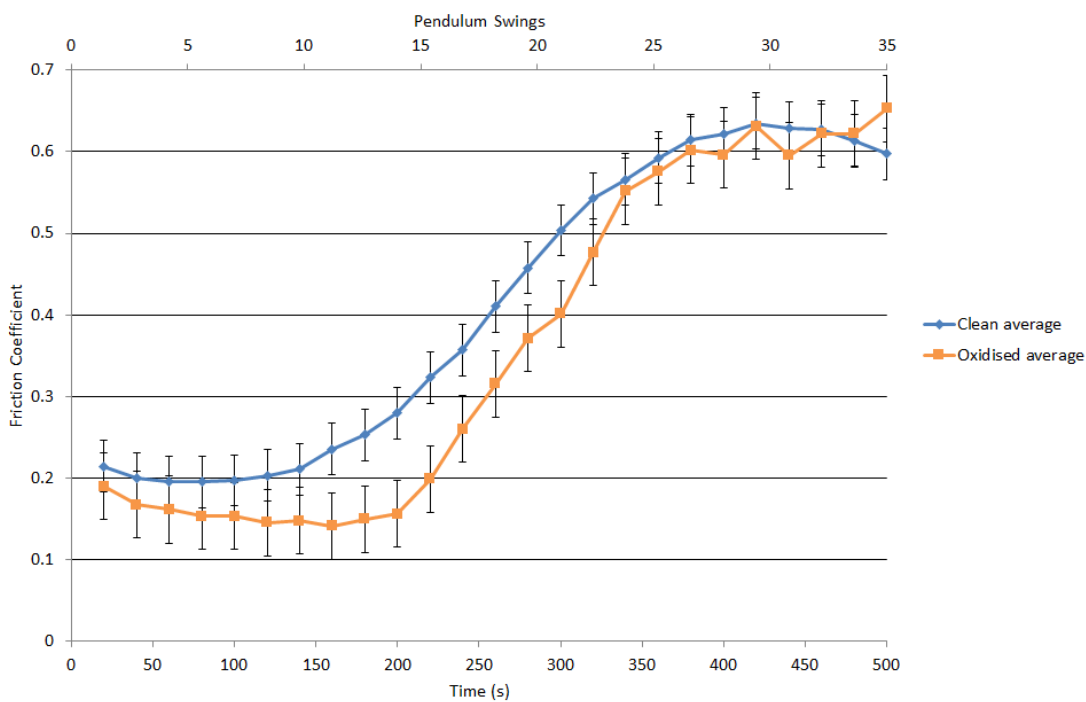


Figure 6.8: Average clean and pre-oxidised railhead friction coefficients



Figure 6.9: railhead wear track after 24 pendulum swings

6.2.4.2 Applied oxide results

The applied magnetite and hematite oxide both followed a similar pattern, with average results for 3 repeats being shown in Figure 6.10. The initial pendulum swing would result in a fairly high friction coefficient, 0.26 for magnetite and 0.30 for hematite. On the second swing for both pastes, the friction coefficient was much lower, 0.21 for magnetite and 0.19 for hematite. At this point both friction coefficients levelled out before rising again on the fourth swing. Overall the hematite friction coefficient seemed to remain lower for longer, but neither produced a very low friction coefficient of below 0.1 as discussed in the literature review. The friction coefficient rose up to approximately 0.5 at 330 seconds for both sets of tests as the railhead dried out.

The previous pendulum tests, using dry and wet conditions, pre-oxidised rail and rail with applied oxide paste, were repeated with a steel slider. The results were plotted against the corresponding lowest friction coefficient for each condition using the rubber slider and shown in Figure 6.11. The greater mass and rigidity of the steel slider removed any oxide with a single strike so the readings for different conditions were very similar and did not vary as much as the rubber slider, the only large difference in friction coefficient was seen between wet and dry values with little difference between oxidised and non-oxidised conditions.

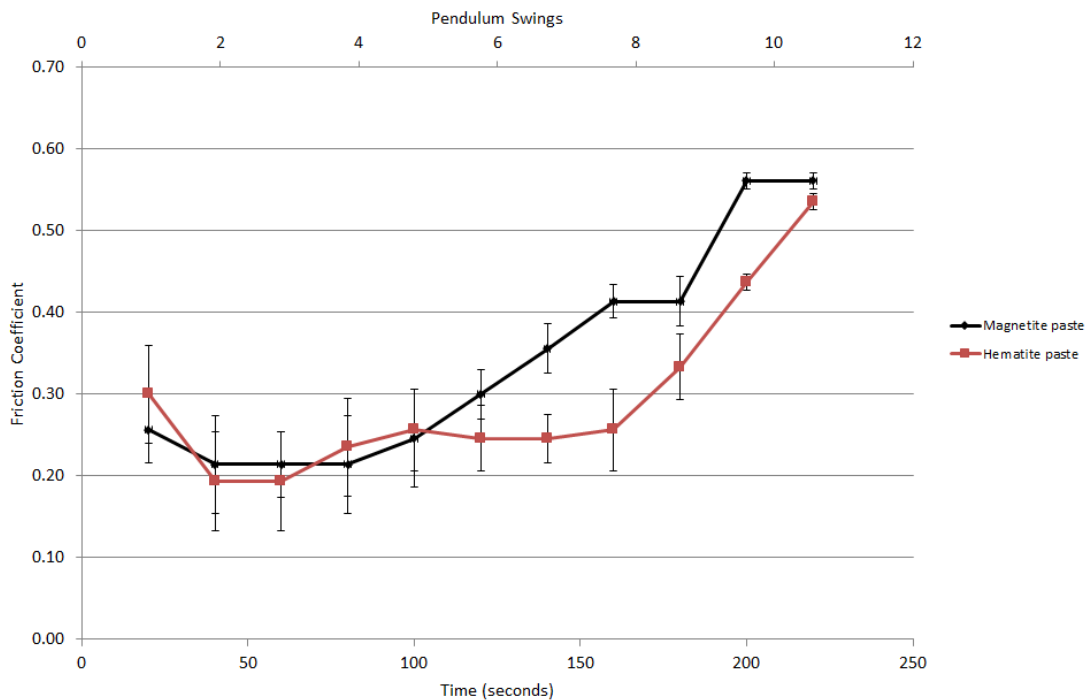


Figure 6.10: Average friction coefficients of 50 wt % magnetite and hematite pastes

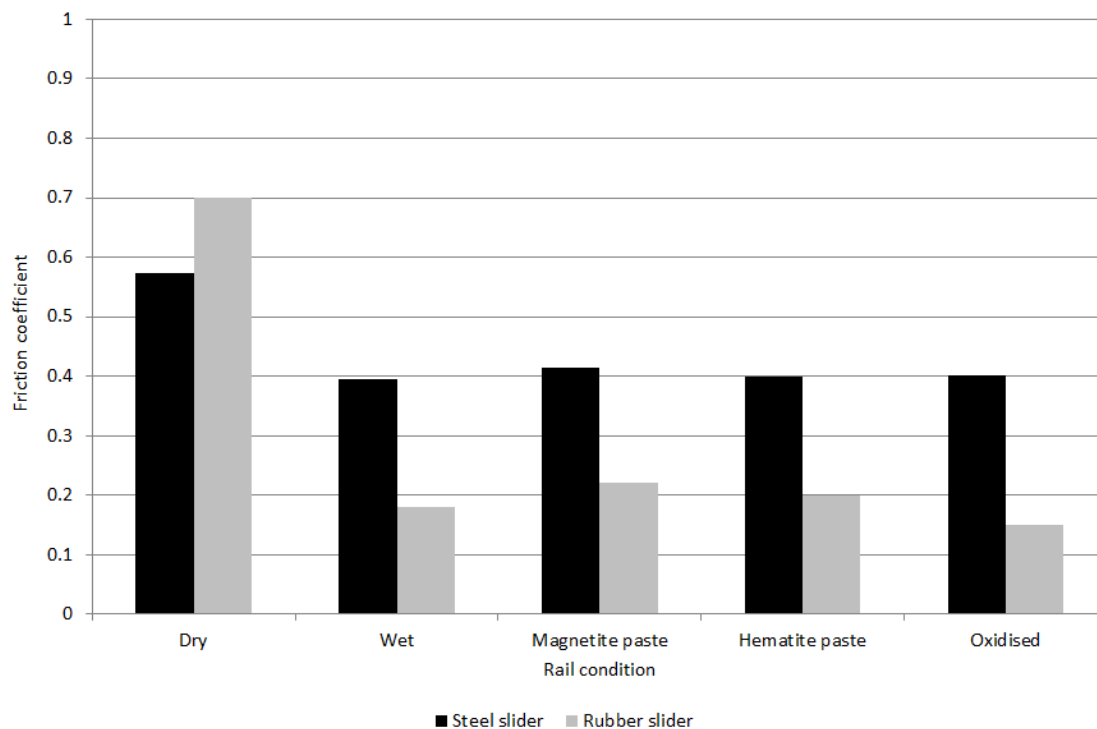


Figure 6.11: Lowest friction coefficient recorded for different railhead conditions using the steel and rubber pendulum sliders

6.2.4.3 Field testing results

Results for pendulum testing on a piece of rail outside in different conditions during November are shown in the following section. The friction coefficient was logged throughout the day, along with the relative humidity and whether there was precipitation falling or dew on the railhead. Three days were tested, each with different weather conditions.

Day 1 began with dew on the rail at 7:00 am. There was then a period of dry weather before heavy rain at around 8:00 am. The railhead remained wet throughout the rest of the day because of light drizzle falling. Results are shown in 6.12.

On day 2, dew was again present in the morning, this time followed by a longer period of dry weather before the railhead was once again wetted by drizzle at 11:30. Results are shown in 6.13.

Finally, conditions over a dry and windy day in winter were plotted in 6.14, the railhead remained dry all day with no dew or precipitation.

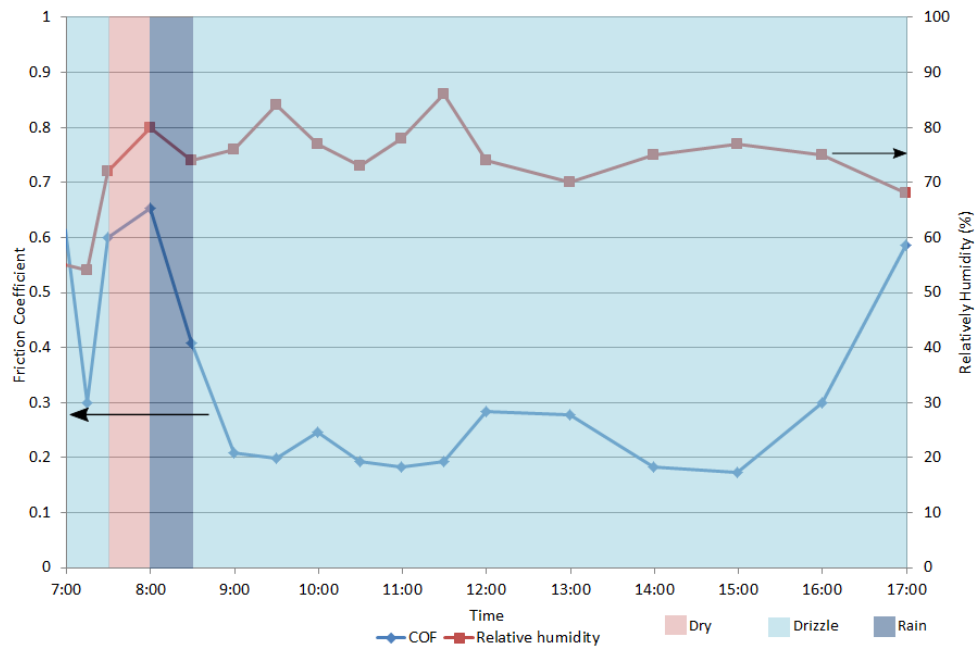


Figure 6.12: Friction coefficient, weather conditions and relative humidity changes over day 1

6.2 Pendulum Testing

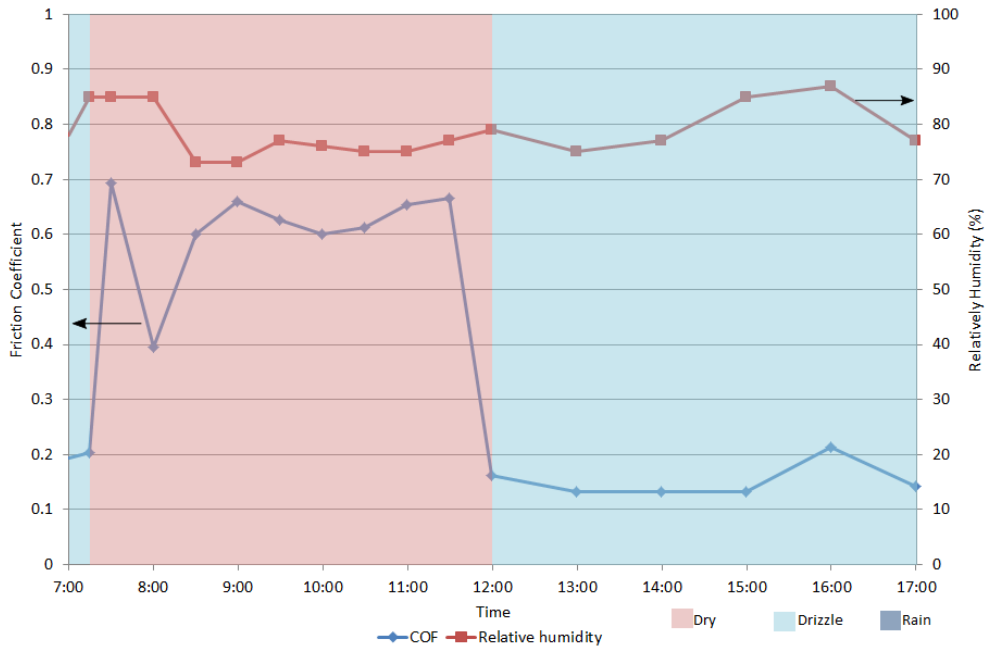


Figure 6.13: Friction coefficient, weather conditions and relative humidity changes over day 2

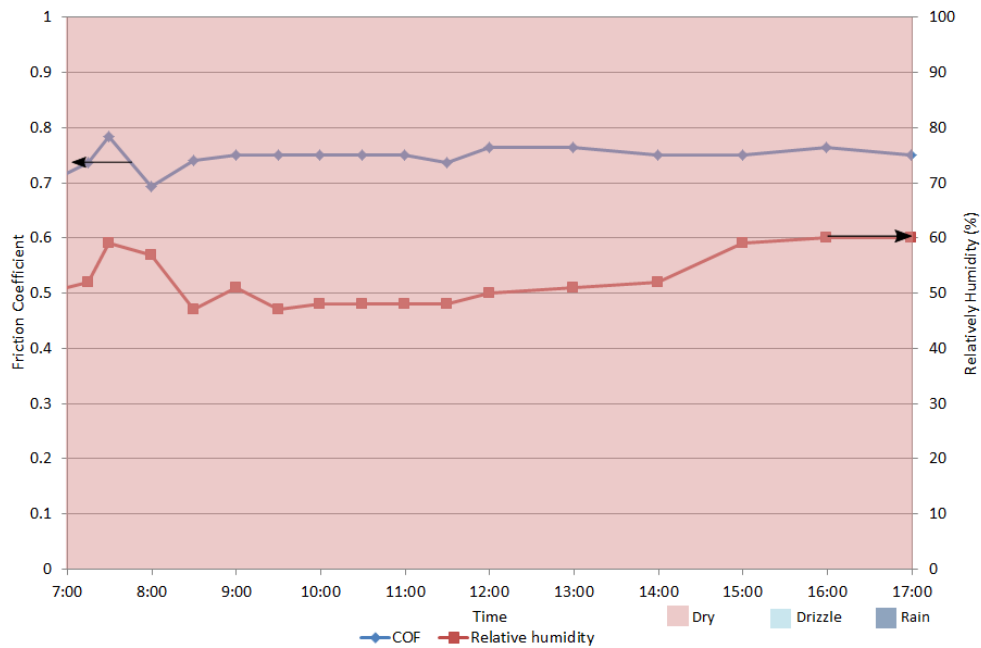


Figure 6.14: Friction coefficient, weather conditions and relative humidity changes over day 3

6.2.5 Discussion

6.2.5.1 Generated oxide

The “generated” oxide laboratory testing showed a clear difference in the friction coefficient between a clean and pre-oxidised railhead. Compared to the clean railhead, the pre-oxidised friction coefficient is lowered as soon as water is added and remains low after wetting for a period of time, before rapidly increasing as the rail dries. After prior oxidation the friction coefficient generally stays at a lower level (below 0.2) for a longer period of time than the rail that had not been pre-oxidised. The clean rail friction coefficient dips below 0.2 briefly, rising above it at 120 s. The friction coefficient of the oxidised rail on the other hand does not rise above 0.2 until 220 s have passed. The oxide layer is removed over a number of cycles and by the end of a 24 cycle test the layer has been virtually completely removed. The increase in friction coefficient seen during the pre-oxidised pendulum testing could be a combination of both the rail drying and the oxide being removed, the oxide seems to be removed at a quicker rate under dry conditions.

It is clear, from visual inspection, that although a thin layer of oxide is being formed in the wear track, the constant pendulum testing is suppressing the bulk of the oxide growth compared to that seen outside the wear track. It can also be noted that the rail used had large amounts of pitting. This creates a more patchy oxide layer which means that the friction coefficient may drop to lower levels if a less damaged railhead was used so a oxide layer with greater coverage could form. The pits would also likely produce a higher surface roughness, which as suggested in the modelling work may prevent low adhesion from occurring.

6.2.5.2 Applied oxides

The friction coefficients of both hematite and magnetite were above those seen in water so neither reduced the friction coefficient to a large extent in this set of tests. Hematite lowered the friction coefficient further than magnetite. The hematite was far more sticky so more remained on the railhead after the initial pendulum strike, whilst the magnetite seemed easier to wash off the railhead and when washed, did not leave as much debris behind.

The extra mass of the steel pendulum slider removed oxides in the wear area in a single swing and did not differentiate as much as the rubber slider between different conditions. Short, 3 swing tests were carried out when it became clear that the results would show little difference between conditions other than wet or dry. This highlights the difference between a sliding and a rolling/sliding contact, where any oxide worn away under a rolling/sliding test rig may remain in the contact, whilst any oxide under a purely sliding contact may simply be pushed aside so the third body layer cannot build up.

The contact patch between rail and pendulum slider will be roughly the same size as the real wheel-rail contact patch but the pendulum is a purely sliding contact, the rubber slider will act very differently to the steel and the pressure and speed used in the pendulum testing are far lower than those seen in the wheel-rail contact. However, the benefit of the test method shown here is that friction coefficient measurements that can be taken in the field and it is able to quickly record changing conditions so can provide useful comparisons. Unlike other small scale test methods, the pendulum rig when using a rubber slider does not provide the forces needed to break the surface oxide layer in a single swing which is useful when testing how the friction coefficient of this oxide layer changes under wet conditions. This means multiple tests can be carried out on a drying railhead without having to re-oxidise the rail for each test.

6.2.5.3 Field testing

Friction coefficients over a winters day show a large dependency on water conditions. Figure 6.12 starts off with a high COF, 0.6, because the railhead has been cleaned with abrasive paper before beginning tests. This was carried out to assess how the friction coefficient would respond to a wheel pass removing oxide and then being left for a period of time in damp conditions to re-oxidised. The coefficient drops to 0.3 very quickly as moisture builds up again, but does not fall to very low values until a drying and re-wetting cycle has taken place. The friction coefficient rises to 0.65 when the rail dries and then quickly falls back down to 0.2 when the rain is re-wetted with drizzle. The relative humidity rises from a low of 75% to a peak of 85% during precipitation.

The railhead was not abraded on the second continuous day of testing, shown in Figure 6.13, so the initial friction coefficient was low at 0.2 when dew was present on the railhead. The friction coefficient then raised to 0.7 as the railhead dried and dropped back down to 0.4, this could be because railhead moisture was pulled back onto the wear track by the pendulum swing. When dry the friction coefficient was slightly above 0.6. When drizzle fell onto the railhead throughout the afternoon the friction on the railhead dropped to 0.15, the lowest values seen during the field testing. On this day the relative humidity was particularly high, around 85 % in the morning and evening.

As predicted, the dry and windy day in Figure 6.14 had a high friction coefficient above 0.6. The high wind meant that relative humidity was far lower than that seen in previous tests, even in the enclosed pendulum area.

The results showed a rapid decrease in friction coefficient as soon as the railhead became wet, both in the morning because of dew and throughout the day with drizzle. The friction coefficient in the period when heavy rain fell only reduced to 0.4 rather than the lower levels seen when drizzle was on the railhead. There was a dry period in between the morning dew and the drizzle in Figure 6.13, which may

have caused more oxidation of the railhead and produced the low friction coefficient in the afternoon.

6.2.6 Conclusions

The pendulum rig provided an efficient method to test a number of friction conditions on the railhead. It showed that an oxidised layer could produce a lower friction coefficient than water alone in this situation and was particularly useful when testing the friction of a railhead left outside, which would not have been possible on laboratory based test rigs. Particularly low friction coefficients were seen when drizzle fell on the railhead, as previously noted in the literature review.

The approximate friction coefficients obtained for the railhead were roughly 0.6 when dry, 0.2 when wet and 0.15 when small amounts of water and oxide were present. Although these friction coefficients are approximated from slip resistance values, they line up well with values seen in the literature when looking at other test rigs. Values below 0.15 may have been seen if the rail used was smoother and less pitted. Approximate friction coefficients from the railhead for applied oxide pastes were similar to those obtained using water alone.

Although useful for gathering comparative data when field testing, the pendulum bears few similarities to a real wheel-rail contact so more comparable laboratory testing was used in the following sections to better understand the wet-rail phenomenon.

6.3 Bruker UMT Tribometer Testing

6.3.1 Introduction to test rig

The exact conditions that cause the wet-rail phenomenon were not understood so a large number of conditions needed to be tested, both physical contact conditions and environmental conditions. The Bruker UMT tribometer could efficiently test a range of conditions with different types of contact using different geometry, speeds and pressures so it was chosen for this work. Unlike the other rigs used in this work, a purpose built humidity chamber could be used to explore the change in friction coefficient using oxide layers at different humidities.

The UMT can only measure the friction coefficient between two sliding surfaces so the contact is different to the rolling-sliding contact found between a rail and wheel, but can still provide important information about changes in friction coefficient under different conditions.

As noted in the literature review in chapter 2, small scale tribometers such as the UMT have been used to measure friction and wear and have been used to investigate low adhesion. Multiple studies [26, 57, 66] have been carried out to look at the effect of iron oxides in the wheel-rail contact and this work was designed to build upon the published work to assess if very low friction can be caused by iron oxides and water alone. Both oxides generated naturally and applied oxide powders will once again be tested under different conditions to assess if any particular conditions will cause a reduction in the friction coefficient.

6.3.2 Test apparatus

A schematic diagram of the Bruker UMT tribometer is shown in Figure 6.15. An upper specimen is mounted to a holder, suspended above a load cell which can move on the X, Y, Z axis. One of two lower modules were used depending on the desired movement type and three types of movement were used over the course of this testing. A linear “reciprocating” module moved the lower specimen forwards and backwards for a set amount of time along the same path, chosen because it was able to be fitted to a humidity chamber. A rotating module rotated the lower specimen either anticlockwise or clockwise, in these tests the upper specimen does not move, but is placed off centre to the lower so a circular path is taken, over the same area with each rotation. This module was chosen because it could produce higher speeds than the reciprocating module. A “spiral” path was also tested where the upper specimen moves on the x axis as the lower specimen rotates, creating a spiraling wear track out from the centre of the specimen and ensuring that the upper specimen does not pass over a previous wear track on the lower specimen. A diagram of each type of movement is shown in Figure 6.16.

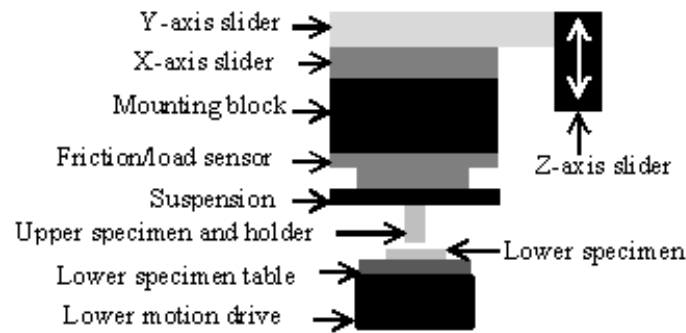


Figure 6.15: A schematic diagram of the Bruker UMT

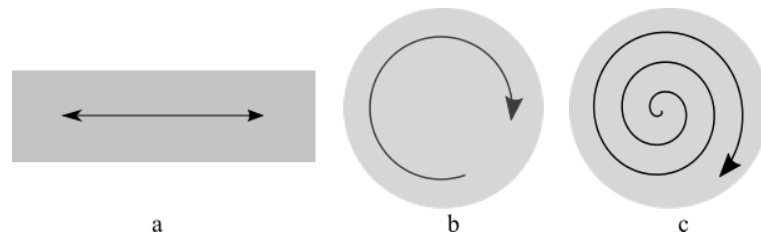


Figure 6.16: a; linear reciprocating movement, b; circular movement, c; spiraling movement

Lower specimens were fixed onto the moving lower module with bolts or a vice. Three types of lower specimen were used in this work, all made using EN24 steel and ground to a surface roughness of $1\ \mu\text{m}$. Rotational specimens were discs with a 75 mm diameter and 5 mm depth, two holes were drilled so it could be bolted onto the module and rotated without slippage. Reciprocating specimens were made in a rectangular shape with a 30 mm width, 60 mm length and 3 mm depth.

A “grooved” disc was also created by machining out a continuous rectangular channel in the steel specimen. This channel allowed oxide paste and other contaminants to sit in the channel and saturate the contact rather than covering the disc surface, as seen in Figure 6.17. This ensured that the paste could not be pushed out the way to leave bare steel during continuous rotational testing.

The upper specimen was a 1010 carbon steel steel ball bearing, the number of ball bearings needed meant that something readily available needed to be chosen rather than replicating real wheel and rail steel. A ball bearing rather than flat pin was used because it was difficult to align a flat pin surface to a flat lower specimen and the continuous ball bearing surface meant that no alignment was needed. The largest size of ball bearing that could be fitted to the UMT, 10 mm, was used.



Figure 6.17: A “grooved” disc filled with hematite paste

A humidity chamber was set up that encompassed both the ball bearing and the disc. The chamber has a metal base that bolts on top of the module holding the lower specimens and still allows movement. The upper section is made from transparent plastic so that the sample is still visible during the test. An air compressor was attached to a humidifier which supplied both dry and humid air to the chamber via a pipe. The UMT rig could control the humidifier so that testing could be carried out at the desired relative humidity (RH).

6.3.3 Methodology

6.3.3.1 Set-up procedure and oxide generation

A script was created for each method to program the UMT to run at the desired speed, load and movement type over the test duration. Samples were cleaned by scrubbing with soapy water and a small brush to remove any oil and debris present after grinding. An ultrasonic acetone bath was then used for 2 minutes to remove any further contamination, then the sample was left to dry. The correct load cell and mounts were fitted and then the samples were fixed into the upper and lower holders.

The 10 mm ball bearing was mounted in the holder, a tapered cylinder which means the ball protrudes out the contacting side, but cannot be pushed out. A grub screw is used to fix the ball in place. The rig was then switched on and both the position and force were zeroed before the script was run and the test carried out.

Oxide pastes were formed to a range of weight percentages using the method described in the introduction to this chapter, both hematite and magnetite were tested. These pastes were applied using a syringe with a modified nozzle to account for the high viscosity. Tests were carried out on flat and grooved specimens to assess any effects involving oxides either remaining in the contact or being pushed aside.

Samples were also pre-oxidised using a humidity chamber to produce an oxide layer that could be tested. Specimens were left in a humidity chamber for 15 minutes to produce a lightly oxidised surface and 30 minutes to produce a heavily oxidised

surface. Images of the lightly and heavily oxidised samples are shown in Figure 6.18 and 6.19. The spotted patches are likely formed where water has condensed onto the substrate surface in droplets which are visible in Figure 6.19.

In the following UMT tests, methods and results will be split into the type of movement rather than oxide type due to the large changes in conditions between rotary, spiraling and linear movement types.

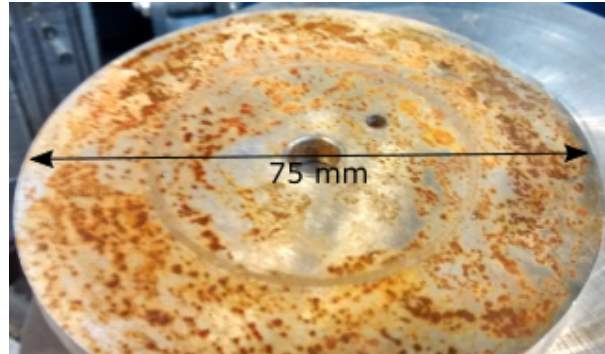


Figure 6.18: A heavily oxidised sample for rotary movement

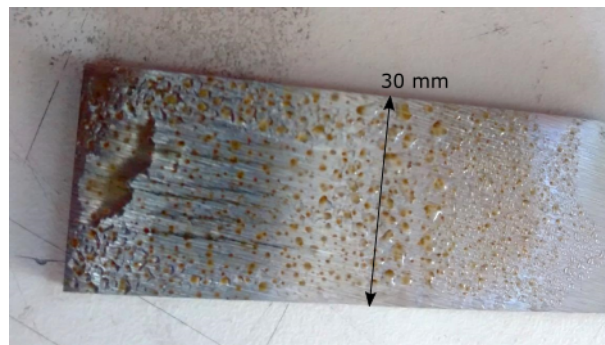


Figure 6.19: A lightly oxidised sample for linear movement

6.3.3.2 Rotary movement

Rotary testing was initially carried out over a range of velocities to assess which would be most useful to carry out a full set of tests. Different velocities were initially tested between 0.03 m/s and 1.8 m/s on wetted steel surfaces. 100 μ l water was applied to the contact using a micro pipette and the friction coefficients compared. The friction coefficient fluctuated at higher speeds, so the initial tests were carried out at 0.12 m/s as a compromise between speed and minimising the deviation in results. Higher speed testing at 1.2 m/s was carried out on oxidised samples but this produced fluctuating results when tested with the thicker oxide pastes. This speed

produced large amounts of wear at high loads so tests were kept short, 6 seconds before the wear track became too large and prevented the pin from rotating.

Hematite and magnetite pastes were tested first, mixed to 50, 60 and 70 wt %. Pastes were added to the contact via a syringe before testing began and two different quantities of paste were tested, 0.5 and 1 g. The lower specimen was rotated to produce a ball bearing velocity of 0.12 m/s under 1 GPa pressure, chosen as a typical contact pressure of the top of the railhead and the wheel of a typical UK passenger locomotive.

Heavily oxidised samples were tested dry and then 3 volumes of water, 10, 50 and 100 μl , were applied by micro pipette to the contact before testing at two speeds, 0.12 m/s and 1.2 m/s. A pressure of 1 GPa was applied and a short test length of 6 seconds was used due to the speed at which the oxide layer was removed.

This previous test was then repeated at a higher speed of 1.2 m/s over 6 seconds using a clean disc, lightly oxidised disc and heavily oxidised disc with the addition of 100 μl water to assess the effect of oxide thickness.

A summary of the tests carried out using rotary movement is shown in Table 6.6.

Test set No.	Movement	Speed (m/s)	Oxide application	Water application
1	Rotary	0.03-1.8	N/A	100 μl
2	Rotary	0.12	1 g Hematite paste (50, 60, 70 wt %)	N/A
3	Rotary	0.12	0.5 g Hematite paste (50, 60, 70 wt %)	N/A
4	Rotary	0.12	1 g Magnetite paste (50, 60, 70 wt %)	N/A
5	Rotary	0.12	0.5 g Magnetite paste (50, 60, 70 wt %)	N/A
6	Rotary	0.12	Heavily oxidised	Dry, 10 μl , 50 μl , 100 μl
7	Rotary	1.2	Heavily oxidised	Dry, 10 μl , 50 μl , 100 μl
8	Rotary	1.2	Clean, lightly oxidised, heavily oxidised	100 μl

Table 6.6: Rotary movement test summary

6.3.3.3 Spiraling movement

A “spiral” pattern was also tested to assess if a single pass, rather than multiple passes over the same contact would be more representative and produce any results that showed low friction. The specimen rotated as usual whilst the ball bearing moved over the X-axis to create a spiral that moved out from the centre of the disc and ensured that the ball bearing would not repeatedly move over the same contact patch. This had to be tested at the lower speed (0.12 m/s) due to poor control at the higher speed. Clean, lightly oxidised and heavily oxidised samples were once again used with 100 μ l of water. The test conditions are summarised in Table 6.7.

Test set No.	Movement	Speed (m/s)	Oxide application	Water application
9	Spiral	0.12 m/s	Clean, lightly oxidised, heavily oxidised	100 μ l via micropipette

Table 6.7: Spiral movement test summary

6.3.3.4 Linear movement

Linear reciprocating tests were beneficial because the sample could be enclosed in a humidity chamber to simulate a high humidity environment. Humidity could be controlled by the UMT program and monitored throughout the test.

Magnetite and hematite oxide powder was also tested without further water addition to assess if the moisture from the humid environment alone could affect the friction coefficient. A new method was also designed to apply dry iron oxide as an evenly distributed powder for this purpose. 0.2 g of iron oxide powder was mixed with 2 ml isopropyl alcohol to form a suspension and mixed thoroughly before applying to the specimen using a syringe. The suspension was left to settle on the level substrate surface before the solvent dried under ambient conditions to leave a well distributed layer of iron oxide on the surface. This was repeated for both hematite and magnetite, images are shown in Figures 6.20 and 6.21. The sample was fixed inside the UMT humidity chamber and sealed in. A humidifier was connected and linked to the UMT so that the program was able to monitor and control humidity.

Lightly and heavily oxidised samples were also tested alongside a clean specimen, each test was run at 60, 70, 80 and 90 % humidity. Tests were carried out at the maximum speed for the linear module, 0.01 m/s, and once again used a 10 mm ball bearing and 1 GPa pressure. A summary of tests carried out using the linear module is shown in Table 6.8.

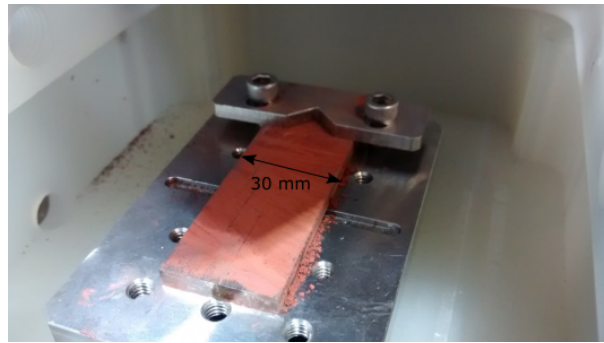


Figure 6.20: Hematite powder application on a linear specimen

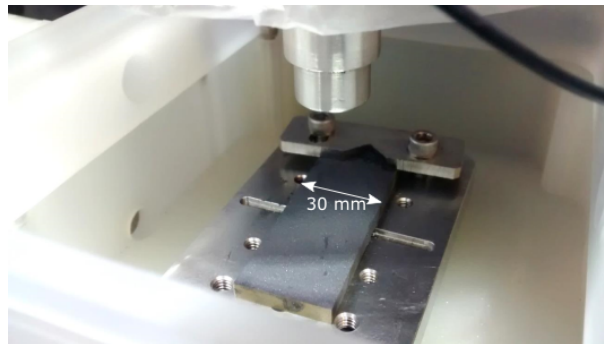


Figure 6.21: Magnetite powder application on a linear specimen

Test set No.	Movement	Speed (m/s)	Oxide application	Humidity (%)
10	Linear	0.01	N/A (clean)	60, 70, 80, 90
11	Linear	0.01	Hematite paste	60, 70, 80, 90
12	Linear	0.01	Magnetite paste	60, 70, 80, 90
13	Linear	0.01	Lightly Oxidised	60, 70, 80, 90
14	Linear	0.01	Heavily Oxidised	60, 70, 80, 90

Table 6.8: Linear movement test summary

6.3.4 Results

6.3.4.1 Rotary movement

The average friction coefficient for test set 1, at different sliding speeds after 100 μ l water application, are shown in 6.22. A large increase in scatter is seen at higher speeds. Average friction coefficients for different wt % and volumes of hematite and

magnetite pastes, test sets 2-5 are shown in Figure 6.23. There is no significant difference between different volumes of paste. Magnetite pastes give a slightly lower friction coefficient than hematite, but the values are still very high.

The raw data for 1.2 m/s with 10, 50 and 100 μl water addition is shown in Figure 6.24 and average friction coefficients for a heavily oxidised sample at two speeds, test sets 6 and 7 are shown in Figure 6.25. There is a large decrease in traction coefficients at the higher speed. The raw data for a non-oxidised sample, lightly oxidised sample and heavily oxidised sample with 100 μl water application, test set 8, are shown in Figure 6.26.

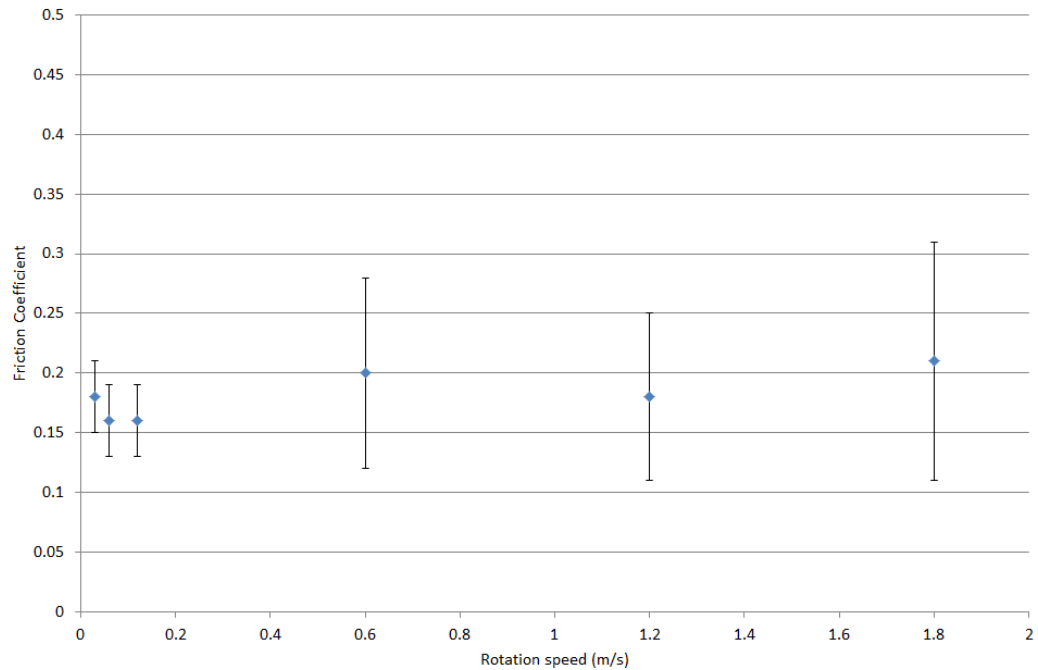


Figure 6.22: Test set 1. Friction coefficient at different speeds using a clean disc with 100 μl water applied

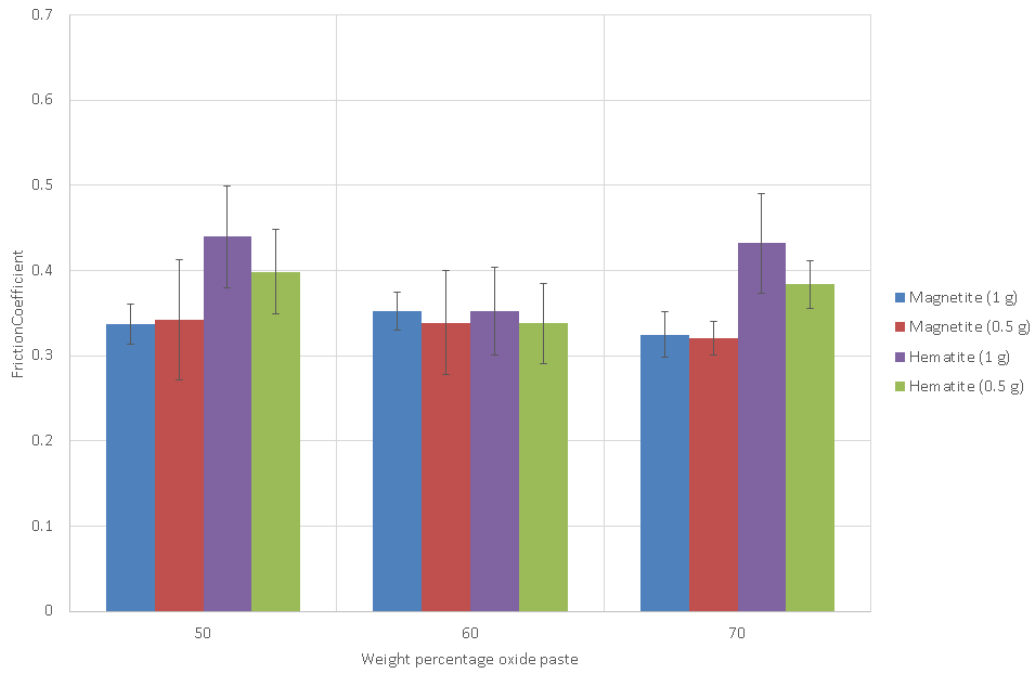


Figure 6.23: Test sets 2-5. Average friction coefficients for different wt % oxide pastes using two different volumes of paste addition

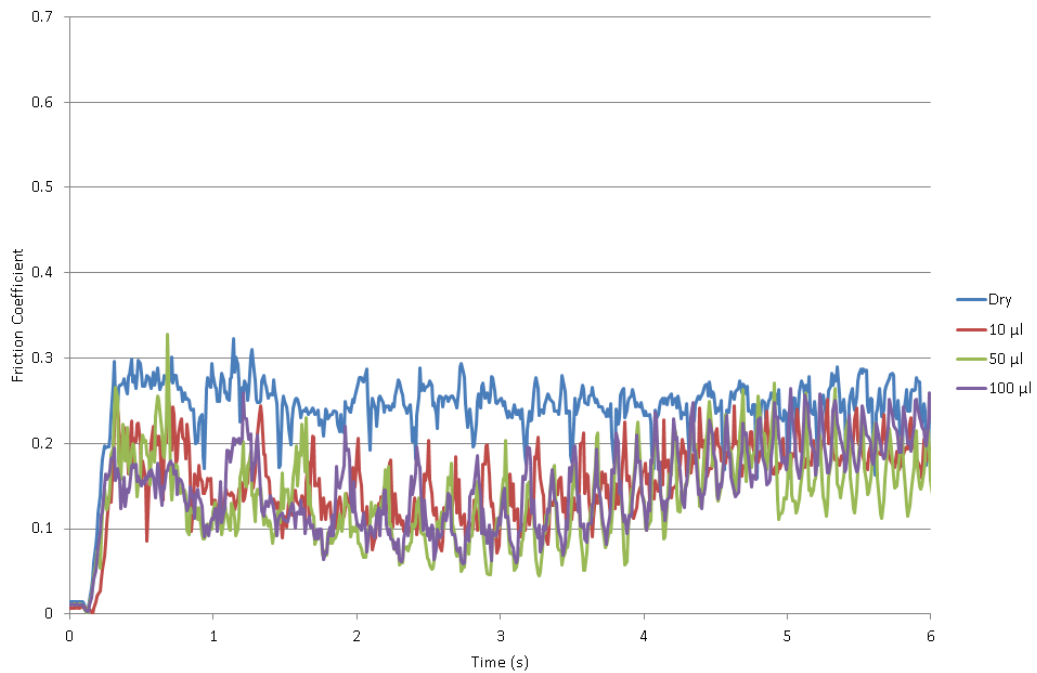


Figure 6.24: Test set 7. Testing a heavily oxidised sample 10, 50 and 100 µl of water addition at 1.2 m/s

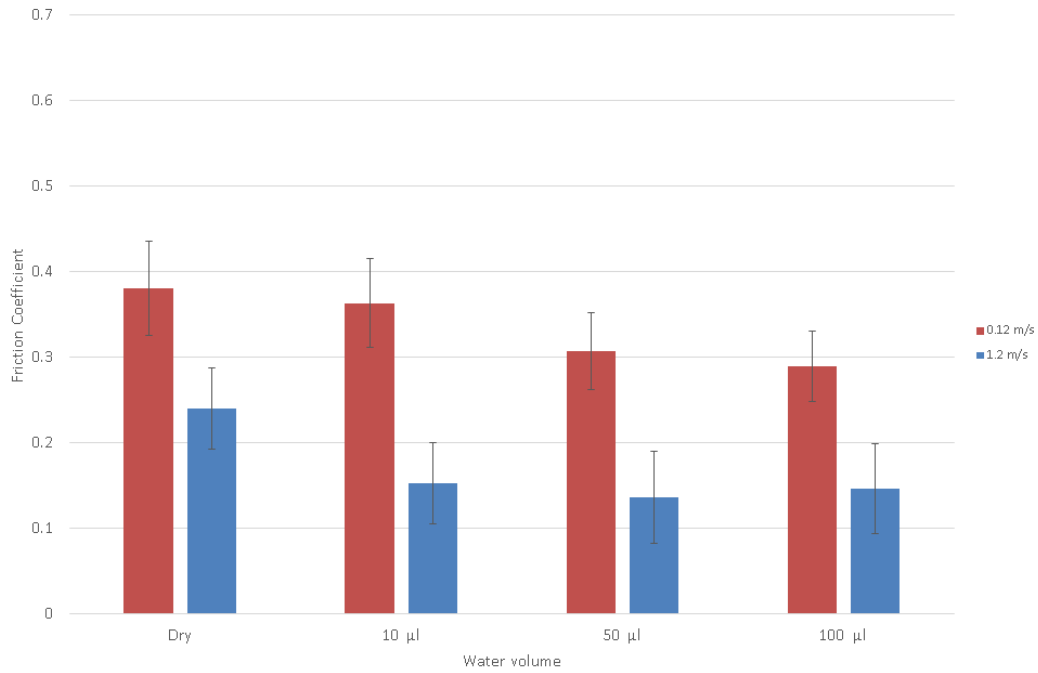


Figure 6.25: Average results for test sets 6 and 7. Friction coefficients for a heavily oxidised sample with different amounts of water added for speeds of 0.12 m/s and 1.2 m/s

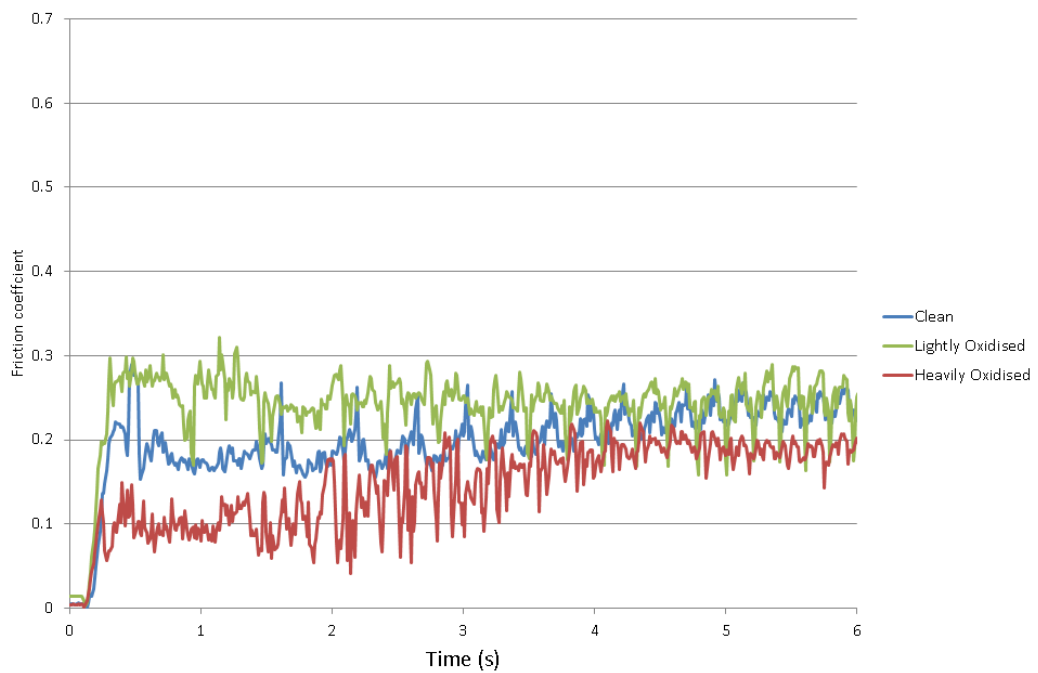


Figure 6.26: Test set 8. Clean, lightly oxidised and heavily oxidised samples with 100 µl water at 1.2 m/s

6.3.4.2 Spiraling movement

Results for the spiralling test, 9, are shown in Figure 6.27. A lower initial friction coefficient is seen for the heavily oxidised sample, but the scatter in the test is large due to fluctuations in results. These fluctuations are larger for the heavily oxidised sample so they are likely due to surface irregularities.

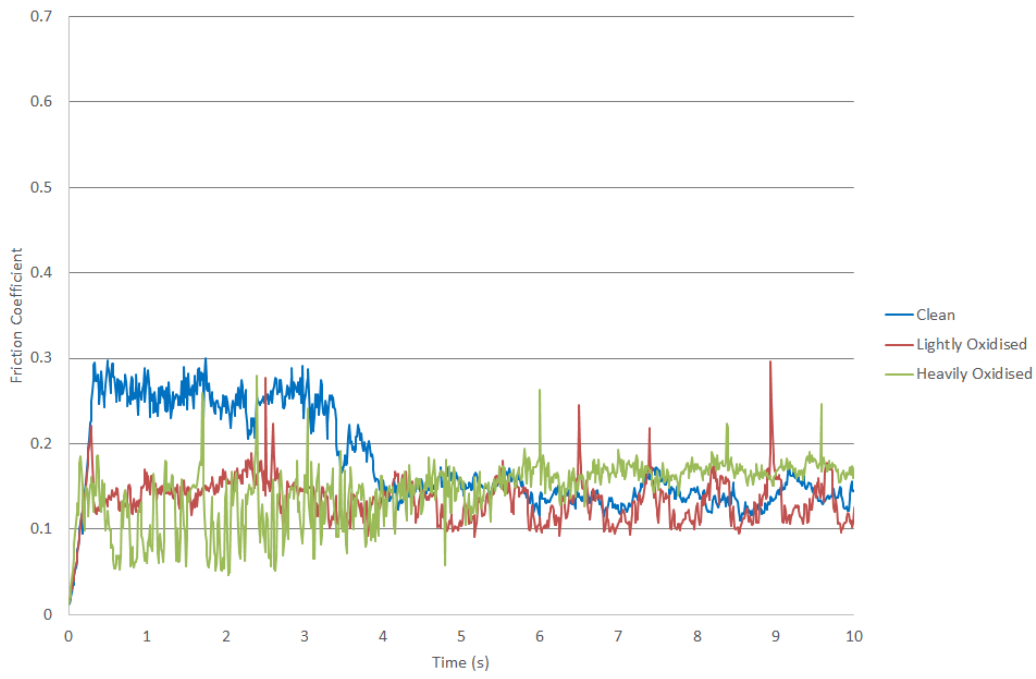


Figure 6.27: Test set 9. Friction coefficient of a clean, lightly and heavily oxidised sample with 100 μ l water and a spiraling ball bearing

6.3.4.3 Linear movement

Average results for tests 10-14 are shown in Figure 6.28. The generated oxide layers have a friction coefficient below that of water alone, shown in the “clean” sample. The oxide pastes produce a higher friction coefficient than water. There is no significant decrease in friction coefficient with increasing humidity.

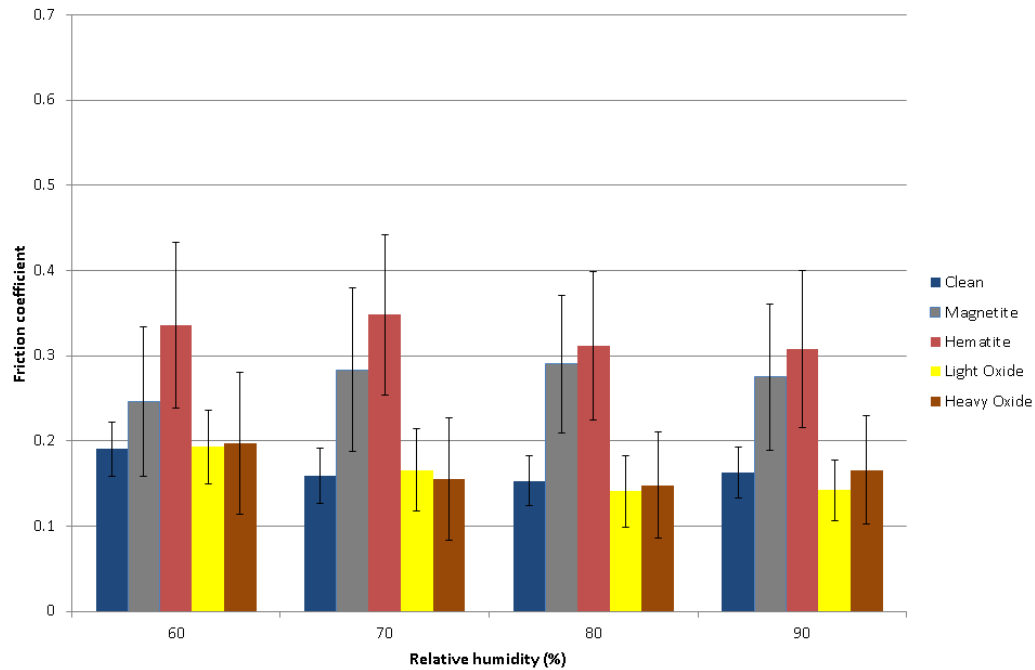


Figure 6.28: Test sets 10-14. Average friction coefficients of a clean and wet sample, magnetite and hematite powder, lightly oxidised samples and heavily oxidised samples at 60, 70, 80, 90 % humidity

6.3.5 Discussion

6.3.5.1 Rotary movement

Sliding speed was initially set low at 0.12 m/s due to difficulties in testing high sliding speeds with a thick layer of oxide pastes. The load and friction coefficient fluctuated dramatically when the speed was set too high. The rotary samples using applied oxide in Figure 6.23 showed magnetite produced a lower friction coefficient than hematite during every condition tested, but this was not significantly lower apart from at 70 wt % and neither friction coefficient was below 0.3 when using iron oxide powder. The ball bearing was visibly plowing through the iron oxide paste and left behind a bare steel trail during its first rotation.

The UMT contact is full sliding rather than the rolling/sliding contact in a real wheel-rail contact, as a result the oxide is more likely to be pushed out of the way under high pressures rather than being rolled over and compressed in the contact, which was seen during the railhead investigations in chapter 4. The dimensions of the ball bearing on flat contact are also very small in comparison to the real wheel-rail contact so the relative size of oxide particles may have an effect. Slow speeds will also be a factor, giving the ball bearing a longer period of time to plough through the iron oxide and push it out of the way.

There is no trend seen between the amount of oxide used and the friction coefficient in the test. This could either be due to even a small amount of iron oxide saturating the contact so any extra is pushed out of the way, or that all the oxide is pushed out the way and there is no oxide powder in the interface. Visually, the metallic wear band seen points towards the second idea being more likely.

An oxide grown naturally through wet and dry cycles or high humidity will be bonded to the substrate and therefore may be less easily pushed out the way in comparison to an applied oxide which may be why lower friction was seen for the naturally generated rather than artificially applied layers. This is a more realistic, but less controllable approach, as it is difficult to grow a repeatable oxide layer due to different rates of oxidation and the oxide growing unevenly across the sample. The grown oxide results fluctuated due to the “spotted” oxide layer resulting in changes in surface profile throughout the sample, at low speed this effect was less severe than at high speeds.

At the slower speed of 0.12 m/s, the friction coefficient of a naturally formed oxide layer decreased as more water was added, between 10 and 100 μl as seen in Figure 6.25, however as the friction coefficient only dropped from 0.36 to 0.28 the iron oxide is not significantly lubricating the contact and all friction coefficients were above that seen in a clean contact.

High speed tests at 1.2 m/s showed a decrease in friction when water was added but no significant drop in friction between different amounts of water. During high speed tests, the accelerated sample wear would cause the tangential force on the ball bearing to become very high after a certain point, possibly due to the ball bearing wearing through the passivating oxide layer or getting “caught” on the wear track, when this occurred the test was stopped to prevent damage to the load cell in the rig and as such the test length is short. The abrupt change in friction coefficient when the layer is worn away shows that the iron oxide is involved in reducing friction in the contact. The natural oxide appeared to be worn away very quickly as the ball bearing ran over the same wear track during every cycle and wore unevenly with some areas of oxide being thicker than others, which is likely to cause the oscillation in friction coefficient as seen in Figure 6.24.

Figure 6.26 showed a lightly oxidised specimen to have a higher friction coefficient than a clean specimen, whilst a heavily oxidised specimen had a lower friction coefficient. It may be that the lightly oxidised specimen had not reached sufficient levels of coverage to reduce the friction in the contact. The friction coefficient of the heavily oxidised specimen stays low at approximately 0.1 for 2 seconds, at this point it starts fluctuating more and steadily rises until it reached a clean value of approximately 0.2 again. This may show a layer in the iron oxide which is worn away after 2 seconds, before hitting a sub-layer which takes another two seconds to wear away and finally reaching the bare steel underneath. Alternatively the wear particles from the iron oxide and increasingly deep wear track could cause the fluctuation in results after 2 seconds

Increasing speed had a larger effect on a heavily oxidised specimen than it did on a clean specimen. The friction coefficient of a heavily oxidised specimen dropped from approximately 0.3 to 0.13 from 0.12 to 1.2 m/s in Figure 6.25 and reached a low value of 0.1 in Figure 6.26. In comparison the clean specimen increased from a friction coefficient of approximately 0.16 to 0.18 between 0.12 and 1.2 m/s, as seen in Figure 6.22.

6.3.5.2 Spiral movement

The results using a “spiral” wear track are seen in Figure 6.27. The test had to be run at 0.12 m/s and results had a lower friction coefficient than the previous set of circular wear track results at that speed, shown in Figure 6.25. This is likely because the iron oxide will reduce the friction coefficient for the first rotation when using the circular motion, but the naturally formed oxide will be very quickly worn through so the oxide layer is not able to lubricate the contact. The friction coefficient of the heavily oxidised sample does drop below 0.1 on several occasions but sustained low friction did not occur, likely due to surface irregularities with the thick oxide coating.

6.3.5.3 Linear reciprocating movement

The linear reciprocating results generally fluctuate more than those seen in rotational testing due to the change in velocity during a cycle. The specimen is moved forwards and backward at 1 mm/s but there is a deceleration, followed by acceleration in the opposing direction as the cycle changes direction and then repeats itself. The main drawback of these tests is the low speed of the reciprocating module, the tests are far slower than those used on other test rigs during this work. As seen previously, the friction coefficient is likely to drop with increasing sliding speed and a lower speed will likely cause the upper ball bearing to plough through the oxide layer more effectively and therefore increase the friction coefficient.

Magnetite once again has a lower friction coefficient when compared with hematite at varying relative humidities, but the friction coefficient does not fall below 0.2 so it cannot be considered low. The lightly and heavily oxidised samples produced a lower friction coefficient than the oxide powders, but this was similar to the friction coefficient of a clean sample. An increase in humidity reduces the friction coefficient of the naturally oxidised samples slightly, but the fluctuation in results means that this is hard to distinguish.

6.3.6 Conclusions

The UMT contact is very different to that in the real wheel-rail interface but it allows closely controlled environmental conditions to be tested. Testing using oxide

pastes has not produced low friction values during this section of testing, with small differences seen between hematite and magnetite pastes, but with friction coefficients much higher than wet baseline values. The heavily oxidised samples reduced the friction coefficient in comparison to the clean samples at higher speeds and briefly produced low adhesion conditions with a friction coefficient of 0.1, but the low adhesion occurred over a very short time period so a different method would be needed to study how it occurred.

The spiral movement provided a far lower friction coefficient at low speeds than the rotating movement, which shows that the oxide is removed very quickly during rotation and may explain the high friction coefficients seen in both the pastes and the naturally generated rotating specimens.

The UMT testing shown here has shown that oxides are able to lower the friction coefficient under some conditions, but has not been able to achieve friction coefficients below 0.1, however this is significantly lower than the friction coefficients seen in a clean specimen. The trends seen in this work need to be validated on a test rig which better represents the wheel-rail contact, which will be covered in the next section.

6.4 SUROS Twin Disc Testing

6.4.1 Introduction to test rig

The Sheffield University Rolling Sliding rig (SUROS) is a twin disc test rig that applies a load to two counter-rotating steel discs, representing a small scale wheel-rail contact. The change in traction coefficient can be logged throughout the test. A schematic diagram of the rig operation is shown in Figure 6.29.

SUROS testing has proved useful in providing friction and wear data for a number of topics [67] [68] and is able to operate with the addition of artificial contaminants throughout the test which makes it suitable for this work.

As well as low adhesion due to leaf contamination [41], SUROS has previously been shown to produce low adhesion using water and oxides [4], which was highlighted in the review in chapter 2. The initial aims of these preliminary tests were to replicate the technique used by Hardwick et al. [4], the test method was then modified to explore how the traction coefficient varied over a number of different conditions. A focus was put upon testing different volumes of water and testing higher creep values.

An investigative approach was used, building up a series of tests in order to understand the conditions required for iron oxides to reduce the traction coefficient and find a reliable method to simulate and create sustained low adhesion on the SUROS rig, which can be used to better understand and mitigate the wet-rail phenomenon.

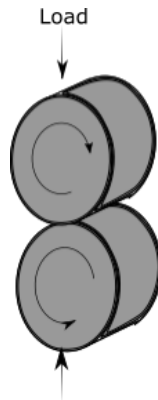


Figure 6.29: A schematic diagram of the two counter-rotating discs

6.4.2 Test apparatus

The SUROS rig consists of a solid machine bed with two independently spinning steel discs. One steel specimen disc in the SUROS rig is driven by a modified Colchester Mascot lathe, the other by an AC motor. The lathe is kept at 400 rpm

whilst the AC motor can be rotated at a higher speed to meet the desired creep value. Creep can be set constant throughout the test or ramped up over a period of time to produce a creep curve.

Load, up to 29 kN, is applied via a hydraulic arm so that the pressures present in the real wheel rail contact can be replicated. The pressure on the discs is controlled manually, with values of 900 MPa or 1500 MPa usually used. Shaft encoders monitor disc speed and revolutions. A shaft-mounted torque transducer is used to provide a traction coefficient value.

A schematic diagram of the SUROS rig is shown in Figure 6.30 and a more detailed description of the rig components is given in [69].

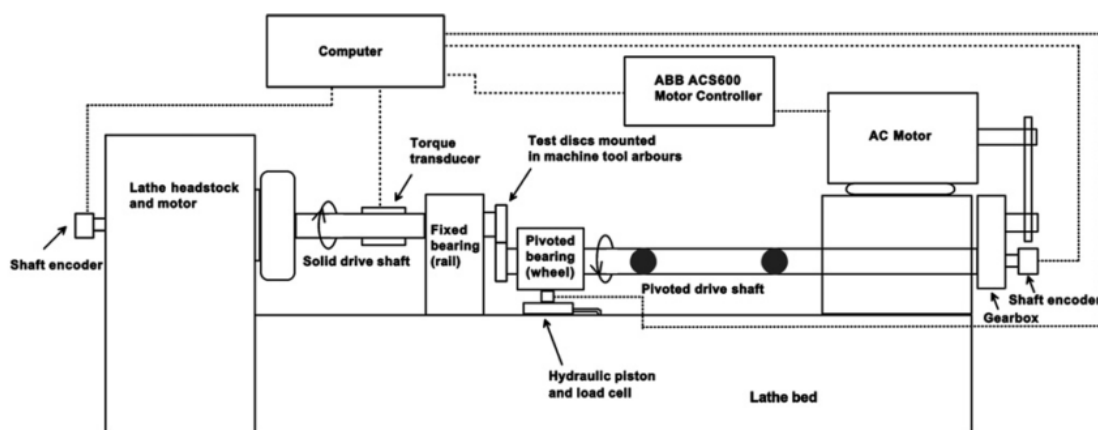


Figure 6.30: A schematic diagram of the SUROS rig and control system [69]

The SUROS discs have a diameter of 47 mm and width of 10 mm and are produced from R8T wheel material and R260 grade rail material to ensure that the chemical properties of the steel are those that are seen in a real railway situation. For this work, the upper disc has been machined from rail steel to act as the braking disc and the lower from wheel steel to act as the driving disc. Discs were ground to an Ra roughness of approximately $1 \mu\text{m}$.

Initially, water was applied drop-wise from a water reservoir that is held above the SUROS rig, with a hose delivering the water to the disc contact. A twist valve is situated at the end of the hose to control the flow of water. This was initially used to replicate the previous low adhesion results, but did not allow the accurate dispensation that would be needed when adding very small volumes of water.

Lower volumes of water application needed to be tested to assess whether it was very low amounts of water mixed with iron oxide that would reduce traction. The syringe pump provided a solution to this, pushing a syringe at a constant speed to release a continuous flow of water that can be programmed to a specific flow rate. A plastic syringe was inserted and connected to a piece of plastic hosing which

was routed along the top of the SUROS rig, ending approximately 3 mm from the upper SUROS disc. The hose was attached so that it dripped water onto the area of specimen that was soon to rotate into contact so that the water was pulled into the contact patch. A schematic of the set-up is shown in Figure 6.31. 5 ml syringes were used for water application rates up to 6 $\mu\text{l/s}$ and 20 ml syringes were used for rates between 6 $\mu\text{l/s}$ and 100 $\mu\text{l/s}$. The syringe plunger could be programmed to account for different volumes and brands of syringe by using the internal diameter of the syringes.

Oxide pastes were too viscous for the syringe plunger to be used. Instead they were applied by hand from a length of tubing that was attached to a 20 ml syringe.

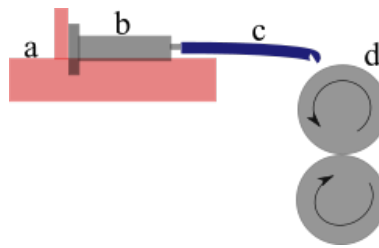


Figure 6.31: A schematic diagram of the syringe plunger set-up: Syringe plunger, (a); syringe, (b); plastic hosing, (c); SUROS discs, (d)

6.4.3 Methodology

6.4.3.1 Generic rig set-up method

This work involved a variety of different methods in order to test the range of conditions needed in this preliminary study, but the initial set-up procedure remained constant. Clean (non-oxidised and ground by the manufacturer) discs were ultrasonically cleaned in acetone to remove any oil-based residue and mounted into the rig and the diameter and width of specimens measured. The wheel disc was mounted to the lower AC motor and rail disc to the upper lathe, care was taken to avoid touching the disc surfaces to ensure no contamination occurred. The discs were aligned and altered using a bolt if necessary and another bolt was used to prevent disc contact when load was applied. The SUROS Labview program was opened and the following variables were added:

- Specimen width
- Specimen diameter
- Youngs modulus of specimen
- Desired contact pressure
- Slip (either as a constant value or a linear ramp)

The AC motor was powered and set-up to operate at the correct acceleration and speed range so that it would create the desired slip in the contact. The load and

torque readings were zeroed, the hydraulic controller was turned on and the hydraulic arm set to the required load for disc contact. The hydraulic arm was then turned off to remove load, the disc separating bolt removed and Labview program set to begin recording data. The lathe and AC motor were then turned on to begin disc rotation and the hydraulic arm turned back on to apply load and enable disc contact.

At this point the PC began recording data and the test was carried out. At the end of each test the load was removed which separated the discs before stopping them.

6.4.3.2 Oxide generation

Both naturally generated oxides and applied oxide pastes were once again tested. Generated oxides were formed on the SUROS discs using a pre-oxidation step by using a method created by Hardwick et al. [4]. Two discs were run together at 0.2 % slip, 1500 MPa and 400 RPM for 4000 cycles under dry conditions, this will be known as the “pre-oxidation” step. An oxide layer was visibly grown on the discs using this method and the discs changed from a reflective bare metal to a duller brown colour, this discolouration started at approximately 1000 cycles and continued over time. The oxide layer was light brown and appeared to be thin and tightly bonded to the metal substrate.

6.4.3.3 Creep ramp

The SUROS Labview software was programmed to perform a creep ramp, where an initial creep was set which could be linearly increased over a period of time. For these tests the creep was programmed to begin and stay at 0.2 % for 1000 cycles to make sure it was consistent and then ramp linearly from 0.2 to 1 % creep over 4000 cycles before remaining at 1 % creep until the test was stopped. Water application was started before the discs contacted and continued throughout the test

6.4.3.4 Investigations of low adhesion due to a generated oxide

The method used previously [4] to generate low traction was first replicated. A list of tests undertaken in this section is shown in Table 6.9. Each test is numbered so it can be referred to in the results section. The generic set-up method was performed at first with a pre-oxidised rail disc and clean wheel disc and conditions were matched to those used in previous work. The water dispenser used previously was then adjusted to a flow rate of two drops per second and a 11000 cycle test was run at 900 MPa and 0.3 % creep.

Test No.	Slip (%)	Load (MPa)	Oxide application	Water application	Number of cycles
1	0.3	900	pre-oxidised rail, clean wheel	2 drops per second	5000
2	0.3	900	clean rail, clean wheel	2 drops per second	5000

Table 6.9: Baseline testing and repetition of previous results

The SUROS rig was set-up with a pre-oxidised rail disc and a clean wheel disc as before. The syringe plunger was set-up as shown in Figure 6.31 to ensure an accurate and variable volume of water could be added. The piping was placed as close to the discs as possible so that water was released more regularly rather than building up into large drops due to water tension. SUROS was programmed to ramp from 0.2 to 1 % creep.

One dry baseline test was carried out in test 3 and then four water application rates were used in tests 4-8; 0.8 $\mu\text{l/s}$, 2.5 $\mu\text{l/s}$, 4 $\mu\text{l/s}$, 15 $\mu\text{l/s}$, 25 $\mu\text{l/s}$ and 100 $\mu\text{l/s}$. A list of tests undertaken in this section is shown in Table 6.10. Test 7 used the same conditions as test 6, but a non-oxidised rail disc was used instead of a pre-oxidised specimen.

Test No.	Slip (%)	Load (MPa)	Oxide application	Water application	Number of cycles
3	0.2-1	900	pre-oxidised rail, clean wheel	Dry	5000
4	0.2-1	900	pre-oxidised rail, clean wheel	2.5 $\mu\text{l/s}$	5000
5	0.2-1	900	pre-oxidised rail, clean wheel	4 $\mu\text{l/s}$	5000
6	0.2-1	900	pre-oxidised rail, clean wheel	25 $\mu\text{l/s}$	5000
7	0.2-1	900	clean rail, clean wheel	25 $\mu\text{l/s}$	5000
8	0.2-1	900	pre-oxidised rail, clean wheel	100 $\mu\text{l/s}$	5000
9a	0.2-2	900	pre-oxidised rail, clean wheel	0.8 $\mu\text{l/s}$	5000
9b	0.2-2	900	pre-oxidised rail, clean wheel	0.8 $\mu\text{l/s}$	5000

Table 6.10: Testing different volumes of water application

6.4.3.5 Investigations of low adhesion due to an applied oxide

SUROS was set-up as described previously. Iron oxide pastes were made to different wt % using the procedure discussed previously and placed in airtight containers before testing to avoid viscosity change due to evaporation. The paste was shaken for 60 seconds until thoroughly mixed before application to minimise any separation. The paste was applied using a 20 ml syringe before and throughout disc contact at different application rates, drops were added to the contact approximately every 20 seconds. The syringe was used in a position that meant the droplets of oxide paste would fall on the upper disc and would be rotated into the contact, as used in the water application.

Hematite pastes were first used at different weight percentages and two different application rates. A list of tests undertaken in this section is shown in Table 6.11.

Test No.	Slip (%)	Load (MPa)	Oxide application	Water application	Number of cycles
10	0.3-1	1500	60 % hematite paste, 2 ml/min throughout	N/A	5000
11	0.3-1	1500	60 % hematite paste, 6 ml/min throughout	N/A	5000
12	0.3-1	1500	N/A	2 ml/min	5000
13	1.5-3	1500	50 % hematite paste, 2 ml/min throughout	N/A	5000
14	1.5-3	1500	60 % hematite paste, 2 ml/min throughout	N/A	5000
15	1.5	1500	pre-coated with 60 % hematite paste	N/A	150
16	1.5	1500	pre-coated with 60 % hematite paste	pre-coated with 2 ml water	700
17	1.5	1500	N/A	pre-coated with 2 ml water	150

Table 6.11: Testing different oxide paste application

6.4.4 Results

6.4.4.1 Investigations of low adhesion due to a generated oxide

The SUROS rig was used under a number of conditions to test the hypothesis that iron oxide and water alone can cause low adhesion between wheel and rail

and therefore cause the wet-rail phenomenon. Rail discs were prepared and pre-oxidised using the previously discussed method. The SUROS discs that have not been subjected to a pre-oxidation procedure will be known as “non-oxidised” for the purposes of this report, although there will still be a thin oxide layer present due to natural oxidation.

Tests were repeated using identical conditions to those used in previous work at 0.3 % slip, 400 rpm and 2 drops of water per second using the water container. The pre-oxidised rail discs were first run against non-oxidised wheel discs and then another test was run using a non-oxidised rail disc and a non-oxidised wheel disc, results are shown in Figure 6.32.

Tests were then carried out using the syringe pump tested a range of water application rates between 2.5 and 100 $\mu\text{l/s}$ with all tests run at 900 MPa. The discs were put into contact and run for 1000 cycles at 0.2% slip so that the AC motor could stabilise, before ramping up to 1% slip over a period of 10 minutes. Results are shown in Figure 6.33. Limitations in the AC motor speed change mean that each individual test had a maximum creep of 1 %, which was acceptable for this testing because the wet tests have reached saturated slip by this point. A comparison of the results is shown in Figure 6.34. Both discs have a water application rate of 25 $\mu\text{l/s}$.

When a lower level of water application, 0.8 $\mu\text{l/min}$, was used the 0.2-1 % slip ramp tests gave anomalous results as seen in Figure 6.35. This graph has been plotted separately because the slip values are not comparable with other results. The test was repeated and the same issue consistently arises, it can be seen that the slip increases dramatically when each droplet of water is added before the feedback mechanism of the rig brings it back down to the desired value. This slip therefore does not follow the linearly increasing pattern of other tests so results are incomparable to the previous slip ramp tests. This anomalous effect may be due to the rapid change in traction values from a high to a very low value being too quick for the SUROS system to process it so could be a sign of very low traction coefficients being reached, but a final conclusion is unclear,

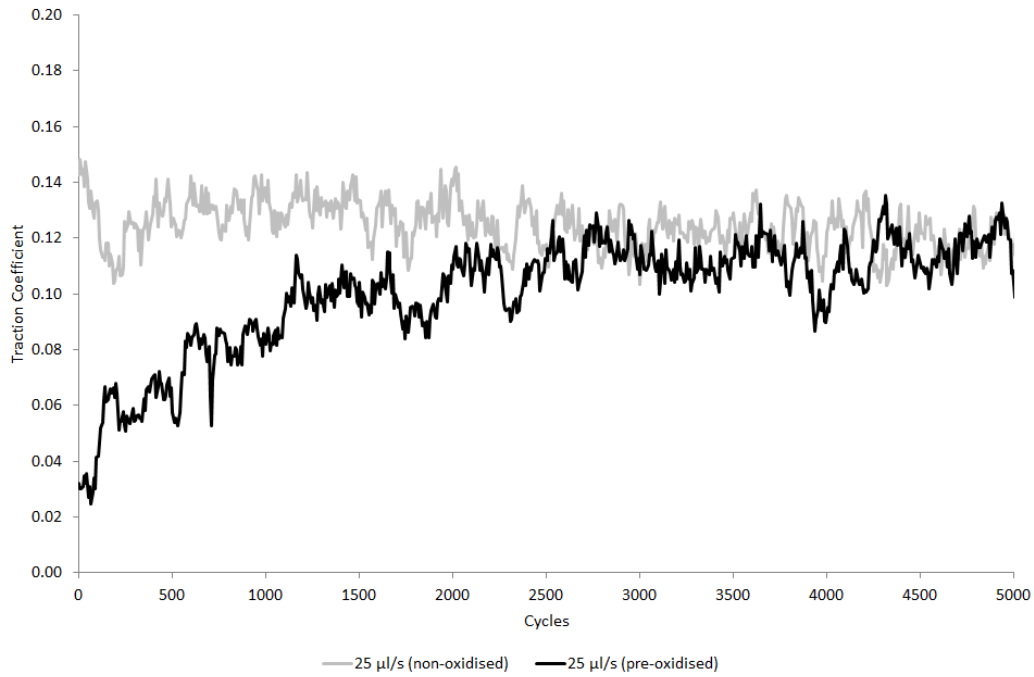


Figure 6.32: Tests 1, 2. Traction coefficients at 0.3 % slip for samples wetted at 25 µl/s, with and without pre-oxidation

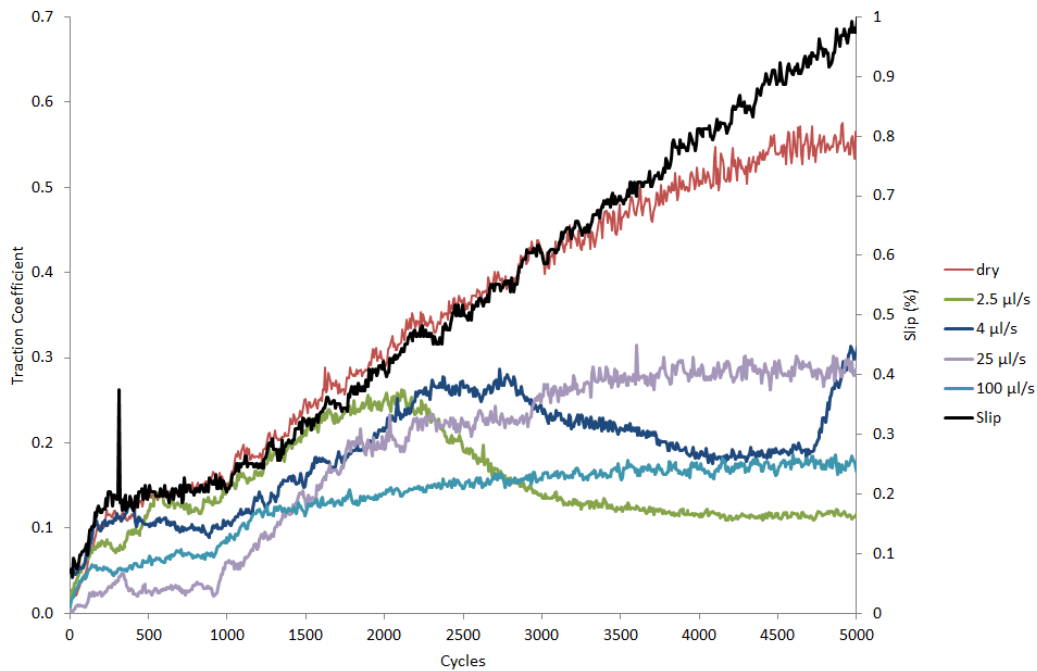


Figure 6.33: Tests 3, 4, 5, 6, 8. Water applied to dry discs, 2.5 µl/s, 4 µl/s, 25 µl/s, 100 µl/s over a 0.2-1 % creep curve

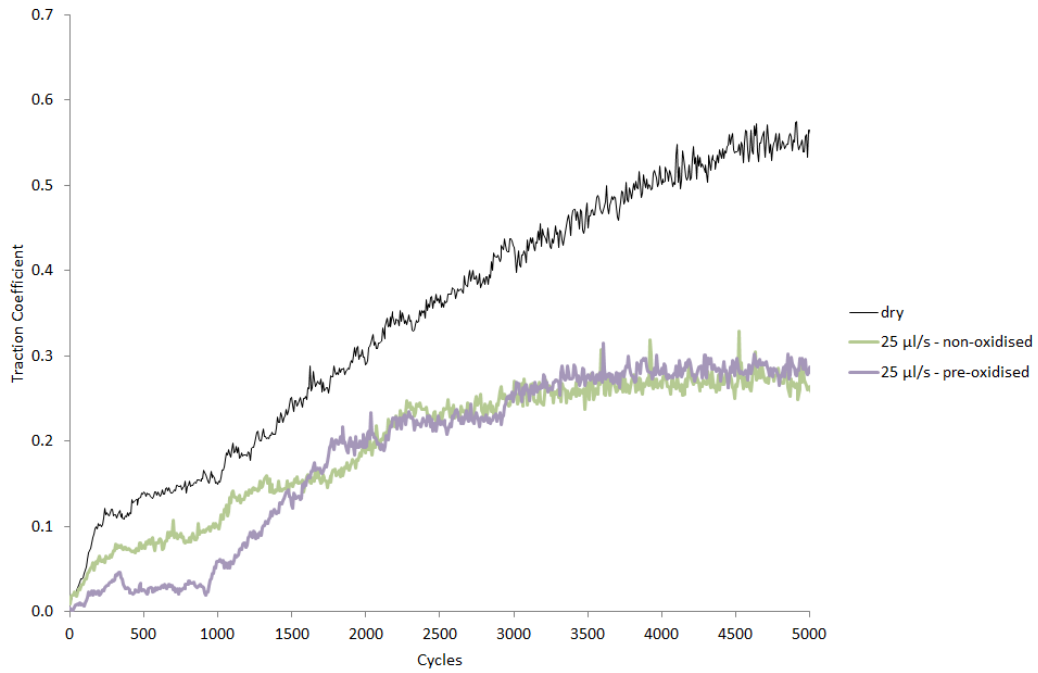


Figure 6.34: Tests 3, 6, 7. Pre-oxidised and non-oxidised rail discs run against non-oxidised wheel discs using a 0.2-1 % slip ramp

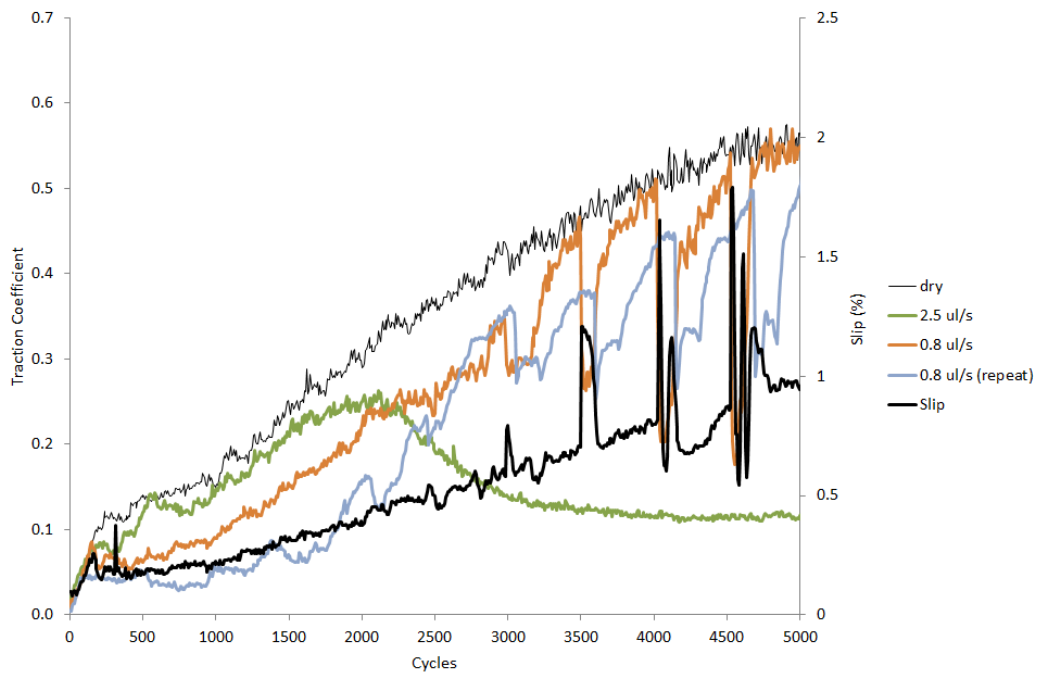


Figure 6.35: Test 9a and 9b. Traction coefficient values at 0.8 $\mu\text{l/s}$ water application

6.4.4.2 Investigations of low adhesion due to an applied oxide

Creep ramp between 0.3 and 1 % over 10 minutes was used to provide a partial creep curve for the 60 wt % hematite suspension, added via syringe at 2 ml/min and 6 ml/min. The results are shown in Figure 6.36. These are plotted against a 2 ml/min application of pure water rather than paste, as well as a dry value.

Higher slips were also tested to assess the effect on increasing slip levels on an iron oxide paste. A 1.5-3 % creep ramp was carried out for 50 and 60 wt % hematite solutions, designed to be a continuation of Figure 6.36. Higher wt % hematite was not successfully tested because the high viscosity meant it was hard to apply and quickly pushed out of the SUROS contact.

It appears that the addition of 50 and 60 wt % oxide pastes produce a low and relatively stable traction coefficient up to approximately 1.5 % slip. For the majority of the low slip stage of the test the 60 wt % has a lower traction coefficient, as low as 0.02 in places, whilst the 50 wt % paste has an average traction coefficient of approximately 0.05. The traction coefficient and slip start to fluctuate above 1.5 % slip. This is similar to that seen in previous tests involving low volumes of water and may be an issue with the SUROS programming system that is unable to process the large change in traction coefficient when a droplet of oxide paste enters to contact and then dries out, this effect is more prevalent for the more viscous oxide paste. Results for this test are shown in Figure 6.37.

It was hypothesised that keeping the slip value constant rather than ramping and not applying any oxides or water may help to reduce the fluctuation at higher slip values. The lower disc was coated in 2 ml of oxide paste before the discs were contacted and the test was run until the traction coefficient started to rise rapidly which indicated the contact was drying and the lubricating effect of oxide or water was over. was reached. In the “hematite” test the top disc was left uncoated. In the “hematite+water” test, 2 ml of water was applied to the top disc before contacting. No water or oxide was added during these tests so the test length was shorter than those undertaken previously because the contact quickly dried out. A value of 1.5 % slip was used to remove the slip fluctuations seen in the creep ramp method. A test was run with just 2 ml of water and no hematite paste to use as a baseline result. Results are shown in Figure 6.38. Tests were stopped early after the initial low traction period before the traction coefficient rose up to a dry value and damaged the surface during these tests so that the discs could be reconditioned and re-used as a limited number were available.

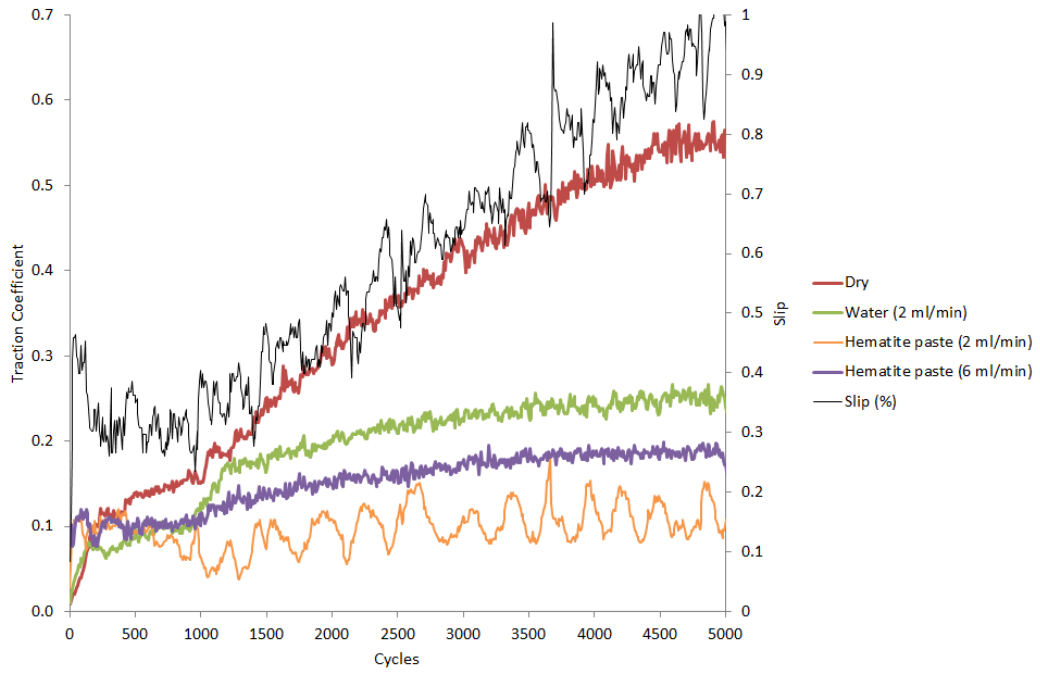


Figure 6.36: Test 3, 10, 11, 12. 60% Hematite at 0.3-1% slip, 2 ml, plotted against dry and wet values

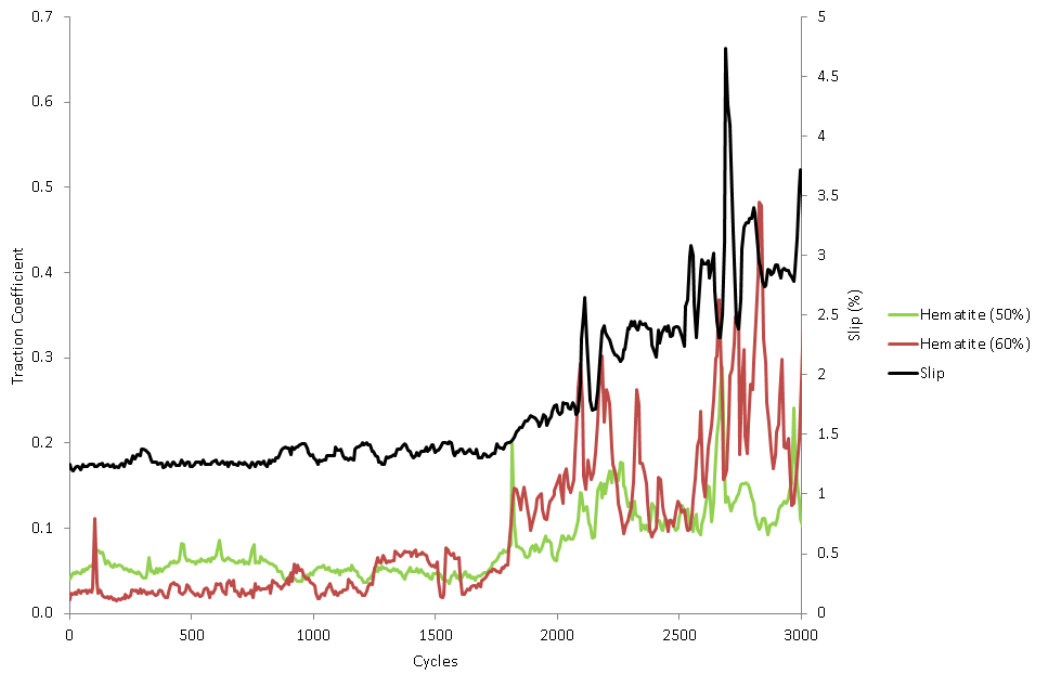


Figure 6.37: Tests 13, 14. 50 and 60 wt % hematite in a 1.5-3 % creep curve

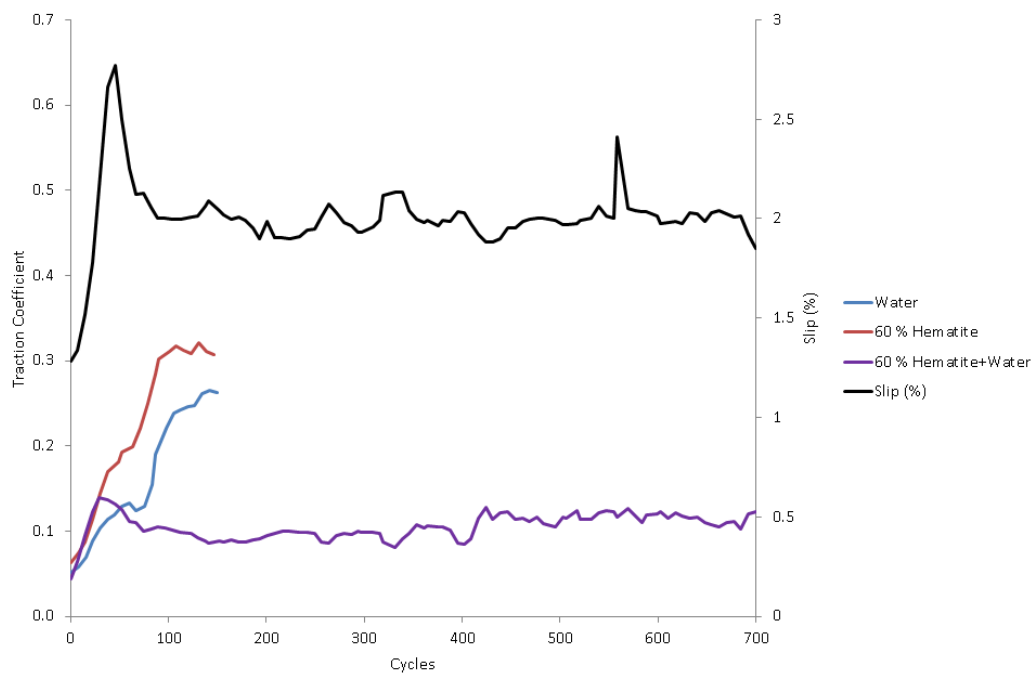


Figure 6.38: Tests 15, 16, 17. Wheel discs pre-coated in hematite paste

6.4.5 Discussion

6.4.5.1 Generated oxide

Very low and sustained traction coefficients due to oxide and water alone have been produced on the SUROS rig using a pre-oxidised specimen and water at low slip values. The traction coefficient during these tests varies greatly depending on how much water is added.

The change in traction coefficient over the creep curve tests with a generated oxide in Figure 6.33 can be split into 4 regions, shown in Figure 6.39. Region 1 is the initial lubrication due to the oxide layer on the rail disc. This occurs during low, linear slip and the traction coefficient starts low, below 0.1. The tightly bonded oxide layer will remain intact at first due to the low slip, but will eventually wear and become present on the previously bare wheel disc, both discs are coated with a brown paste at this point. Region 1 continues if slip ramp is not used and creep values remain low. The period of time that region 1 occurs for varies between tests, depending on both contact conditions, water application and the amount of previous oxidation.

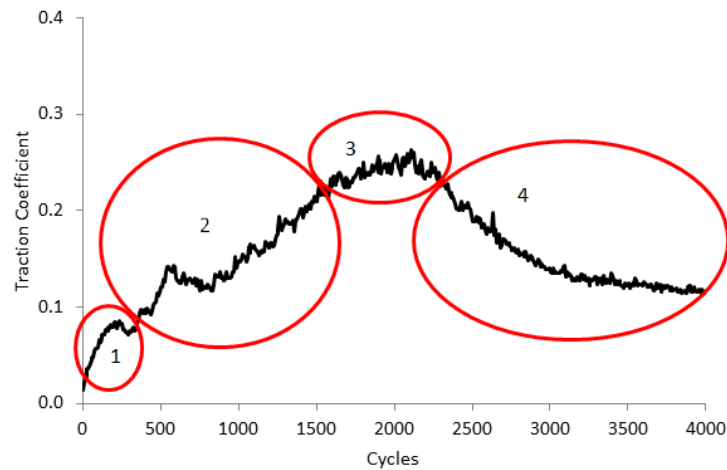


Figure 6.39: Traction regions

It is impossible to keep conditions constant during the pre-oxidation step and a visible difference in oxidation is seen, the oxide is noticeably thicker and more coloured in some tests than others. Factors that could affect the growth of the oxide layer include humidity, temperature, small changes in load and slip and any contamination still present on the discs after the acetone bath. These could affect rate, type and morphology of oxide growth so there may be chemical differences as well as physical differences such as thickness and roughness. The initial low traction coefficient rises very quickly in dry tests, presumably the water helps protect the initial oxide layer which provides the low traction when combined with water.

This brown oxide layer disappears and the discs return to their bare metallic appearance during region 2. This is where the traction coefficient rises to a value of about 0.2. The time taken to reach this value varies between tests, depending on the slip value, rate of water addition and amount of previous oxidation. The traction coefficient stays largely constant in region 3 and provides a similar traction coefficient to wet baseline tests where the rail has not been pre-oxidised. Region 3 seems to occur for most samples at around 1000-2000 cycles which is 0.4 % slip. Both discs have a bare metallic appearance. This is similar to the wet and non-oxidised baseline value so it is hypothesised that the initial oxide coating has no effect on this region. Some tests will stay in region 3 until water application stops, but other tests enter traction region 4.

The traction coefficient will start to decrease in region 4, this is accompanied by an audible and visual change from the SUROS rig. The traction coefficient decreases and a brown layer reappears as a band in the centre of the contact. The traction coefficient drops to a lower value and seems to remain low as long as conditions remain constant. A pool of brown viscous liquid is seen in between the contact discs, presumably formed from iron oxide, wear debris and the added water.

In terms of the tribological circuit that was discussed in the literature review, these naturally generated oxides would constitute the internal source flow. The oxides are created in the simulated wheel-rail contact under the heat, pressure and moisture present. Hypotheses were made in the literature review as to why the wet-rail phenomenon occurs and these can be revisited again after analysing these results. The hypothesis that there is a viscous and low shear strength paste formed between wheel and rail could be correct in this case. During “region 1” as proposed in Figure 6.39, all results are similar in that the oxide layer will produce very low traction coefficients at low slip when compared to a non-oxidised sample. At this stage there is a tightly bonded oxide layer on the surface as well as a mixture of water, iron oxide and wear debris present on top. This mixture will presumably produce a more viscous liquid in the contact. The combination of the oxide layer coated with paste is described in the literature review hypotheses.

During region 4 the thick surface layer of iron oxide seen in region one is no longer present having been worn away. Region 4 only seems to occur at very low levels of water which may be due to the paste becoming viscous enough to lower the traction coefficient. In the tests carried out so far, region 4 was also only entered after pre-oxidation. A brown layer of oxide was seen to appear as the traction coefficient was reduced. This method worked on some attempts but did not on others, possibly due to the water application needing to be stopped at a particular point in the test where a suitable amount of wear debris has built up. Too early and there may be not enough wear debris, too late and the wear debris may have been flung from the contact as the water droplets were flung out.

Very low levels of water were tested during the slip ramp method but these seemed to give anomalous results. At $0.8 \mu\text{l/s}$ the traction coefficient followed the pattern seen previously, starting low and climbing once the initial oxide layer was worn away. However, at the higher slip values the rig could not maintain slip when water is applied. The slip increased suddenly when a water droplet is added and the traction coefficient was lowered. The slip value then fluctuated until the control system brought the slip value back to its desired value, this process repeated itself whenever a water droplet was added. This could be due to the drop of water briefly creating a traction reducing paste, but then the paste is dried or spread out by the contact too rapidly so that the traction level rises to a dry level once again. The feedback mechanism in the rig may not be able to process this and the slip changes.

The initial traction coefficients of the oxidised rail disc in Figure 6.34 was significantly lower than the non-oxidised rail disc, approximately 0.02 rather than 0.06 and stayed lower for a longer period of time. Both traction coefficients increased to 0.2 at 2000 cycles, the surface oxide layer had been visibly removed by this point. The traction coefficient then stayed at a similar level for the remainder of the test, presumably the initial oxide layer had been removed and therefore the traction coefficient became similar to that of a non-oxidised wet baseline test.

Pre-oxidation seemed to have two effects on the traction coefficient. It firstly reduced

the traction coefficient during stage one, with the oxide protected from wear by the water. Secondly, no tests without pre-oxidation have been seen to enter region 4 where traction is once again reduced. This could be due to the wear particles from the initial oxide layer building up and remaining on the disc. They could mix with the water but only reduce the traction coefficient under certain conditions. These conditions could be the correct ratio of particles to water in the contact, a chemical change in the particles or a physical change such as roughness or higher slip.

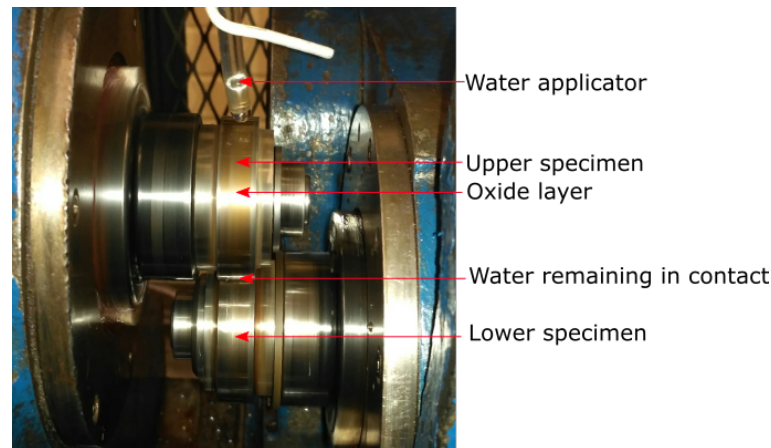


Figure 6.40: An oxide layer on SUROS discs during region 4

6.4.5.2 Applied oxides

The artificial pastes seemed to drop the traction coefficient to levels similar to those seen during the “natural test”, the main difference being that the naturally formed oxide layers produced a more stable traction coefficient with only water added, rather than fluctuating depending on how much oxide paste was added. This could be due to differences in either chemical or physical oxide properties or because the oxide paste is more easily pushed out whilst the natural layer remained in the contact. The results show that both the quantity and viscosity of paste have a large impact on the traction coefficient.

An oxide application rate of 2 ml/min appears to be the quantity that produces the lowest traction coefficient because upon oxide addition the traction coefficient rose to a maximum value then dropped to a minimum and rose slightly again before more hematite was added to repeat the cycle, creating an oscillating traction coefficient. A closer view of the 2 ml/min application of hematite paste at 60 wt % with labelled points at which the hematite paste is added is shown in Figure 6.41.

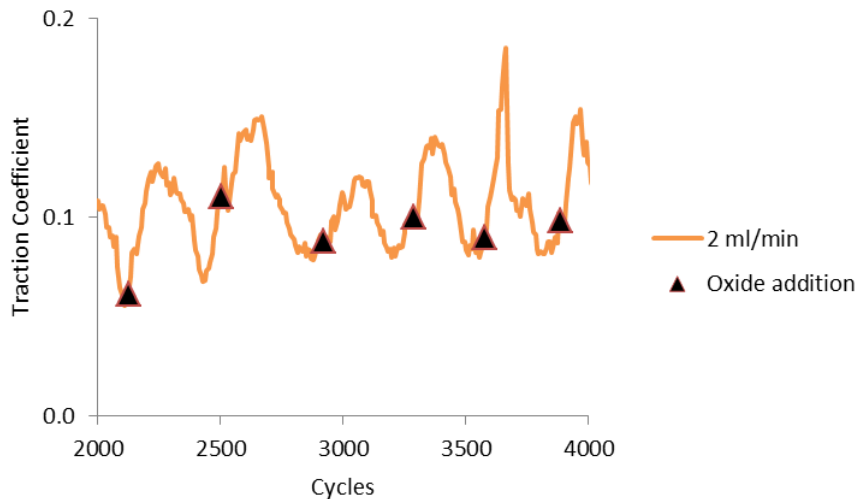


Figure 6.41: Labelled diagram of test 10, showing hematite addition

The 2 ml/min of paste application has a more fluctuating traction coefficient than 6 ml/min, possibly because of the large difference in conditions as the contact dries out. The larger quantity of 6 ml/min may be enough to prevent the contact drying out and therefore generating a stable traction coefficient, but it is the point at which the contact starts to dry that seems to produce very low traction conditions.

The initial paste application causes an increase in traction coefficient at 2 ml/min and 60 wt % oxide pastes and low traction is not observed until a period of time after paste addition where the paste layer appears to become thinner and less visible on the disc. The paste could be either not viscous enough or the quantity could be too high, upon addition of paste it takes a period of time to either be removed, spread out or for water to be squeezed out of it before it reduces the traction coefficient. Alternatively the oxide particles may need to be crushed smaller over a number of rotations or crushed into the steel surface to reduce the traction. Time may also be needed to build up a layer of oxide paste on the disc surfaces.

Applying oxide before, rather than during a test as seen in Figure 6.38 seemed to stabilise the slip and traction coefficient of the SUROS results and may provide a better platform when adding compounds which may cause or prevent low adhesion. There is still a short period at the beginning of the test where the rig adjusts to disc contact and has to ramp up the slip to the desired value, but this seems to be unavoidable using the current control system.

All the pastes were pushed out of the contact rapidly, leaving only a thin layer behind and with visible pooling of oxide outside the contact band. It is as yet unclear whether the whole paste is pushed out of the contact or whether the water component is pushed out to leave more viscous oxide powder in the contact, which was suggested in the railhead investigations. These applied oxides would initially

represent the external source flow in the tribological circuit discussed in the literature review, with particles flowing into the simulated contact from external sources. once in the contact, the powder would become part of the internal circuit.

6.4.6 Conclusions

Unlike many other test methods such as the pendulum and UMT, the SUROS can produce a rolling/sliding contact and real wheel and rail steel can be used which creates an excellent method to test the traction response when conditions are changed or contaminants are added. Low adhesion conditions, with traction coefficients far below 0.1, have been produced over significant periods of time at saturated slip values using iron oxides and water alone during these tests, which was not seen previously in the literature review.

The main drawbacks to the SUROS method are speed limitations and the repeated and “recycling” rolling contact. The speed is an issue with many small scale test rigs, 400 rpm on a 47 mm SUROS disc is equivalent to a 1 m/s velocity which is far slower than would be seen in a real low traction situation. This could have large effects on the behaviour of third body layers in the contact patch, especially when looking at shearing oxide layers, as highlighted in the rheometry work.

The second issue is that the discs also roll and slide over the same area every rotation in the SUROS rig which is problematic, especially in this situation looking at oxide layers. When adding oxide paste there will be a constant refreshment of oxide in the contact but when running on “natural” layers, any build-up of oxide is likely to be removed or changed with repeated contact cycles and the layer will be “recycled”. In a real situation the surface layer of the rail will only be contacted by the number of wheel sets on the train which may mean that the oxide layer will stay intact for a longer period of time or that any third body paste remains present on the railhead rather than being pushed out of the contact quickly as seen in these SUROS tests. When the discs rotate at 400 rpm this will accelerate the wear of any layer formed.

The two creep methods used in the previous results, constant and ramping, both have their merits and drawbacks. If a specific creep is needed for low adhesion to occur then a creep ramp may be more useful to test a range of values in a single test, for the majority of tests here the creep ramp was more useful when comparing conditions. The drawback of this method is that the SUROS control system could not keep a stable creep value during some tests when ramping the creep, particularly when artificially applying oxides.

If a paste from wear particles or surface oxidation is formed that causes low adhesion during a test, a constant creep is more likely to keep conditions stable that will allow this paste formation and therefore produce low adhesion for a longer period of time. If substrate conditions change or if oxide and water is “consumed” during low adhesion, either modified in the contact or ejected from the disc surface during rotation, then the conditions that produce the lowest traction levels at low slip or at

the start of the test will not necessarily produce the lowest traction levels at higher slip or at the end of the test so static creep tests are important to carry out.

Testing with naturally formed oxide showed that the traction coefficient can become very low and stable with iron oxide and water alone, without any other contaminants. Low traction coefficients have been seen in both the initial low slip period as well as at higher slip values.

The tests involving an artificially added oxide also reach very low traction coefficient values as long as paste was continuously added which implies that the paste is either modified in the contact or flung out of the disc contact. In comparison, the long periods of low traction seen in the natural tests can occur with only water being applied. The following have been hypothesised as to why these two different behaviours are observed:

1. The natural oxide layer is bonded to the SUROS discs and harder to push out of the contact than the oxide pastes
2. The natural oxide layer is removed but recycled in the contact rather than being removed
3. The natural oxide layer is formed as well as being destroyed or removed in the contact

The 2 ml/min hematite paste produced a lower but fluctuating traction coefficient as the contact dried whilst the 6 ml/min produced a higher but stable traction coefficient as the contact was consistently saturated and did not reach a point of drying. This reinforces the suggestion in the literature review that transient conditions could result in the wet-rail phenomenon, where the track has very low moisture levels and that the lowest traction is seen just before the track dries out. This was also discussed in the modelling work where the traction coefficient becomes a minimum as the wt % of hematite is increased, shortly before rising up to its maximum when the contact becomes too dry.

The results from this section have shown that oxides both in the internal and external source flows that occur in the tribological circuit can produce low adhesion. The knowledge gained in this section has been used to perform a more comprehensive set of tests in the next chapter, where variables can be altered and specimens analysed after testing to better understand why the wet-rail phenomenon occurs and how we can mitigate the problem.

6.5 Investigative Test Conclusions

The following conclusions can be made from work in the previous chapter:

- Using small scale test rigs under laboratory conditions, mixtures of iron oxides and water can produce lower friction conditions than water alone, but only under specific conditions
- Low adhesion due to iron oxide and water seems to be dependent on velocity
- Out of the three test rigs, only SUROS is able to repeatably produce low traction due to iron oxides and water alone, for an extended period of time

Because of the large range of conditions that could occur, a scattered approach has been used. A broad array of different conditions using different methods has been tested, but due to the variation in rigs it was difficult to use a systematic way of moving from one condition to another and keeping test conditions constant between test rigs was especially difficult. The more scattered approach has worked and been able to discover conditions using purely iron oxide and water that have caused low adhesion, whilst a more focussed and systematic approach may not have covered the range of conditions needed to find a method to produce low adhesion.

Each of the three different rigs used in the previous chapter has provided further knowledge into how the wet-rail phenomenon may occur. No rig has fully represented the wheel-rail contact but each has simulated an individual aspect of the contact conditions between wheel and rail.

The pendulum rig, although being the furthest from representing the wheel rail contact itself, was the most useful test in measuring a real railhead under a variety of conditions outside because it was the only portable method used here. Because of the ease of setup, it was useful when measuring transient conditions such as dew drying or drizzle beginning to fall and it was able to differentiate between railhead conditions with approximate friction coefficients being 0.6 for dry, 0.2 for wet and 0.15 when small amounts of water and oxide were present. It was useful in being able to test the top of a railhead without any further cutting or machining.

Although the UMT contact was more representative because it was a steel-steel contact, it was still completely sliding rather than rolling. The UMT could technically be programmed to run at a higher velocity than any other rig available, but in practice this produced fluctuating results due to the third body oxide layers necessary in this testing. It was the only rig available that could be easily used with a humidity chamber, although very little difference in friction coefficients was seen when using this, possibly due to the type of contact. A low friction coefficient of 0.1 was briefly seen when testing with a heavily oxidised sample, a small amount of water and high velocity.

Although like all the rigs used here it has its limitations, the SUROS rig has provided the best platform for testing low adhesion due to iron oxides and water alone. A rolling contact with creep control provides a contact that although smaller, replicates

the rolling and sliding motion of a real wheel-rail contact. It has the benefit of conditions being far more controllable than full scale laboratory testing and real field testing. The specimen discs can be made from authentic materials and are relatively inexpensive so that a large range of conditions can be tested. Changing the environmental conditions such as temperature and humidity would be difficult to achieve but the specimens can be oxidised and water or other contaminants can be easily applied. Even using the controllable laboratory conditions the naturally “grown” iron oxides were difficult to produce consistently, which highlights how difficult it would be to generate repeatable conditions in the field. Low adhesion was produced using both generated and applied oxides, but the applied oxides produced far more repeatable low adhesion conditions

Now that methods that produce low adhesion have been found, a more focussed approach is needed to assess how low adhesion may occur in certain situations and look at how progressively changing certain conditions will effect the friction levels in the contact patch. Information from this chapter, as well as ideas and hypotheses fed in from the modelling work, will be used to provide a more in depth analysis using just one test method to better understand how the wet-rail phenomenon occurs, why it occurs and then look at how the problem could be mitigated.

Based on this, the SUROS rig will be used in the next chapter to perform a series of tests that will look in more detail at the specific conditions that may cause the wet-rail phenomenon. The work will focus upon achieving low adhesion and analysing the specimens more thoroughly to better understand the mechanisms that result in the wet-rail phenomenon.

7 Simulation of the Wet-Rail Phenomenon

7.1 Introduction

The preliminary tests in chapter 6 showed that low adhesion due to iron oxide and water was achievable using small scale laboratory testing, but were not able to show exactly how it occurred. The tests in this chapter used the knowledge gained in the previous chapter to carry out a more in-depth series of tests using a single test rig to investigate the mechanism and conditions that cause the wet-rail phenomenon.

After assessment of the preliminary tests and modelling work, the SUROS rig was chosen to use for this test series. It was able to recreate a realistic rolling/sliding contact and generate low traction conditions using oxide and water alone, with both naturally generated oxides and applied oxide pastes. Oxide pastes were easy to apply during a test and the specimens were able to be analysed afterwards.

Oxide pastes were chosen for this series of tests rather than naturally occurring oxide layers. This was because the naturally occurring layers were difficult to repeatably generate and seemingly identical conditions would form a different thickness and colour of oxide layer with different traction coefficients. Oxide pastes on the other hand could repeatably cause low traction and the observations of railhead conditions in chapter 4 suggest that a paste is likely to play a role in the wet-rail phenomenon so these conditions could realistically occur.

The modelling work suggested that the traction coefficient would vary with different oxide paste viscosities, decreasing with increased viscosity up to a certain point and then rapidly rising. A test series was designed to assess whether this model was valid. Roughness analysis was carried out to assess how the test specimen surface changes throughout the tests so that the mechanisms causing low traction could be better understood.

7.2 Methodology

7.2.1 SUROS traction testing

Hematite powder and water pastes were made to 30, 40, 50, 60 and 70 wt % pastes using the methodology outlined in chapter 6. Hematite was chosen for the main body of testing because the literature review had highlighted that it was often found on the railhead and it was readily available as a powder. Previous analysis had been carried out on it in this work and it had been used previously for low adhesion modelling, which allowed the results of these tests to be compared to the modelling work.

A 6 % bentonite clay solution was also used in this work which, although viscosity testing was not able to be carried out at the time of these tests, seemed to have a similar viscosity to 60 % hematite and was able to be pumped using a syringe into

the contact using the same method as the oxide pastes. Clay forms a suspension with similar chemistry to that seen in the hematite pastes, insoluble particles form a viscous colloid when mixed with water and remain suspended in the liquid phase due to electrostatic interactions, so this test helped assess whether the oxide particles could be substituted in the paste and still result in low traction. In this situation clay particles are used as a substitute for oxide particles but clay could be deposited naturally from the surrounding soil and a similar suspension could be formed from ballast dust.

Any results averaged in this chapter, unless otherwise mentioned, are taken as the mean over the first 400 cycles of a test after oxide application. 400 cycles were chosen because it provided enough data to show a stable traction coefficient, but was a short enough time period to prevent difficulties in application of the very viscous oxide pastes to the SUROS contact. Some tests are shown for much longer time periods to show that the traction coefficient can remain low and stable for as long as the oxide paste is applied consistently.

The SUROS rig was set up using the methodology described in section 6.4. The discs were then contacted and paste application continued at 2 ml/min by syringing onto the upper disc throughout the test. Paste addition was started 10 seconds before contact and then continued at 2 ml/min throughout the test. Baseline water tests and dry hematite powder at 2 g/min were tested to generate data for 0 wt % and 100 wt % hematite. Tests were run 2 % constant creep as well as a 1.3-3 % creep ramp, the creep curve will be fully saturated at 2 %, but the change in traction coefficient before and after this point was analysed to generate a creep curve. The creep value of 1.3% was tested as a minimum because of limitations in the maximum creep range that SUROS was able to effectively cover in a single test.

Magnetite pastes were tested, made up to 50, 60 and 70 wt % and added to the contact at 2 ml/min at 2 % slip. A 6 wt % clay solution was also applied at 2 ml/min. A summary table of the SUROS tests carried out in this chapter is shown in Table 7.1.

Test No.	Slip (%)	Load (MPa)	Paste application	Water application	Length of test
1	2	1500	30 % hematite paste, 2 ml/min	N/A	400 cycles
2	2	1500	40 % hematite paste, 2 ml/min	N/A	400 cycles
3	2	1500	50 % hematite paste, 2 ml/min	N/A	400 cycles
4	2	1500	60 % hematite paste, 2 ml/min	N/A	400 cycles
5	2	1500	70 % hematite paste, 2 ml/min	N/A	200 cycles
6	2	1500	hematite powder, 2 g/min	N/A	400 cycles
7	2	1500	N/A	2 ml/min	400 cycles
8	2	1500	6 % clay solution, 2 ml/min	N/A	400 cycles
9	1.3-3	1500	50 % hematite paste, 2 ml/min	N/A	3000 cycles
10	1.3-3	1500	60 % hematite paste, 2 ml/min	N/A	3000 cycles
11	2	1500	50 % magnetite paste, 2 ml/min	N/A	400 cycles
12	2	1500	60 % magnetite paste, 2 ml/min	N/A	400 cycles
13	2	1500	70 % magnetite paste, 2 ml/min	N/A	200 cycles

Table 7.1: A summary of SUROS tests carried out in this chapter

7.2.2 SUROS specimen roughness analysis

SUROS specimens were analysed using an Alicona 3D roughness profilometer. The optical profilometer had the benefit of being able to generate a profile of a sample without needing physical contact with the specimen, which may have broken any oxide layer on the test specimens before disc separation. Roughness analysis was carried out on specimens at different traction coefficients to assess how the surfaces may be different between a sample causing a very low traction coefficient and one with a higher traction coefficient after paste addition.

Repeated tests were carried out using 60 wt % hematite and a 1.3-3 % creep curve. Tests were stopped and specimens analysed at different points in the test to assess how the oxide layer changes throughout testing. An unused SUROS specimen was

first analysed as a baseline. The test was then stopped after 400 cycles at 1.3 % slip with a very low traction coefficient of 0.03. Another test was stopped at 3000 cycles, where the slip value had increased up to 3 % and the traction coefficient had increased to 0.15. The three stages will be labelled as “before”, “during” and “after” the low traction period.

The specimens will continue to oxidise after testing and the morphology of the oxides may change over time. To minimise any changes, the specimen was put in a vacuum jar containing silica gel packets immediately after testing and taken out shortly before analysis.

Specimens were wiped gently with a paper towel before analysis. This was carried out in order to remove any excess powder left over from the oxide paste so the profile was taken only of the strongly bonded oxide and the metal surface, rather than of loosely bonded oxide powder that had settled on the steel surface. Specimens were then scanned over 3 positions under the Alicona 3D profilometer.

Roughness has been split into longitudinal and lateral roughness so that the two directions can be compared, a schematic of the two roughness profiles in relation to a SUROS specimen is shown in Figure 7.1.

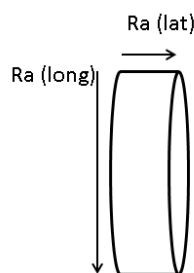


Figure 7.1: A schematic showing longitudinal and lateral roughness of a SUROS disc

7.3 Results

7.3.1 SUROS traction testing

Raw results for tests 1-7 are shown in Figure 7.2 and a box plot of traction data for these tests is shown in Figure 7.3. The box plot includes data for the first 400 test cycles for all pastes except 70 % hematite, which could not be applied for long enough due to its very high viscosity. 0 % oxide is water alone, generating a stable traction coefficient of approximately 0.18 when added to the contact at 2 ml/min. All oxide pastes produced a lower traction coefficient than water, the more viscous oxide pastes produce a lower traction coefficient until 60 wt % which produces a

traction coefficient below 0.05 at some points. This was the highest wt % paste that could produce a stable low traction period, which remained low for a prolonged period of time, as long as oxide paste could be continuously added to the contact.

70 wt % hematite initially produced a minimum traction coefficient as low as 0.02 when the paste entered the contact, but was difficult to apply due to the very high viscosity. The paste was too viscous to travel continuously down the tubing and often “bounced” off the discs rather than entering the contact so low traction was only produced until approximately 50 cycles, at which point the traction coefficient rose back up because oxide was not entering the contact. If the application method could be improved, the traction coefficient may stay at the very low value of 0.02 for a long period of time. In a real wheel-rail situation the application would not be an issue because the paste would remain on the railhead so very low adhesion could occur.

Raw results for a clay suspension in test 8, plotted against tests 3, 4 and 7 for comparison is shown in Figure 7.4. The clay suspension gives a low traction coefficient similar to that seen in the hematite suspensions, with a traction coefficient starting lower than the 50 % and 60 % oxides at 0.05, before rising slightly.

Raw results for tests 9 and 10 are shown in Figure 7.5 and 7.6 Low adhesion conditions, with a traction coefficient of approximately 0.06, were produced for long periods of time as long as oxide paste was applied continuously. The slip value fluctuated whilst increasing rather than the expected linear increase which meant that it is difficult to analyse any data for these creep ramp tests, this effect had been seen previously in the preliminary testing.

Average results for magnetite in tests 11-13 are shown in Figure 7.7, low adhesion was not seen for these tests so the raw results are not included. The traction coefficient remained above 0.16 for all tests, which was not significantly below that of water alone.

7.3 Results

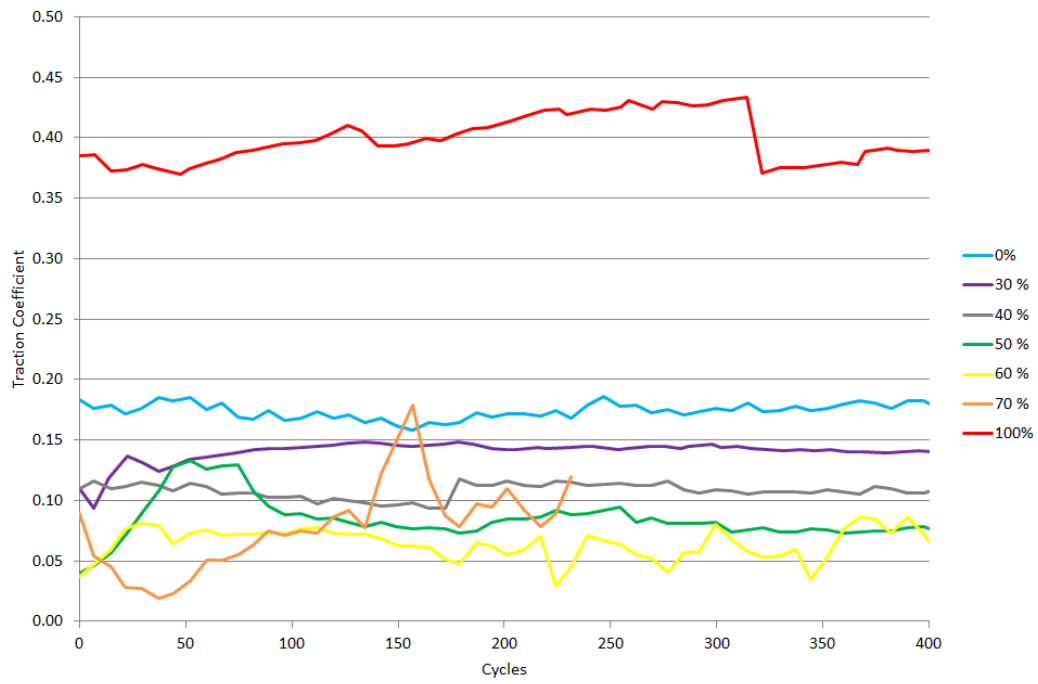


Figure 7.2: Traction coefficient for 30, 40, 50, 60 and 70 wt % hematite at 2 % slip

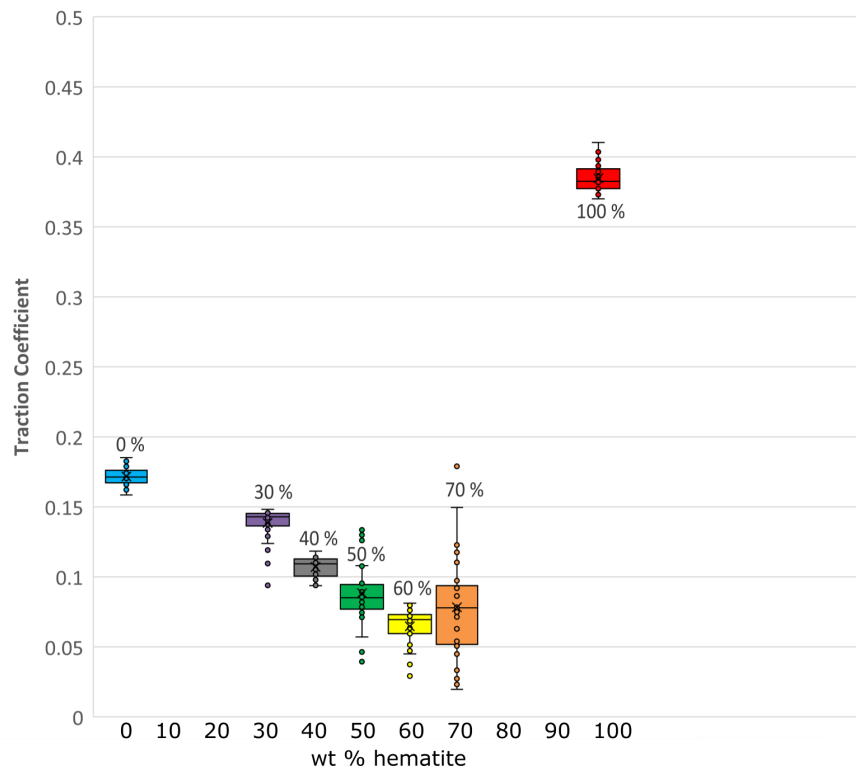


Figure 7.3: Traction coefficient for 0, 30, 40, 50, 60, 70 and 100 wt % hematite at 2 % slip

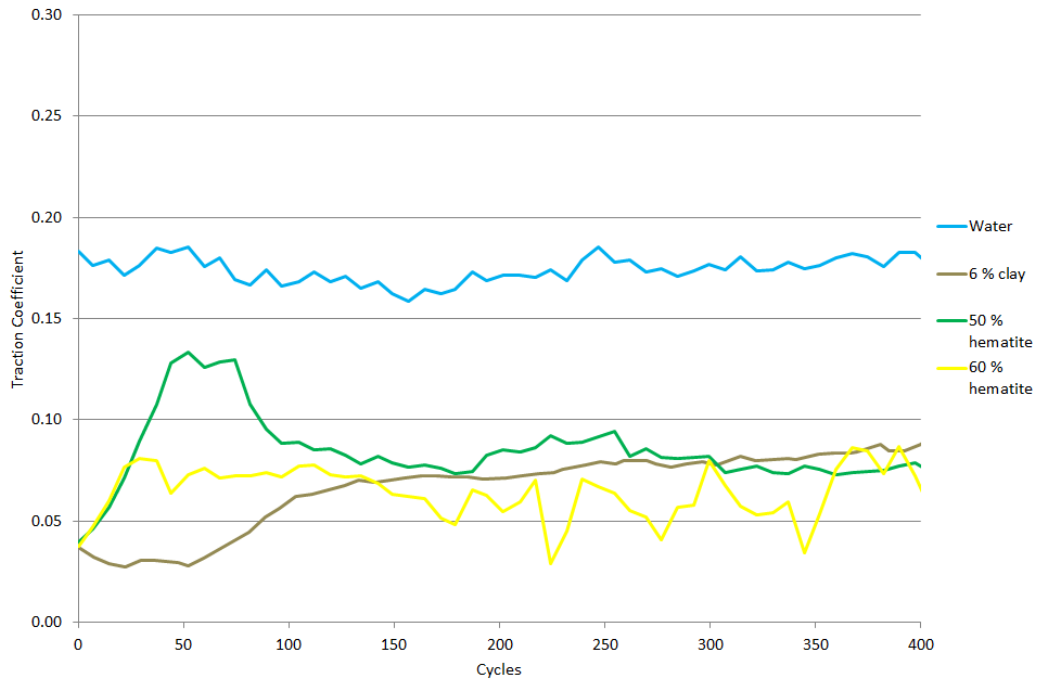


Figure 7.4: The traction coefficient when a 6 % clay solution was added to the SUROS contact, plotted against water and hematite pastes

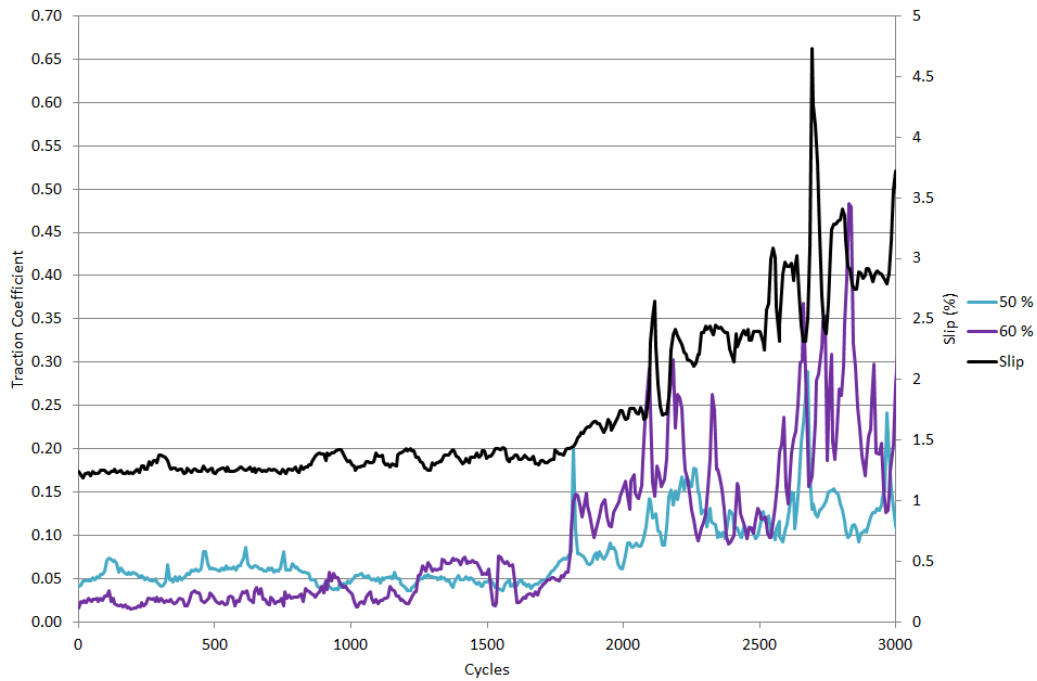


Figure 7.5: Traction coefficient for 50 and 60 wt % hematite at 1.3-3 % slip

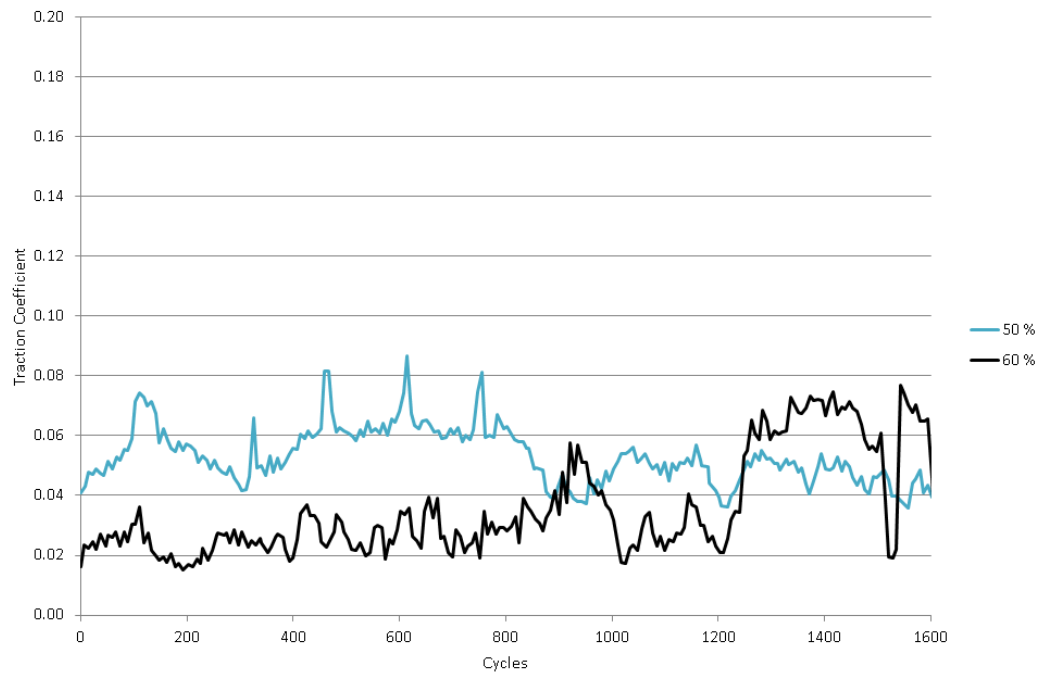


Figure 7.6: Traction coefficient for 50 and 60 wt % hematite at 1.3 % slip

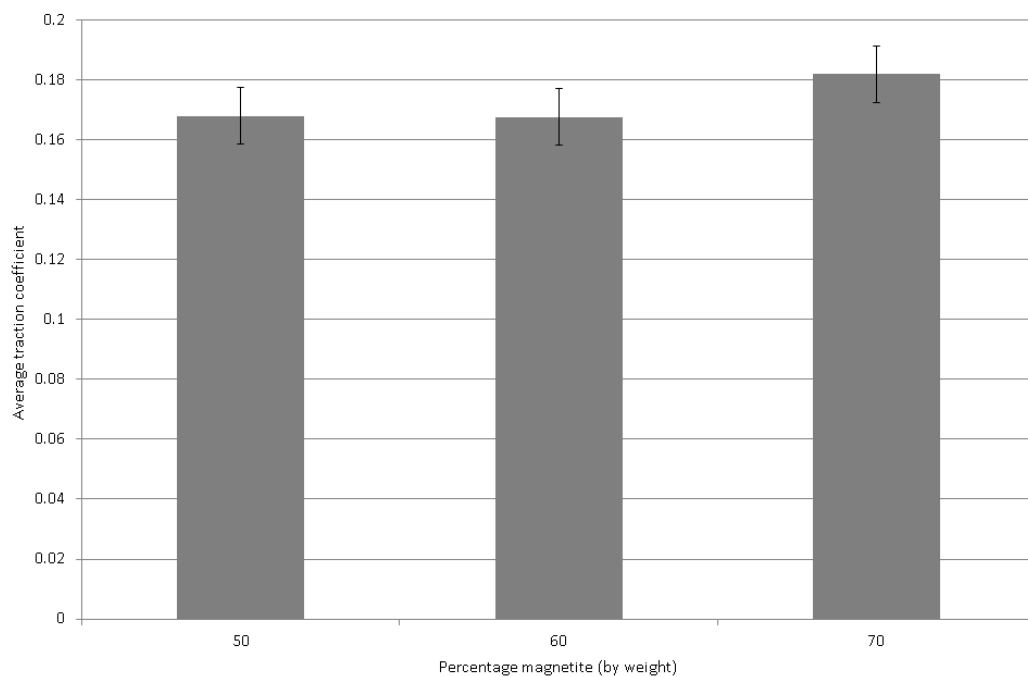


Figure 7.7: Average friction coefficients for 50, 60, 70 wt % magnetite paste at 2 % slip

7.3.2 SUROS specimen roughness analysis

Three tests were run using 60 wt % hematite paste under the conditions shown in Figure 7.5. Images of specimen discs before the test, during low traction at 300 cycles and after the low traction period at 3000 cycles are shown in Figure 7.8. Images through the Alicona optical microscope are shown in Figure 7.9. An example profile of one of the pits seen in the microscopy, areas of bare steel where the oxide layer has been removed, found on the rail discs after 3000 cycles is shown in Figure 7.10.

Average roughness for each disc is shown in Figure 7.11, with combined roughness of wheel and rail discs for each stage of testing shown in Figure 7.12. An example graph of raw results for the rail disc is shown in Figure 7.13.



Figure 7.8: SUROS wheel and rail discs before, during and after testing

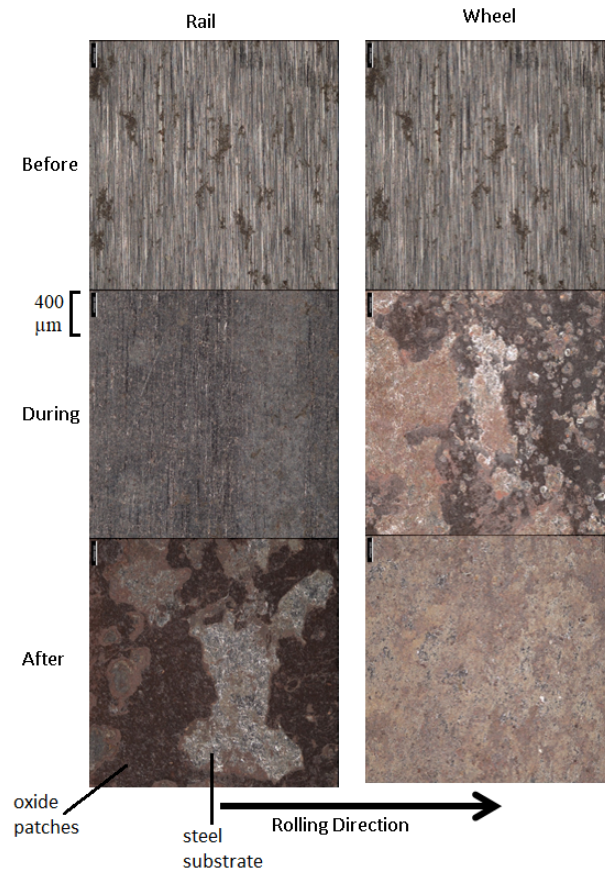


Figure 7.9: Alicona microscope images of rail and wheel surface before, during and after testing

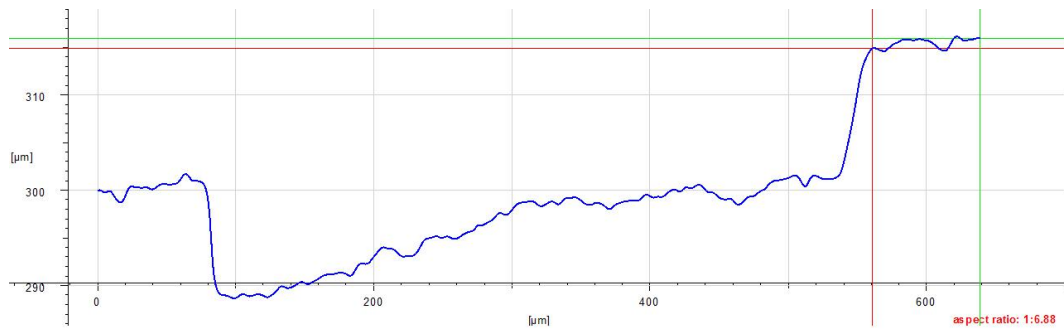


Figure 7.10: A pit in the oxide layer on the “after” rail disc

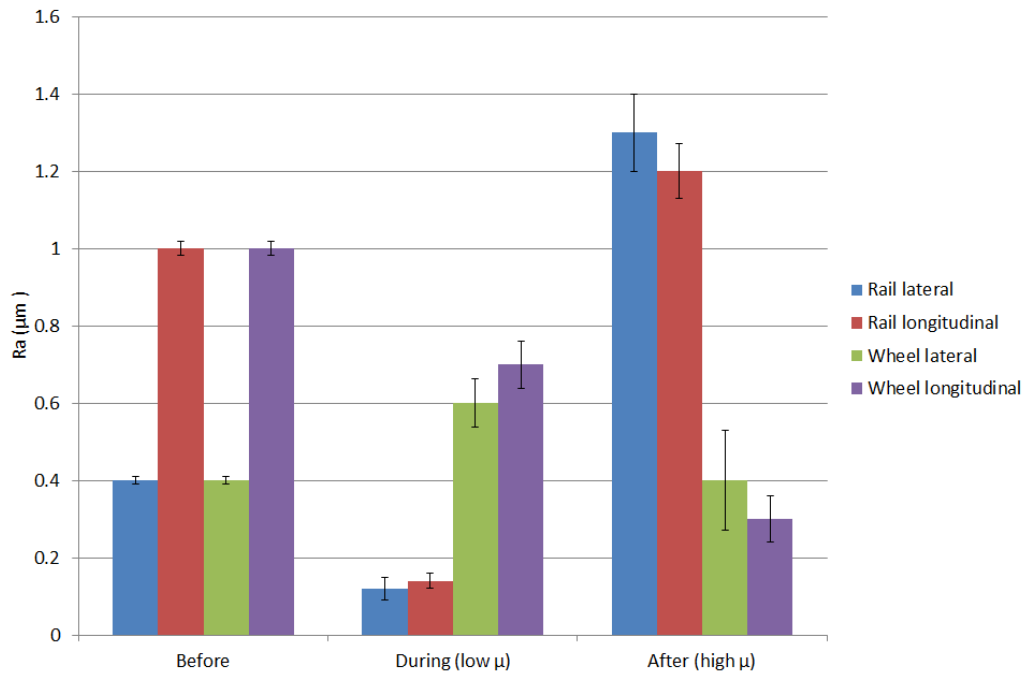


Figure 7.11: Longitudinal and lateral roughness of SUROS wheel and rail discs, before, during and after testing

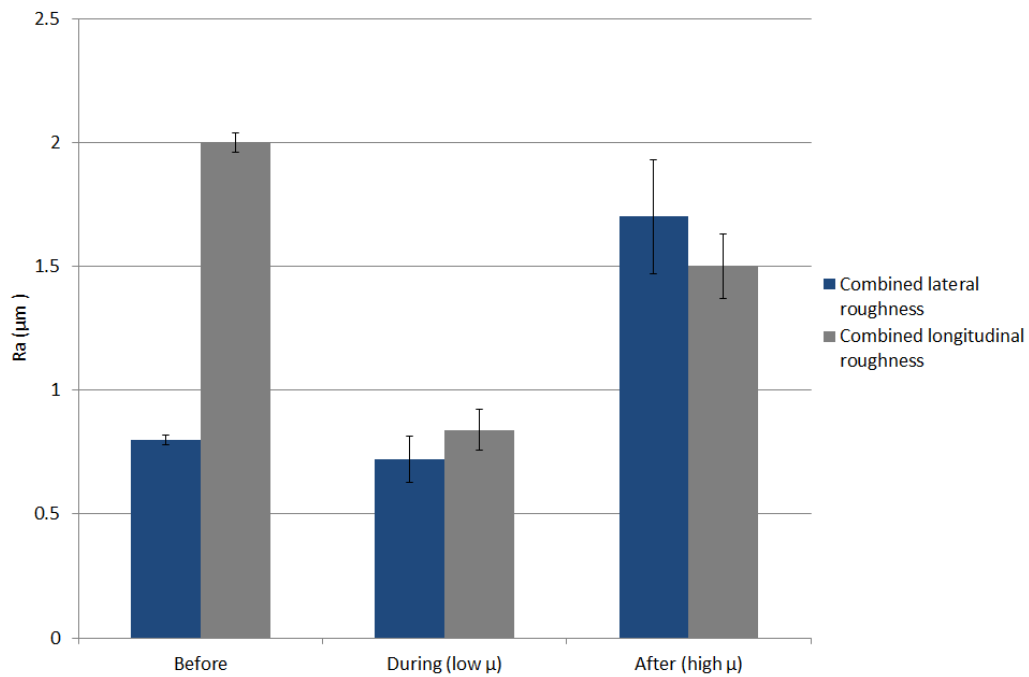


Figure 7.12: Combined wheel and rail roughness for lateral and longitudinal directions, before, during and after testing

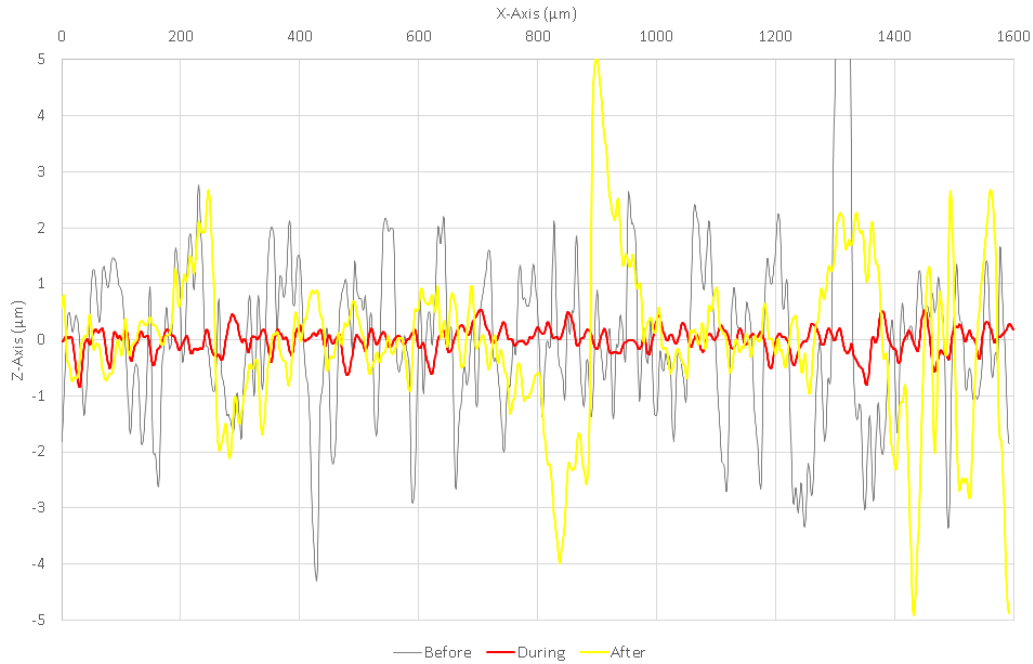


Figure 7.13: Example raw lateral roughness data for rail discs before, during and after testing

7.4 Discussion

7.4.1 SUROS traction testing

The hematite pastes show a substantial drop in traction coefficient at higher weight percentages, seen in Figure 7.3. 30 wt % at 2 % slip gives an average traction coefficient of approximately 0.14, lowering the traction coefficient slightly from a wet value of 0.17. The traction coefficient drops to approximately 0.06 at 60 wt %.

The lower wt % pastes could be easily applied to the SUROS discs, but the 60 and 70 wt % pastes became much more viscous which made application difficult, especially when trying to achieve a steady rate. 70 wt % hematite gave an extremely low minimum traction coefficient of 0.02 at 2 % slip when it was able to enter the contact, as seen in Figure 7.2. However it could not be applied at a steady rate, the highly viscous consistency meant that it was difficult to apply to the discs consistently for an extended period of time so the test had to be stopped and the traction coefficient fluctuated due to the varying amount of paste in the contact.

As carried out in the methodology in chapter 6, the oxides pastes had to be applied to the upper disc and pastes up to 60 wt % stuck to the upper disc and were pulled into the contact. 70 wt % hematite behaved differently and often “bounced” off the upper disc and fell out of the contact area rather than sticking to it and being

pulled into the contact so the contact was often dry with no paste in it. The traction coefficient dropped to a minimum whenever any paste stuck to the disc and was able to be pulled into the contact. In a real contact the paste on a rail would be trapped between wheel and rail and would not have to rotate into the contact, so higher viscosities may cause low adhesion in a real railway situation but are unable to using the SUROS rig.

The large fluctuations during the slip ramp as shown in Figure 7.5 are not present in the constant creep tests at 2 % slip. This suggests that there may be issues with the SUROS rig stabilising the slip value when trying to increase creep during oxide paste applications, which was why a second set of results were carried out at 2 % slip rather than using the creep ramp technique throughout.

Magnetite does not produce low traction when pastes are added to the contact. This is likely due to the magnetite and water suspension being far less stable than hematite and water as seen in the introduction to chapter 6. The magnetite particles separate from water very quickly so likely separate very quickly in the contact rather than remaining as a paste.

7.4.2 SUROS specimen roughness analysis

The Alicona profilometer was able to measure the roughness of any compacted iron oxide layer, as well as the steel substrate. The discs visibly change colour throughout the test due to the build up of iron oxide on the contact surface which remained on the specimens when the tests were stopped. The loosely bonded oxide is rubbed from the disc before analysis so what is visible in Figure 7.8 is a strongly bonded layer. It can be seen that even after 400 cycles a layer is built up on the wheel disc. At 4000 cycles this layer is much thicker but has transferred to the rail disc, with only a thin layer present on the wheel disc.

The roughness seems to be lowered substantially during low adhesion, especially the rail disc. This could either be due to mild wear of the steel or the build up of a solid oxide layer may create a smoother surface on top of the steel. The low combined roughness, below 1 μm , has been recorded on railway lines previously as discussed in the literature review.

The build-up of the oxide layer suggests that the water is squeezed out of at least some of the iron oxide paste in the contact, leaving the dry powder behind to become compressed and build up the layer seen on the test specimens. The darkening colour of the layer throughout the test is likely to be caused by the mixing of hematite powder with steel wear particles and naturally oxidised steel.

This layer appears to have been flaked off in sections to leave holes which expose the bare metal underneath. The profile of the pits, shown in Figure 7.10, shows that the layer is approximately 12 μm thick in places. The third body layer on a railhead was found to be 15 μm in the literature review so this is representative of real railhead

conditions, This is thicker than the combined roughness of the wheel and rail steel discs so leads to the suggestion that under certain conditions, the wheel disc could be entirely contacting the third body oxide layer on the rail disc, rather than the steel disc. The remaining oxide layer on the steel specimens was very tightly bonded to the steel and was difficult to remove after testing so it is likely that this layer could prevent wheel and rail contact on the railhead, at least at lower creep values.

7.4.3 Links to the adhesion model

The adhesion model discussed in chapter 5 was used with conditions that were as similar as possible to SUROS, with hypotheses formed as to how the curve would change when the SUROS geometry and dynamic effects were taken into account. This curve for the SUROS “best fit” using a combined wheel and rail roughness of 0.7, as gathered during this work, has been plotted alongside the average values for the hematite paste collected during this work at 2 % slip, except 70 % where a minimum value has been used and shown in Figure 7.14.

The experimental results show a decrease in traction coefficient earlier than predicted in the model, but both reach a very low value and rise back up quickly. Hematite weight percentages between 70 and 100 % were not tested due to difficulties applying the viscous pastes to the discs, but given the trend observed it seems reasonable to suggest that the traction coefficient will continue to be lowered until the paste reaches the limit of the packing structure and the paste is saturated by hematite, as discussed in the modelling work. After this point, any excess hematite added will be found as a powder and is therefore likely to substantially increase the traction coefficient. It is currently unclear where this saturation point will be, but it is likely to vary with particle size, temperature, pressure and the presence of any contaminants. therefore finding this point for a hematite and water paste would not be beneficial to the understanding of the low adhesion problem.

The wt % that is fed into the upper disc is not necessarily the wt % of paste that will enter the contact. The build-up of a dry iron oxide layer suggests that water can be squeezed out or evaporated in the contact so the paste may become more viscous than when added, perhaps explaining why a lower traction coefficient than previously predicted will occur at lower hematite weight percentages.

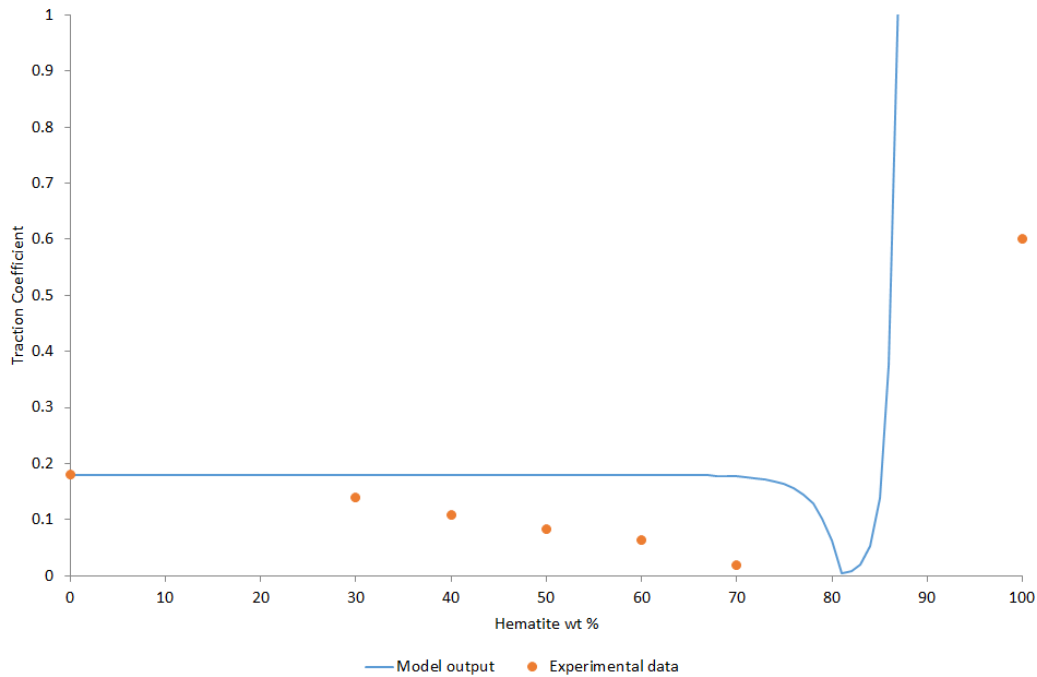


Figure 7.14: The change in traction coefficient, experimental results plotted against the modelling output from chapter 5

7.4.4 Hypotheses validation

A mechanism for low adhesion that was suggested after the literature review is that oxide and water alone could create a paste that results in loss of traction. The paste was thought to be either on top of the bare steel substrate, or covering a second tightly bonded layer that lowers the roughness of the steel.

The work carried out in this chapter supports the hypothesis that a paste alone can lower the traction coefficient without the need for an intact oxide sub-layer. Although an oxide layer is built up throughout the test, the raw data in Figure 7.2 shows a low traction coefficient immediately which suggests that a sub-layer of compacted powder is either formed within a few cycles, before the slip stabilises and the first data point is collected, or either a sub-layer is not required for low adhesion or a layer is formed very quickly. There is a small decrease in traction coefficient during some tests from the initial value which could be due to the oxide layer lowering the roughness or mild wear, but the low roughness values seen here are similar to those noted on actual track which may mean that an underlying oxide layer would not be necessary in a real situation to decrease the roughness.

As a result, it is likely that the viscous paste on top of the rail, without needing an intact layer of oxide, is sufficient to produce low adhesion. An underlying layer will likely cause similar low adhesion as long as the roughness remains low, but the

images in chapter 4 of a railhead after a wheel slide suggest that any underlying layer will be removed by the first wheelset if WSP is not present and the wheel slides. The clay substituted tests show that other similarly shaped particles that form a stable suspension can produce low adhesion and the problem is not just restricted to hematite alone. As a result, the low adhesion causing paste that is seen on a real railhead does not have to be made from oxide and water alone, it will likely contain other contaminants that were discussed in the literature review. Low adhesion did not occur when using magnetite, likely due to the instability of the suspension that resulted in rapid separation of oxide particles and water.

7.5 Conclusions

Hematite and clay suspensions are able to decrease the traction coefficient to levels that would be classed as low adhesion when added to the SUROS twin disc test rig whilst magnetite suspensions do not, which could be due to magnetite forming a less stable suspension. The higher wt % hematite pastes produce a lower traction coefficient, this trend is likely to occur until the paste is completely saturated by hematite. Hematite powder, without any water addition, produces the same traction as a dry test with no contaminants. On a real track, a small amount of water could mix with iron oxide and wear debris to form a thick paste and produce the very low adhesion conditions seen in the laboratory during this chapter.

The low traction coefficients seen in this work occur at low roughness values, which are realistic in comparison to roughness values of wheel and rail as discussed in the literature review. The data collected supports the model discussed in chapter 5 which predicts a significant reduction in adhesion coefficient at high wt % of oxides. The model, carried out to fit SUROS as best as possible, shows low adhesion occurring at a higher wt % of oxide than results obtained using experimental testing but suggestions for why the model may predict these higher values were discussed in the modelling chapter.

8 Chemical Analysis of the Wet-Rail Phenomenon

8.1 Introduction

X-ray photoelectron spectroscopy, XPS, was noted in the literature review as a potential method to generate information on what type of oxide was found in the contact as it could provide details on elements including iron and oxygen on a sample. It can measure the elemental composition and chemical state of a material, typically up to 10 nm below the surface.

XPS works by irradiating the sample with x-rays which causes photoelectrons to be emitted from the surface. The binding energy and intensity of these electrons can be measured which can be used to gather elemental data.

XPS analysis was carried out using 6 samples to try and understand how oxide and organic contamination changes after entering the wheel-rail contact and how the artificially added contamination differs from a layer that occurs naturally on the railhead. XPS was carried out on the following samples:

1. A sample of hematite powder of the same type that has been used to make hematite pastes for SUROS testing in chapter 7
2. A layer that was formed on the SUROS disc surface, after hematite was mixed with tap water to form a 60 weight % suspension and added to a test at 2 % creep for 1000 cycles which produced low traction
3. A sample of pectin powder, before it was mixed with water and added to the SUROS rig
4. A layer that was formed on the SUROS disc surface, after pectin powder was mixed with tap water to form a 7.5 wt % solution and added to a test at 3 % creep which produced low traction
5. A sample of a leaf layer created by adding leaves to a railhead, before wetting and rolling over with a full scale locomotive to produce a layer which caused low adhesion during a braking test
6. A sample of a leaf layer formed naturally on the railhead on a Northern Rail line near Barnsley, which is a notorious low adhesion hotspot

Although organic contamination is not the focus of this thesis, the results from the pectin layer are included in this section because they show the formation of hematite during the test.

8.2 Methodology

Samples were removed from the railheads and SUROS specimens with a metal spatula and transported in aluminium foil. The XPS tests were carried out by the University of Sheffield Surface Analysis Centre using a Kratos Supra with a monochromatic aluminium source, two points of each sample were analysed and a low resolution “sweep” was carried out before obtaining high resolution spectra for each element present. Samples were in the form of powders and pressed into soft

indium foil for analysis. A low resolution survey scan was performed to determine which elements and then high resolution scans were taken for each element.

8.3 Results

The results from the two survey scans for each sample are shown in Table 8.1. The XPS analysis generated a large number of spectra, but six spectra that show the key outcomes of this XPS analysis are included in this chapter.

Figure 8.1 shows an XPS survey scan of pectin powder before it was added to the SUROS contact, with Figure 8.2 showing the spectrum after contact. An increase in iron oxide, likely to be hematite, is seen in the spectrum at 707 eV. No oxide powder was added to these tests which means that the steel is being oxidised into hematite during pectin addition. The carbon spectrum also shows that the type of bonding has changed in the pectin, although it was unclear what transformation has taken place.

Figure 8.3 shows a high resolution O 1s XPS spectrum of the hematite powder before it was made into a paste, whilst Figure 8.4 shows the O 1s spectrum of powder taken from the surface of a SUROS disc after testing with a 60 weight % hematite paste at 2 % slip. The survey scan of the hematite samples show that the oxide has remained in the same oxidation state, but these high resolution scans show an increase in the oxygen peak at 531.7 eV which is likely because some of the hematite has been converted to an oxyhydroxide.

An XPS survey scan on the leaf layer that was generated by placing wetted leaves onto a railhead at the Long Marston test track and then rolling over with a locomotive is shown in Figure 8.5. The layer was blackened and loosely bonded, with pieces of leaf matter visible.

An XPS survey scan of a black layer that has been formed on top of a railhead on a Northern Rail line during the autumn season is shown in Figure 8.6. The area that this layer was taken from is a known low adhesion hotspot. The layer was black and tightly bonded, the powder was removed as a solid that did not resemble organic matter.

Sample	Na	Fe	Mn	O	N	Ca	C	Cl	Si
Pectin (before) N1	1.0	<0.1	<0.1	37.4	0.6	<0.1	61	<0.1	<0.1
Pectin (before) N2	0.9	<0.1	<0.1	37.3	0.9	<0.1	60.9	<0.1	<0.1
Pectin (after) N1	<0.1	1.1	<0.1	29.4	3.8	<0.1	61.7	<0.1	4.1
Pectin (after) N2	<0.1	0.8	<0.1	29.6	4	<0.1	61.9	<0.1	3.7
Hematite (before) N1	1.3	15.1	0.7	53.6	<0.1	2.6	15.9	0.5	6.5
Hematite (before) N2	1.2	16.5	0.7	53	<0.1	2.5	15.1	0.6	6.9
Hematite (after) N1	1.3	11.3	0.4	50.2	<0.1	5.6	19.8	0.5	5.7
Hematite (after) N2	1.3	10.3	0.3	50.5	<0.1	6.1	20.3	0.5	5.4
Northern Rail N1	<0.1	4.8	<0.1	42.1	1.1	0.4	36.7	<0.1	12.8
Northern Rail N2	<0.1	4.4	<0.1	42.9	0.9	0.4	36.7	<0.1	12.7
Long Marston N1	<0.1	0.2	<0.1	19.6	0.7	0.6	77.9	<0.1	1.1
Long Marston N2	<0.1	0.1	<0.1	18.2	0.7	0.5	79.5	<0.1	1

Table 8.1: Surface compositions (atomic %) determined by XPS survey scans

8.3 Results

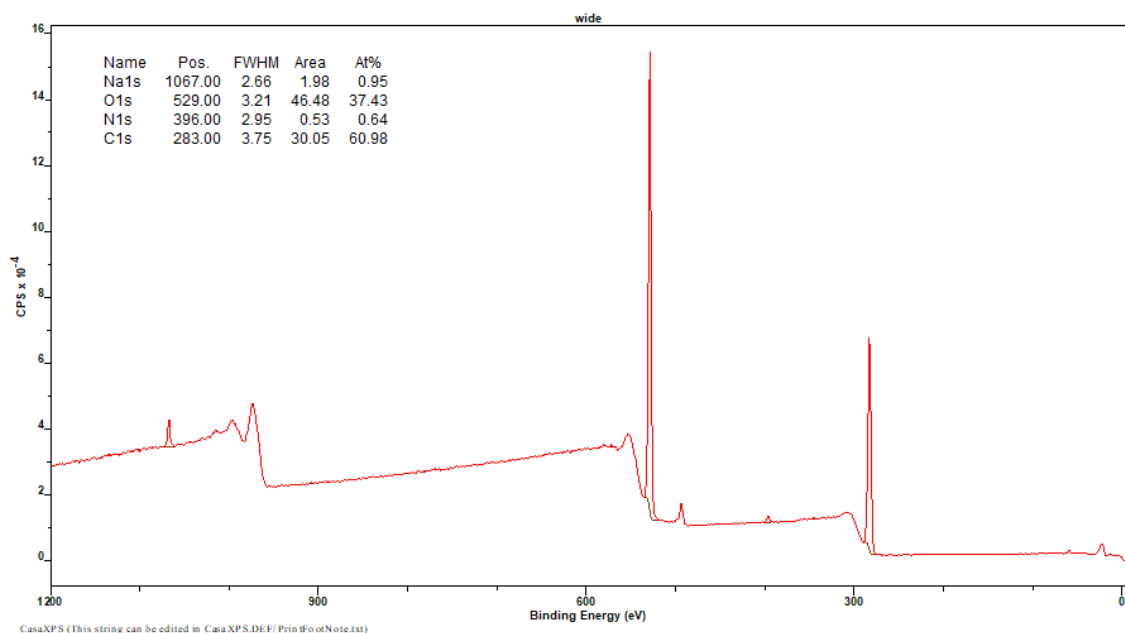


Figure 8.1: XPS survey scan of pectin before disc contact

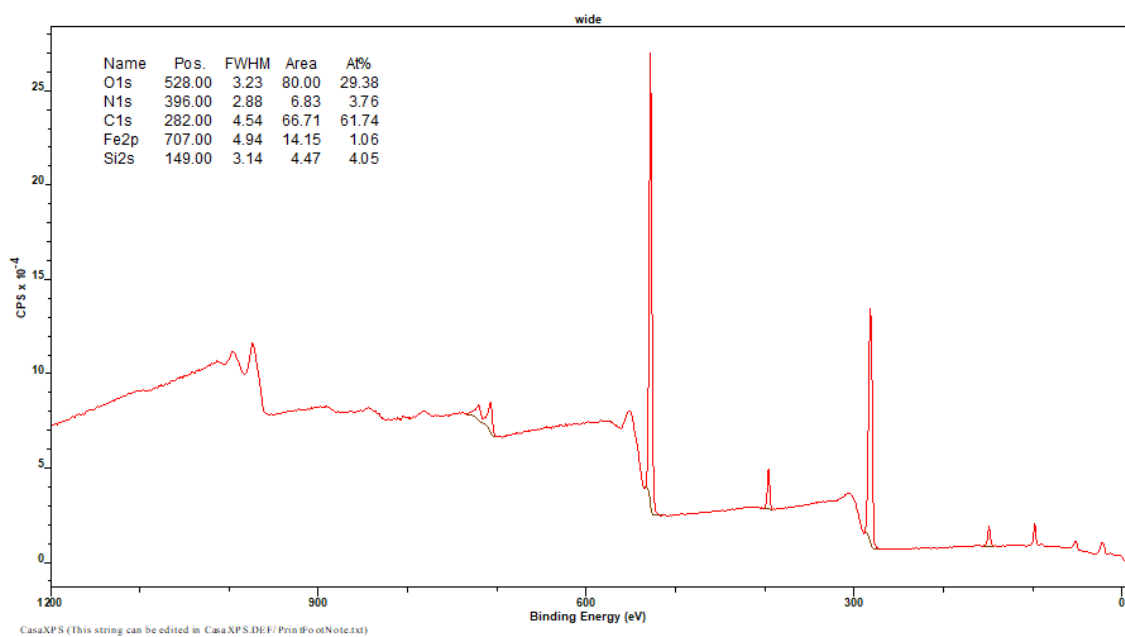


Figure 8.2: XPS survey scan of pectin after disc contact

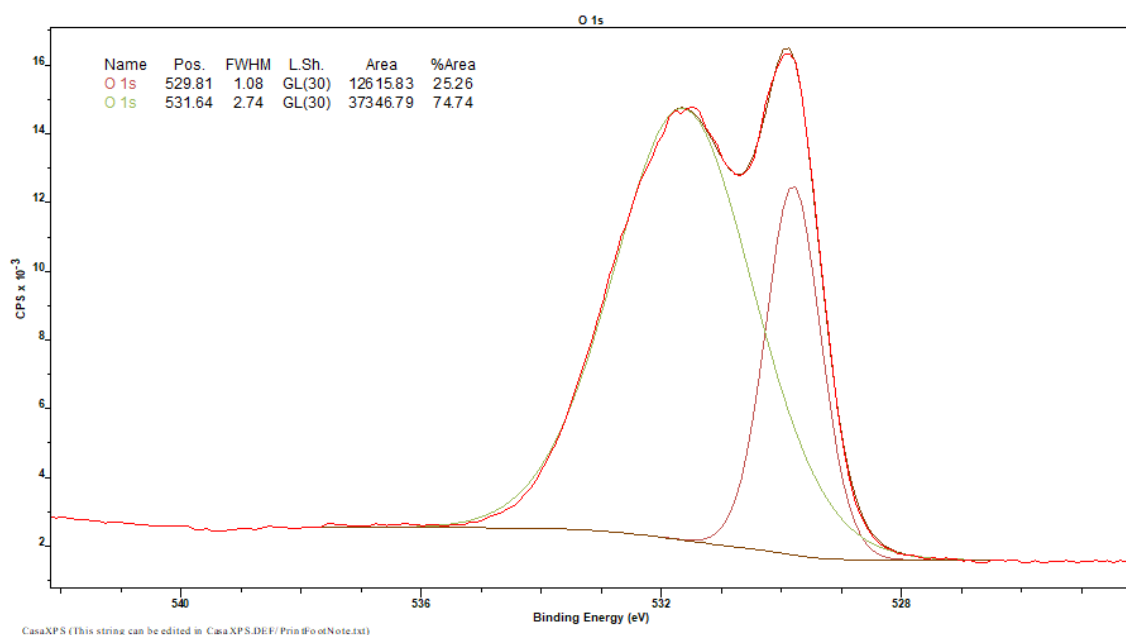


Figure 8.3: High resolution O 1s XPS spectrum from hematite before disc contact

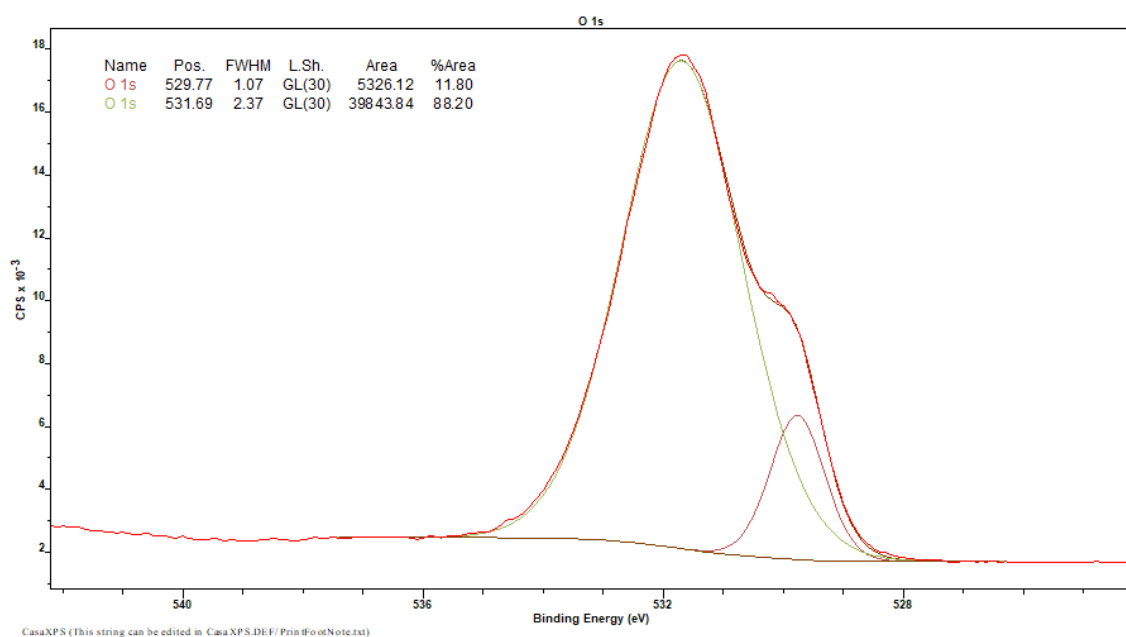


Figure 8.4: High resolution O 1s XPS spectrum of a hematite layer after disc contact

8.3 Results

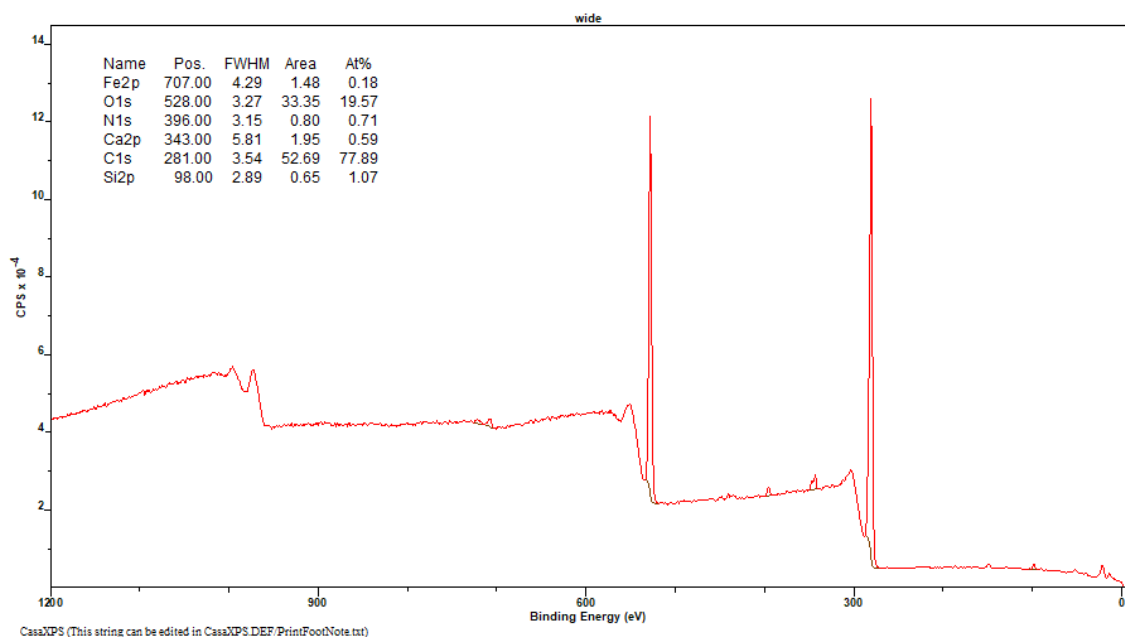


Figure 8.5: XPS Survey scan from the Long Marston sample

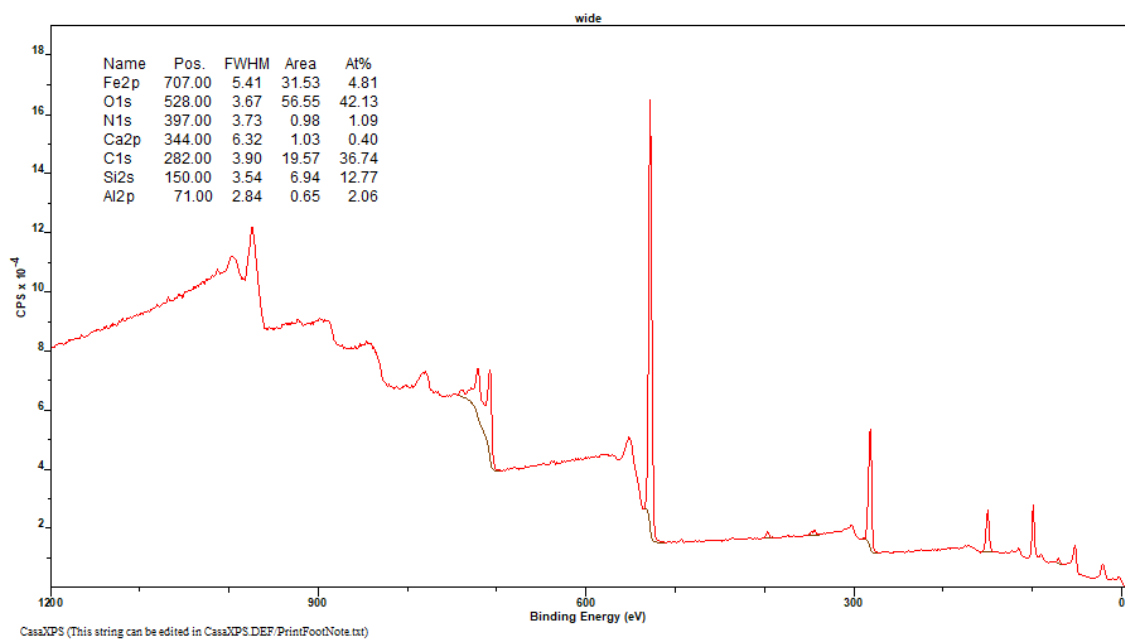


Figure 8.6: XPS Survey scan from the Northern Rail sample

8.4 Discussion

The pectin layer sampled from the SUROS specimen surface showed a small concentration of iron, probably as Fe_2O_3 , but also silicon and organic nitrogen, along with more carbon in C-C and C-H type environments. The Fe_2O_3 suggests that the steel has oxidised and this oxide has mixed with the organic layer during disc contact.

This validates the use of hematite powder to simulate low adhesion, as it appears as an oxidation product of steel in the SUROS contact and therefore will likely occur in the real wheel-rail contact. The increase in nitrogen and the changing carbon environments suggests that the organic constituents of pectin change during the test when a layer is created but it would be difficult to determine what has been formed from this data.

Hematite contained more than just Fe_2O_3 which was expected due to it being a natural mineral. The elements seen in the survey scan are shown in Table 8.1. During the test the hematite remained as Fe(III), but some Fe_2O_3 may have become hydrated to $\text{Fe}(\text{OH})_3$, an oxyhydroxide, which would explain the change in oxygen spectrum as shown in Figures 8.3 and 8.4. Four polymorphs of the oxyhydroxide exist, goethite, akaganeite and lepidocrocite. The result of this it may be the product that hematite is transformed into that causes low adhesion, rather than hematite itself, but this cannot be verified from these results alone and is unlikely due to the small amount of oxide that is transformed in the contact in comparison to the volume of hematite added.

The hematite coating that was removed from the SUROS disc after testing included additional calcium, probably as calcium carbonate, silica and what was likely aluminosilicate. The calcium is likely due to the tap water used to create the oxide paste. The silica and aluminosilicate is likely because of the bag that the hematite was shipped in and the aluminium foil that was used to transport the powder to the test facilities.

Organic contaminated samples rather than pastes were used because unless the sample could be taken straight after a low adhesion incident, it would be difficult to collect a paste sample that would be known to produce low adhesion.

The Long Marston samples were predominantly carbon, as expected from its appearance of a blackened leaf layer. There was not as much oxygen present in this sample as the Northern Rail sample, likely because the layer was created shortly before testing so there was less time for oxidation of both the steel and the organic matter. The Long Marston layer was more loosely bonded to the railhead than the Northern Rail sample so this oxidation may be required to produce the tightly bonded layer seen in low adhesion situations.

The Northern Rail sample was approximately 10% iron oxide, probably Fe_2O_3 , 40% silica and 50% carbon compounds with some calcium carbonate and aluminosilicate. The percentage of iron oxide in this sample is less than has been seen in previous reports, but it still makes up a significant portion of the black layer on the railhead.

8.5 Conclusions

XPS analysis was successful in distinguishing between different types of iron oxide and showing when iron oxide was generated in the contact. The pectin layer tests showed that hematite was formed as a likely product from steel oxidation during the test.

The hematite powder, after addition to the SUROS contact to simulate low adhesion, was hydrated to an oxyhydroxide which was discussed in the literature review. It is unknown whether the hematite alone causes low adhesion or whether this transformation would need to take place for the wet-rail phenomenon to occur.

The two leaf layers, one “natural” and one “artificial” produced similar elemental results with each containing a large amount of carbon matter. One key difference was the lack of iron oxide and oxygen in the artificially produced leaf layer, which may be required for a strong bond between rail and organic contamination to be formed.

9 Mitigation of the Wet-Rail Phenomenon

9.1 Introduction

A short test series was designed at the end of this work to assess potential mitigation methods which could help prevent the wet-rail phenomenon. At the time of this work it was unclear whether standard traction gels, designed to remove organic contamination, would be able to prevent a low adhesion simulation of the wet-rail phenomenon using hematite paste.

Products designed to modify friction levels are used extensively across the rail network. One class of products are known as traction gels, solid particles suspended in a gel that are applied to the railhead and designed to abrade any layer that may cause low adhesion between wheel and rail. Traction gels can either be applied to the railhead from wayside applicators or the train itself. A traction gel, TG60, which is approved and used on railways was added to a wet-rail simulation in this chapter and the results assessed.

An alternative method that could be used to mitigate the wet-rail phenomenon by separating the paste was also proposed and assessed. Magnetite paste, used during previous tests in chapter 7, was not stable and when completely separated into a layer of water on top of the oxide it did not produce low adhesion, even when the oxide phase was added. It was proposed that a coagulant such as aluminium sulfate may provide a potential wet-rail mitigation method because it may be able to separate the hematite paste and produce similar results.

Aluminium sulfate is used in waste water treatment to coagulate particles in a suspension. It works by neutralising the charge on the particles so that they are no longer repelled by each other and “clump” together. If successful, the aluminium sulfate could be used alone or as a component in traction gels.

9.2 Methodology

A 60 weight % hematite paste was prepared and the SUROS rig set up as described in chapter 7. All tests in this section were run at 900 MPa and 2 % slip in order to provide a comparison with work that has been carried out looking at organic contamination in another project.

Traction gels were tested first. The 60 % hematite paste was added at 2 ml/min for approximately 450 cycles and then 0.5 g, followed by 2 g of TG60 traction gel was added to the upper specimen using a wide nosed syringe, whilst the specimen discs were in contact, the gel was pulled into the contact and the traction coefficient logged until 950 cycles.

Another test was run by adding 2 g of aluminium sulfate to a beaker containing 20 g of 60 weight % hematite paste and water suspension. The aluminium sulfate was left in the beaker for 30 minutes to coagulate the hematite particles and then the

suspension was added to a running SUROS test via syringe at 2 ml/min. The entire beaker of paste was added because in the wheel-rail contact, the wheel would roll over the entire paste and not just the upper layer if there was separation. A visibly more viscous layer settled on the bottom of the beaker.

9.3 Results

The results for traction gel addition are shown in Figure 9.1, labelled with the point at which traction gel was applied. A small amount, 0.5 g, of TG60 was added to the contact initially and the traction coefficient rose and then fell back down again, a larger amount of 2 g was then added to the contact which caused the traction coefficient to quickly rise up to a dry value.

The results for hematite paste with aluminium sulfate addition is shown in Figure 9.2. The point at which the added suspension became visibly more viscous is labelled. This was accompanied by an increase in traction coefficient at first, followed by a sudden drop to a very low traction coefficient of 0.07. The traction coefficient then rose again to 0.2 before dropping down to 0.04.

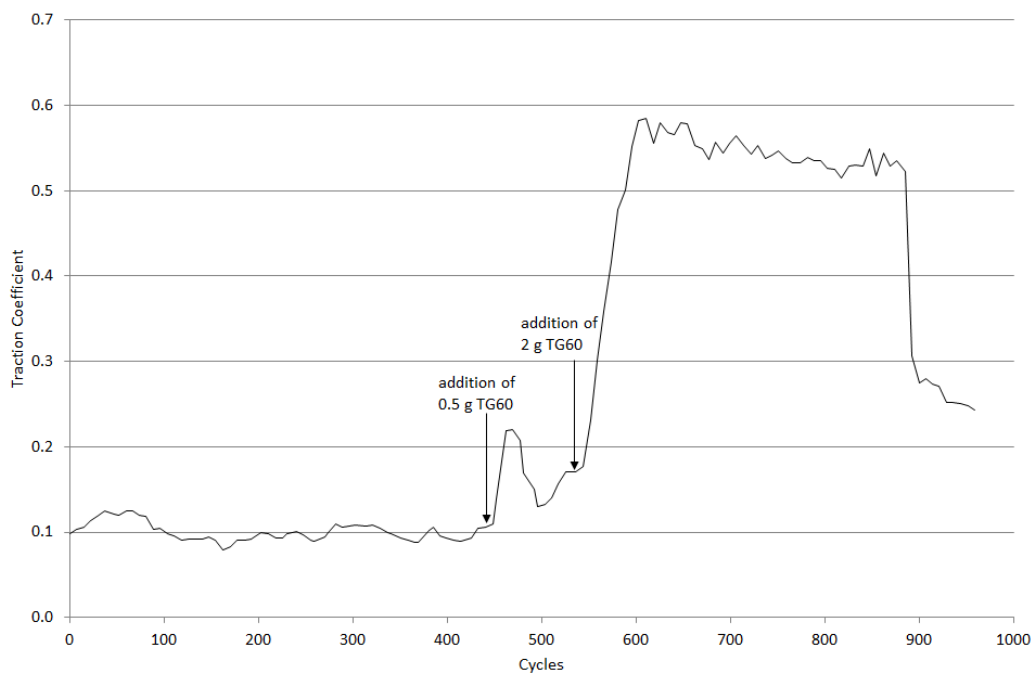


Figure 9.1: The traction coefficient of a 60 weight % hematite paste when 0.5 g and 2 g TG60 traction gel is applied

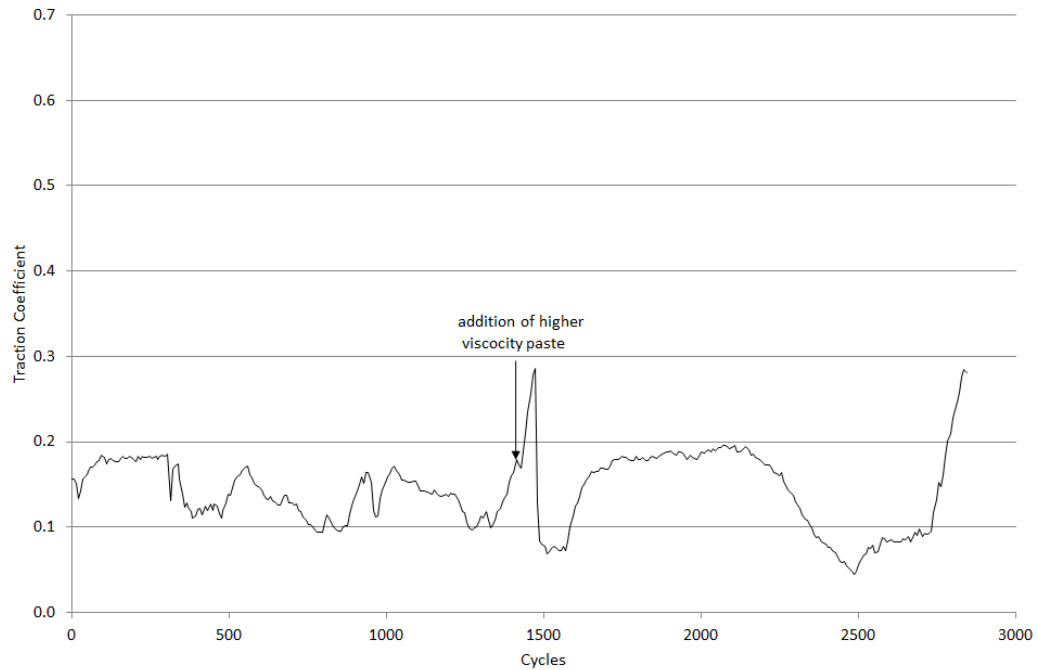


Figure 9.2: The traction coefficient of a 60 weight % hematite paste containing 2 g aluminium sulfate

9.4 Discussion

The traction gel worked effectively to increase the traction coefficient in a wet-rail simulation. Prior to gel addition the traction coefficient remained at approximately 0.09, this was not as low as seen in previous tests but still provided conditions that would be classed as low adhesion. Traction recovery after paste addition happened very quickly and the traction coefficient rose up to dry values.

During traction gel addition, the disc surface became visibly cleaner and coated in less oxide paste, which leads to the suggestion that the traction gel was able to remove the thin layer of hematite that had built up on the disc surface. The layer would be broken up and either pushed out of the disc contact or remain mixed with the traction gel which prevents further traction reduction. The abrasive traction gel may also increase the roughness of the sample which would increase the traction coefficient and may prevent low adhesion as seen in the previous modeling work.

A visible effect was seen when aluminium sulfate was added to the hematite suspension, with gas being produced as the particles coagulate. The mixture continued to effervesce over 30 minutes so the suspension was left until the reaction had completed. The particles coagulated, but did not separate as much as expected, there was a more viscous slurry on the bottom of the beaker, but the upper layer still contained iron oxide particles.

The initial application of the hematite suspension with added aluminium sulfate produced a high traction coefficient of up to 0.18, a similar value to tests run with water alone and much higher than has occurred previously for a 60 weight % hematite paste. The traction coefficient then starts fluctuating, presumably because the viscosity of the added hematite paste changes due to the separation in the beaker.

The sharp rise followed by a sudden drop in traction coefficient to very low levels was seen when the main viscous phase at the bottom of the beaker was added. This rise and fall in traction coefficient occurs again because of the non-homogeneous suspension as different viscosities of paste were added to the contact. The traction coefficient of 0.04 is one of the lowest seen during a wet-rail simulation.

As a result, this method of mitigation was deemed to be ineffective because if the paste was separated using aluminium sulfate on the railhead, the wheel would still have to roll over the more viscous paste and may even squeeze away the upper layer preferentially to the more viscous lower layer, which would produce very low traction coefficients.

9.5 Conclusions

A conventional traction gel was able to recover the traction coefficient to dry values during a wet-rail simulation using hematite paste. The proposed alternative method for mitigating the wet-rail phenomenon was not effective because paste separation still results in the viscous paste entering the contact patch which may create even lower adhesion levels. If current traction gels are effective then efforts need to be made to make sure that they can be quickly applied to known areas of low adhesion when conditions such as dew or drizzle occur to help prevent the wet-rail phenomenon.

10 Discussion

10.1 Introduction

The five overall benefits of this work that could improve the knowledge of low adhesion due to the wet-rail phenomenon are as follows:

1. highlighting the frequency of incidents that may have been caused by the wet-rail phenomenon and concluding environmental factors that are likely to cause low adhesion
2. better understanding the behaviour of pastes on the railhead
3. simulating low traction caused by the wet-rail phenomenon
4. providing mechanisms and hypotheses as to how the wet-rail phenomenon may occur
5. showing the effectiveness of certain mitigation methods

The following chapter will discuss these outputs, suggestions for future work that could be carried out on each section are also described.

10.2 Incident Frequency and Weather Conditions

The data analysis at the beginning of this work showed that many of the station overruns that Network Rail attributed to weather conditions with no other explainable factors could be linked to the wet-rail phenomenon. The incidents that did not occur around precipitation often took place during the early morning and late evening, likely because of dew formation but the low resolution data meant that any exact conditions that could cause low adhesion were difficult to conclude. This data was still able to steer the test methodologies towards using low volumes of water to create dew and damp conditions.

Useful information that could be gained from this chapter was also that the wet-rail phenomenon was unlikely to be caused by “extreme” conditions, very high or low temperatures did not produce an increase in weather related station overruns, at least during the autumn season. This meant that lab testing did not have to be focused around any very high or low temperatures. Very low temperatures result in far more wheel flats during the Swedish case study but the large number of incidents in the UK study that occurred at higher temperatures meant that there were other causes.

The hourly weather data was still not high resolution enough to be able to attribute very specific weather conditions to low adhesion. During the later part of this work a micro weather station was designed that could be placed next to a railhead and provide detailed rainfall, temperature and humidity data. This has currently only been used on closed loop testing but could be expanded to low adhesion hotspots in order to link low adhesion to more specific weather conditions.

10.3 Oxide Paste Behaviour

The behaviour of third body layers, simulated with hematite paste, were looked at by assessing how particles are pushed along the railhead. This behaviour analysis would be difficult to achieve without regular track access but the full scale rig provided a useful base for assessing oxide paste behaviour. The rheology of hematite pastes was carried out previously but had not been repeated on modern equipment which has provided new data. A summary of the hematite paste behaviours and how they could play a part in the wet-rail phenomenon are described in this section.

The rapidly increasing shear stress at the higher weight percentages shows why there is large difference between paste behaviour at different water levels. The properties of a paste will change rapidly as the paste dries out which may explain why the wet-rail phenomenon only occurs in certain situations.

The hematite paste separates into both hematite and water during both rheometry and FSR testing. The water is also seen be squeezed out of the contact during FSR testing. Although it could not be replicated under the low loads of a modern rheometer, the oxide paste is likely to “jam” when high shear and load is applied between wheel and rail which would produce a rapid increase in shear stress.

The hematite pastes likely showed time dependent shear thinning so an initial shear may produce very high stresses, but the shear stress of the paste will decrease over time as the particles begin to flow. The effect of this is difficult to predict but may not be relevant as the wheel will pass over each particle in a very short time period.

The oxide paste is spread down the railhead running band with each wheel pass and paste outside the running band seems to be pulled in during a wheel pass. The movement of oxide as the wheel moves over the rail acts in two different ways dependent on the viscosity of the paste. Water is needed as a “carrier” to push the oxides down the railhead so if the amount of water is below a certain threshold, as seen between 50 and 60 wt % hematite suspensions, the oxide will be deposited as a thick layer and cannot be pushed any further. If there is enough water, the paste will be spread a long way down the railhead. This may mean that a less viscous paste can be spread down the railhead and then be compressed into a thick layer when it dries.

These behaviours have only been assessed for hematite paste during this work so a more realistic and complex paste of wear particles and different iron oxides could be created to assess the differences in paste movement.

Even the smaller amount of 2 ml paste seemed quite large compared to the volume of paste that is seen on the railhead so smaller volumes could be used to assess if the behaviour changes. Finally, multiple wheel passes with a longer period of time between them could be made to assess how the paste behaviour changes as it dries.

10.4 Simulation of the Wet-Rail Phenomenon

A large number of tests under different conditions were carried out without low adhesion occurring, but this was explainable due to the narrow window of conditions that was thought to produce the wet-rail phenomenon. During these early tests it became apparent that although the conditions resulting in low adhesion could be narrowed down with a literature review, the fact that nobody had successfully produced repeatable low adhesion due to “wet-rail” conditions or were able to show the exact weather conditions meant that a large range of conditions would need to be tested.

There was a possibility that there was a velocity dependence to the wet-rail phenomenon and that very low adhesion could only be achievable at high velocities which are often not obtainable in small scale test rigs, so reductions in friction were noted and analysed even if very low friction, below 0.1, was not achieved. This meant that information was still valuable from test methods such as the pendulum rig, which showed a reduction in friction with an oxide layer, but did not show very low friction values.

The achievement of sustained low adhesion, initially through tests with generated oxide layers and then more repeatedly with applied oxide pastes using the SUROS rig was a large step forward for this work, as it had not been achieved previously at saturate slip values on a small scale rig. It showed that low adhesion could be produced even at low speeds and could occur either using oxides generated in the contact itself or with artificial paste addition. It was able to show that low traction could be produced even without an intact oxide layer.

The wet-rail simulation method was discovered towards the end of this work which means that there are a number of future tests that could be carried out to better understand how this low adhesion occurs.

The first suggestion would be to simulate the wet-rail phenomenon on a more sensitive test rig than SUROS. The current SUROS control system does not apply the correct load and slip instantly when the discs are contacted, especially when a solid contaminant is added. If a more sensitive test set up was used the data could be analysed over the first 10 cycles of each test which could be able to assess if the shear behaviour and traction of the oxide pastes changes with each cycle, either due to non-Newtonian behaviour or water being squeezed out.

The second would be to compare the traction coefficient when hematite paste is added to test specimens both with and without an underlying oxide layer, which would help understand whether the underlying layer produces even lower traction. A more sensitive test set up would also help with this, detecting the change in traction coefficient if the layer was removed quickly.

Attempts to simulate the wet-rail phenomenon on the full scale rig were unsuccessful but this has been attributed to the wear scar on the test wheel having a very high

roughness. Simulating the wet-rail phenomenon on larger scale tests or full scale field testing would help validate the hypotheses that have been concluded in this work.

Hematite paste has been used as a wet-rail simulation, in this case it is easily visible on the full scale rig due to its bright red colour and is able to produce low traction on the SUROS rig. The XPS analysis showed formation of hematite during an organic based test using a pectin layer which shows that it can be formed in the wheel/rail contact. The analysis of hematite powder used shows that although it may be formed in the contact, it may then be transformed into an oxyhydroxide. It is currently unclear whether this is necessary to produce low adhesion. The paste formed on a railhead will likely contain many other contaminants but the formation of hematite in the contact helps to justify its use as a wet-rail simulant.

10.5 Mechanisms and Hypotheses

The mechanism for low adhesion has been discussed in this work and concluded that a paste is the cause of low adhesion due to the wet-rail phenomenon, as simulated in laboratory tests.

Low adhesion due to iron oxides was initially thought to be due to the chemical properties of the iron oxide, which was analysed in the literature review. This may still be partially correct because the small oxide particles produce a stable paste due to electrostatic repulsion between the adsorbed ions on the particle surface, but these properties are not specific to iron oxides alone. The SUROS test that produced low adhesion with a clay suspension showed that low adhesion was likely to be due to the rheological paste properties. Low adhesion has been previously reported on a railway due to coal or clay industrial contamination which supports these findings and could include any other contaminant that forms a viscous paste.

It is likely that any paste seen in the field will be composed of a mixture of third body components and different types of oxide rather than hematite and water alone but the mechanism of low adhesion would remain the same. If both oxide and clay pastes can cause low adhesion year round, it is likely that the organic components will also mix with these and add to the problem. Iron oxides were found in the “natural” organic contamination that was studied in this work, as well as in previously studied leaf layers.

It is important to bear in mind that for low adhesion to occur over long distances of track as has been previously reported, then there must be either consistent low adhesion conditions over many kilometres of track, or some sort of propagation mechanism occurring.

The first proposal, that the conditions will remain consistent, seems unlikely. This work has shown that the wet-rail phenomenon is likely to only occur under very

specific conditions which are unlikely to occur over very long distances as both physical and environment conditions are likely to change over the distance of wheel slide.

A “propagation” mechanism may take place which causes low adhesion to occur over the large distances, even if conditions do not remain consistent. The mechanism of low adhesion due to the paste formation has been proposed previously and simulated in a laboratory using the twin disc testing but the mechanism of how the low adhesion could propagate down the railhead would be difficult to simulate on small scale rigs due to the likely velocity effects, although some hypotheses can be made using the information gained from this work.

The full scale testing showed that oxide could be spread down the railhead, both the paste sticking to the wheel and being pushed in front of the wheel would squeeze out moisture and the oxide would be compacted under the wheel as seen in the full scale testing and discussed in the literature review, meaning subsequent wheelsets encounter a denser and compacted paste layer on the running band. This will have two effects, the compacted paste may become solid enough to fully support the wheel load and mean that the rail surface effectively becomes smoother over time, which has been noted to reduce friction. The compaction will also increase the viscosity of any paste which has been shown to also reduce adhesion. In the full scale tests, the oxide paste is seen to be “pulled” into the contact from outside the running band, so the amount of paste in the running band may increase with multiple wheel passes. It seems likely that a sliding wheelset will more effectively push the oxide paste along the railhead which may extend the distance of low adhesion.

A wheelset with saturated creep may shear the oxide paste more effectively than a wheel with less creep. If increased shear will increase the separation of oxide and water which leads to further jamming then, once adhesion is lost, the higher creep will lead to further jamming, which in turn will lead to low adhesion which could provide a reason why the long sliding distances occur.

The rheological study showed other oxide paste behaviour that could explain the low adhesion propagation. Firstly is the “shear banding” phenomenon, that water can create a shear plane when pulled into the oxide paste, rather than mixing to create a homogeneous suspension. This shear plane could be created between the oxide in the contact and a thin layer of water on the surface, providing a lubrication mechanism. The second oxide behaviour seen was that the separation of hematite and water would likely lead to “jamming” when the oxide is sheared, which is likely why the previous results lead to shear thickening behaviour whilst the new results showed time dependent shear thinning. The jamming would increase the viscosity of any paste on the railhead, which according to the previous results would decrease adhesion levels.

Many of these oxide behaviours were not documented before this work so all could be analysed further to see how they could produce the wet-rail phenomenon. Without a full sized test rig that operates at high speeds, mechanisms and especially

propagation mechanisms can be proposed but are difficult to assess. If the wet-rail phenomenon could be simulated using oxide paste during field testing then high speed cameras could be used to look at the paste behaviour when low adhesion occurs.

10.6 Mitigation

The suspension is likely stabilized by opposing charges of ions that have adsorbed on the solid oxide particles, these form an electric double layer and the particles repel each other which prevents agglomeration or “clumping” of particles and sedimentation.

Attempts to break this layer were not successful when testing the traction coefficient on SUROS tests. Changes to pH and addition of agglomerating agents such as aluminium sulfate were attempted but two issues were encountered.

The additives caused visible agglomeration of the particles but this occurred over time rather than instantly, even with large quantities of agglomerating agent. This would not be suitable to a rail situation because the traction enhancer would need to work quickly to prevent low adhesion.

When the samples of hematite paste were left for 30 minutes to agglomerate and added to the SUROS rig, two stages of traction occurred due to the sedimentation. Initially the traction coefficient was as high as water and low adhesion was prevented. However, the entire sample was added to SUROS so when the sediment was added the traction coefficient dropped to very low values.

Traction gel successfully increased the traction coefficient when added to a wet-rail low adhesion simulation, with a rapid increase to dry values showing that any layer formed due to the iron oxide paste is being worn away.

The wet-rail phenomenon has been difficult to predict but this work has highlighted the occurrence of low adhesion because of dew formation or drizzle. Traction gels could be automatically applied if the rail temperature falls below the dew point and condensation is formed on the railhead.

11 Conclusions

11.1 Project conclusions

The original thesis aim was to better understand the wet-rail phenomenon and this was achieved in this work. The key points described in this thesis that increase the knowledge of the wet-rail phenomenon are shown below:

- Low adhesion due to iron oxides and water alone at saturated slip values has been successfully and repeatedly generated on the SUROS test rig for the first time, validating the hypothesis that iron oxides play a large role in the wet-rail phenomenon
- Analysis of these tests has validated the hypothesis that iron oxides and small amounts of water can form a paste that will reduce adhesion, especially when both wheel and rail are worn with a low combined roughness
- This paste can likely be formed from different types of solid particles that form a viscous paste, mixed with small amounts of water on the railhead, as shown by the clay substitution. This viscous paste was observed on the railhead during field testing and is likely to form whenever small amounts of water are added to the railhead, especially after being mechanically mixed by a wheel pass
- The paste formed would be easily spread down the railhead which would mean that the wet-rail phenomenon could occur over long distances
- The paste lowers adhesion to a minimum shortly before it dries so could be spread down the railhead when wet and then cause low adhesion when drying, which could mean that the railhead would appear dry when inspected after an incident

This work can conclude that hematite, when mixed with small amounts of water, can form a paste which causes low adhesion under certain conditions. Visibly, this is similar to pastes seen to occur naturally during field testing when dew has been present on the railhead. The surprising conclusion to this work is that this adhesion reducing paste is not limited to iron oxides alone, it has been repeated using clay as a substitute and is likely to occur with a range of small particles when mixed with water to produce stable and high viscosity pastes.

Testing with organic layers has not been the subject of this thesis so data collected involving these layers has not been included, but organic substances such as pectin, arabic gum and carboxymethyl cellulose all form thick gels when hydrated with water and have resulted in very low traction coefficients during twin disc simulation tests, this data will be published in future. Pectin in particular is found in leaves and does not cause low traction when dry, but can be hydrated to form a thick gel which results in very low traction when wetted. Particles of iron oxide have been found to be suspended in this gel layer when it has been analysed after twin disc testing. The fact that low adhesion has been produced on SUROS using both inorganic and organic viscous pastes and gels, leads to the suggestion that the mechanism of adhesion loss during the autumn season may be similar to that seen throughout the

year in the wet-rail phenomenon, but further work would need to be carried out on the subject to validate this theory.

Water has, as expected, been found to play a key role in the wet-rail phenomenon. Large amounts of water will help to wash contamination off the railhead so this will effectively mitigate this problem, but small amounts of water will form pastes similar to those seen in this work. Any paste formed will become more viscous as water evaporates and at some point will reach the specific viscosity needed to lower adhesion. Given the specific conditions needed, short period of time of a wheel pass and the fact that the train would need to be accelerating or braking for a problem to arise, the wet-rail phenomenon is likely to occur sporadically. However, the wheel flats, station overruns and SPAD events that can be attributed to the wet-rail phenomenon show that the results of it can be disastrous.

Because of the previously mentioned conditions needed, the wet-rail phenomenon is likely to remain very difficult to predict. Although there are contributing factors, the answer is unfortunately not as simple as testing for a specific type of iron oxide or watching for specific weather conditions. There is unlikely to be a single test that can distinguish whether a low adhesion producing paste can be formed as it could be formed from many different types of particles.

The increased knowledge of the contributing factors of this form of low adhesion can help with mitigation methods. Particular attention should be paid to areas with a thick third body layer build up such as oxidised track, areas contaminated with solids such as crushed ballast, clay, organic contamination or perhaps even soil matter, especially when the railhead is likely to be wetted. Current adhesion models could be improved by adding areas where rail is likely to oxidise quickly or contamination is likely to be found and precautions should be taken when these areas are wetted, especially by dew or light rain after a dry period. A smooth contact between wheel and rail has been shown to produce the lowest traction so a rough and freshly ground wheel may prevent the wet-rail phenomenon, but previous data has shown that the metal will quickly become smoother. Traction gels, which are used to remove organic contamination, have been found to mitigate the wet-rail phenomenon and increase the traction coefficient back up to dry values in small scale tests. This should be recreated in future on larger scale tests to validate this, but the challenge will be to ensure that they are present in the field in areas where the low adhesion producing paste will form. There are likely to be “hotspots” for this but the reality is that this paste is able to form anywhere due to rail oxidation and the build-up of other debris. As a result, trainborne traction gel dispensers may be most effective, as long as they are able to ensure that sufficient paste can enter the contact.

The thesis plan was designed around an interdisciplinary approach, using both chemistry and tribology, to better understand the wet-rail phenomenon. It is fitting that the hypothesis for the wet-rail phenomenon produced as a result of this work is also interdisciplinary; the chemistry of steel corrosion causes the iron in the steel to

oxidise and creates an iron oxide layer, which is mixed with water to form a paste and causes low adhesion due to its tribological and rheological effects in the contact.

11.2 Publications Arising From This Work

- White, B. T., Nilsson, R., Olofsson, U., Arnall, A. D., Armitage, T., Fisk, J, Lewis, R. Effect of the presence of moisture at the wheel – rail interface during dew and damp conditions. *Proc. Inst. Mech. Eng. Part F J. Rail Rapid Transit*, 2016, <https://doi.org/10.1177/0954409717706251>.
- White, B. T., Lewis, R., Olofsson, U., & Lyu, Y. The Contribution of Iron Oxides to the Wet-Rail Phenomenon. *Under review for the International Journal of Railway Technology (IJRT)*, 2016.
- White, B. T., Lewis, R., Olofsson, U., & Lyu, Y. The Contribution of Iron Oxides to the Wet-Rail Phenomenon. *Proceedings of Civil-Comp Press Conferences-Railways 2016*. Sardinia, 2016.
- White, B. T., Arnall, A. D., Evans, M. D., Fletcher, D. I., Lewis, R. A Study into the Effect of the Presence of Moisture at the Wheel/Rail Interface during Dew and Damp Conditions. *Proceedings of the 20th International Conference on Contact Mechanics and Wear of Rail/Wheel Systems*, Colorado, USA, 2015.

References

- [1] K. Ishizaka, S.R. Lewis, and R. Lewis. The low adhesion problem due to leaf contamination in the wheel/rail contact: Bonding and low adhesion mechanisms. *Wear*, 2017.
- [2] S. Descartes, C. Desrayaud, E. Niccolini, and Y. Berthier. Presence and role of the third body in a wheel/rail contact. *Wear*, 2005.
- [3] Y. Berthier, S. Descartes, M. Busquet, E. Niccolini, C. Desrayaud, and L. Baillet. The role and effects of the third body in the wheel - rail interaction. *Fatigue and Fracture of Engineering Materials and Structures*, 2004.
- [4] C. Hardwick, R. Lewis, and U. Olofsson. Low adhesion due to oxide formation in the presence of salt. *Proceedings of the Institution of Mechanical Engineers, Part F: Journal of Rail and Rapid Transit*, 2013.
- [5] RSSB. www.sparkrail.org. Investigation into the Effect of Moisture on Rail Adhesion- Project Report T1042. Technical report.
- [6] W.A Skipper and R. Lewis. A Review of the Use of Abrasive Particles as an Adhesion Enhancer in the Wheel / Rail Contact. *Submitted to Tribology - Materials, Surfaces Interfaces*, 2017.
- [7] P.A. Murkin. An Investigation of Possible Meteorological Factors Affecting Low Rail Adhesion Events in Autumn 2003. *Adhesion Working Group*, 2005.
- [8] O. Arias-Cuevas. *Low Adhesion in the Wheel-Rail Contact*. PhD thesis, The University of Sheffield, 2010.
- [9] U. Olofsson and R. Lewis. *Tribology of the wheel-rail contact*. CRC Press, 2006.
- [10] E.A. Gallardo-Hernandez and R. Lewis. Twin disc assessment of wheel/rail adhesion. *Wear*, 2008.
- [11] E. Magel. A survey of wheel/rail friction. *Federal Railroad Administration*, 2017.
- [12] J. Lundmark, E. Hoglund, and B. Prakash. Running-in Behaviour of Rail and Wheel Contacting Surfaces. *International Conference on Tribology*, 2006.
- [13] S. Iwnicki. *Simulation of wheel/rail contact forces*. PhD thesis, Manchester Metropolitan University, 2003.
- [14] H. Tournay. Supporting Technologies Vehicle Track Interaction. *Guidelines to Best Practice for Heavy Haul Railway Operations: Wheel and Rail Interface Issues*, 2001.

-
- [15] R. Lewis, R.S. Dwyer-Joyce, U. Olofsson, J. Pombo, J. Ambrósio, M. Pereira, C. Ariaudo, and N. Kuka. Mapping railway wheel material wear mechanisms and transitions. *Proceedings of the Institution of Mechanical Engineers, Part F: Journal of Rail and Rapid Transit*, 2010.
- [16] J. Suzumura, Y. Sone, A. Ishizaki, D. Yamashita, Y. Nakajima, and M. Ishida. In situ X-ray analytical study on the alteration process of iron oxide layers at the railhead surface while under railway traffic. *Wear*, 2011.
- [17] K J Sawley. Calculation of temperatures in a sliding wheel / rail system and implications for wheel steel development. *Transit*, 2007.
- [18] D. Godfrey. Iron oxides and rust (hydrated iron oxides) in tribology. *Journal of the society of tribologists and lubrication engineers*, 1999.
- [19] S. Hoerlé, F. Mazaudier, P.H. Dillmann, and G. Santarini. *Advances in understanding atmospheric corrosion of iron. II. Mechanistic modelling of wet-dry cycles*. 2004.
- [20] R.M. Cornell and U. Schwertmann. *The Iron Oxides*. 1996.
- [21] E. Paterson. *Iron Oxides in the Laboratory. Preparation and Characterization*. Wiley-VCH, 1992.
- [22] W. Chen, L. Hao, J. Dong, and W. Ke. Effect of sulphur dioxide on the corrosion of a low alloy steel in simulated coastal industrial atmosphere. *Corrosion Science*, 2014.
- [23] S Descartes, C Desrayaud, and Y Berthier. Experimental identification and characterization of the effects of contaminants in the wheel-rail contact. *Proceedings of the Institution of Mechanical Engineers, Part F: Journal of Rail and Rapid Transit*, 2008.
- [24] V. Cerezo Y. Hichri and M. Do. Effect of dry deposited particles on the tire/road friction. *Wear*, 2017.
- [25] T.M. Beagley. The rheological properties of rail contaminants and their effect on wheel/rail adhesion. *Proceedings of the Institution of Mechanical Engineers, Part F: Journal of Rail and Rapid Transit*, 1976.
- [26] Yi Zhu, Ulf Olofsson, and Hua Chen. Friction Between Wheel and Rail: A Pin-On-Disc Study of Environmental Conditions and Iron Oxides. *Tribology Letters*, 2013.
- [27] S.R. Lewis, R. Lewis, and U. Olofsson. An alternative method for the assessment of railhead traction. *Wear*, 2011.
- [28] Yi Zhu, Huayong Yang, and Wenjian Wang. Twin-disc tests of iron oxides in dry and wet wheel-rail contacts. *Proceedings of the Institution of Mechanical Engineers, Part F: Journal of Rail and Rapid Transit*, 2015.
- [29] RSSB. www.sparkrail.org. Modelling and quantifying the influence of water wheel/rail adhesion levels - Project Report T1077. Technical report, 2015.

- [30] M. Ishida, F. Aoki, Y. Sone, T. Ban, and K. Shirouze. Rail corrugations caused by low coefficient of friction in a submarine railway tunnel. *Proceedings of WTC 2005 world tribology congress III*, 2005.
- [31] B. Panda, R. Balasubramaniam, and G. Dwivedi. On the corrosion behaviour of novel high carbon rail steels in simulated cyclic wet-dry salt fog conditions. *Corrosion Science*, 2008.
- [32] U. Olofsson, Y. Zhu, S. Abbasi, R. Lewis, and S. Lewis. Tribology of the wheel/rail contact. Aspects of wear, particle emission and adhesion. *Vehicle System Dynamics*, 2013.
- [33] T.M. Beagley, I.J. McEwen, and C. Pritchard. Wheel/rail adhesion - the influence of railhead debris, 1975.
- [34] K. Xiao, C. Dong, X. Li, and F. Wang. Corrosion Products and Formation Mechanism During Initial Stage of Atmospheric Corrosion of Carbon Steel. *Journal of Iron and Steel Research, International*, 2008.
- [35] T. Nakahara, K. Baek, H. Chen, and M. Ishida. Relationship between surface oxide layer and transient traction characteristics for two steel rollers under unlubricated and water lubricated conditions. *Wear*, 2011.
- [36] T. Misawa, K. Hashimoto, and S. Shimodaira. The mechanism of formation of iron oxide and oxyhydroxides in aqueous solutions at room temperature. *Corrosion Science*, 1974.
- [37] Y. Zhu, U. Olofsson, and R. Nilsson. A field test study of leaf contamination on railhead surfaces. *Proceedings of the Institution of Mechanical Engineers, Part F: Journal of Rail and Rapid Transit*, 2012.
- [38] U Olofsson. A multi-layer model of low adhesion between railway wheel and rail. *Proceedings of the Institution of Mechanical Engineers, Part F: Journal of Rail and Rapid Transit*, 2007.
- [39] S.R. Lewis, R. Lewis, U. Olofsson, D.T. Eadie, J. Cotter, and X. Lu. Effect of humidity, temperature and railhead contamination on the performance of friction modifiers: Pin-on-disk study. *Proceedings of the Institution of Mechanical Engineers, Part F: Journal of Rail and Rapid Transit*, 2012.
- [40] Y Zhao, J Liu, and L Zheng. The oxide film and oxide coating on steels under boundary lubrication. *Proceedings of the 16th Leeds-Lyon symposium on tribology*, 1990.
- [41] S.R. Lewis, R. Lewis, J. Cotter, X. Lu, and D.T. Eadie. A new method for the assessment of traction enhancers and the generation of organic layers in a twin-disc machine. *Wear*, 2016.
- [42] D.H. Klein, A.W. Andren, J.A. Carter, J.F. Entergy, C. Feldman, W. Fulkerson, W.S. Lyon, J.C. Ogle, Y. Talmi, R.I. Hook, N. Bolton, N.S. McIntyre, and D.G. Zetaruk. X-ray Photoelectron Spectroscopic Studies of Iron Oxides. *N.Y. Science Environ. Sci. Technol*, 1975.

-
- [43] Engineering Toolbox. <https://www.engineeringtoolbox.com/water-dynamic-kinematic-viscosity-d596.html>.
- [44] Y. Zhu, U. Olofsson, and K. Persson. Investigation of factors influencing wheel-rail adhesion using a mini-traction machine. *Wear*, 2012.
- [45] H. Chen, T. Ban, M. Ishida, and T. Nakahara. Influential Factors on Adhesion between Wheel and Rail under Wet Conditions. *Quarterly Report of RTRI*, 2012.
- [46] H. Chen, T. Ban, M. Ishida, and T. Nakahara. Adhesion between rail/wheel under water lubricated contact. *Wear*, 2002.
- [47] J. Garforth. Woodland trust autumn analysis document. <https://naturescalendar.woodlandtrust.org.uk/media/1681/2016-autumn.pdf>, 2016.
- [48] P.M. Cann. The leaves on the line problem. A study of leaf residue film formation and lubricity under laboratory test conditions. *Tribology Letters*, 2006.
- [49] D.J. Watkins. Exploring adhesion with british rail's tribometer train. *Railway Engineering Journal*, 1975.
- [50] D.A. Garrec and I.T. Norton. The influence of hydrocolloid hydrodynamics on lubrication. *Food Hydrocolloids*, 2012.
- [51] E.D. Tingle. The importance of surface oxide films in the friction and lubrication of metals. Part I-The dry friction of surfaces freshly exposed to air. *Transactions of the Faraday Society*, 1950.
- [52] B.H. Gu, J. Schmitt, Z.H. Chen, L.Y. Liang, and J.F. McCarthy. Adsorption and Desorption of Natural Organic-Matter on Iron Oxide - Mechanisms and Models. *Environmental Science Technology*, 1994.
- [53] www.smtweather.co.uk.
- [54] T.M. Beagley. The rheological properties of solid rail contaminants and their effect on wheel/rail adhesion. *Proceedings of the Institution of Mechanical Engineers, Part F: Journal of Rail and Rapid Transit*, 1976.
- [55] A.D. Arnall, D.I. Fletcher, and R. Lewis. Geospatial and temporal analysis of wheel slide events. *Proceedings of the 10th international conference in contact mechanics of the wheel-rail contact, Colorado, USA*, 2015.
- [56] P. Brimblecombe. Temporal humidity variations in the heritage climate of South East England. *Heritage Science*, 2013.
- [57] Y. Zhu, Y. Lyu, and U. Olofsson. Mapping the friction between railway wheels and rails focusing on environmental conditions. *Wear*, 2015.
- [58] L. Chapman, J.E. Thornes, Y. Huang, X. Cai, V.L. Sanderson, and S.P. White. Modelling of rail surface temperatures: a preliminary study. *Theoretical and Applied Climatology*, 2007.

- [59] H.A. Barnes. Shear Thickening in Suspensions of Nonaggregating Solid Particles Dispersed in Newtonian Liquids. *Journal of Rheology*, 1989.
- [60] N Willenbacher and K Georgieva. *Product Design and Engineering: Formulation of Gels and Pastes*. Wiley-VCH, 2013.
- [61] Peter Schall and Martin van Hecke. Shear Bands in Matter with Granularity. *Annual Review of Fluid Mechanics*, 2010.
- [62] L.E Buckley-Johnstone, G. Trummer, P. Voltr, A. Meierhofer, and K. Six. New understanding of the impact of small amounts of water and iron oxides on adhesion in the wheel / rail interface using novel high Pressure Torsion testing and an innovative adhesion model. *Submitted to Tribology International*.
- [63] G.H. Covey and B.R. Stanmore. Use of the parallel-plate plastometer for the characterisation of viscous fluids with a yield stress. *Journal of Non-Newtonian Fluid Mechanics*, 1981.
- [64] T.M. Beagley and C. Pritchard. Wheel/rail adhesion - The overriding influence of water. *Wear*, 1975.
- [65] R. Lewis, S.R. Lewis, Y. Zhu, S. Abbasi, and U. Olofsson. The modification of a slip resistance meter for measurement of railhead adhesion. *Proceedings of the Institution of Mechanical Engineers, Part F: Journal of Rail and Rapid Transit*, 2012.
- [66] U. Olofsson and K. Sundvall. Influence of leaf, humidity and applied lubrication on friction in the wheel-rail contact: pin-on-disc experiments. *Proceedings of the Institution of Mechanical Engineers, Part F: Journal of Rail and Rapid Transit*, 2004.
- [67] O. Arias-Cuevas, Z. Li, and R. Lewis. Investigating the Lubricity and Electrical Insulation Caused by Sanding in Dry Wheel/Rail Contacts. *Tribology Letters*, 2009.
- [68] D.I. Fletcher and S. Lewis. Creep curve measurement to support wear and adhesion modelling, using a continuously variable creep twin disc machine. *Wear*, 2013.
- [69] D.I. Fletcher and J.H. Beynon. Development of a Machine for Closely Controlled Rolling Contact Fatigue and Wear Testing. *Journal of Testing and Evaluation*, 2000.